# FLUVIAL SUSPENDED SEDIMENT CHARACTERISTICS BY HIGH-RESOLUTION, SURROGATE METRICS OF TURBIDITY, LASER-DIFFRACTION, ACOUSTIC BACKSCATTER, AND ACOUSTIC ATTENUATION

A Dissertation

Presented to

The Academic Faculty

By

**Mark Newton Landers**

In Partial Fulfillment

of the Requirements for the Degree

Doctor of Philosophy in the

School of Civil and Environmental Engineering

Georgia Institute of Technology

May, 2012

**FLUVIAL SUSPENDED SEDIMENT CHARACTERISTICS**

**BY HIGH-RESOLUTION, SURROGATE METRICS OF TURBIDITY, LASER-DIFFRACTION, ACOUSTIC BACKSCATTER, AND ACOUSTIC ATTENUATION**

Approved by:


Dr. Terry Sturm, Advisor
School of Civil and Environmental Engineering
*Georgia Institute of Technology*

Dr. Aris Georgakakos
School of Civil and Environmental Engineering
*Georgia Institute of Technology*

Dr. Jian Luo
School of Civil and Environmental Engineering
*Georgia Institute of Technology*

Dr. Phillip Roberts
School of Civil and Environmental Engineering
*Georgia Institute of Technology*

Dr. David Mueller
*U.S. Geological Survey*


Date Approved: December 13, 2011

# Acknowledgements

The U.S. Geological Survey made this research possible through support, funding, and above all a community of applied researchers committed to furthering the science and practice of sediment monitoring. Dr. Terry W. Sturm was a steady, reliable advisor and friend. My children, extended family, friends, and Church were patient and encouraging during this journey. Especially, my wife of 28 years, Aleta McNair Landers, gives me inspiration and support that are critical to all of my accomplishments.

# Contents

# List of Tables

# List of Figures

# Symbols and Abbreviations

| | |
|---|---|
| ADCP | acoustic doppler current profiler |
| $a_s$ | sediment radius, in microns |
| $a_{nv}$ | sediment radius for sizes in non-viscous attenuation range, in microns |
| $a_T$ | sediment radius for transition zone of acoustic attenuation, in microns |
| $a_v$ | sediment radius for sizes in viscous attenuation range, in microns |
| cfs | cubic feet per second |
| cm/s | units of centimeters per section |
| dB | decibels, acoustic amplitude, logarithmic scale |
| EWI | equal width increment method of cross section sampling |
| FNU | formazin nephelometric units |
| ft/s | units of feet per section |
| MHz | megahertz, frequency of acoustic signal |
| PSD | sediment particle size distribution |
| *Q* | streamflow discharge, typically in cubic feet per second |
| *RB* | relative acoustic backscatter, adjusted for spreading, attenuation in dB |
| *RL* | acoustic reverberation level (measured backscatter intensity) in dB |
| SSC | general suspended sediment concentration, mg/L |
| $SSC_{xs}$ | cross section average suspended sediment concentration, mg/L |
| $SSC_{point}$ | suspended sediment concentration from fixed-point pump sample, mg/L |
| $SSC_V$ | volumetric suspended sediment concentration |
| *T* | turbidity in formazin nephelometric units |
| TL | two-way acoustic transmission loss in dB |
| TS | acoustic intensity of signal echoed by the suspended particles in dB |
| *VPC* | laser-diffraction metric of volumetric particle concentration in µl/L |

| | |
|---|---|
| $\alpha_S$ | attenuation of acoustic energy by sediment in dB/cm |
| $\alpha_w$ | attenuation of acoustic energy by water in dB/cm |
| $k$ | waver number equal to $2\pi$ / (acoustic wavelength) |
| $\Psi$ | factor accounting for non-uniform acoustic signal spreading in near field |
| $<f>$ | mean form function for the suspended sediment in acoustic scattering |
| µl/L | micro-liters per Liter |
| µm | microns |

## Summary

Sedimentation is a primary and growing environmental, engineering, and agricultural issue around the world. However, collection of the data needed to develop solutions to sedimentation issues has declined by about three-fourths since 1983. Suspended-sediment surrogates have the potential to obtain sediment data using methods that are more accurate, of higher spatial and temporal resolution, and with less manually intensive, costly, and hazardous methods. The improved quality of sediment data from high-resolution surrogates may inform improved understanding and solutions to sedimentation problems. The field experiments for this research include physical samples of suspended sediment collected concurrently with surrogate metrics from instruments including 1.2, 1.5, and 3.0 megahertz frequency acoustic doppler current profilers, a nephelometric turbidity sensor, and a laser-diffraction particle size analyzer. This comprehensive data set was collected over five storms in 2009 and 2010 at Yellow River near Atlanta, Georgia. Fluvial suspended sediment characteristics in this study can be determined by high-resolution surrogate parameters of turbidity, laser-diffraction and acoustics with model errors 33% to 49% lower than traditional methods using streamflow alone. Hysteresis in sediment-turbidity relations for single storm events was observed and quantitatively related to PSD changes of less than 10 microns in the fine silt to clay size range. Suspended sediment particle size detection (PSD) is significantly correlated with ratios of measured acoustic attenuation at different frequencies; however the data do not fit the theoretical relations. Using both relative acoustic backscatter (*RB*) and acoustic attenuation as explanatory variables results in a significantly improved model of *suspended sediment* compared with traditional sonar equations using only *RB*. High resolution PSD data from laser diffraction provide uniquely valuable information; however the size detection limits of the instrument is a significant limitation.

# 1 Introduction and Motivation

Sedimentation (erosion, transport, and deposition) is a primary and growing environmental, engineering, and agricultural issue around the world. Success in managing and solving sedimentation problems requires improved data and understanding of fluvial suspended sediment characteristics. Despite a growing need, the collection of sediment transport data has steadily declined in recent decades, due largely to high costs and difficult field methods. New technologies may be applied to collect sediment flux data of higher resolution and greater accuracy with potentially lower costs. This thesis presents research and results of methods to determine fluvial suspended sediment characteristics such as concentration, size, and flux by high-resolution, surrogate metrics of turbidity, laser-diffraction, acoustic backscatter, and acoustic attenuation.

Environmental impacts of sedimentation include loss of benthic aquatic habitat with resultant decreased biodiversity, ecological disruption due to changes in photosynthesis and visibility, and impacts from contaminants attached to and transported by sediments (Wood and Armitage, 1997). Most trace metals such as zinc, copper, and mercury as well as total phosphorus are strongly associated with sediments, particularly for sediments having smaller sizes (less than 63 microns) and resultant larger surface areas for a given diameter or concentration (Horowitz, 1991). More than 75 percent of the annual fluvial flux of most trace metals and total phosphorus is associated with suspended sediments in rivers and streams ranging from the lower Mississippi River to Peachtree Creek and other Metropolitan Atlanta streams (Horowitz et al., 2001, Landers et al., 2007, Horowitz et al., 2008). Sediment is the third most frequent cause of impairment in EPA's 303(d) list; it, accounts for 6,749 stream segments or 10.6 percent

of all impairments (U.S. EPA, 2008). All of the top five causes of stream impairment (pathogens, mercury, sediment, other metals, and nutrients) are sediment associated.

Figure 1.1 - Chattahoochee River at Morgan Falls Dam in Atlanta, Georgia, September 2009 Flood

The total maximum daily load (TMDL) studies required under the Clean Water Act for most of these impaired steam segments often lack sound methods to reliably estimate fluxes of sediment and sediment-associated constituents. Prevention and mitigation of the environmental impacts of sediment and stream habitat restoration require improved information on sedimentation.

Sedimentation also represents a major engineering problem. Sedimentation reduces waterway values for purposes of flood-control, recreation, and navigation, and increases water-treatment requirements for municipal and industrial uses. The average annual sediment load to reservoirs and aquatic systems in the United States from agricultural land use alone has been estimated to be 880 X $10^6$ tons (Pimentel, et.al, 1995). Dredging costs for United States waterways were over $966M per year in 2006 and 2007 (U.S. Army Corps of Engineers, 2008). Erosion of roadways and bridge scour represent a major engineering challenge. More bridges fail due to channel erosion than

all other causes combined, yet prediction of bridge scour continues to be a significant engineering problem (Landers and Mueller, 1996; Sturm, 2006). More recent engineering challenges include decommissioning and removal of dams, stream restoration, and contaminated sediment removal. Informed solutions to these problems require an increase in quality and quantity of sediment data and a deeper understanding of the physics of sediment erosion, transport, and deposition.

Erosion of arable lands is a primary threat to agricultural productivity and sustainability. The impacts of erosion on agriculture vary with agricultural practices, soil type, crop, and topographic setting. Erosion causes total annual costs (1992 dollars) estimated as high as $17 billion for all non-agricultural costs, plus $27 billion for agricultural productivity losses (Pimentel, et.al, 1995); although actual costs may be considerably lower (Crosson, 1997).

Sedimentation is a worldwide problem; however there has been a decreasing amount of fluvial sediment data collected in recent decades. The number of sediment monitoring stations where the U.S. Geological Survey (USGS) collects consistent and comparable data has declined by about three-fourths from 1982 to 2008 (Gray and Gartner, 2009). The declining number of sediment stations is due to factors that include high costs, manually intensive methods, and safety considerations. In view of the problems caused by sedimentation and the relative paucity of data collection efforts, the National Research Council (NRC, 2004) has stated that improved sediment monitoring is a crucial need. The increasing need is not only for collection of basic sedimentation data, but also for acquisition of more detailed, higher resolution data. Suspended-sediment surrogates, which are measured variables that indirectly relate to sediment concentration but are more easily measured, have the potential to provide sediment data using methods that are more accurate, of higher spatial and temporal resolution, and with less

manually intensive and hazardous procedures. If the surrogates can be developed from acoustic devices that are already being deployed in rivers, then costs may be lower than traditional methods.

Traditional methods are typically used at locations where sediment flux (discharge) is being monitored. Sediment fluxes are often integrated over a runoff event or a specific time period, such as a year, and are referred to as sediment loads. Many current methods for measuring sediment fluxes or loads have inherent limitations, particularly on dynamic rivers of medium and small size watersheds, where there is a growing need for sedimentation research. Such methods rely on relationships established between water discharge and sediment concentration; however, these relationships often exhibit hysteresis over a flow event. Some sediment surrogates may have a more unique relationship with sediment concentration, with the potential to define sediment transport hysteresis and to compute more accurate sediment fluxes (Gippel, 1989). Information on event hysteresis provides valuable clues about sediment sources in the watershed. For example, sediment concentrations that are higher on the rising limb than on the falling limb of a hydrograph (leading or clockwise hysteresis) may indicate that the limiting factor for sediment transport is the capacity or energy of the flow; whereas concentrations that are higher on the falling than on the rising limb of a hydrograph (trailing or counterclockwise hysteresis) may indicate that the limiting factor for sediment transport is the supply of fluvial sediment in storage (Julien, 1995).

Surrogates of fluvial suspended-sediment characteristics, including acoustic, optical turbidity, and laser diffraction metrics, can complete measurements (including averaging and filtering) with temporal resolutions of less than one minute; and with individual measurements of less than one second. High temporal resolution data are needed to describe processes in smaller and urbanizing watersheds where flow and sediment

conditions change rapidly. Traditional, manual methods of sediment sampling cannot provide high temporal resolution needed to define rapidly changing sediment concentration, size, and flux. Acoustic methods can measure (ensonify) and delineate a larger volume of water than traditional methods; and the profile of acoustic data may provide profiles of sediment concentration, resulting in much better spatial resolution. In addition to concentration, multi-frequency acoustics and laser diffraction may measure changes in sediment-size characteristics. Sediment size is indicative of absorbed, sediment-associated contaminants, and of biological impacts (Horowitz, 1991, Wood and Armitage, 1997). Sediment size also is an indicator in fingerprinting sediment source areas (Collins et al., 1997). The potential for high-resolution data on sediment concentration and size is significant to many sediment problems.

Data on sediment load, not concentration alone, are needed to address most of the sedimentation problems described previously. This is because environmental, engineering, and agricultural impacts of sedimentation are primarily due to cumulative effects over time of sediment, which are quantified in sediment load. Sediment load also is an effective measure of cumulative watershed effects from interactive processes affecting watershed hydrology and constituent yield over time (Horowitz, 2008). These cumulative processes include changing land use, climate, and watershed management practices. Acoustic metrics have the potential benefit of providing data to compute water discharge (via index velocity and stage area ratings) and sediment concentration needed for sediment-flux computations.

Although much has been done to develop and apply suspended-sediment surrogate technologies, the following literature review indicates that there are unaddressed and under-addressed questions, particularly in the application of acoustics. Much of the research into suspended-sediment surrogates has been conducted in marine

environments rather than fluvial environments. In fluvial environments, turbidity (nephelometric and optical backscatter sensors) has been used as a sediment surrogate for several decades (Walling, 1977; Downing et al, 1981; Lewis, 1996; Uhrich and Bragg, 2003; Rasmussen and others, 2005; Horowitz et al., 2008); although its limitations have also been broadly documented (Conner and De Visser, 1992; Downing, 1996; Sutherland et al., 2000; Jean et al., 2008; Landers, 2003). Acoustic surrogates of suspended sediment concentration (SSC) have been broadly investigated using principles of acoustic scattering and attenuation by SSC, as discussed in greater detail in the next chapter (Crawford and Hay, 1993; Gartner, 2004; Thorne et al., 1991; Wall et al., 2006). The relationship between acoustic metrics and sediment characteristics is rendered complex and dynamic by the acoustic effects of other environmental factors and instrument properties. In contrast to the methods of previous authors, Topping et al. (2004, 2006, 2007) use a more direct, empirical calibration method developed on the Colorado River that may have practical and accuracy advantages over the approach used by other authors to estimate SSC and flux from acoustic backscatter and attenuation. This empirical methodology needs further testing in other environments. Studies that compare at least two surrogate technologies to direct measurements to obtain sediment flux in rivers were found only for the Hudson River, New York (Wall et al., 2006) and for the Colorado River in the Grand Canyon, AZ (Topping et al., 2004, 2006, 2007).

The objectives of the research are to:

(1) Propose, develop, and test a new method for evaluation of sediment size from multi-frequency acoustics;

(2) Evaluate and further develop recently introduced empirical methods for estimating acoustic attenuation by sediment for the purpose of improving acoustic backscatter estimates and estimating sediment size;

(3) Assess accuracies and compare results for sediment concentration, load, and size estimates using each of the surrogate metrics of turbidity, acoustic backscatter, acoustic attenuation, and laser-diffraction; and

(4) Compare sediment surrogate technologies on the basis of reliability and operational considerations.

Methods to determine fluvial suspended sediment characteristics by high-resolution, surrogate metrics have been reviewed, developed, tested, and evaluated for measured data in this research. The research methodology involved collection of physical samples of suspended sediment concurrently with surrogate metrics from instruments including 1.2, 1.5, and 3.0 megahertz (MHz) frequency acoustic doppler current profilers, a nephelometric turbidity sensor, and a laser-diffraction particle size analyzer installed at the USGS stream gauge on Yellow River at Gees Mill Road near Milstead Ga (02207335), in the metro-Atlanta area. The extensive data are analyzed to address the objectives of this research.

# 2 Literature Review

This Chapter contains a review of previous investigations of surrogates of suspended-sediment characteristics including acoustic, turbidity, and laser-diffraction surrogates. The literature review provides background information that forms the context for the research and describes the technology and principles for each class of sediment surrogate.

## 2.1 Acoustic Surrogates

Characterization of suspended sediment using backscatter and attenuation of acoustic signals in water has been described and developed for several decades (Urick, 1948, 1975, Flammer, 1962, Hay, 1983, Sheng and Hay, 1988, Flagg and Smith, 1989, Thorne et al., 1991, Hay and Sheng, 1992, Lynch et al., 1994, Thorne and Hardcastle, 1997, Holdaway et al., 1999, Gartner, 2004, Topping et al., 2006, Wall et al., 2006, Gray and Gartner, 2009, Simmons et al., 2010, Guerrero et al., 2011, Thorne et al., 2011). The basic principles are that acoustic waves passing through a water-sediment mixture will scatter and attenuate as a function of sediment, fluid, and instrument characteristics. The acoustic metrics of backscatter and attenuation relate functionally to sediment characteristics (concentration, size, and shape) within an ensonified volume after adjusting for the influence of fluid and instrument characteristics. This literature review of acoustic surrogates of suspended sediment was published in the proceedings of the Joint Federal Interagency Sedimentation Conference (Landers, 2010).

### *2.1.1 Acoustic Attenuation*

Rayleigh (1896, § 334) developed the theory and expressions for the pressure disturbance (scattering) due to planar acoustic waves impinging on fluid spheres in an

inviscid medium. Sewell (1910) derived expressions for the energy loss (absorption) for rigid, fixed spheres in a viscous fluid. Lamb (1916, § 296-298) extended Sewell's method for rigid spherical objects that are free to move in the sound field. Urick (1948) extended Lamb's theoretical absorption equation to include scattering and viscous loss components for a given concentration of spherical particles. Urick (1948) wrote his equation as a coefficient for the attenuation of acoustic energy by sediment, $\alpha_S$, expressed in dB/cm so that larger values quantify larger acoustic attenuation per unit length. This equation is plotted in figure 2.1 and may be expressed in dB/cm as:

$$\alpha_S = SSC_V \left[ k(\gamma - 1)^2 \left\{ \frac{s}{s^2 + (\gamma + \tau)^2} \right\} + \frac{1}{6}(k^4 a_s^3) \right] 4.34 \qquad (1)$$

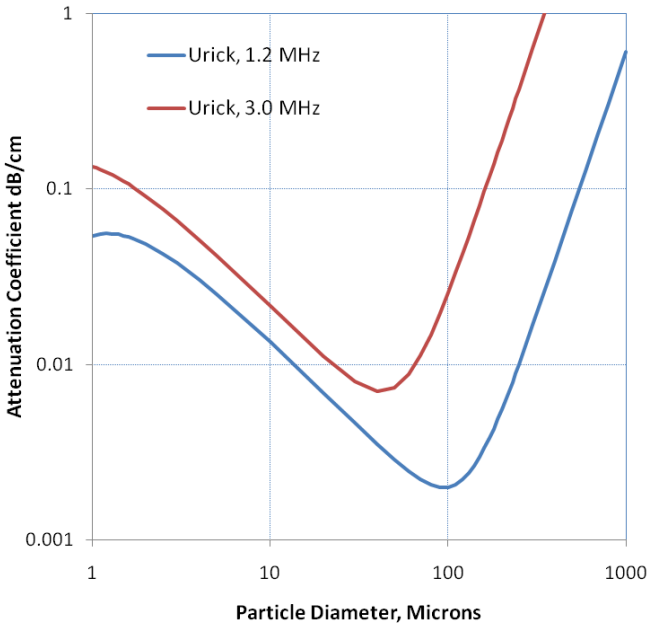


Figure 2.1. - Coefficient of acoustic attenuation due to suspended sediment and particle size, for 1.2 and 3.0 MHz frequencies at concentration of 1000 ppm from Urick's equation (1948)

where $SSC_V$ is the volumetric sediment concentration (SSC divided by sediment density), $k$ is the wave number, $2\pi/\lambda$, in which $\lambda$ is the wavelength in cm, $\gamma$ is the specific gravity of the sediment, $a_s$ is the mean sediment radius in cm, $s$ is equal to $[9/(4\beta a_s)][1+1/(\beta a_s)]$, $\tau$ is equal to $[0.5+9/(4\beta a_s)]$, in which $\beta$ is equal to $[\omega/2\upsilon]^{0.5}$, $\omega$ is $2\pi f$, $f$ is frequency in Hz, $\upsilon$ is the kinematic viscosity of water, in stokes, and 4.34 is the conversion from nepers to decibels for the attenuation. The first term of the sum within the brackets is the acoustic attenuation due to viscous losses and the second is the acoustic attenuation due to scattering losses. This form is dimensionally consistent and has been used by several subsequent researchers (Flammer, 1962; Hay, 1983; Gartner, 2004; Wall, 2006).

Urick (1948) tested equation 1 with laboratory data using quartz and kaolinite particles with median diameters of 2.2 and 0.9 microns, respectively in frequencies of 1 to 15 MHz. Urick found good agreement between equation 1 and laboratory results and noted that viscous losses accounted for nearly all of the absorption for the small particle sizes investigated in the frequency range of 1 to 15MHz.

Flammer (1962) tested Urick's theoretical expression for scattering attenuation, but did not investigate viscous losses because of equipment limitations for smaller particle sizes. Flammer conducted experiments over a range of frequencies from 2.5 to 25MHz, and sediment size distributions with mean diameters from 44 to 1000 microns. Flammer developed an expression in addition to viscous and scattering losses for attenuation due to diffraction by particles where $\lambda << 2\pi a_s$. Flammer found 'reasonably good' agreement between measured and computed geometric mean sediment size for a range of sediment gradations.

Sheng and Hay (1988) investigated methods of estimating attenuation due to scattering loss using data from four prior investigations, with most of the data coming from Flammer (1962). They observed a maximum scattering loss that is not represented in Urick's (1948) equation. Their expression was further developed in Crawford and Hay (1993) and is shown in figure 2.2 and expressed as:

$$\alpha_S = SSC_V \left[ \frac{k^4 a_s^{\,3}}{5(1 + 1.3k^2 a_s^{\,2} + 0.24k^4 a_s^{\,4})} \right] 4.34 \qquad (2)$$

This expression has been used by many authors investigating sediment surrogates in near bed marine environments where particle sizes larger than 63 microns are dominant (Thorne et al., 1991, Hay and Sheng, 1992, Thorne and Hardcastle, 1997, Holdaway et al., 1999, Thorne and Hanes, 2002).

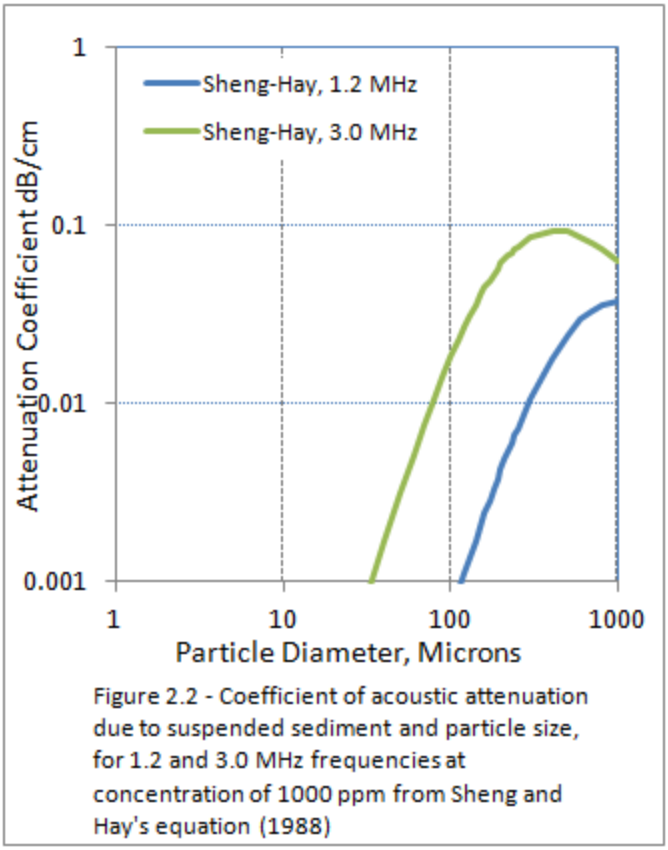


Figure 2.2 - Coefficient of acoustic attenuation due to suspended sediment and particle size, for 1.2 and 3.0 MHz frequencies at concentration of 1000 ppm from Sheng and Hay's equation (1988)

In many fluvial environments the size distribution of suspended sediments may include significant fractions of both silt/clay (less than 63 microns) and sand (greater than 63 microns) sizes. Some investigators (*personal communication, Scott Wright, USGS*) including this author have proposed replacing the scattering loss function in Urick's equation with that of Sheng and Hay to produce the following estimator of acoustic attenuation by SSC shown in figure 2.3 and equation 3.

$$\alpha_S = SSC_V \left[ k(\gamma - 1)^2 \left\{ \frac{s}{s^2 + (\gamma + \tau)^2} \right\} + \left\{ \frac{k^4 a^3}{5(1 + 1.3k^2 a^2 + 0.24k^4 a^4)} \right\} \right] 4.34 \quad (3)$$

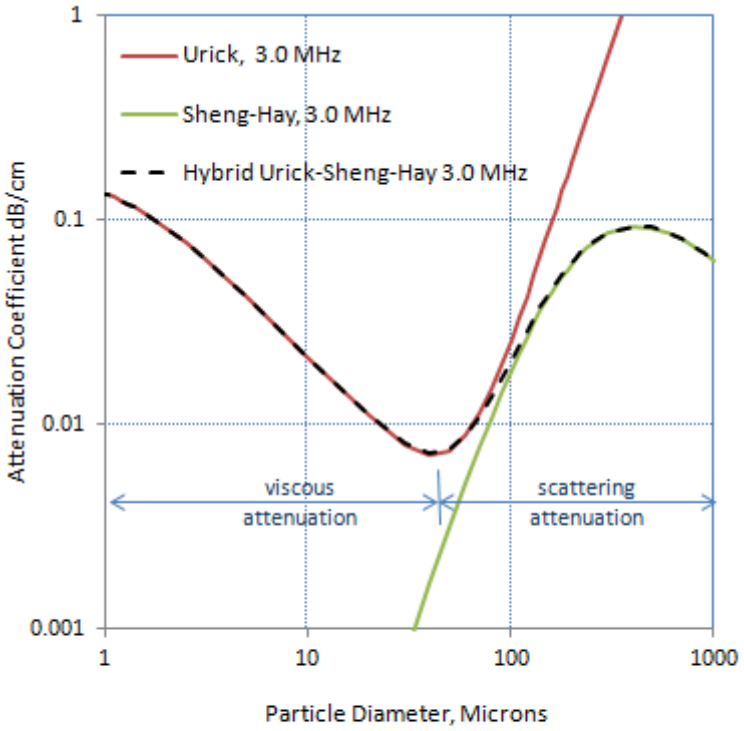


Figure 2.3 - Coefficient of acoustic attenuation due to suspended sediment and particle size, for 3.0 MHz frequencies at concentration of 1000 ppm from hybrid Urick-Sheng-Hay equation

Viscous losses are primarily due to the concentration of finer particles while scattering losses are primarily due to coarser particles. The acoustic attenuation due to viscous loss is caused by shear at the fluid-particle boundaries because of a lag between the sound-wave induced vibration of the particle and that of the fluid. The magnitude of the viscous loss is a function of the particle surface area, sound frequency, fluid viscosity,

and the ratio of particle to fluid density. As particle size (and inertia) becomes very small (left edge of figure 2.3), viscous loss approaches a maxima because the increased surface area is offset by a decreased lag for these very small particles. As the total particle surface area decreases with increasing particle size for given suspended sediment concentration (SSC) in figure 2.3, there is decreasing shear and viscous loss. Scattering of acoustic energy is related primarily to sediment diameter, rather than surface area (as for viscous losses). The scattering loss, represented in the second term within brackets in equation 1, or by equation 2, is generally negligible in the viscous loss particle size range. The minimum acoustic attenuation occurs at the transition between viscous and scattering losses. The particle size associated with this minimum attenuation increases with wavelength (decreasing frequency; figure 2.1). The minimum acoustic attenuation occurs, according to equation 3, at particle diameters of 90, 74, and 42 microns for frequencies of 1.2, 1.5, and 3.0 MHz, respectively, using 1,484 meters per second as the speed of sound in water. These particle diameters are in the silt to very fine sand range.

The scattering loss is due to reradiation of the acoustic energy incident on a particle. Scattering loss is a function of the ratio of acoustic wavelength, $\lambda$, to particle circumference $2\pi a_s$. For $\lambda >> 2\pi a_s$ scattering is concentrated in the backward direction and scattering losses rise rapidly with increasing sediment size. As $\lambda$ approaches $2\pi a_s$ scattering becomes complex and changes rapidly with sediment size and frequency (Urick, 1948; Flammer, 1962). The scattering attenuation reaches a maximum at particle diameters of about 1,050, 840, and 420 microns for frequencies of 1.2, 1.5, and 3.0 MHz, respectively. For $\lambda << 2\pi a_s$ half of the scattering propagates in the forward direction and the remainder scatters through all directions.

Theoretical acoustic absorption varies linearly with $SSC_V$ for a given frequency and sediment size. Linear variation of absorption with concentration implies that the absorption effects from individual particles are independent, because the particles are 'far enough apart' so that the scattering from one does not affect that of its neighbors. This assumption has been proven valid for a range of sediment sizes for concentrations up to 10,000 mg/l (Urick, 1948; Flammer, 1962; Sheng and Hay, 1988).

Some authors have recently reported that acoustic attenuation is dominated by the influence of fine particles (*hydroacoustics.usgs.gov/training/webinars/SAW-Acoustics-Sediment.ppt;* Topping et al, 2007*)*. This general assumption, however, is not supported by theoretical or experimental results. For example, using equation 3, the total acoustic attenuation for a suspension of uniform 250 micron sand is equal to that for a suspension of uniform 10 micron silt, independent of concentration, for a 1.5 MHz system and a speed of sound in water of 1,484 meters per second. The relative contribution of silt-clay sediment (viscous losses) and sand sediment (scattering losses) to total attenuation will depend on the gradation of the sediment mixture in the sampled volume. Flammer's (1962) thorough and often cited work, which verified Urick's equation, used sediments sizes primarily in the fine sand range. Also, Thorne and Hanes (2002) note that for noncohesive sediments ensonified at MHz frequencies the scattering component dominates.

Researchers investigating sound attenuation in fluids have often noted an 'excess attenuation' that was assumed to be related to turbulence (Brown and Clifford, 1976). The attenuation of sound by turbulence is due to two mechanisms. The first mechanism is direct transfer of sound energy to the turbulence (production of turbulent energy), and occurs only at low frequencies (less than a few kilohertz), where acoustic wavelengths are much greater than the turbulence correlation scale (Noir and George, 1978). The

second mechanism is scattering of sound waves by the turbulent microstructure and occurs at frequencies much higher than characteristic turbulent fluctuations. Brown and Clifford (1976) investigated this scattering loss using order of magnitude approach, while Ross and Lueck (2005) used concurrent shear and acoustic measurements at relatively high frequency (a 307 kHz). Both found that sound attenuation by turbulent scattering is a function of frequency to approximately the one-third power, and of fluid properties of viscosity, temperature, pressure, and total dissolved solids.

### *2.1.2 Acoustic Backscatter*

Early investigations of acoustic surrogates relied on instruments with a separate sound source and receiver, rather than a combined source and receiver such as modern transceivers (referred to here and typically as transducers). The transducer emits an acoustic pulse and then, after an interval just long enough to stop 'ringing', it receives the echoes backscattered from particles suspended in the acoustic path, as illustrated in the simplified cartoon of figure 2.4. Acoustic doppler current profilers (ADCPs) measure the doppler shift in the frequency of the backscattered signal to determine the velocity of the particles scattering the signal (the assumed water velocity) relative to the transducer. Two or three transducers at fixed beam angles may be used to resolve a 2- or 3-dimensional flow velocity vector. As hydroacoustic transducers became available researchers began to investigate the amplitude of backscattered sound at the transducer as a surrogate for sediment concentration. In an investigation of fluvial sediment, Braithwaite (1974) measured SSC and backscatter amplitude from a 1MHz transducer in seven rivers in England. Limitations in the methods make the results qualitative, but good correlation was proven for backscatter amplitude and sediment concentration in fluvial environments. Investigations in marine environments using single-frequency acoustic backscatter include those of Young et al. (1982), Hay (1983), and Hess and

Bedford (1985). Flagg and Smith (1989) showed good correlations between acoustic backscatter amplitude and zooplankton abundance with high temporal and spatial resolution.

### *2.1.3 Acoustic Surrogates – semi-empirical method*

A semi-empirical backscattering theory and acoustic surrogate methodology was progressively developed by several researchers working in marine environments (Sheng and Hay, 1988; Thorne et al., 1991; Hay and Sheng, 1992; Downing et al, 1995; Crawford and Hay, 1993; Thorne and Hardcastle, 1997). This methodology has been tested across a wide range of frequencies and sediment sizes in laboratory and marine environments by these and other authors (Hamilton et al., 1998; Holdaway et al, 1999; Thorne and Hanes, 2002; Thorne et al., 2011). Fluvial environments have rarely been

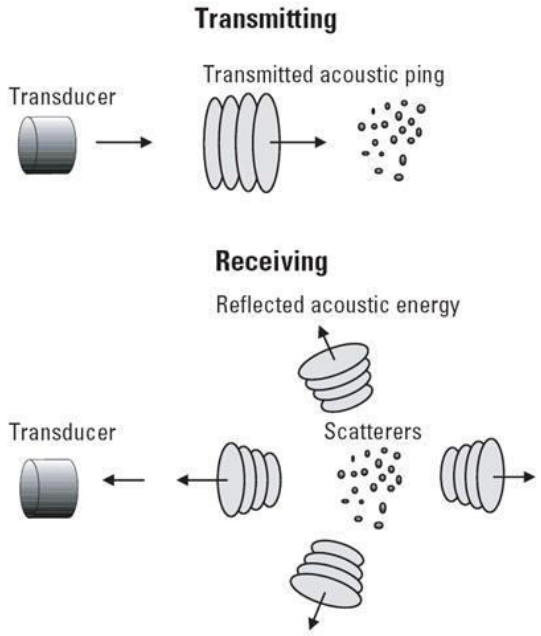


Figure 2.4 - Acoustic backscatter from suspended particles (from Simpson, 2001)

evaluated by this method. The general expression for average (root mean square) backscatter amplitude ($P_{rms}$ as pressure) from an ensemble of measurements for a specific ensonified volume is:

$$P_{rms} = \frac{K_s K_t}{r\psi} \sqrt{SSC}\ e^{-2r(\alpha_w + \alpha_s)} \qquad (4)$$

where

$$K_s = \frac{< f >}{\sqrt{\rho < a_s >}}, \quad K_t = \frac{0.96 P_o r_o}{k a_t} \left\{ \frac{3\tau c}{16} \right\}^{0.5}, \quad \psi(r) = 1 + \frac{1}{(1.35r/r_n) + (2.5r/r_n)^{3.2}}$$

where, $r$ is the range from the transducer to the ensonified volume, *SSC* is the mass concentration of suspended sediment, signal attenuation is expressed in the coefficients for sediment absorption, $\alpha_s$, and water absorption, $\alpha_w$, $K_s$ and $K_t$ account for sediment scattering and instrument effects, and $\psi(r)$ accounts for nonuniform energy spreading in the transducer near field, $r_n$, which is also known as the Rayleigh distance. Equation 4 is dimensionally inconsistent.

Many authors using equation 4 have assumed $\alpha_s$ to be negligible; others have used equation 1 or, more often, equation 2. Water absorption is a function of water temperature, salinity, and pressure and can be obtained by equations or tables (Ainslie and McColm, 1998; Fisher and Simmons, 1977). For most freshwater fluvial environments (at depths less than 100 meters), only temperature will significantly affect $\alpha_w$ .

The parameter $K_s$ accounts for variations due to the size, density, and scattering properties of the sediment, in which $<f>$ is the mean form function for the suspended

sediment taken over the range of sediment sizes, $\rho$ is the sediment density and $<a_s>$ is the mean sediment radius. The variation in form function with particle size and frequency is explored by Thorne and Hanes (2002), and Thorne and Hardcastle (1997). The parameter $K_t$ accounts for variations due to instrument electronic characteristics and transducer characteristics in which $P_o$ is the backscatter amplitude at reference distance $r_o$ , usually 1 meter, $a_t$ is the transducer radius, $\tau c$ is the pulse length equal to the product of pulse duration, $\tau$, and the speed of sound, $c$.

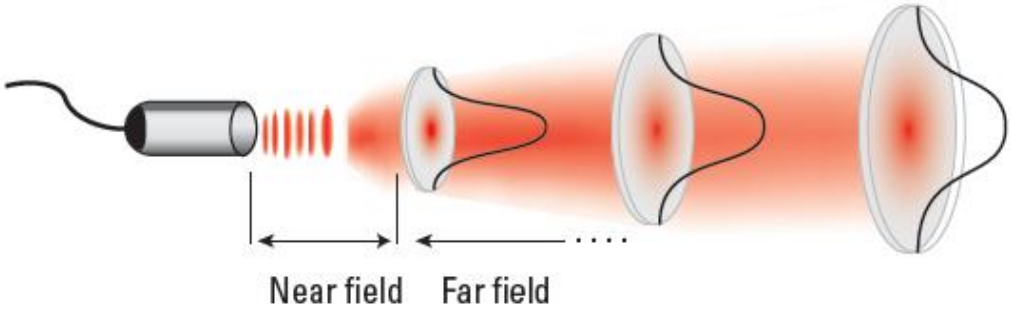


Figure 2.5 - Spherical spreading of acoustic energy

Backscatter amplitude from reflections in the transducer far field varies with the inverse range (*1/r*) to the measured volume due to spherical spreading of the acoustic energy from the sound source, as illustrated in figure 2.5. For measurements made near the transducer surface, in the near field, the energy spreading is nonlinear. The parameter $\psi(r)$ accounts for the departure of the acoustic signal from spherical spreading in the near field, $r_n = \pi a_t^2 / \lambda$, in which $\lambda$ is the wavelength. In marine studies, transducers often are down-looking from a platform resting on the bed, so that near field corrections often are needed. In fluvial studies the measurement volume may be beyond the near field, but near field correction was included here for completeness.

The $P_{rms}$ of equation 4 results from averaging $P^2$ over several realizations and integrating over the ensonified volume. The conversion from the mean backscattered pressure of individual particles to mass concentration contains an implicit sediment density and equivalent spherical size. Particles within the measurement volume are assumed to be randomly and uniformly distributed, which is likely for measurements from profiling, multi-cell ADCPs, in which the return signal is evaluated (digitally sliced) into smaller, user-specified cell lengths (a pulse time slice). The effects of irregular sediment shape and density will be discussed later.

Rearranging, equation 4 may expressed as

$$\therefore SSC = \left[ \frac{P_{rms} r \psi}{K_s K_t} \right]^2 e^{4r(\alpha_w + \alpha_s)} \qquad (5)$$

The limitations of this methodology are obvious in that information for the unknown sediment size and SSC are needed to evaluate the $K_s$ and $\alpha_s$ parameters on the right hand side of the equation. These will be discussed further in the limitations section. Investigators using equation 5 have evaluated $K_t$, $K_s$ and $\alpha_s$ using laboratory measurements and assumptions, with $\alpha_s$ often assumed to be negligible. Potential attenuation due to turbulence was not considered to be significant by any of the reviewed studies.

### *2.1.4 Acoustic Surrogates – Urick's method*

A different expression relating acoustic surrogates to sediment concentration begins with Urick's (1975) sonar equation and has been used by several authors (Thevenot and

Kraus, 1993; Reichel and Nachtnebel, 1994; Gartner, 2004; Wall et al, 2006, Topping et al, 2007). The sonar equation is written in logarithmic units of decibels as:

$$RL = SL - 2TL + TS \quad (6)$$

*where*

$$2TL = 20\log_{10}(\psi r) + 2r(\alpha_s + \alpha_w) \quad (7)$$

In this method *RL* is the reverberation level (measured backscatter intensity) of the received signal and is equal to $10\log_{10}(P_{rms}^2)$, *SL* is the source level of the emitted signal, *2TL* is the two-way transmission loss equal to the sum of the spherical spreading and attenuation, and *TS* is the intensity of the signal echoed by the particles in the ensonified volume, equal to $10\log_{10}(SSC)$. Equation 6 can be derived from equation 4, except for parameters $K_t$ and $K_s$, which are handled empirically by most authors using this method, and source level (*SL*) which is generally not evaluated in this method (Thevenot and Krause, 1993; Gartner, 2004). The relative backscatter (*RB*) is computed as *RB = RL+2TL,* which is equivalent to the total scattering by suspended particles. Then, $\log_{10}(SSC)$ is a function of *RB* and:

$$SSC = 10^{(A+B*RB)} \quad (8)$$

The coefficients *A* and *B* are evaluated using regression for paired physical *SSC* and acoustic measurements. Source level is generally not evaluated in this method (Thevenot and Krause, 1993; Gartner, 2004), and sediment acoustic attenuation is sometimes assumed to be negligible (Gartner and Cheng, 2001; Wall and others, 2006).

Gartner (2004) described the methodology and accounted for water absorption, spreading loss, near field distortion, receiver signal sensitivity, and sediment absorption using Urick's (1948) equation. Gartner used downward looking 1.2 and 2.4MHz

broadband ADCPs, mounted about 2 meters above the bed at two locations in San Francisco Bay and calibrated the systems using optical backscatter (OBS) turbidity readings adjacent to the ADCPs. Estimates of SSC of clay to fine sand sizes from acoustic surrogates agreed to within about 8 to 10 percent of those estimated by OBS.

Wall and others (2006) used a bottom mounted, broadband, 4 beam, 0.614 MHz ADCP on the Hudson River at the U.S. Geological Gage 01372058. They collected concurrent SSC samples from the ensonified volume to calibrate the sonar equation. They also measured depth and width integrated SSC for the stream cross section and developed the relation between sediment flux in the acoustic sampling area and in the river cross section. Their work resulted in the computation of daily sediment flux for this tidally affected location of the Hudson River which is shown in near real time on the USGS data National Water Information System.

### *2.1.5 Multi-Cell Acoustic Surrogates*

Measurements of the acoustic return signal can be digitally sliced into specific range-gated 'cells' to provide data on velocity and acoustic metrics at integral points along the acoustic beam. These data offer an effective means to directly measure the sediment acoustic attenuation at a high temporal resolution. Figure 2.6 shows the acoustic backscatter in decibels (dB) measured by a 3.0 MHz unit with 10 cells of 20cm axial distance each measured between 0.2 and 2.2 meters from the transducer face.

The average SSC in the channel cross section was about 694 milligrams per liter (mg/l) at the time of this acoustic measurement. The measured values are assigned to the center location of each cell (0.3, 0.5,…2.1m) and the near field boundary for this instrument is 0.77 m. The *RL* line is the measured backscatter intensity and its slope is the combined two-way signal strength loss due to spherical spreading plus fluid and

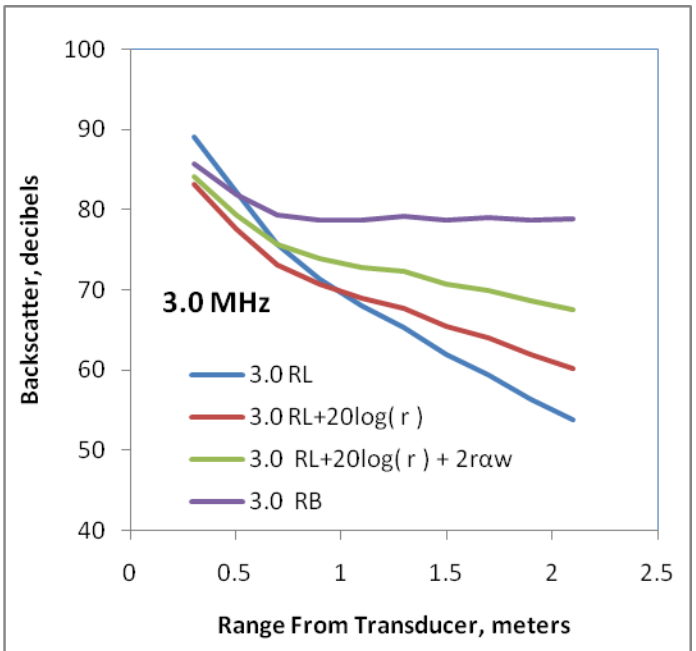


Figure 2.6 - Backscatter amplitude profiles along axial range ro 3.0 MHz acoustic doppler profiler

sediment acoustic attenuation. The ($RL+20log_{10}(\psi r)$) line is the measured backscatter intensity corrected for spherical spreading and the ($RL+20log_{10}(r) + 2r\alpha_w$) line is further corrected for fluid attenuation. Solving for the slope of this line provides the two-way acoustic attenuation, $2\alpha_s$. Topping et al (2004, 2006, 2007) first used this method to solve for $\alpha_s$. The sediment acoustic attenuation is then used to compute the relative backscatter ($RB=RL+2TL$) for each cell as shown. The *RB* for a given cell varies with scattering properties of the ensonified volume, having been corrected for all other factors. This analysis is performed for each time step to obtain a time series of the acoustic surrogates of acoustic attenuation by sediments and normalized acoustic backscatter.

This multi-cell method has the powerful advantages of measuring $\alpha_s$ and of normalizing for the effects of sediment scattering properties, $K_s$, and transducer specific characteristics, $K_t$. The effects of $K_t$ would be constant from cell-to-cell in the same measurement, as would the effects of $K_s$, so long as sediment scattering properties are not changing significantly along the acoustic beam. In other approaches these effects have been assumed to be constant over time, but this method can be applied to normalize measurements at each time-step so that changing sediment scattering properties or changes due to power supply variations can be accounted for.

### *2.1.6 Multi-Frequency Acoustic Surrogates*

A significant limitation of single-frequency systems is that the metrics of acoustic attenuation and relative backscatter change in response to changes in both sediment concentration and sediment size, creating a size-concentration ambiguity. Relative acoustic backscatter from sediment may increase with increased concentration at a fixed size distribution or with increased sediment size at a fixed concentration; and acoustic

attenuation also varies with size as discussed previously. Multi-frequency acoustic systems, however, have been successfully used to estimate both sediment concentration and general size characteristics (Crawford and Hay, 1993; Gartner, 2004; Hay and Sheng, 1992; Thorne et al., 1991; Thorne and Hardcastle, 1997; Smith et al, 2006; Topping et al., 2007). Two approaches have been developed that use multi-frequency acoustics to evaluate sediment size, one by Hay and Sheng (1992) and one by Topping et al (2007).

In the multi-frequency method developed by Hay and Sheng (1992) and further described by others (Crawford and Hay, 1993; Thorne et al., 1991; Thorne and Hardcastle, 1997; and Thorne and Hanes, 2002, Thorne et al., 2011), sediment size is obtained from the ratio of form function at different frequencies by inversion of equation 5 as:

$$\frac{< f_i >}{< f_j >} = \left[ \frac{P_{rmsi} / K_{ti}}{P_{rmsj} / K_{tj}} \right]^2 e^{2r(\alpha_i - \alpha_j)} \qquad (9)$$

in which

$$< f_i > = 1.1 \left\{ 1 - 0.25 e^{-\left( \frac{ka_s - 1.4}{0.5} \right)^2} \right\} \left\{ 1 + 0.37 e^{-\left( \frac{ka_s - 2.8}{2.2} \right)^2} \right\} \left\{ \frac{1.1(ka_s)^2}{1 + 1.1(ka_s)^2} \right\} \qquad (10)$$

Where $k$ is the wave number, as before, and $i$ and $j$ refer to different frequencies and $\alpha = (\alpha_w + \alpha_s)$. The ratio of the form function to sediment size only varies over a limited range of the product of the wave number and sediment size. If $k\langle a_s \rangle$ is larger than about 2 or less than about 0.2, then there is no size information in $\langle f_i \rangle / \langle f_j \rangle$. Methods to determine

$K_t$ are reviewed by Thorne and Hanes (2002) and include full electronic and acoustic calibration of the system (most used method); laboratory calibration using a known concentration of glass spheres (so that $K_s$ is known); and methods using field sediments by assuming $K_s$ (and thus PSD) is invariant. Note that the complexity and/or assumptions in estimating $K_t$ is a significant limitation to the generalized application of this method using commercial ADCPs. Also in this method, the backscatter is the primary measured quantity and $\alpha_s$ is either assumed to be negligible or an iterative approach is used to resolve the unknown $\alpha_s$.

Hay and Sheng (1992) developed and applied a multi-frequency acoustic backscatter system to measure vertical profiles of sand concentration and size near the sea bed (<1 meter) using 1, 2.25, and 5MHz systems. Hay and Sheng also deployed OBS turbidity sensors near the monitoring bins of the acoustic system. Their laboratory measurements indicated that the three frequency system was able to measure mean concentration with about 10 percent accuracy and mean size with 10 to 20 percent accuracy. The method required averaging measurements over about one-half hour to obtain this accuracy because of high measurement variance. Field measurements indicated that concentrations from the multi-frequency acoustic system and the optical backscatter sensors are within 10 percent. The OBS turbidity sensors were calibrated in the laboratory with local bottom sediments.

Smith et al (2006) apply a similar approach using form-factor ratios to estimate particle sizes for natural sands using a multi-frequency transducer measuring suspensions in a turbulent jet in a laboratory. They found maximum errors of 36 percent for particle diameters from 300 to 950 microns and 160 percent for particle diameters of 150 to 300 microns.

Three frequencies have been used in most multi-frequency sediment surrogate studies. In some applications with little silt and clay, sediment acoustic attenuation is assumed to be negligible and $<a_s>$ can be extracted from the form function ratio at different frequencies (Thorne and Hanes, 2002). As noted in Thorne and Hardcastle (1997) the form function to sediment size relationship for a given frequency is not always monotonic so that multiple solutions are possible; but this can normally be resolved if at least three frequencies are used.

Thorne et al. (2011) evaluate a new dual frequency inversion procedure to obtain sediment concentration profiles in the near bed boundary layer. The dual frequency approach is based on inversion of the backscatter signal (as with previous methods). The result improved estimated SSC, compared to previous approaches as reviewed in Thorne et al. (2002); however its restrictive conditions are a known and constant particle size distribution. Thorne et al. (2011) also discuss how acoustic attenuation due to sediment is a major source of uncertainty in their method; and that this attenuation is greatest during high concentration conditions which are of primary interest.

Topping et al (2004, 2006, 2007) have used laser and acoustic metrics as surrogates of suspended sediment for the Colorado River in the Grand Canyon, Arizona, USA. In this river, sediment load is typically controlled by the supply of sediment (supply limited) rather than by the capacity of the flow (capacity limited). Thus, discharge is not a good surrogate of sediment concentration and flux. The suspended sediment size distribution in the study reach is typically bimodal and is highly variable depending on rainfall patterns in the watershed. The calibration data set (2007) has silt and clay concentrations from 10mg/l to 20,000 mg/l with median size of 14 μm and sand concentrations from 10mg/l to 3,000 mg/l with median sizes of up to about 400 μm.

Topping et al (2007) observe the transition from viscous to scattering losses in sediment acoustic attenuation as noted previously for Urick's equation (figure 2.1) and from this describe two acoustic size classes of sediment; a finer acoustic size class in which viscous attenuation is dominant and a coarser acoustic size class in which scattering attenuation is dominant and backscatter is more significant. The upper limit of the finer acoustic size class is frequency dependent and is defined as 62.5 *μm* for 2 MHz; 105 *μm* for 1 MHz, and 177 *μm* for 0.6 MHz. The range of coarser acoustic size class assigned to each frequency is 62.5-105 *μm* for 2 MHz, 105-177 *μm* for 1 MHz, and greater than 177 *μm* for 0.6 MHz. These upper limits are approximately equal to the sizes producing minimum acoustic attenuation at these frequencies.

In the method developed by Topping et al (2007) the sediment acoustic attenuation coefficient is determined from multi-cell measurements as described in the previous section and a regression equation is developed between measured silt-clay concentration (less than 63 μm) and $\alpha_s$ for the 2 MHz frequency to obtain a predictive surrogate relation for the concentration of fines. Next, the measured backscatter is normalized for spherical spreading, water attenuation, sediment acoustic attenuation, and a factor for the influence of the fine sediments on increased backscatter for each frequency. Measured sand concentration within the frequency-specific coarse size class is then regressed against this normalized backscatter for each frequency. The total suspended sand concentration is obtained as the sum of the computed concentrations of sand in each grain-size range. The median sand grain size is computed by logarithmic interpolation between the acoustically computed concentrations in each grain-size range. Applying this method, Topping et al (2007) report computed concentrations within 5% of the values computed using conventional data; and median sand grain size typically within 10% of the values obtained by conventional measurement.

### *2.1.7 Acoustic Instrument Technology*

Acoustic doppler current profilers (ADCP) are commercially available and broadly used to measure velocity profiles in laboratory and environmental applications (Cobb and Landers, 1993; Muste, et al., 2007 (special edition ASCE Journal of Hydraulic Engineering);). A fixed array of 2 to 4 transducers measure axial velocities that are used to obtain a 2- or 3-dimensional stream velocity. A transducer is a (typically piezoelectric)

Figure 2.7 - Concept of a multi-cell, 2-beam ADCP (Sontek, Inc.)

device that transfers voltage to a sound-wave producing pulse, and vice versa. The transducer sends an acoustic pulse, and then measures the returned backscatter signals as illustrated previously in figure 2.4. If the suspended scatterers have a non-zero velocity along the axis of the acoustic beam, then there will be a doppler shift in the backscattered signal. Assuming the suspended particles are moving at the same velocity as the water, the axial water velocity can then be computed from the change in frequency phase of the backscatter as:

$$u = \frac{c\, f_D}{2 f_0} \qquad (11)$$

Where *u* is the axial water velocity, $c$ is the speed of sound in water, $f_O$ is the system frequency, and $f_D$ is the doppler shifted frequency measured at the transducer. ADCPs measure temperature continuously and store a user-specified total dissolved solids to compute $c$ for each measurement. The return voltage signals are digitized and sliced by time interval into ranges or bins so that a velocity profile can be computed (figure 2.7).

As a velocity measuring instrument, the ADCP records the backscatter amplitude as a data-quality indicator. Velocity measurement requires the magnitude of the measured backscatter to be greater than that of ambient acoustic noise. The maximum range of an ADCP, if it does not intersect a boundary, is dependent on the signal attenuation, which is a function of water, sediment, and instrument characteristics. Figure 2.8 shows an example of recorded backscatter amplitude (as signal to noise ratio) for 5 cells of one beam, and computed velocity for beams one and two for a 3.0 MHz Sontek ADCP.

At least one instrument using multi-frequency (3 to 4 frequencies from 0.5 to 4 MHz) acoustic technology to estimate sediment characteristics is commercially available (Aquatec Group, 2011). This instrument provides information on SSC for concentrations from 100 to 20,000 mg/L for sediments from 20 to 2000 microns. The sampling range varies with the transducer frequency. This author is not aware of this device being used in fluvial environments at this time. The approximate cost of an AQUAscat survey unit in 2011 is $30,070.

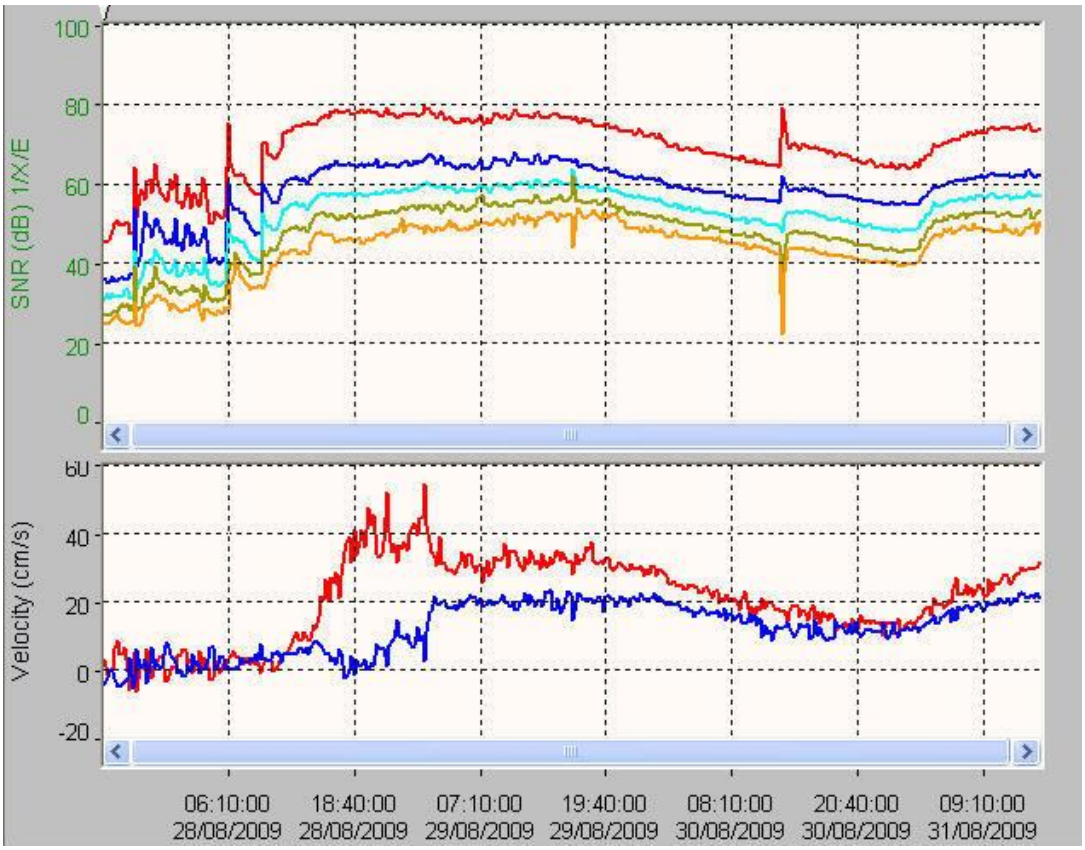


Figure 2.8—Backscatter amplitude as signal to noise ratio (SNR) for five cells, and computed velocity for 3.0 MHz ADCP

### *2.1.8 Limitations and Assumptions of Acoustic Surrogates*

As discussed previously, acoustic metrics from single-frequency systems may change due to changes in sediment concentration or sediment size, creating a size-concentration ambiguity. This limitation may be overcome using multi-frequency acoustic systems, although these systems increase complexity and cost. Also, methods to quantify and adjust for sediment size characteristics using acoustic metrics have had very little testing and have not been generalized for broad application. Acoustic metrics are sensitive to the ratio of sediment size to wave number and a somewhat narrow frequency is optimal for evaluation of particle size distribution using multi-frequency

acoustics (Gray and Gartner, 2009). The sensitivity of acoustic surrogates of suspended sediment is limited for low concentrations and generally may not be applicable for concentrations less than about 10 mg/l for frequencies in the 0.5 to 5MHz frequency range (Gray and Gartner, 2009). All methods that use measurements of a subsection or single point of the channel cross section require concurrent point and cross-section SSC measurements for calibration to the entire cross section and assumed stability of those calibrations. This limitation is more restrictive for surrogates based on small point volume measurements than for acoustic surrogates which typically are based on a much larger volume than point measurements.

The irregular shape of natural sediments can significantly affect acoustic backscatter and attenuation. Two cross sections of natural sediments affect acoustic surrogates. The backscatter cross section, or the effective particle area incident to the acoustic wave affects the backscattered energy; and the total scattering cross section, which affects the energy scattered in all directions (Hay and Sheng, 1992). Expressions for the effects of irregular shaped particles on acoustic scattering were developed by Sheng and Hay (1988).

Because the semi-empirical method requires estimation of $K_S$ and $K_T$, additional assumptions are required that are not required where these affects are normalized for empirically using the multi-cell approach. Knowledge or assumptions of SSC, particle size, and particle scattering characteristics are required to compute $K_s$. Thorne and Hanes (2002) review methods such as estimating sediment size from bed-material samples, assuming $\alpha_s$ is negligible, and solving equation 5 using an iterative approach. In fluvial environments, scattering characteristics likely would be more variable than in marine environments, increasing uncertainty in $K_s$ estimates.

Full electronic and acoustic evaluation of $K_t$ requires measurements of the transmit signal level, receiver amplification, time variable electronic gain, analog to digital conversion, and the transducer beam pattern. These characteristics can vary with power supply and environmental conditions, and characteristics for each transducer are unique, even for the same multi-transducer instrument. Experimental determination of these characteristics is very difficult and requires specialized laboratory instrumentation (Holdaway et al, 1999; Thorne and Hanes, 2002). $K_s$ and $K_t$ have often combined into a single calibration coefficient because of their complexity and because they may have a limited variance in specific marine sediment conditions for a single, specialized instrument set up.

## 2.2 Turbidity Surrogates

Turbidity is a metric of the optical properties of a water-sediment mixture causing opaqueness because of the scattering and absorption of light by suspended and dissolved matter such as organic and inorganic particles, organisms, and dyes (Anderson, 2005; ASTM International, 2007). Semi-quantitative measurements of water opacity have been measured since the 1860's as the depth of disappearance of a white or white and black 30cm diameter Secchi disk. A systematic study of this method was presented by Angelo Secchi in 1866 (Preisendorfer, 1986). Turbidimeters were introduced around 1958 and have progressed steadily in instrument technology to standardized instruments that can be deployed in situ to measure streamflow turbidity (Hach, 1972). The two types of turbidity sensors in common use at this time are based on nephelometric or optical-backscatter (OBS) principles.

Turbidity is the most widely used sediment surrogate for regular estimates of sediment concentration and load; and has been endorsed for sediment-monitoring programs by the U.S. Geological Survey, the Federal Interagency Sedimentation Project, and others (Rasmussen et al, 2009). Recognizing the value of turbidity as a surrogate, many States have established regulations using turbidity, particularly for drinking water sources. However, turbidity is not a physical property of water and its measured values are affected by suspended-sediment and water characteristics including particle size, shape, and color. (Hach, 1972; Conner et al, 1992; Lewis 1996; Davies-Colley and Smith, 2001; Landers, 2003; Ziegler, 2003a,b; Anderson, 2005; Downing, 2006; Loperfido, et al., 2010).

Turbidity has been used as a quantitative surrogate of SSC in marine and fluvial environments for several decades. (Walling, 1977; Downing et al, 1981; Kineke and

Sternberg, 1992; Lewis, 1996; Christensen et al, 2000; Warner and Sturm, 2002; Schoellhamer and Wright, 2003; Uhrich and Bragg, 2003; Rasmussen and others, 2005). Several of these studies found significant improvements in accuracy of computed suspended sediment loads using turbidity compared with loads computed from streamflow alone (Rasmussen et al, 2005; Jastram et al, 2009). Several studies also have used turbidity as a surrogate of other constituent concentrations, including total nitrogen, total phosphorus, and pathogen indicator bacteria (Rasmussen et al, 2005; Lawrence, 2006; Jastram et al, 2009)

Jastram et al (2009) compared estimates of SSC based on turbidity and streamflow surrogates for three major tributaries to Chesapeake Bay and found that the mean absolute error of turbidity-based SSC estimates was 50 to 87 percent less than the corresponding over-predicted results from streamflow-based models, with resultant improvements in suspended sediment load estimates. They also found significant

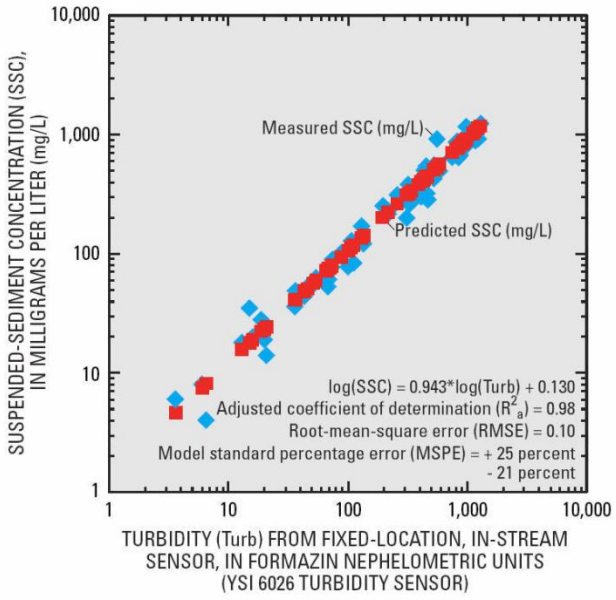


Figure 2.9 - Example of simple linear regression of log-transformed turbidity and SSC for Little Arkansas River near Sedgwick, Kansas (from Rasmussen et al, 2009)

improvements in estimates of total phosphorus, which is highly sediment associated.

The methods used in these studies are fairly straightforward. Turbidity readings from a fixed point may or may not be calibrated to cross sectionally averaged turbidity values in fluvial studies. Concurrent turbidity and cross-section average SSC measurements are used to develop a turbidity to SSC model. The model is usually obtained by curve fitting as with linear regression (figure 2.9). This model is combined with continuously monitored turbidity to create SSC time series that can be used with the concurrent streamflow data to compute continuous suspended sediment load. In some cases streamflow was as a second explanatory variable in the model to estimate SSC. In October of 2009 the USGS released a report documenting methods for computing time-series of SSC and suspended sediment load from turbidity and streamflow data (Rasmussen et al, 2009). This report provides detailed guidance on using turbidity as a SSC surrogate and generally will be used as a guideline for the turbidity methods used in this research.

### *2.2.1 Turbidity Instrument Technology*

The two types of turbidity sensors in common use at this time are based on nephelometric or OBS principles. Nephelometric turbidimeters measure the optical properties of a water-sediment mixture that cause light to be scattered or attenuated rather than transmitted in straight lines through the solution; with increased scattering resulting in increased turbidity values. Nephelometry is the measurement of light scattering using a light detector 90 degrees from the incident light (U.S. Environmental Protection Agency, 1999). Approved methods (in 2008) for the measurement of turbidity include those that conform to one of three protocols. These are stated in: (1) U.S. Environmental Protection Agency (USEPA) Method 180.1 (U.S. Environmental

Protection Agency, 1979), (2) ISO Method 7027 (International Organization for Standardization, 1999), and (3) standard methods recommended by the American Water Works Association and the Water Environment Federation (Clesceri and others, 1998). Both nephelometric and OBS turbidimeters may use white or near-infrared light sources. OBS turbidimeters operate by the same principles as nephelometric meters but the angle between the light source and the detector it typically smaller than 90 degrees.


Figure 2.10- Three self-cleaning nephelometric turbidity sensors: (A) YSI (Yellow Springs Incorporated) model 6136, (B) Hydrolab, and (C) Forest Technology Systems model DTS-12

Designated measuring units for turbidimeters have changed over time. The most common in use at this time are nephelometric turbidity unit (NTU) and formazin nephelometric unit (FNU). Nephelometric sensors typically have a maximum reading of 1000 to 2000 NTUs; while OBS sensors generally do not have a cut off or censoring level. A review of available turbidity sensor technologies is provided by Anderson (2005), with recommendations for specific applications and guidelines for calibration, operation,

quality-assurance procedures, and reporting of data. Turbidimeters are particularly subject to fouling by biological and other sources, so that wipers have become standard for many models as shown in figure 2.10.

### *2.2.2 Limitations and Assumptions of Turbidity Surrogates*

Although the methodology is straightforward, there are significant limitations to using turbidity as a sediment surrogate. As noted previously, turbidity is not a physical property of water such as Ph, temperature, or SSC. The optical measurement is affected by the size, shape, and color of the suspended sediment mixture, as well as by dissolved, light absorbing substances. Turbidity readings are also variable with instrument design (light source, detector, and spectra) and with specific instruments of the same design. Many of these issues are summarized by Downing (2006).

The size-concentration ambiguity found for acoustic surrogates also occurs with turbidity surrogates. Measured turbidity for a given concentration of suspended particles increases with decreasing particle size due to increased light scattering from smaller particles as seen in figure 2.11B (Conner and DeVisser, 1992; Sutherland et al, 2000). Sediment shape also affects optical scattering and absorption, with typically higher turbidity measured for plate-shaped particles than for more rounded particles (Downing, 2006). Turbidity metrics also are affected by the reflectivity of the suspended sediment, which is generally tied to its color as seen in figure 2.11A, with increased turbidity readings for increased sediment reflectivity. Dissolved materials that absorb light cause lower scattered light intensity and therefore lower values of turbidity. An example of such materials is the tannins common in some swamp and estuarine environments. The effect of sediment reflectivity and dissolved materials would not be a factor for acoustic or laser sediment surrogates.

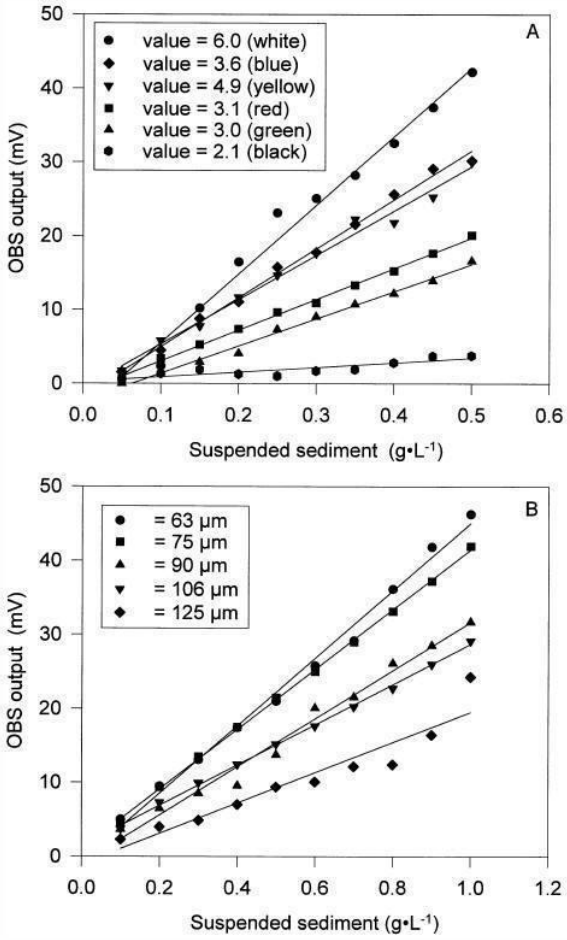


Figure 2.11- Turbidity (OBS) output versus suspended sediment concentration for various sediment colors (A) and various sediment sizes (B). The sediment grain size of the colored sediment was 90 $\mu$m (from Sutherland et al, 2000)

These sediment-water mixture properties often are assumed to be unchanging for a given site, so that a relation for turbidity to SSC can be developed and used. The effects of these factors can be further evaluated by additional analyses of sediment size and water color, as well as by residual analysis of regression results. However, these effects render any turbidity to SSC relation site specific, as with acoustic surrogates.

In addition to the effects of sediment-water mixtures on measured values for a given turbidimeter, different turbidimeters can provide different turbidity readings for the same sample (Landers, 2003; Ziegler, 2003a; Rasmussen and others, 2009). Landers (2003)

describes bench tests conducted as part of a workshop in which variances in measurements from nine different types of turbidimeters using blind reference samples were evaluated. These differences may be due to design differences relating to light wavelength, reflector measuring angle, ambient light filters, or other factors. Because of these effects, changes in the type of turbidimeters will likely produce a change in any turbidity to SSC relation that has been developed. If two sensors can be compared against identical standards, then a conversion factor may be developed to allow continuity of turbidity time series data. One additional significant limitation applies to nephelometric turbidimeters, which typically have a maximum reading of 1000 to 2000 NTUs, so that readings above this limit are censored. This censoring is particularly troublesome because it occurs at the higher concentrations where information is particularly needed. OBS turbidity sensors generally do not have a cut off or censoring level.

## 2.3 Laser-Diffraction Surrogates

Laser diffraction instruments have been used in the laboratory for several decades to measure volumetric particle concentration (*VPC*) and particle size distribution (PSD). Although PSD is highly significant to the engineering, water-quality, and ecological roles of sediment in the environment, it is rarely measured in field studies and no single method provides a complete description of the PSD (Reynolds, et al., 2010). The availability of this technology for in-situ measurement is providing high temporal and spatial resolution measurements of volumetric PSD that can significantly expand the field of environmental particle measurement and related research. The Laser In-Situ Scattering and Tranmissometry (LISST) series of instruments being developed by Sequoia Scientific, Inc. are the first such instruments to be commercially available (Agrawal and Pottsmith, 2000).

Laser diffraction instruments characterize the suspended particle size distribution by measuring the small forward scattering angles produced by laser-generated light hitting small particles in suspension. The small forward-scattering angle from a particle is essentially the same as the angle of diffraction of light passing through an aperture of the same size as the particle. The forward-scattering angles from all particles in the mixture are sensed on a 'ring detector' (figure 2.12). The scattering angles are inverted to obtain a particle size distribution and the count of angles provides the particle count in each size range. The volumetric particle concentration ($\mu$l/l) is obtained from the total count of particles for the sampled volume (Agrawal et al, 1991; Agrawal and Pottsmith, 1994, 2000).

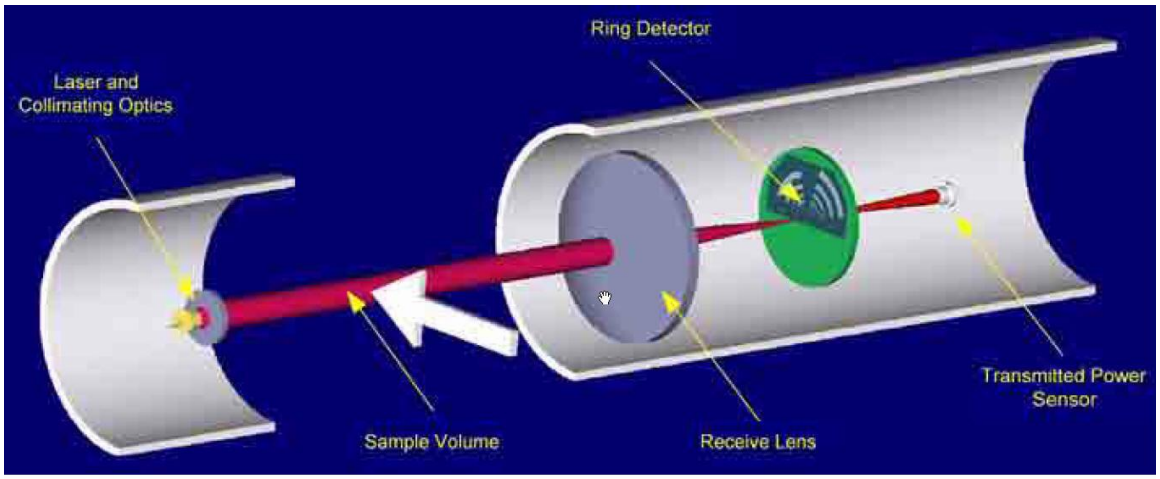

Figure 2.12 - LISST laser-diffraction measurment concept (from Sequoia Scientific, 2008)

Since field-deployable, laser-diffraction instruments became available, they have been used in several investigations in marine environments (for example: Agrawal and Pottsmith, 1994; Gartner et al, 2001, Shao, et al., 2011). Thevenot and Kraus (1993) compare SSC measured by physical samples, laser diffraction, and acoustic surrogates sampled for one day in an estuarine environment and found the acoustic surrogate had accuracy comparable to the laser diffraction for this data set. Laser-diffraction measurements have been used alongside physical SSC samples in order to validate methods using acoustic and turbidity surrogates (Holdaway et al, 1999; Lynch et al, 1994).

Studies using laser-diffraction in fluvial environments are rare. Topping et al (2004, 2006, 2007) used laser-diffraction measurements to calibrate and extend the analysis of sediment characteristics using multi-frequency acoustic surrogates and physical samples. In their research a LISST-100X was suspended by cable in a deep, strong eddy zone of the Colorado River at Phantom Ranch, Grand Canyon, AZ (USGS Station 09402500).The point location laser-diffraction readings were calibrated to cross-section averaged measurements of: median grain size, the concentration of fines (less than 63

μm), and the concentration of sand (greater than 63 μm). The resulting accuracies are 5 percent or better for load of silt and clay, load of sand, and median size.

### *2.3.1 LISST Laser-Diffraction Instruments*

Two Sequoia Scientific Inc. laser-diffraction instruments that can obtain a continuous time series of volumetric concentration and particle size distributions are the LISST-100X and the LISST-Streamside. Both these instruments measure scattered light on a 32-ring light detector from which angles are inverted to obtain a 32-size class particle size distribution. The upper and lower particle size limits vary depending on the LISST model, but are typically from 2 to 380 microns for the LISST-100 and LISST-Streamside as designed for use in fluvial environments. The typical sample path of these LISST instruments is a cylinder of 6mm diameter and 50mm length. The LISST-100 can be deployed *in situ*, while the LISST-Streamside samples water pumped from the stream. The LISST-Streamside is preferable in environments conducive to organic growth that can quickly foul the LISST-100 which does not have a mechanical wiper. The LISST-Streamside flushes the sample chamber with clean water prior to each sample to both rinse the chamber and, by measuring laser diffraction metrics for clear water, recalibrates the unit before each measurement. A recently introduced instrument, the LISST-SL, uses the LISST measurement technology in an isokinetic sampler that can be deployed from a suspension cable for stream cross section measurements with high spatial resolution (Agrawal and Pottsmith, 2006; Gray and Gartner, 2009).

Laser-diffraction measurement has the significant advantage over acoustic and turbidity surrogates that it is not affected by a size-concentration ambiguity and provides environmental, volumetric size distribution data. Also, the measurements are not affected by particle reflectivity as are turbidity measurements. Laser diffraction is

described by LISST instrument makers as a measure of sediment size and concentration rather than as a surrogate; and it has been successfully used to measure these in field environments (Melis et al, 2003). Laser diffraction instruments provide unique access to high resolution, environmental PSD data; however the technology has several limitations that must be considered.

### *2.3.2 Limitations and Assumptions of Laser-Diffraction Surrogates*

Limitations of laser-diffraction measurements of concentration and PSD include: the instrument particle size limits of detection, the effect on measured light scattering from particles outside the measurement size limits, the effects of particle shape, and the effects of sediment density in converting volumetric to mass concentration. The first three of these issues are reviewed by Andrews et al. (2011) for low oligotrophic systems. In addition to these technological limitations, the instrumentation has had operational limitations in fluvial environments.

The LISST-Streamside instrument particle size detection limits are 2 and 381 microns. The particle sizes for the midpoint of the 32 measurement bins for the LISST-Streamside used in this study are given in table 4.1. While previous studies have found that LISST instruments provide reliable PSD measurements within its measured range, sediment sizes outside the instrument limits are unmeasured. As shown in the results of this study, this is an important limitation in both *VPC* and PSD measurements from laser-diffraction analyzers for fluvial environments where large fractions of the suspended sediment often are clay sized and/or larger than medium sand sized.

The effect of particles smaller or larger than the instrument measurement limits was evaluated by Andrews et al. (2011) for a LISST-100 with measurement limits of 1.25 to

250 microns. They found that particles larger than the maximum measurement range have little impact, while particles smaller than the minimum measurement range have a notable impact on measured PSD. Particles smaller than the minimum measurement size were found to inflate the measured concentration of the smallest size bin for the LISST.

In past studies, spherical particle shapes have been assumed in the use of laser-diffraction *surrogates* of sediment characteristics, which can result in errors in measurement of natural particles (Baker and Lavelle, 1984; Traykovski et al 1999). A recent study by Agrawal et al (2008) using natural sediments developed procedures to adjust measurements assuming random-shaped particles; and these methods have been implemented in the LISST processing software.

Laser-diffraction instruments measure volumetric particle concentration (*VPC*), while SSC in fluvial environments has historically been measured as mass concentration by gravimetric analysis. In most applications mass SSC data are needed for characterization of impacts from sediment load. In many environments the majority of sediment is silica based and *VPC* can be converted to SSC using a specific gravity of about 2.65. However, studies in marine environments have found highly variable particle densities (for example Braithwaite et al., 2010) and few studies have evaluated particle density variation over the PSD in fluvial systems. Flocculation of fine particles can affect both the size analysis and the conversion to mass concentration. If the LISST measures a floc as a particle, then the specific gravity of the floc (a bulk specific gravity) will be much less than that of the composite particles.

Several investigators have found significant operational problems using laser-diffraction devices (personal communication, USGS personnel in GA, ID, FL, IN). The LISST-100X

instrument is extremely sensitive to fouling or scratching of the sensor window and may require thorough weekly or daily cleaning in organically productive environments typical of many streams of the USA in summer. The LISST-Streamside is designed to overcome this problem; but this author had to work with the manufacturer to obtain updated firmware to flush the sample chamber before *and* after each sample, and perform thorough weekly cleanings to maintain reliable operation of the unit.

In this study the LISST measured *VPC* is used as a surrogate which is calibrated to SSC using concurrent measurements. Thus limitations due to unmeasured sediment sizes and unknown sediment density can be accounted for in the SSC to *VPC* calibration curve, so long as these characteristics do not change significantly over the event. Previous studies (as summarized in Gary and Gartner, 2009; Andrews et al., 2011) have shown that laser-diffraction based PSD data are reliable within the measurable particle size limits of the instrument. This study has shown these PSD data to be extremely valuable for interpreting sediment transport characteristics and the surrogate metrics in this study as discussed further in the results for this study. It is essential to know and assess the limitations and assumptions of any surrogate metric of SSC; but those limitations need not prevent the data from being highly valuable.

# 3 Hypothesis and Questions

The fundamental hypothesis of this research is that fluvial suspended sediment characteristics may be determined by high-resolution, surrogate metrics of multi-frequency acoustic, optical turbidity, and laser-diffraction characteristics with greater accuracy and resolution than traditional methods that are based on streamflow alone; and that some metrics will be more accurate and informative sediment surrogates than others. More specifically, it is hypothesized that if acoustic attenuation is driven by both viscous losses associated with fine sediments and scattering losses associated with coarser fractions, and if the total acoustic attenuation is measured, then the representative size of these finer and coarser fractions may be estimated using an optimization procedure that minimizes the difference between the measured and computed acoustic attenuation.

Some of the key questions associated with the hypothesis are:

- Can estimates of fine and coarse sediment sizes, associated with viscous and scattering attenuation, be estimated using optimization of the hybrid Urick-Sheng-Hay acoustic attenuation equation when SSC is known; or ratios of the Urick-Sheng-Hay equation for two frequencies when SSC is unknown?
- Do the methods proposed by Topping et al. (2007) to empirically determine acoustic attenuation apply for a stream of the southeastern USA, and how should the methodology be specifically applied?
- Are some surrogates more accurate or more reliable for higher or lower total sediment concentrations, and for different particle size distributions?
- What are the effects of different acoustic frequencies or frequency ratios in the use of acoustic surrogates?

- What are the operational and maintenance aspects of using these surrogate technologies?

The hypothesis and these questions will be tested in this research plan, following the experimental approach and analytical methods described.

# 4 Experimental Approach

## 4.1 Site Selection

Selection of a river or stream location for conducting the experiments for this research involved setting selection criteria, reviewing records, and visiting potential sites. Selection criteria for potential sites included: existing USGS stream gaging stations, driving distance from Metropolitan Atlanta area, adequate depth for instrument deployment, adequate mixing for point to cross-section calibration of measurements, safe sampling conditions, and ideally an ongoing sampling program to supplement data collection. Some 28 USGS-operated monitoring stations in Metropolitan Atlanta were reviewed and several sites were visited to select a good site for sediment surrogate experiments.

The selected site, Yellow River at Gees Mill Road, near Milstead, GA ( USGS station number 02207335) is located at latitude 33$^{o}$40'01", longitude 83$^{o}$56'17" (North American Datum of 1983), in Rockdale County, Hydrologic Unit code 03070103 within the Georgia International Horse Park (figures 4.1, 4.2). The gage was installed in November 2001 and elevations are referenced to a local gage datum only.

Yellow River at Gees Mill has a 260 square mile watershed that originates in northeast metropolitan Atlanta, Georgia on the Eastern Continental Divide and drains south-southeast within the Ocmulgee River Basin. The watershed has a population of about one-half million people and developing urban land use with about 16 percent impervious surfaces in 2000, based on the National Land Cover Dataset (MLRC, 2001). Principal land uses in 2009 were residential (56%), commercial and industrial (15%), and forest (14%), with only 2 % in agriculture (ARC Landpro 2009). The gage is located about 30 miles east of Georgia Tech at the location of an old mill.

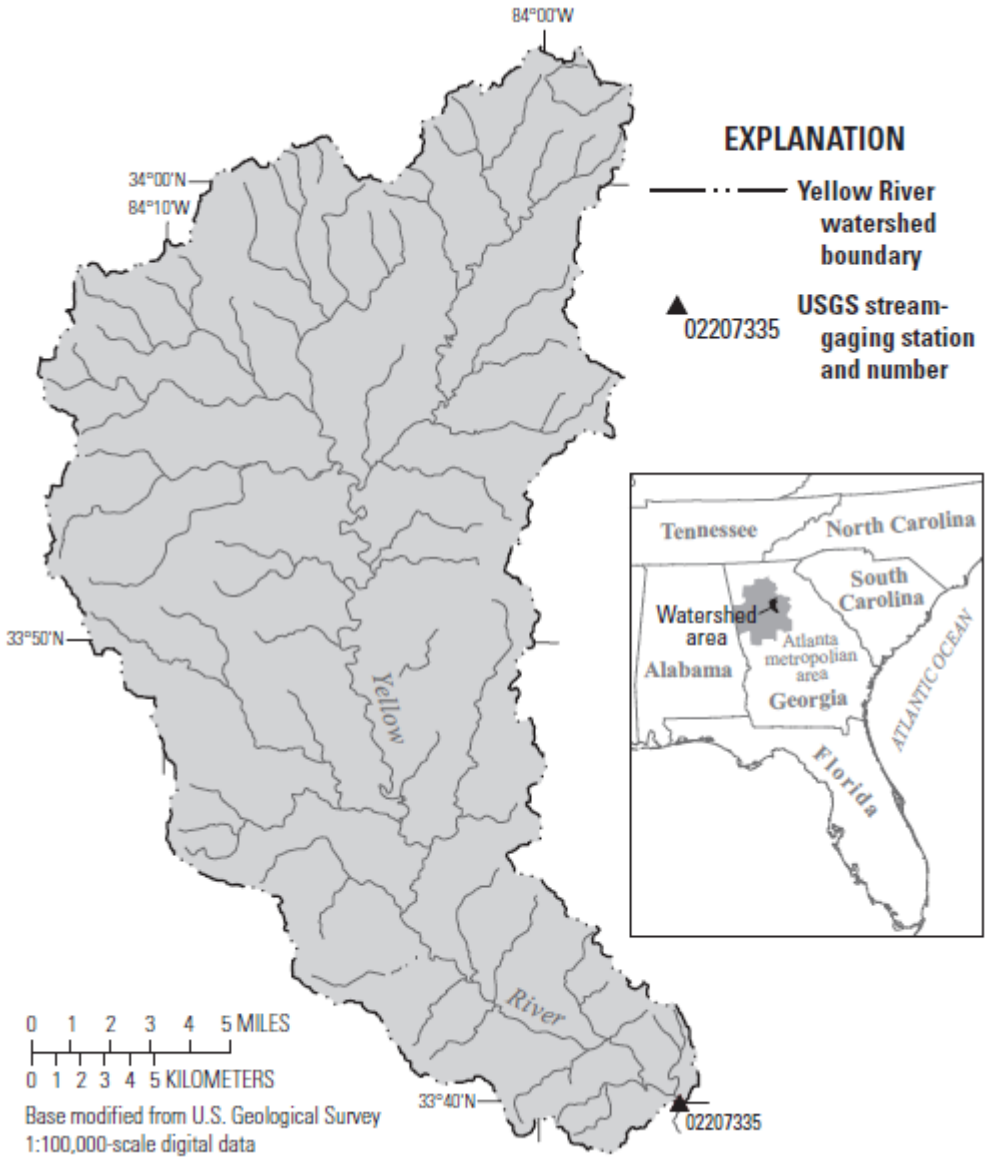


Figure 4.1—Yellow River watershed above Gees Mill Road in northeast metropolitan Atlanta, Georgia (watershed area is 260 square miles)


Figure 4.2a—Aerial view of Yellow River at Gees Mill Road

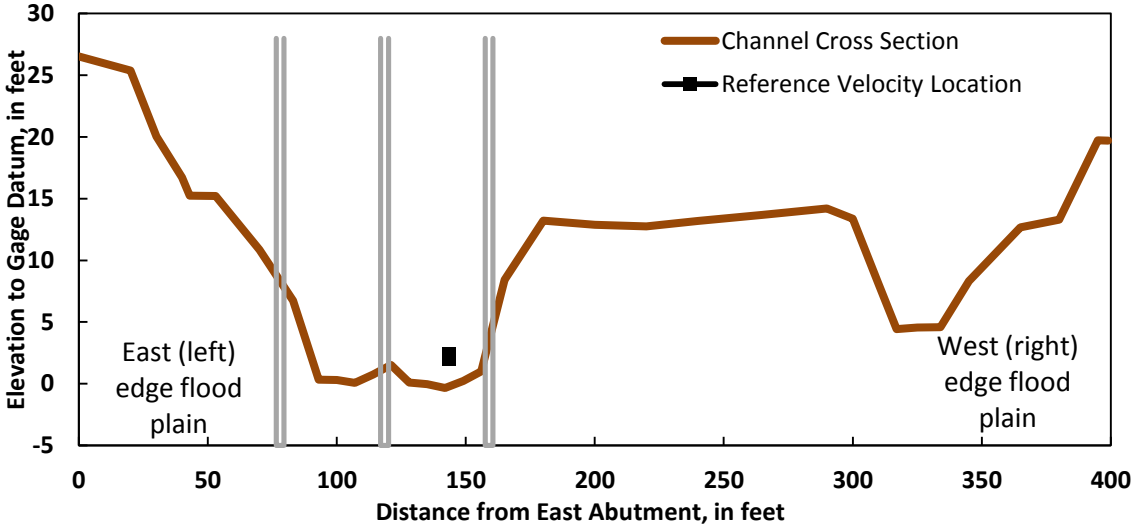


Figure 4.2b-- Yellow River at Gees Mill Road (02207335) Cross section at downstream side of bridge

The cross section at the downstream side of the bridge is plotted in figure 4.2b. The dug mill raceway channel for the old Gees Mill is evident on the west edge of the floodplain. Flow enters this raceway channel about 325 feet upstream from the bridge where the main channel is bending eastward, effectively cutting across a natural meander bend. It reenters the main channel about 250 feet below the bridge. Flow in the mill raceway begins at a stream stage of about 4.5 feet. As shown in the data summary, concentrations of SSC in the mill channel are not significantly different from those at the edges of the main channel. Measurements for streamflow discharge and $SSC_{xs}$ always include the mill channel when it is flowing, and for practical purposes it is encompassed in discussion of main channel flow and sediment transport.

After this research project began, this watershed experienced extreme flooding that crested in September 24, 2009 at a stage of 22.54 feet and a discharge of 20,800 cfs. The annual exceedence probability of this event was about 0.5 percent (200-year flood). During this event, which overtopped the roadway just west of the bridge, discharge was measured near the peak, but sediment samples were not collected. Fortunately, the water-quality sonde and the laser-diffraction analyzer had been removed for servicing; otherwise they would have been lost along with the ISCO sampler, shelter, and the cabling and intake tubing for the water-quality sonde and laser-diffraction analyzer; as the anchors were damaged and the shelter was lost. Purchasing and re-establishing the shelter, pump tubing, and control cables for the pumping sampler and laser-diffraction analyzer required several months which delayed the data collection between the first and second sampling period for this research.

The stage-discharge relation at this cross section is well established by the USGS, and verification measurements are made about every 6 weeks. The controls for the stage-discharge relation are: 1) an exposed rock ledge downstream of the bridge during low

flows; 2) the main channel shape and roughness during medium flows, and; 3) the main channel plus flood plain shape and roughness during high flows. The low-flow control was damaged at the east edge of the channel during the September 2009 flood, which was measured for streamflow but was not sampled for this study. Several subsequent discharge measurements reestablished the shifted stage-discharge curve for low flow.


Figure 4.2c – Upstream east (left) edge channel from bridge during September 2009 flood on Yellow River at Gees Mill Road

Exposed granite forms the eastern bank providing a good deployment area for instrumentation 100 feet upstream of the downstream side of the bridge (figures 4.2 and 4.3). The stage sensor, multi-parameter water-quality sonde, and fixed-point sampler intakes were anchored about 0.5 feet above this rock shelf, about 3 feet below the low-water stage. Pipes were anchored to the granite bedrock to convey to the gage shelter the sensor cable, bubbler pressure line for stage measurement, the pump intake lines for the fixed-point sampler and for the laser-diffraction analyzer. Stage, discharge (by a stage-discharge rating), precipitation, turbidity, temperature, and conductance are continuously monitored, with 15-minute measurement intervals. Data are transferred hourly via satellite to publically-accessible USGS databases.

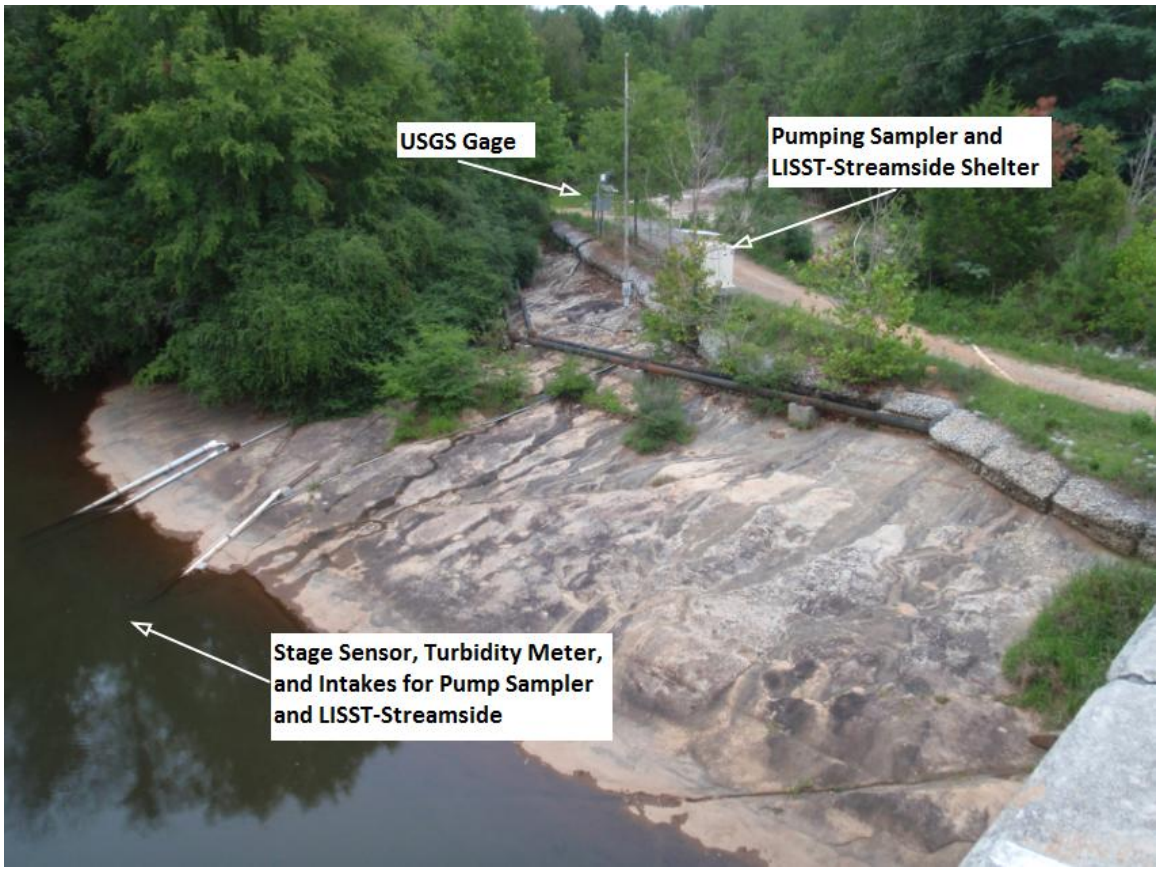


Figure 4.3 – Upstream east (left) edge channel from bridge and locations of instruments and shelters for stage, turbidity, laser-diffraction (LISST), and pump sampler

## 4.2 Instruments and Field Methods

### *4.2.1 Physical Sediment Samplers*

Physical sediment samples were collected from the fixed-point pumping sediment sampler as well as from depth and width integrated samplers deployed from the bridge using methods described by Edwards and Glysson (1999), Nolan et al. (2005) and Gray et al. (2008). The Equal-Width-Increment (EWI) sampling method uses an isokinetic sampler (see figure 4.4) that integrates a sample proportionally by velocity and area and results in a discharge-weighted sample representative of the suspended material in transport through the cross section at the time of sample collection. Ten to 12 vertical locations across the cross section were sampled for each EWI measurement, including at least one vertical in the mill channel when flowing. Samples from individual verticals were analyzed separately for many of the EWI measurements to evaluate concentration changes across the section; while verticals from other EWI samples were composited for a single analysis, often including full PSD analysis. Where individual samples were analyzed separately, a volume weighted concentration was computed for the EWI.

The isokinetic depth-integrating sampler selected for this study is a US DH-95 sampler (Serial Number 12401) which was developed by the Federal Interagency Sedimentation Program (FISP; Davis, 1995). The US DH-95 weighs 29 pounds and holds a 1-liter polypropylene bottle to which a nozzle and cap assembly is screwed (figure 4.4). A 5/16 inch nozzle was used throughout the study; though the nozzle was replace several times whenever it was scuffed on the bridge hand rail. All sample bottles were labeled with the site number, cross section station, date, time, bottle number, and sampler initials; and this information also was recorded on the field sample sheet.

Figure 4.4 - D-95 isokinetic depth-integrating water-quality sampler

In addition to the fixed-point and cross section integrated EWI samples, depth-integrated samples were collected also at single verticals located at either station 144.3 or 137 (see figure 4.2b for station locations). These single verticals supplement the EWI samples and often were large volume (8 to 12 liters) so that full particle size analyses could be performed. The relation between concentrations from the cross section integrated EWI samples and single vertical samples was established for each event with very good fit, so that single vertical samples could be used to supplement the EWI data set. Of the 33 concurrent samples, 9 of the EWI concentrations were estimated from single verticals.

The ideal measuring section is one without any obstructions, such as bridge piers, and with a very long straight reach approaching the measurement section. The stream is straight for about 170 feet upstream from the bridge, but flow velocities are somewhat higher on the west side of the channel. Samples were collected from the downstream side of the bridge (as is often done) to minimize hazards of the sample hitting or getting caught in the bridge piers; or being struck by debris. However, the downstream section may have turbulence due to the piers that affects the velocity and sediment distribution.

Fixed-point sediment samples were collected using a pumping sampler located 100 feet upstream from the downstream side of the bridge on the east bank. The intake for the sample tubing is shown in figure 4.3. An ISCO (Teledyne ISCO, Inc.) Model 6712 programmable sampler was used. This instrument pumps samples from the stream through a 3/8 inch inside diameter tubing using a peristaltic pump. The unit was set up with 24 1-liter bottles and programmed to sample hourly or every other hour, depending on the projected storm duration. The pump was calibrated to collect between 750ml and 900ml for each sample. The sample tubing also can be diverted to discharge into a separate container for large volume samples as needed for particle size analysis (figure 4.5). The sampler and housing were destroyed during the September 2009 flood, and replaced with a near-identical (non-refrigerated) sampler. After each event, sample bottles were pulled and labeled, and the programmed sample times were verified against the times stored in the ISCO. This sampler performed very well throughout the study.

Figure 4.5—Fixed-point ISCO pumping sampler and shelter

### *4.2.2 Turbidity Meter*

The turbidity meters used in this research are nephelometric meters manufactured by Yellow Springs Incorporated (YSI). A model YSI 6136 turbidity meter, serial number 08G100269, shown previously in figure 2.8A, was used in conjunction with YSI 6920 multi-parameter water quality sonde (figure 4.8). The YSI 6136 conforms to the ISO Method 7027 and ASTM D-7315 measurement standards. The light source has a wavelength of 860 ± 30 nanometers (nm) with a single detector oriented at 90 degrees from the incident light path. A YSI 6920 with YSI 6136 was deployed in situ on the east stream bank at the location of the stage sensor and sample intake lines (figure 4.3). The sonde was deployed in a PVC pipe with a 'cage' at the stream end to permit water measurement and to minimize fouling by debris. The in situ sonde was calibrated against commercially provided turbidity standards, using a two point calibration at zero and 1000 NTU standards. After installation, the in situ sonde was pulled from the stream, cleaned, and checked against standards after each sampled flood event and at regular

Figure 4.6—Multi-parameter water-quality sensor (YSI 6920) including turbidity, and DH-95 sediment sampler

intervals from one to four weeks depending on conditions. (Warmer weather promotes biological growth which requires more frequent cleaning.) A second, identical YSI model was used as the *field sonde* (figure 4.8). As part of the quality assurance process, the field sonde was used to obtain concurrent measurements of the stream at the fixed location of the *in situ* sonde when the *in situ* sonde was cleaned and checked. The *in situ* sonde was recalibrated if its readings varied from the calibration standard by more than ±5 percent. The field sonde also was used to obtain turbidity readings across the stream cross section at the locations of EWI verticals for selected events.

### *4.2.3 Laser-Diffraction Analyzer*

The laser-diffraction instrument used in this study is a LISST-Streamside, serial number 3022, which uses the principles described previously to obtain continuous measurements of volumetric particle concentration (*VPC*) and particle size distribution (PSD). The PSD is measured in 32 logarithmically spaced size classes with the upper size in each class equal to 1.1809 times the next lower size class. The mid-point for the 32 size classes for the list is shown in Table 4.1.

Table 4.1 - Mid-point of 32 particle size classes, in µm, measured by LISST-Streamside

| | | | | | | | |
|---|---|---|---|---|---|---|---|
| 2.06 | 2.43 | 2.87 | 3.39 | 4.01 | 4.73 | 5.59 | 6.60 |
| 7.79 | 9.20 | 10.86 | 12.83 | 15.15 | 17.89 | 21.12 | 24.95 |
| 29.46 | 34.79 | 41.08 | 48.51 | 57.29 | 67.65 | 79.89 | 94.34 |
| 111.41 | 131.56 | 155.36 | 183.47 | 216.66 | 255.85 | 302.13 | 356.79 |

A submersible pump carries stream water to the LISST-Streamside where it measures the water sample while it is being pumped through the sample chamber. The unit can obtain a 600 measurement average reading in 15 seconds, and can sample at any interval from 1 minute or longer. Figure 4.10 shows the instrument LISST-Streamside in the instrument shelter initially designed for it in this investigation. The 20-gallon capacity

cylindrical tank provided about 8 to 14 days of clean water for instrument flushing and background measurement using the settings selected for this study.

The LISST-Streamside has a RS-232 data cable by which it can be programmed and downloaded. The unit can also be programmed using a touch screen interface. For each deployment, the unit records one binary file for the background measurements and one for the river water measurement. The unit also records an ASCII file of processed size and concentration data, and a system configuration text file.


Figure 4.7—LISST-Streamside laser-diffraction analyzer, clean water tank, and instrument shelter

Operation and maintenance of the LISST-Streamside may present challenges and limit data quality. In this study the firmware for the unit initially allowed only for a pre-sample rinse of clean water; however this meant that stream water stayed in the chamber between samples which caused rapid fouling. At the author's request, the firmware was upgraded so that pre- and post-flushing could be programmed. A detailed cleaning procedure was established for the unit which prevented fouling.

After extensive testing in the spring and summer of 2009, programmable sampling parameters for the LISST-Streamside were set as follows:

- Measurement Interval: One (usually) or two hours depending on storm duration
- Sample Duration: 120 seconds in which 4677 measurements are averaged
- River Pump Pre-Flush Duration: 270 seconds
- Clean Water Background Measurement: before every sample
- Post-Sample Clean Water Flush Duration: 30 seconds (clean water remains in the sample chamber until the next sample)
- Pre-Sample Clean Water Flush Duration: zero seconds

During testing of the LISST-Streamside during the summer of 2009, the data indicated significant errors with a diurnal pattern, associated with very high daytime temperatures. The manufacturer determined this was because of flow issues due to differences in the temperature of the sample chamber and the stream water. Longer sample pre-pump periods were established, and the instrument shelter was painted white, given a shade cover, and installed with a high-volume cooling fan. After the first fully sampled event in August 2009, the unit was sent back to Sequoia Scientific and the temperature issues were resolved by modifying the plumbing inside the instrument.

### *4.2.4 Acoustic Doppler Current Profilers*

Three acoustic doppler current profilers (ADCPs) were used in this research. All have two primary beams and are designed for fixed-location deployment for channel velocity measurement, primarily for use in computing streamflow discharge. Two are manufactured by Sontek, Incorporated and are a 1.5 MHz Sontek Argonaut SL, serial number E408 (figure 4.6B) and a 3.0 MHz Sontek Argonaut SW, serial number T597 (figure 4.6C).


Figure 4.8—Acoustic doppler current profilers: (A) 1.2 MHz RDI, (B) 1.5MHz Sontek, (C) 3.0MHz Sontek

Figure 4.9—Acoustic doppler current profilers mounted on downstream bridge pier at west edge of main channel

The third unit is manufactured by Teledyne RD Instruments (RDI) and is a 1.2 MHz RDI Channel Master, serial number 7199 (figure 4.6A). They were mounted on a high-density plastic board as shown in figure 4.6, and attached to the downstream side of the downstream bridge pier located on the west bank of the Yellow River at Gees Mill Road using pipe connection fittings and concrete anchors. The units were mounted perpendicular to the flow, in line with the pier face, about 1 to 2 feet above the bed at the channel edge and 0.3 to 2.0 feet below the water surface at variable low-flow conditions (figures 4.7 and 4.8). The centerline of the horizontal beams is a 2.20 feet, gage datum. The sensor cables were run up the pier to an instrument shelter bolted to the bridge handrail which also contains a battery and solar panel.

Table 4.2 – Operational characteristics of the ADCPs used in this study

| ADCP description | Maximum number of cells | Minimum Cell Size (cm) | Beam Angle | Reported Velocity Accuracy |
|---|---|---|---|---|
| Sontek/YSI 1.5MHz | 10 | 40 | 25 | 0.5% |
| Sontek/YSI 3.0MHz | 10 | 20 | 45 | 1% |
| RDI 1.2MHz | 128 | 10 | 20 | 1% |

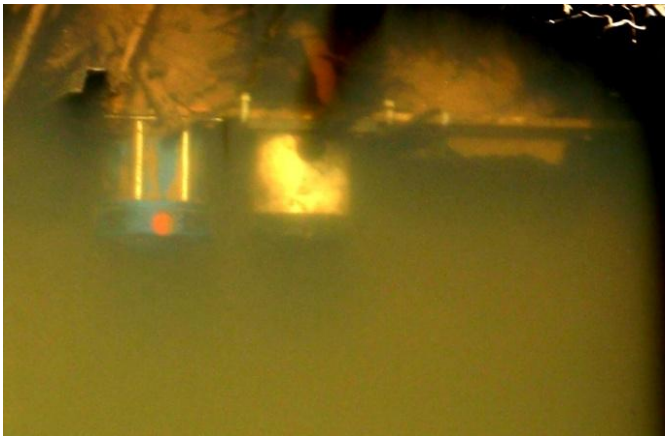

Figure 4.10 – Submerged side-looking acoustic doppler current profilers on downstream, west pier

Selected operational characteristics of the ADCPs are noted in table 4.2. The maximum range for the 3.0MHz unit is limited by the attenuation of this high frequency signal, and was usually less than 10 feet. Beyond this distance, the signal-to-noise ratios became too high for meaningful data. The maximum range of the 1.2MHz and 3.0MHz units was limited by interference with the center bridge pier or the channel bed. The cell size and blanking distance were programmed for each ADCP to optimize the ability of the instruments to indicate sediment backscatter and attenuation. The blanking distance is the unmeasured zone between the transducer face and the beginning of the first measurement cell. Readings from the acoustic meters were carefully evaluated to select appropriate blanking distance, cell sizes, and maximum range for the measurements and to check for any boundary interference in any of the beams. Adjustments were made to all three meters after the August 2009 event and to the 3.0MHz unit after the March 2010 measurements; then the settings were held constant. These settings are shown in table 4.3 to 4.5 and in figure 4.9.

Prior to each event, each ADCP was checked for operation and its program was reviewed. All three meters were programmed to record a 120 second average velocity measurement every 15 minutes. The measurement initiation time for each meter was offset by 5 minutes to eliminate any potential problems with acoustic interference between the meters. The ‘concurrent’ acoustic measurements were thus offset by at most 10 minutes. The acoustic backscatter amplitude and acoustic attenuation was converted to decibels (dB) for all units. The RDI 1.2MHz unit operates in broadband mode in default setting; and was set to operate in narrowband mode in order to facilitate data comparisons with the Sontek/YSI units. This setting of the RDI 1.2 MHz unit was done after the first, August 2009 event. The setting does not affect the measured velocities, but does affect the measured backscatter and attenuation. After each event, the data from each unit was downloaded and reviewed.

Table 4.3 Settings for ADCPs for event of August 28 to September 2, 2009. Distances are in meters from face of transducer to centers of cells.

| | 1.2MHz RDI | 1.5MHz Sontek | 3.0 MHz Sontek |
|---|---|---|---|
| Blank (m) | 0.26 | 0.5 | 0.2 |
| Cell Size (m) | 0.1 | 0.4 | 0.2 |
| No. of Cells | 16 | 10 | 10 |
| End Last Cell | 1.86 | 4.5 | 2.2 |
| Cell No. | 1.2MHz Cell Center | 1.5MHz Cell Center | 3.0MHz Cell Center |
| 1 | 0.31 | 0.7 | 0.3 |
| 2 | 0.41 | 1.1 | 0.5 |
| 3 | 0.51 | 1.5 | 0.7 |
| 4 | 0.61 | 1.9 | 0.9 |
| 5 | 0.71 | 2.3 | 1.1 |
| 6 | 0.81 | 2.7 | 1.3 |
| 7 | 0.91 | 3.1 | 1.5 |
| 8 | 1.01 | 3.5 | 1.7 |
| 9 | 1.11 | 3.9 | 1.9 |
| 10 | 1.21 | 4.3 | 2.1 |
| 11 | 1.31 | | |
| … | … | | |
| 15 | 1.71 | | |
| 16 | 1.81 | | |

Table 4.4 Settings for ADCPs for event of March 10–16, 2010. Distances are in meters from face of transducer.

| | 1.2MHz RDI | 1.5MHz Sontek | 3.0 MHz Sontek |
|---|---|---|---|
| Blank (m) | 1.16 | 1.0 | 0.9 |
| Cell Size (m) | 0.2 | 0.5 | 0.2 |
| No. of Cells | 20 | 10 | 10 |
| End Last Cell | 5.16 | 6.0 | 2.9 |
| Cell No. | 1.2MHz Cell Center | 1.5MHz Cell Center | 3.0MHz Cell Center |
| 1 | 1.26 | 1.25 | 1 |
| 2 | 1.46 | 1.75 | 1.2 |
| 3 | 1.66 | 2.25 | 1.4 |
| 4 | 1.86 | 2.75 | 1.6 |
| 5 | 2.06 | 3.25 | 1.8 |
| 6 | 2.26 | 3.75 | 2 |
| 7 | 2.46 | 4.25 | 2.2 |
| 8 | 2.66 | 4.75 | 2.4 |
| 9 | 2.86 | 5.25 | 2.6 |
| 10 | 3.06 | 5.75 | 2.8 |
| 11 | 3.26 | | |
| … | … | | |
| 19 | 4.86 | | |
| 20 | 5.06 | | |

Table 4.5 Settings for ADCPs for events of April, May, and September, 2010. Distances are in meters from face of transducer.

| | 1.2MHz RDI | 1.5MHz Sontek | 3.0 MHz Sontek |
|---|---|---|---|
| Blank (m) | 1.16 | 1.0 | 1.0 |
| Cell Size (m) | 0.2 | 0.5 | 0.4 |
| No. of Cells | 25 | 10 | 10 |
| End Last Cell | 6.16 | 6.0 | 5.0 |
| Cell No. | 1.2MHz Cell Center | 1.5MHz Cell Center | 3.0MHz Cell Center |
| 1 | 1.26 | 1.25 | 1.2 |
| 2 | 1.46 | 1.75 | 1.6 |
| 3 | 1.66 | 2.25 | 2.0 |
| 4 | 1.86 | 2.75 | 2.4 |
| 5 | 2.06 | 3.25 | 2.8 |
| 6 | 2.26 | 3.75 | 3.2 |
| 7 | 2.46 | 4.25 | 3.6 |
| 8 | 2.66 | 4.75 | 4.0 |
| 9 | 2.86 | 5.25 | 4.4 |
| 10 | 3.06 | 5.75 | 4.8 |
| 11 | 3.26 | | |
| … | … | | |
| 24 | 5.86 | | |
| 25 | 6.06 | | |

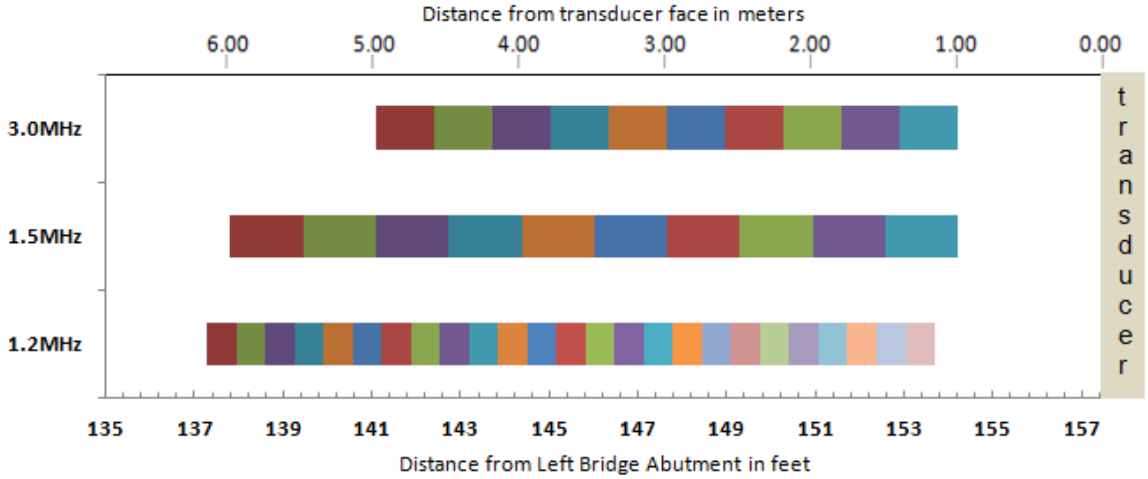


Figure 4.11 – Locations of acoustic profile cells, in feet from left abutment, and meters from transducer faces; configuration for events of April, May, and September 2010. Face of transducer is at station 157.5 feet. Stationing decreases with distance from transducer.

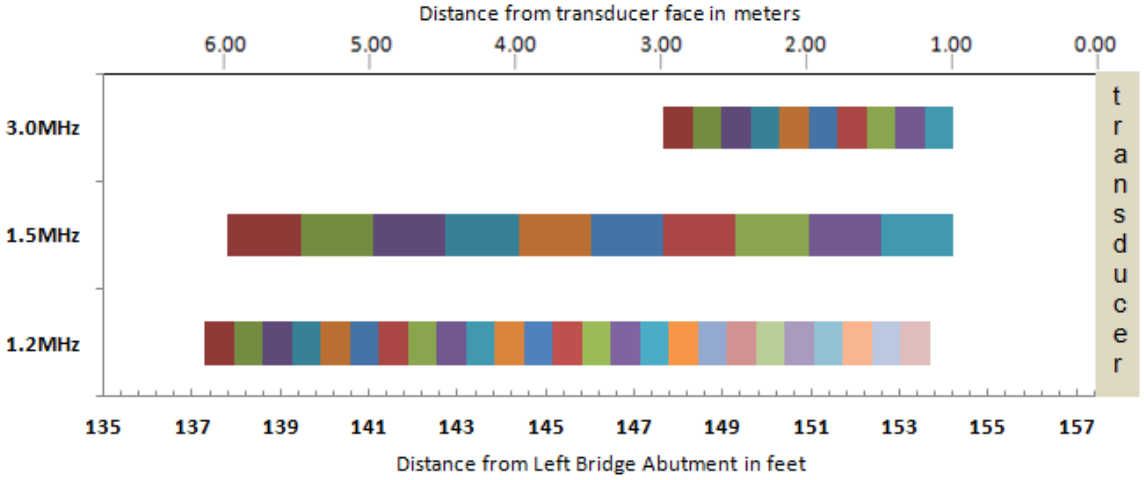


Figure 4.12 – Locations of acoustic profile cells, in feet from left abutment, and meters from transducer faces; configuration for event of March 2010. Face of transducer is at station 157.5 feet. Stationing decreases with distance from transducer.

## 4.3 Sample Processing and Analysis

Sediment samples were collected, labeled, and transported to the USGS Georgia Water Science center sediment laboratory for analysis. Labels were placed on every sample bottle denoting site number, sample number, sample date and time, sample method (EWI or point), sample location along the cross section (for EWI samples), and initials of sampling party. This information was repeated on a field sheet for each EWI sample group and each carrousel of fixed-location samples. Additional data on stream stage, temperature, environmental conditions, sampler identification numbers, and any associated concurrent data, such as turbidity measurements, were recorded on the field sheet. Information from each sample was summarized in a spreadsheet that was included with the samples as they were delivered to the sediment laboratory. Each sample was analyzed for total SSC as well as the percent of SSC less than 63 microns (percent fines). One or two large volume samples were collected for each event and sent to a USGS laboratory for full particle size distribution analysis. Data returned from the laboratories was stored in the project data base, described further below.

## 4.4 Data Management

This research project produced voluminous quantities of raw data and computed results. The concurrent SSC and averaged 1- and 2-hour data for each surrogate used for this study, as well as supporting data and computed values are included in the tables within this thesis. All of analyses from fixed point and cross section EWI SSC samples are listed in the thesis and stored in the USGS National Water Information System (NWIS), data base available via the NWIS web at http://waterdata.usgs.gov for the station 02207335, Yellow River at Gees Mill Road near Milford, Ga. The 15-minute interval

stage, discharge, and precipitation data also are stored in the permanent NWIS database, with daily values available via the NWIS web and 15-minute data available by request. The 15-minute turbidity, specific conductance, and temperature data also are stored in the permanent NWIS data base and are available on request.

The acoustic metric data were retrieved from the instruments in their native binary format and stored in the permanent project files. The binary files were processed using the ADCP manufactures' software to obtain ASCI-format files which were imported to Microsoft Excel ® and thence imported to statistical and graphical software for further analyses. The laser-diffraction binary data files and calibration files were downloaded from the LISST-Streamside and stored in the permanent project files. The laser-diffraction files were processed using MATLAB® codes developed by this author and by Sequoia Scientific, Inc. All of the project files are permanently backed up and stored on the USGS computer system.

# 5 Summary of Results

Comprehensive, concurrent hydrologic, sediment, and multi-parameter surrogate measurements were obtained at Yellow River at Gees Mill Road near Atlanta, Georgia for five storm events that began in August 2009, and March, April, May, and September 2010. The sediment and surrogate metric data were collected specifically for this thesis and are the basis for the evaluations and comparisons of fluvial suspended sediment characteristics by high-resolution, surrogate metrics.

## 5.1 Hydrologic and Velocity Data Summary

### *5.1.1 Hydrologic Data Summary*

The hydrologic and velocity characteristics of the five measured storms are summarized in table 5.1 and figures 5.1 to 5.13. Two storms were measured in the fall of 2009 and 2010, and three in the spring and summer of 2010. The events cover the range of typical annual storm events, as per the experimental plan and as indicated in figure 5.1b. The minimum event, which began on September 27, 2010, rose only 1.6 feet above seasonal baseflow and peaked at 368 cubic feet per second (cfs). The maximum event began on May 3, 2010, and rose 9.4 feet above seasonal baseflow to approximately bank full stage, at a discharge of 5070 cfs (figures 5.8-9, and 5.12-13). This event had an annual exceedence probability of about 50-percent based on flood-frequency relations for long-term upstream and downstream gages.

Streamflow discharge is determined from 15-minute stream stage measurements and the stage-discharge relation at this cross section. This stage-discharge relation is well established by the USGS, and verification measurements are made about every 6 weeks. The controls for the stage-discharge relation, as described previously in chapter

4 of this thesis are: 1) an exposed rock ledge downstream of the bridge during low flows; 2) the main channel shape and roughness during medium flows, and; 3) the main channel plus flood plain shape and roughness during high flows. The stage-discharge relation for Yellow River at Gees Mill Road is shown in figure 5.1a. Discharge data are essential for understanding watershed sediment transport processes and for computation of sediment flux and sediment load.

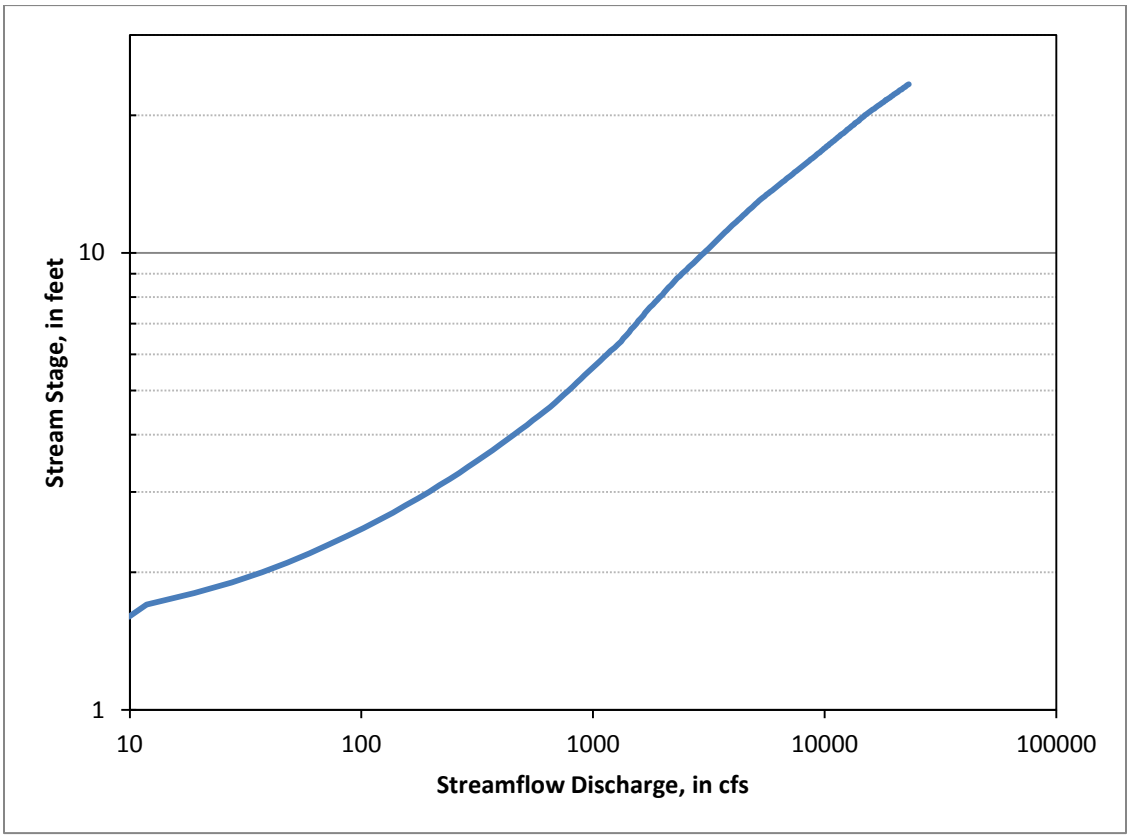


Figure 5.1a—Stage to Discharge rating curve for Yellow River at Gees Mill Road (station number 02207335)

Precipitation was measured at the stream gage and is an inconsistent indicator of the total precipitation over the 260 square mile watershed, depending on the spatial uniformity of the precipitation. For example, the May 3—6, 2010 event apparently had much larger rainfall in the upper basin, as indicated by the magnitude and atypical, lagging-peak shape of the hydrograph (figure 5.9). The total runoff is an indicator of the watershed precipitation, the dry antecedent conditions, and the seasonal variation in evapotranspiration. The approximate number of prior days since runoff producing rainfall, also shown in table 5.1, can indicate hydrologic conditions and the supply of sediment recently stored in the channel and immediately available for suspension and transport.

The index or reference velocity location was taken as cell 7 of the 1.5MHz system, which is at or near the channel thalweg. Cell 7 is 1.31 feet long, centered at station 143.6, at gage elevation 2.20, about 2.34 feet above the channel bed at this location on March 10, 2010 (figure 5.1). Average and maximum velocity at station 143.6 (cell 7 of the 1.5MHz ADCP) for each event are shown in table 5.1.

Table 5.1 -- Summary of hydrologic and reference velocity characteristics of measured storms

| Event Begin Date | 8/28/2009 | 3/10/2010 | 4/24/2010 | 5/3/2010 | 9/27/2010 |
|---|---|---|---|---|---|
| Start and End Time, Month/Day | 01:00 08/28<br>12:00 09/02 | 13:00 03/10<br>13:00 03/15 | 14:00 04/24<br>04:00 04/27 | 04:00 05/03<br>00:00 05/06 | 14:00 09/27<br>12:00 10/01 |
| Peak Flow, cfs | 1800 | 2640 | 1270 | 5070 | 368 |
| Peak Stage, feet | 8.56 | 9.36 | 6.43 | 12.85 | 3.89 |
| Total Precipitation, inches | 2.67 | 2.33 | 1.49 | 2.23 | 2.18 |
| Total Runoff, inches | 0.58 | 0.86 | 0.26 | 1.16 | 0.15 |
| Event Duration, days | 5.5 | 4.0 | 2.6 | 2.8 | 3.9 |
| Prior Dry Days | 23 | 5 | 14 | 7 | 14 |
| Average Reference Velocity, ft/s | -- | 3.78 | 3.24 | 4.03 | 2.44 |
| Peak Reference Velocity, ft/s | -- | 4.52 | 4.11 | 5.20 | 3.22 |
| Average Water Temperature C° | 22.90 | 11.10 | 18.80 | 21.20 | 21.20 |

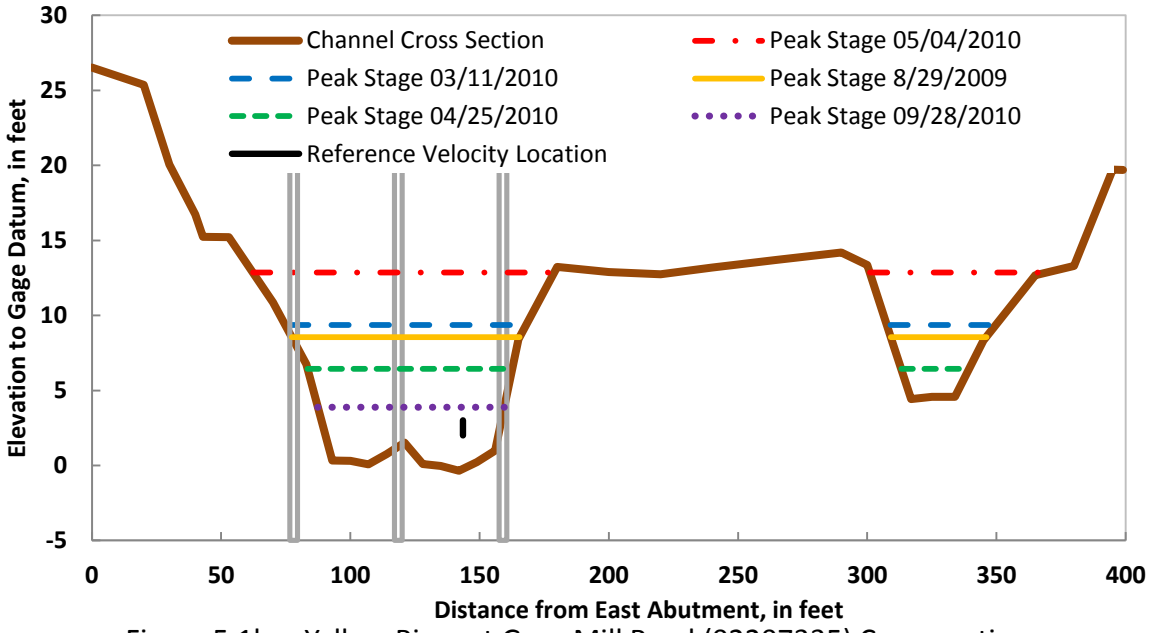


Figure 5.1b -- Yellow River at Gees Mill Road (02207335) Cross section at downstream side of bridge

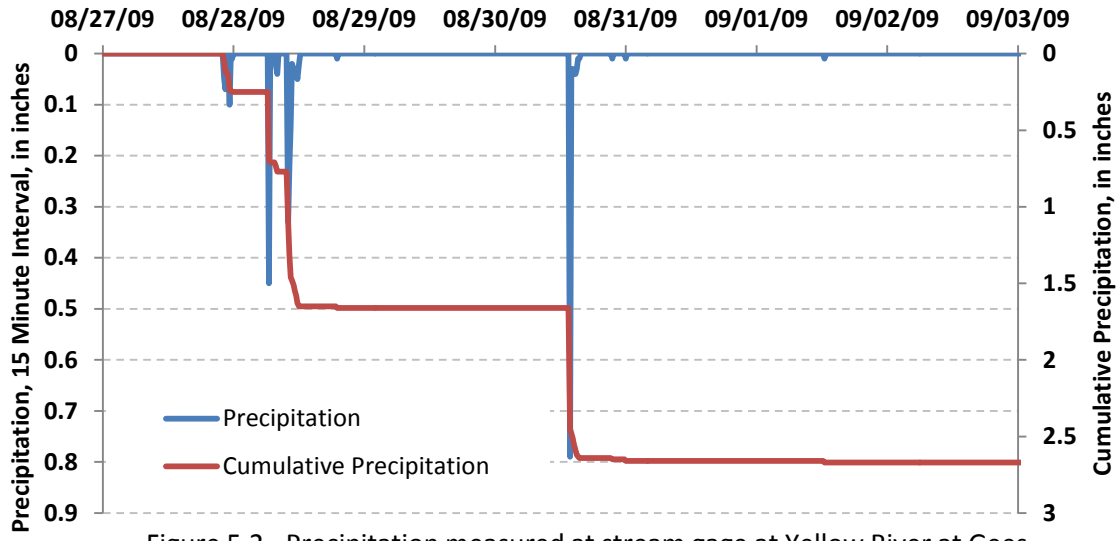


Figure 5.2 - Precipitation measured at stream gage at Yellow River at Gees Mill Road (02207335) from August 28–September 2, 2009

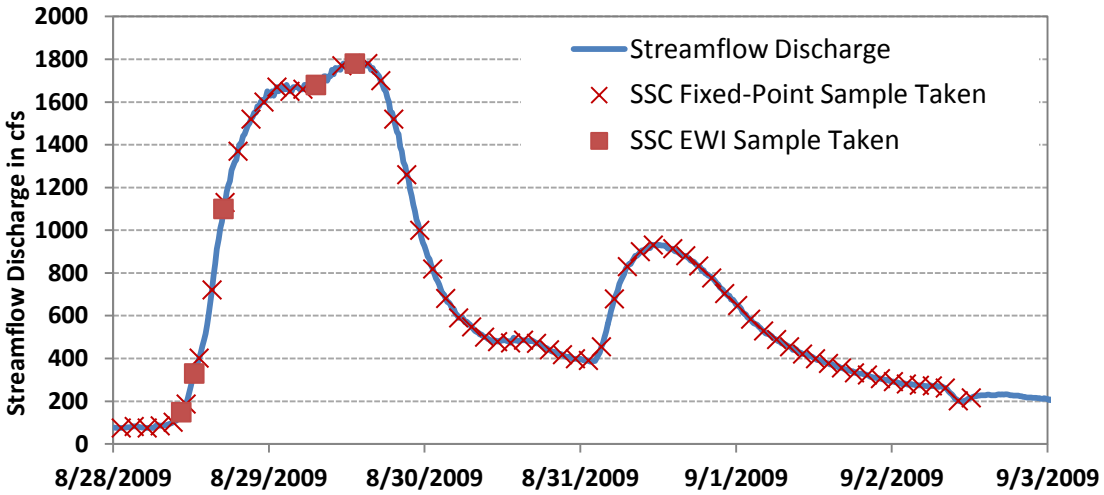


Figure 5.3 - Streamflow discharge Hydrograph and physical sediment sample times for Yellow River at Gees Mill Road (02207335), August 28–September 2, 2010

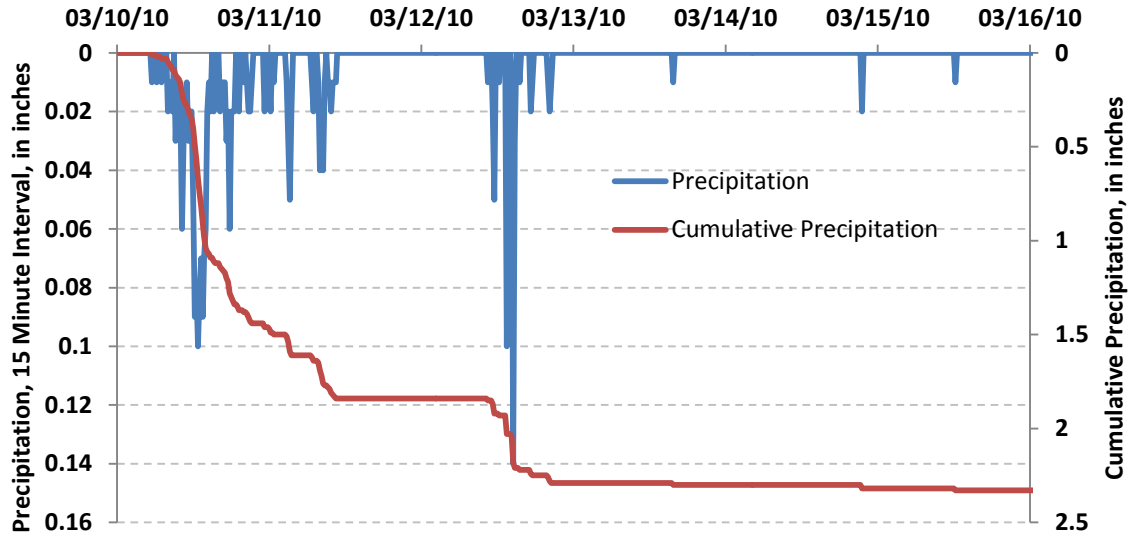


Figure 5.4 - Precipitation measured at stream gage at Yellow River at Gees Mill Road (02207335) from March 10–15, 2010

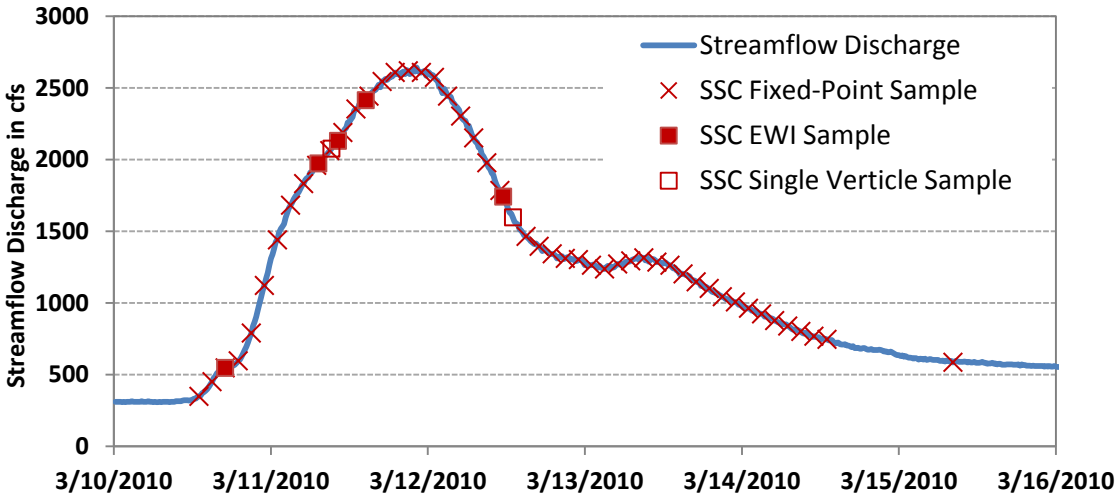


Figure 5.5 - Streamflow discharge hydrograph and physical sediment sample times for Yellow River at Gees Mill Road (02207335), March 10–15 2010

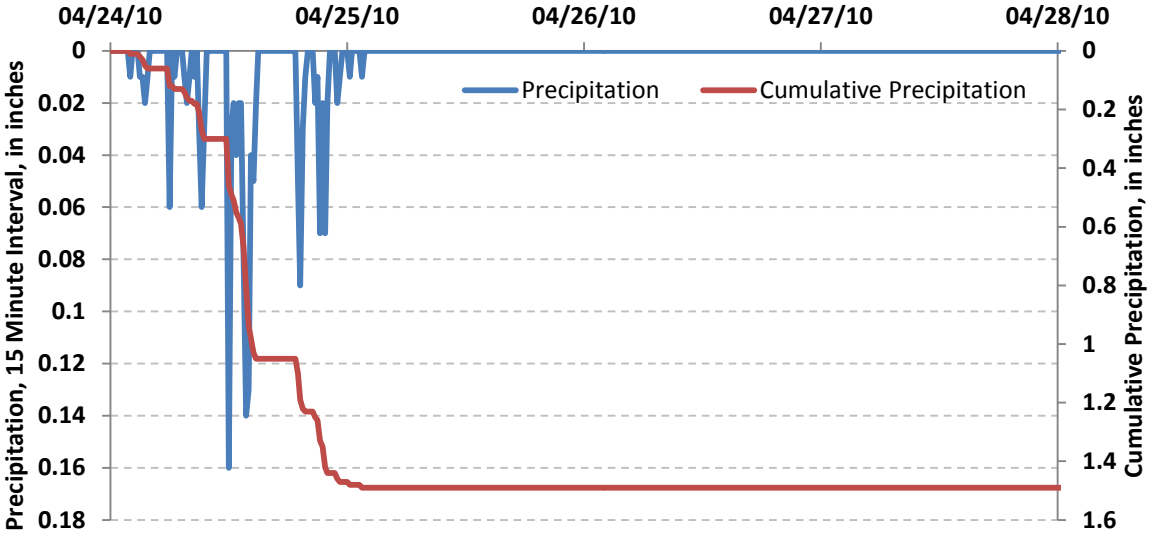


Figure 5.6 - Precipitation measured at stream gage at Yellow River at Gees Mill Road (02207335) from April 24–27, 2010

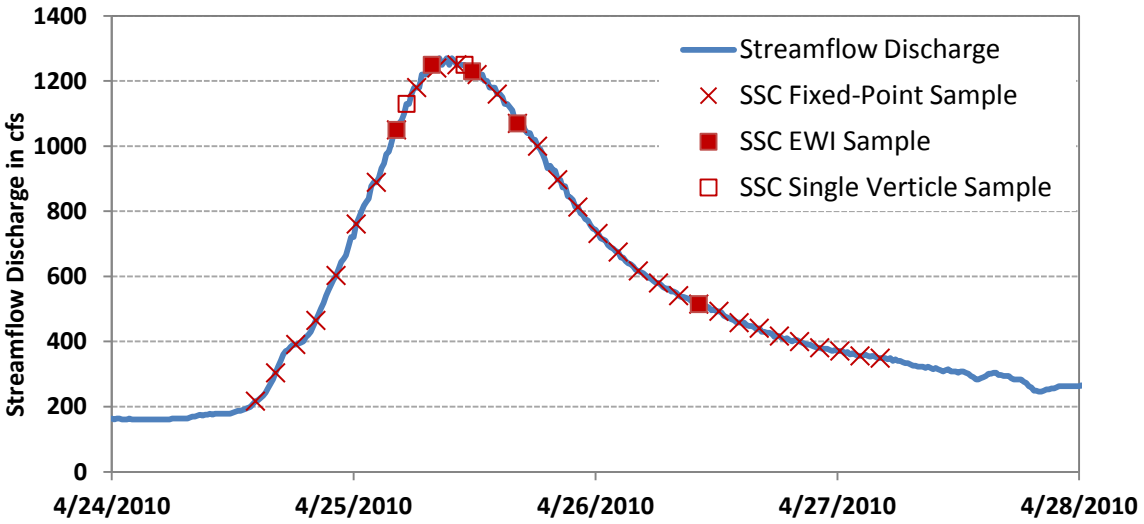


Figure 5.7 - Streamflow discharge hydrograph and physical sediment sample times for Yellow River at Gees Mill Road (02207335), April 24–27, 2010

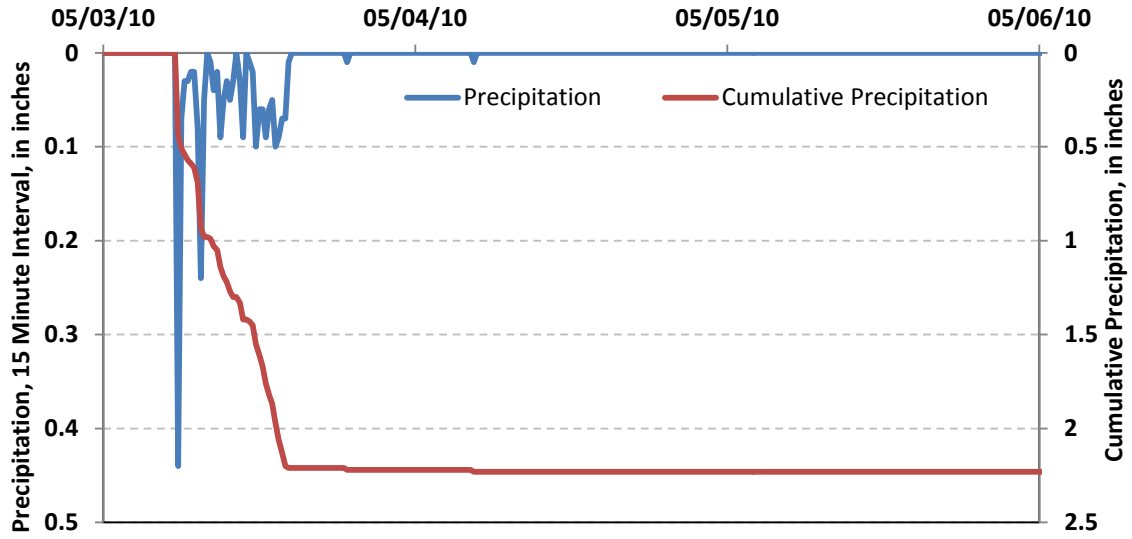


Figure 5.8 - Precipitation measured at stream gage at Yellow River at Gees Mill Road (02207335) , May 3–6, 2010

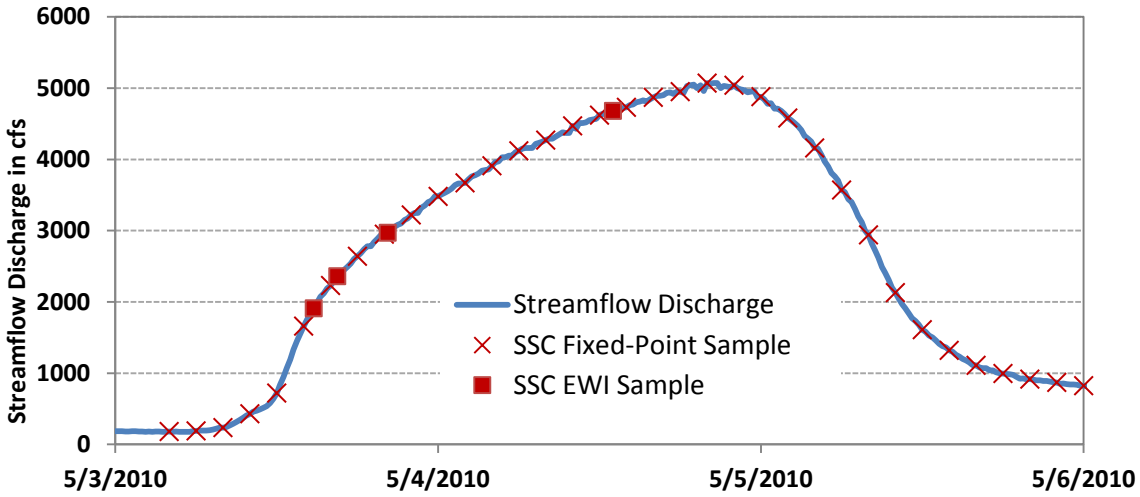


Figure 5.9–Streamflow discharge hydrograph and physical sediment sample times for Yellow River at Gees Mill Road (02207335), May 3–6, 2010

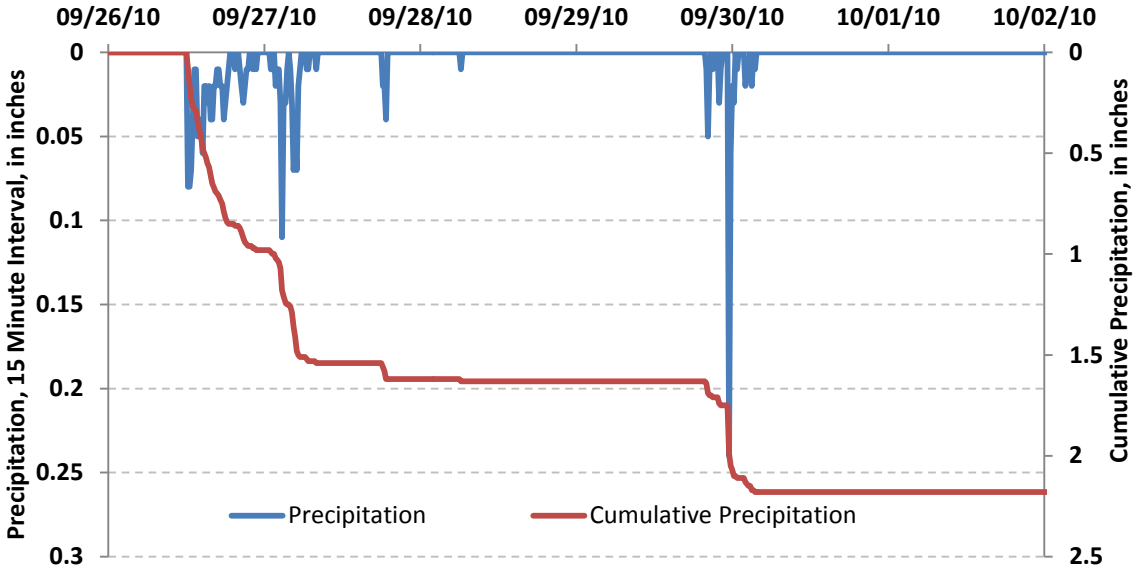


Figure 5.10 - Precipitation measured at stream gage at Yellow River at Gees Mill Road (02207335), Sept 26–Oct 2, 2010

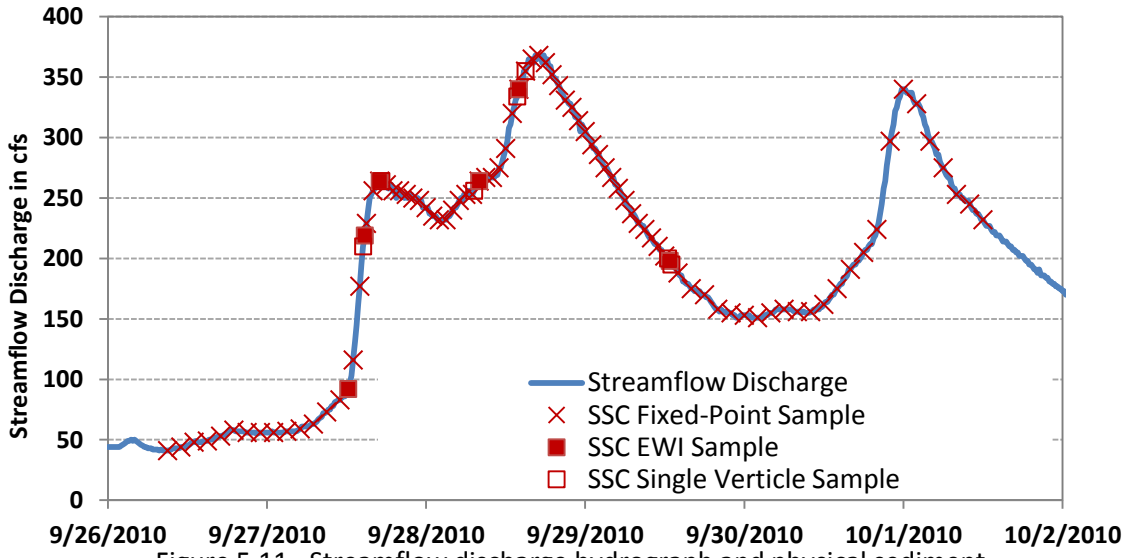


Figure 5.11 –Streamflow discharge hydrograph and physical sediment sample times for Yellow River at Gees Mill Road (02207335), Sept 26–Oct 2, 2010

Figure 5.12 Yellow River at Gees Mill Road looking downstream from bridge during bank full flow event on May 4, 2010.

Figure 5.13 Yellow River at Gees Mill Road looking downstream from gage during bank full flow event on May 4, 2010.

### *5.1.2 Velocity Data Summary*

Continuous horizontal profiles of velocity were measured using 3 ADCPs mounted on the downstream bridge pier at the west bank, at a gage elevation of 2.2 feet, as described in section 4.1.4. The data were processed using software developed for each instrument by the manufacturers, and using Microsoft Excel ® and MATLAB®. The data from these devices are voluminous, including velocities for each beam, overall velocity magnitude and angle of flow, and acoustic backscatter for each cell every 15 minutes.

Selected velocity data are summarized for each event from the 1.5MHz Sontek ADCP in figures 5.14 to 5.18. These figures show the velocity data from cells 1, 3, 5, 7, and 9 (cell locations noted in tables 4.3 to 4.5). The direction of the average measured flow for each time step, shown in these figures, is referenced to zero degrees perpendicular to the face of the transducers. The flow direction is typically about 100 degrees; that is 10 degrees west of perpendicular to the bridge alignment.

Similar analyses were completed with similar results for the 1.2MHz and 3.0MHz velocity data. The acoustic backscatter and attenuation data for each device are discussed in detail in the results section. During the May 2010 flow event, the 1.2MHz RDI ADCP was not recording because the memory card was full. After this event, the memory was cleared and the unit performed and recorded without error.

There is interference in the velocity data for the August 2009 event, apparently from tree limbs, and likely from a large tree that was lodged on the upstream central pier and extended into the flow near the west bank. The data in figure 5.14 appear to follow a noisy but somewhat meaningful pattern (after much post processing); however the analysis indicates that the magnitude and direction of these data are not comparable

with any subsequent events. The interference affected readings from all three ADCPs. The data from this event was not used in the analysis because it could not be corrected or adjusted to obtain representative data. Bridge maintenance crews removed the trees from the bridge pier after this event.

Velocities are notably smaller near the west channel edge and increase toward the channel centerline, as expected for fluvial systems. There is little change in average velocity between cell 7 (1.5 MHz) at station 143.6 feet (4.25 meters from the transducer face), and cell 9 at station 140.3 feet (5.25 meters from the transducer face). The 1.5 MHz ADCP was selected as the primary velocity reference device because the range of the 3.0MHz unit did not reach to the higher velocities near the channel thalweg and because the 1.2MHz system was not functioning during the May 2010 event.

The incipient motion critical velocity was computed for the reference velocity location using the methods described by Sturm (2001), for a range of sediment sizes. These were computed assuming a logarithmic vertical velocity profile, water temperatures of $20^{o}$C, and silica sediments having specific gravity of 2.65. The critical velocities for 16 (silt), 62 (silt-sand break), and 1000 (coarse sand) micron sediments at 2.34 feet above the channel bed are 0.62, 0.96, and 2.4 ft/sec (19, 29, and 72 cm/s), respectively. The critical velocities for these sizes are shown in figures 5.15 to 5.18.

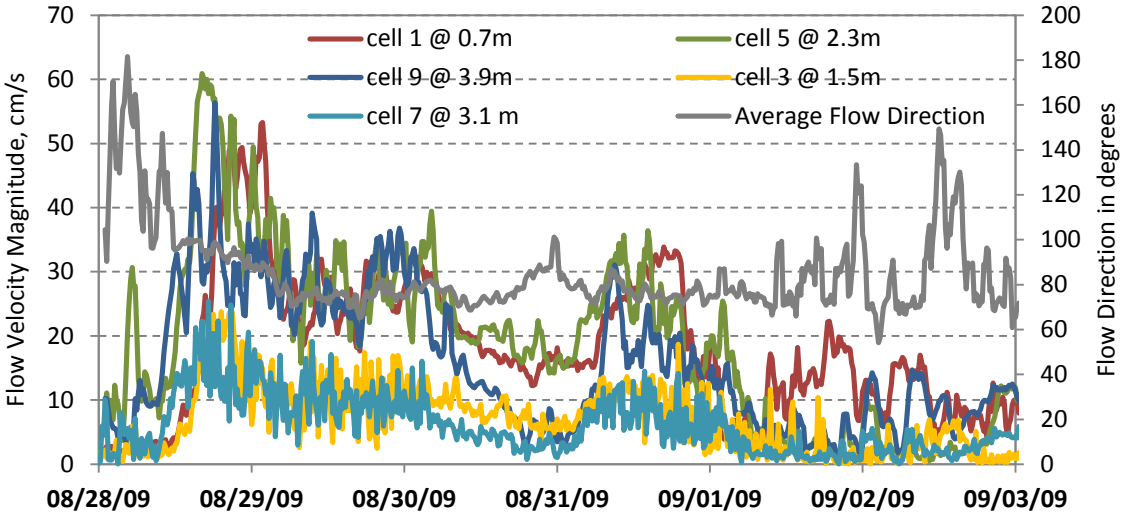


Figure 5.14 - Flow velocity magnitude and direction, average hourly, measured by 1500kHz instrument, for cells 1, 5, and 9, for event of August 28-Sept 2, 2010. Data are corrupted by debris caught on bridge piers.

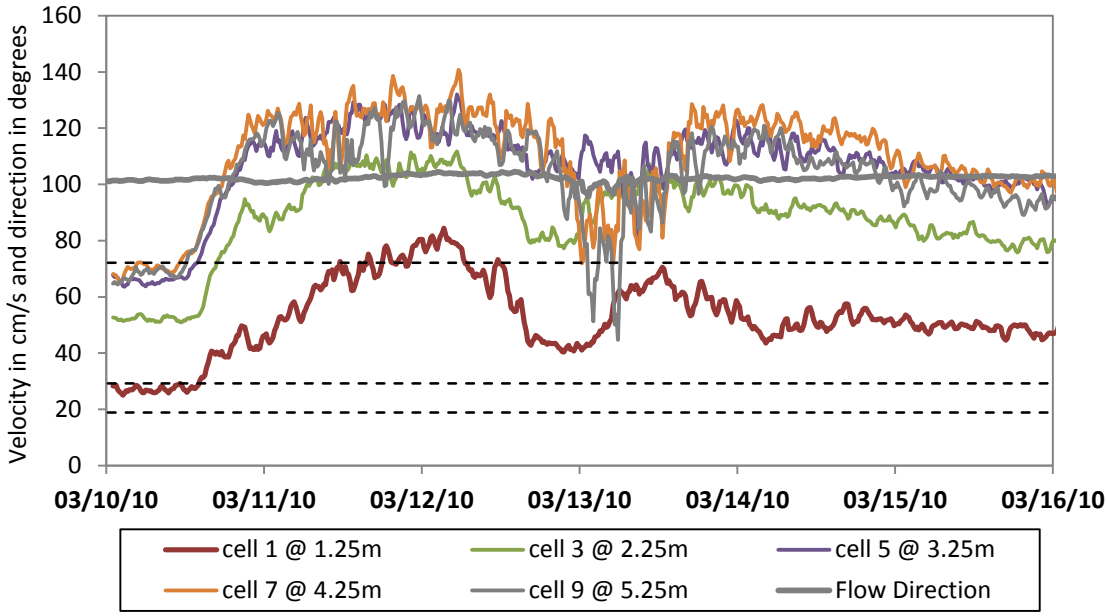


Figure 5.15 - Flow velocity magnitude and direction, hourly average, measured by 1500kHz instrument, for cells 1, 3, 5, 7, and 9, for event of March 10-16, 2010, and critical velocities (dashed lines) for 16, 62, and 1000 micron sediment at cell 7.

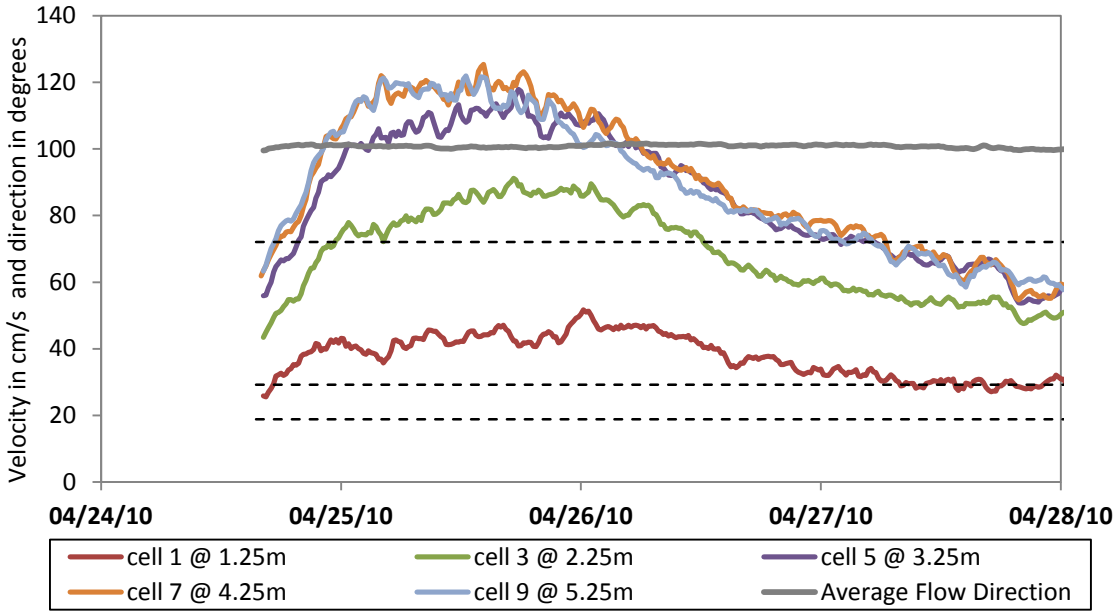


Figure 5.16 Flow velocity magnitude and direction, hourly average measured by 1500kHz instrument, for cells 1, 3, 5, 7, and 9, for event of April 24-28, 2010, and critical velocities (dashed lines) for 16, 62, and 1000 micron sediment at cell 7.

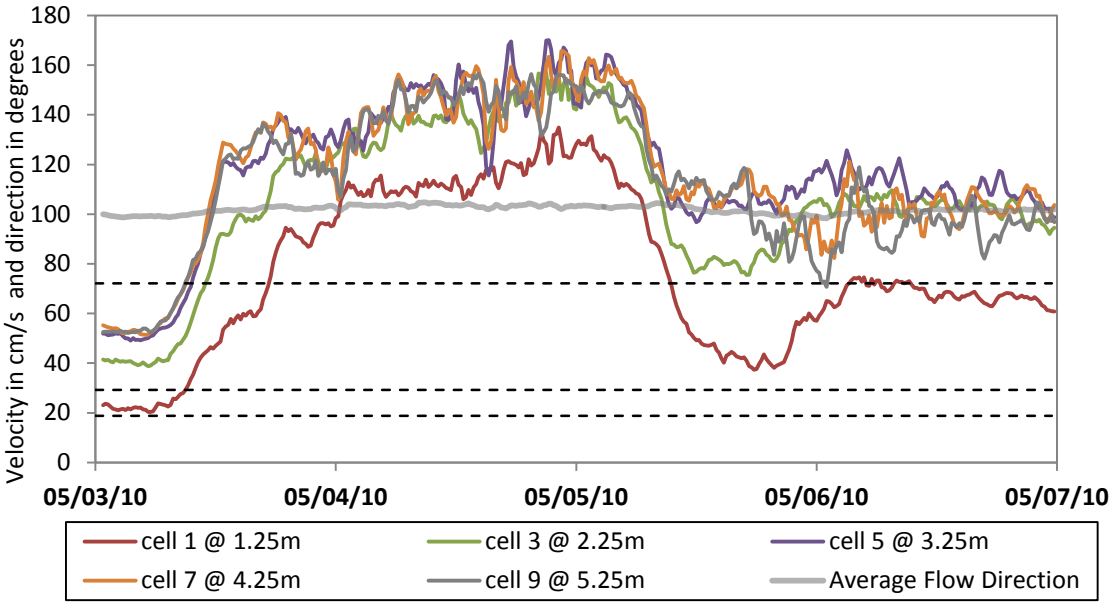


Figure 5.17 - Flow velocity magnitude and direction, hourly average, measured by 1500kHz instrument, for cells 1, 3, 5, 7, and 9, May 3-6, 2010, and critical velocities (dashed lines) for 16, 62, and 1000 micron sediment at cell 7.

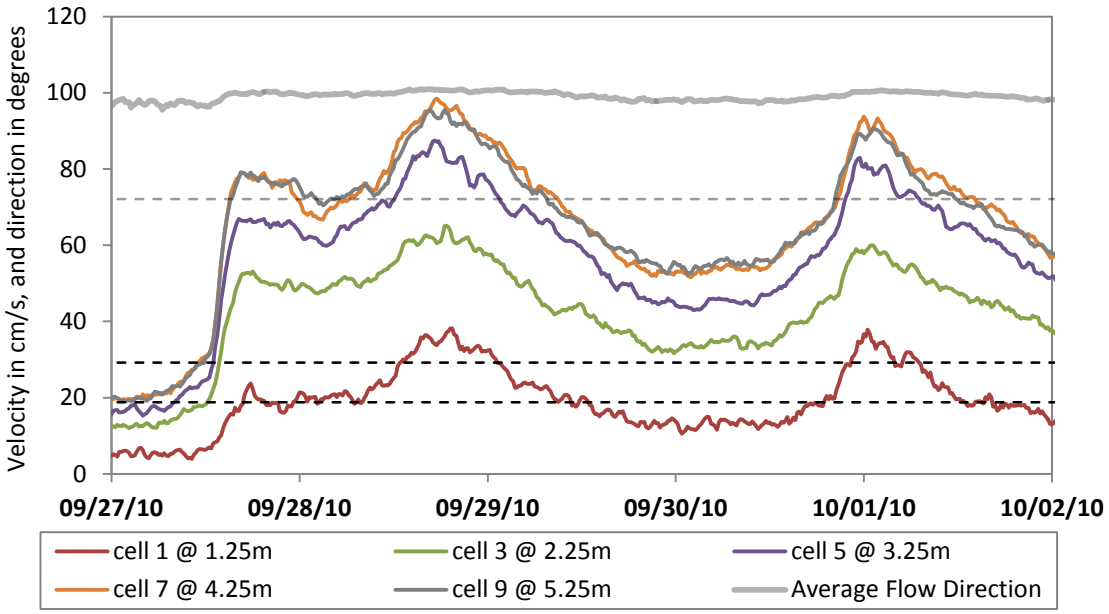


Figure 5.18 - Flow velocity magnitude and direction, hourly average, measured by 1500kHz instrument, for cells 1, 3, 5, 7, and 9, for Sep 27-Oct 1, 2010, and critical velocities (dashed lines) for 16, 62, and 1000 micron sediment at cell 7.

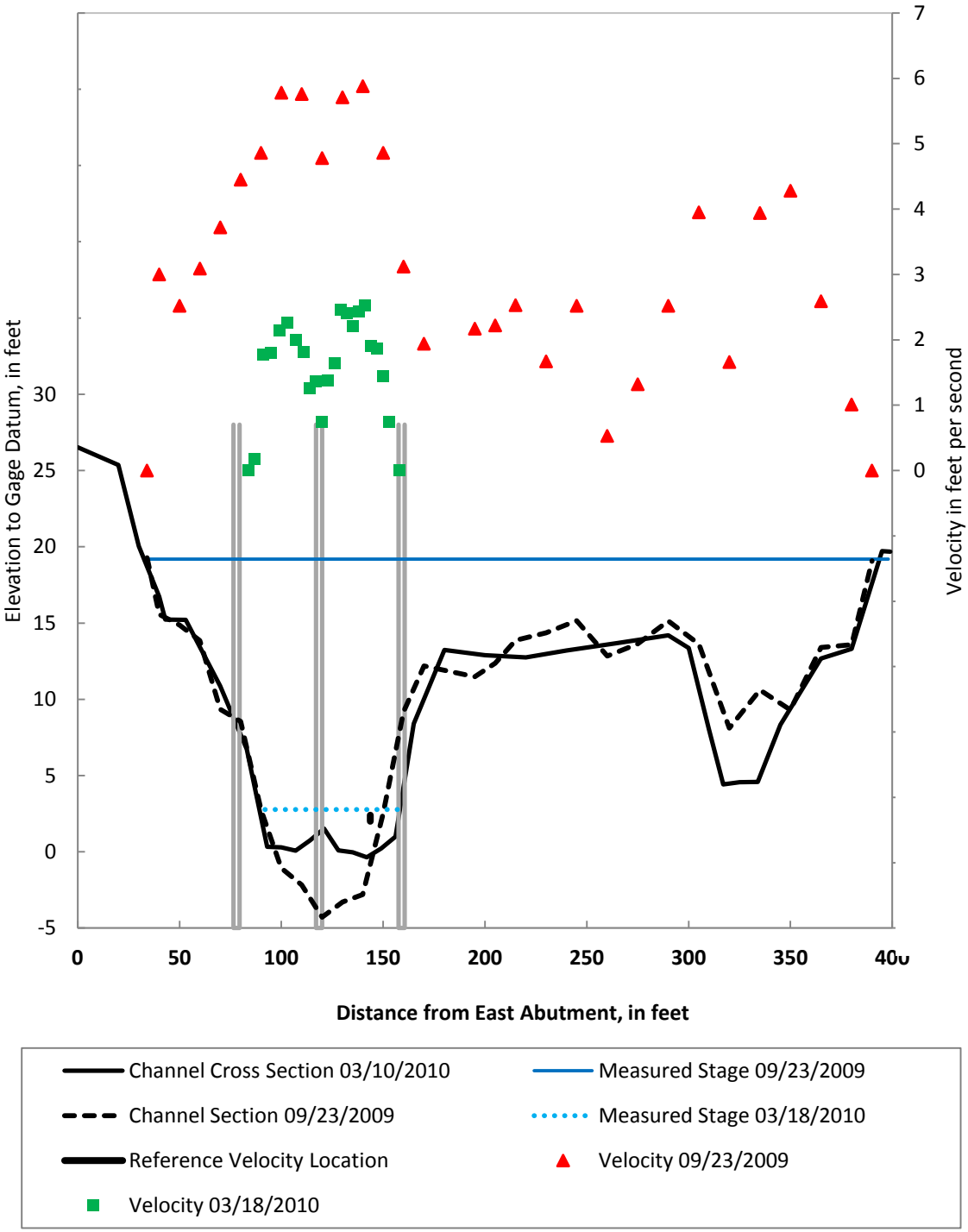


Figure 5.19 -- Yellow River at Gees Mill Road (02207335) Cross sections and velocity magnitude for measurements at downstream side of bridge

Two cross section discharge measurements using traditional Price-AA velocity meters and sounding weights were made from the bridge section during the period of this study. (Because of manpower limitations, the author was not able to obtain cross section velocity measurements during the sampled events.) Figure 5.19 shows the resulting cross section velocities from these traditional measurements. The measurement of September 23, 2009 was made on the rise of the 0.5-percent annual exceedence (200-year) flood at a stage of 19.20 feet and discharge of 12,700 cfs. The average cross section velocity for the September 23, 2009 measurement was 3.93 feet per second (ft/s), and the maximum measured point velocity was 6.50 ft/s at station 140 (5.88 feet per second average for the vertical). The channel section from this measurement is different from that measured on 03/10/2010, because the sounding weight was carried downstream from the vertical and/or because of channel scouring during this extreme event. The measurement of March 18, 2010, obtained only 3 days after one of the events sampled for this study, was made at a stage of 4.15 feet and discharge of 541 cfs. The average cross section velocity of the March 18, 2010 measurement was 1.57 ft/s and the maximum point velocity was 2.77 ft/s at station 138. The station of the maximum measured velocity for both of these measurements is in close proximity to the reference location at station 143.6 used for the continuous time series data.

Two historical cross section velocity measurements were also reviewed for this study. These measurements were both made using a downward looking ADCP deployed from a floating tri-maran downstream from the bridge. A measurement made on 08/27/2008 at a stage of 7.97 feet and discharge of 2050 cfs had an average cross section velocity of 2.89 ft/s and a maximum point velocity of 7.17 ft/s. A measurement made on 12/11/2008 at a stage of 8.56 feet and discharge of 2058 cfs had an average velocity of 3.35 ft/s and maximum point velocity of 7.07 ft/s. These historical cross section ADCP measurements

have higher measured maximum point velocities than the measured maximums from Price-AA meter measurements of the September 23, 2009 flood, because ADCP meters have much higher spatial resolution than the traditional Price-AA meters. The average velocities of these events are less than that of the extreme flood measurement of September 23, 2009.

## 5.2 Physical SSC Data Summary

Physical samples of SSC were collected at the downstream bridge section using equal-width-integrated (EWI) methods (24 samples) and single vertical samples that were then calibrated to EWI concentrations (9 samples); and at the fixed-point pumping sampler on the east stream bank (251 samples). The SSC data collection and calibration methods are described in the experimental approach. The relation between EWI and fixed-point pumped samples was defined and used to provide estimates of cross section SSC ($SSC_{XS}$) throughout each measured event. Samples were collected over rising and falling hydrograph conditions, as illustrated in figures 5.(3,5,8,9,11). All samples were analyzed in USGS sediment laboratories for total concentration and percent finer than 63 microns. Selected large volume samples were analyzed in the laboratory for full PSD. The physical sample concentrations, turbidity, and volumetric concentration and PSD are summarized for each event in table 5.2. The average concentrations are the average of one- or two-hour time interval samples obtained over the duration of event.

Table 5.2 - Average and maximum SSC (cross section and fixed-point), turbidity, laser-diffraction *VPC*, and average volumetric PSD for the 5 measured storm events

| Event Begin Date | 8/28/ 2009 | 3/10/ 2010 | 4/24/ 2010 | 5/3/ 2010 | 9/27/ 2010 |
|---|---|---|---|---|---|
| Average Cross Section SSC, mg/L | 146 | 84 | 99 | 157 | 33 |
| Maximum Cross Section SSC, mg/L | 648 | 198 | 190 | 496 | 93 |
| Average Fixed-Point SSC, mg/L | 120 | 71 | 83 | 130 | 29 |
| Maximum Fixed-Point SSC, mg/L | 508 | 163 | 157 | 393 | 79 |
| Number of SSC Samples | 64 | 49 | 32 | 34 | 72 |
| Average Turbidity, FNU | 89 | 55 | 44 | 99 | 20 |
| Maximum Turbidity, FNU | 286 | 129 | 93 | 274 | 74 |
| Average Fixed-Point *VPC*, µl/L | 188 | 54 | 89 | 110 | 30 |
| Maximum Fixed-Point *VPC*, µl/L | 596 | 143 | 201 | 369 | 56 |
| Average *D10*, microns | 6 | 4 | 6 | 4 | 5 |
| Average *D16*, microns | 8 | 6 | 7 | 5 | 6 |
| Average *D50*, microns | 23 | 17 | 21 | 16 | 15 |
| Average *D84*, microns | 83 | 69 | 61 | 76 | 57 |
| Number of *VPC* Measurements | 27 | 48 | 30 | 30 | 60 |

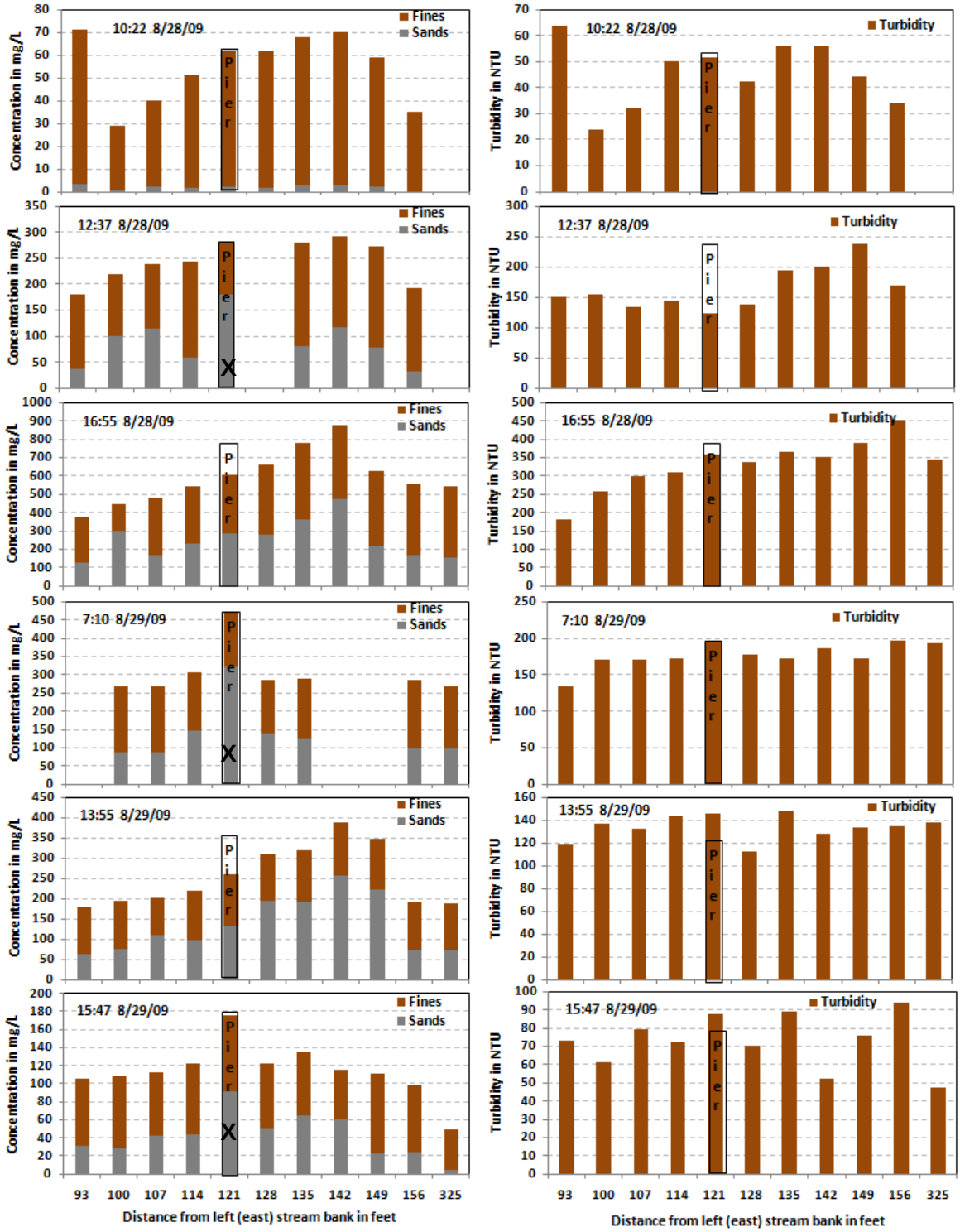


Figure 5.20 – Concentration of sands (greater than 63 microns) and fines, and sample turbidity across cross section at downstream side of bridge, Yellow River at Gees Mill Road, for August 28—29, 2009 (An "X" indicates a sample that was not used to compute the composite EWI)

### *5.2.1 EWI Cross Section Samples from Bridge Section*

The EWI samples were collected using methods described in the experimental approach section. The EWI samples collected at 10 to 12 verticals were analyzed individually for some samples to evaluate the cross sectional variation in concentration; and were composited in a single container for other samples to save analytical costs and to obtain enough sediment for full PSD analysis.

The cross sectional variation in concentration is illustrated in figure 5.20 for August 28-29, 2009. This event has the highest SSC concentration and highest percent larger than 63 microns of the 5 measured storms. The sampling vertical stations shown in this figure were those consistently sampled for all EWI samples during this research. Station 121, behind the central bridge pier, was sampled each time but in some cases was excluded from the composite EWI where this vertical was obviously higher than the other samples due to pier-induced turbulence. For example, a “X” in the pier bar in figure 5.20 indicates those samples where this vertical was not used to compute the composite EWI for those samples.

The concentrations increase from east to west across the channel section following the velocity distribution (as shown in figure 5.19) and, to a lesser extent, flow direction and increasing depth. Although the channel passes perpendicular to the bridge, the flow direction is consistently about 10 degrees west of center (equal to 100 degrees as illustrated in figures 5.15—5.18) as measured on the west side of the channel by the 2-dimensional ADCPs. The cross sectional variation in SSC is primarily due to changes in the sand (>63 microns) concentration. The fines (<63 microns) concentration is relatively

spatially uniform, which explains why the turbidity has less variance than SSC across the section in figure 5.20, because turbidity is more responsive to fines than to sands as discussed further in the results section. Thus, cross sectional non-homogeneity in SSC will increase with increasing sand concentrations, as has been observed in prior sediment studies (Vanoni, 2006). An exception in which the fines vary across the section is observed in the measurement of 10:22 08/28/09. This exception is probably due to poor mixing at the beginning of runoff for this event, which was visually apparent in the stream at the time of sample collection.

Concentrations in the mill channel (station 325), when flowing, are slightly less than those at the west edge of the main channel (station 156) for most EWI samples. In figure 5.20 this is evident except for the last sample of the set, for which the stage was nearly below the threshold for zero flow in the mill channel. The EWI sample results for all five measured events are summarized in table 5.3, along with the concurrent fixed-point sample results, discharge, velocity, and temperature. These data will be discussed further in following sections.

Table 5.3 Suspended sediment concentration and percent fines from concurrent EWI and fixed-point pumping sampler, and discharge, water temperature, and velocity measured by side-looking ADCP taken at station 143.6
(a: EWI concentration estimated from single vertical near middle of channel)

| Sample Month Year | Day | EWI Time (EST) | EWI Conc Total (mg/l) | EWI Percent Fines | Fixed-Point Time (EST) | Fixed-Point Conc Total (mg/l) | Fixed-Point Percent Fines | Discharge cfs | Velocity Station 143.6 cm/s | Temperature C |
|---|---|---|---|---|---|---|---|---|---|---|
| Aug '09 | 28 | 10:22 | 55 | 97 | 11:00 | 55 | 84 | 167 | 31 | 23.1 |
| Aug '09 | 28 | 12:37 | 240 | 68 | 13:00 | 297 | 66 | 366 | 37 | 22.8 |
| Aug '09 | 28 | 14:40 | 250[a] | 52[a] | 15:00 | 258 | 54 | 638 | 60 | 23.4 |
| Aug '09 | 28 | 16:55 | 591 | 58 | 17:00 | 508 | 65 | 1070 | 66 | 23.1 |
| Aug '09 | 28 | 18:15 | 525[a] | 55[a] | 19:00 | 461 | 71 | 1330 | 65 | 23.3 |
| Aug '09 | 28 | 19:57 | 479[a] | 55[a] | 21:00 | 386 | 52 | 1495 | 70 | 23.3 |
| Aug '09 | 29 | 7:10 | 282 | 60 | 7:00 | 256 | 67 | 1685 | 39 | 22.3 |
| Aug '09 | 29 | 13:15 | 255 | 50 | 13:00 | 204 | 84 | 1780 | 35 | 22.6 |
| Aug '09 | 30 | 15:47 | 108 | 67 | 15:00 | 126 | 90 | 485 | 38 | 23.2 |
| Mar '10 | 10 | 17:01 | 73 | 83 | 17:00 | 71 | 92 | 545 | 102 | 10.7 |
| Mar '10 | 11 | 7:22 | 193 | 65 | 7:00 | 151 | 87 | 1956 | 101 | 10.6 |
| Mar '10 | 11 | 9:15 | 209[a] | 64[a] | 9:00 | 159 | 90 | 2056 | 102 | 10.6 |
| Mar '10 | 11 | 10:16 | 192 | 64 | 11:00 | 163 | 87 | 2185 | 102 | 10.6 |
| Mar '10 | 12 | 13:00 | 55[a] | 88[a] | 11:00 | 62 | 88 | 1796 | 121 | 11.1 |
| Apr '10 | 25 | 4:20 | 215 | 55 | 4:00 | 125 | 89 | 1021 | 100 | 18.4 |
| Apr '10 | 25 | 5:15 | 144[a] | 73[a] | 6:00 | 153 | 89 | 1163 | 100 | 18.3 |
| Apr '10 | 25 | 7:45 | 186 | 67 | 8:00 | 145 | 88 | 1240 | 101 | 18.2 |
| Apr '10 | 25 | 11:00 | 191[a] | 65[a] | 10:00 | 146 | 90 | 1258 | 100 | 18.3 |
| Apr '10 | 25 | 11:45 | 166 | 73 | 12:00 | 148 | 89 | 1228 | 101 | 18.5 |
| Apr '10 | 25 | 16:15 | 285 | 43 | 16:00 | 138 | 92 | 1095 | 101 | 19.2 |
| Apr '10 | 26 | 10:15 | 52 | 84 | 10:00 | 52 | 94 | 520 | 101 | 18.7 |
| May '10 | 03 | 14:45 | 529 | 78 | 14:00 | 270 | 87 | 1602 | 101 | 18.0 |
| May '10 | 03 | 16:30 | 423 | 78 | 16:00 | 393 | 93 | 2208 | 103 | 17.9 |
| May '10 | 03 | 20:15 | 330 | 66 | 20:00 | 260 | 90 | 2038 | 103 | 18.5 |
| May '10 | 04 | 13:00 | 216 | 45 | 12:00 | 128 | 89 | 4598 | 104 | 16.7 |
| Sep '10 | 27 | 12:18 | 8 | 82 | 11:00 | 8 | 100 | 83 | 96 | 23.0 |
| Sep '10 | 27 | 14:50 | 54 | 91 | 15:00 | 45 | 91 | 224 | 97 | 24.0 |
| Sep '10 | 27 | 17:01 | 42 | 92 | 17:00 | 41 | 93 | 263 | 98 | 23.7 |
| Sep '10 | 28 | 7:15 | 28[a] | 88[a] | 7:00 | 21 | 97 | 254 | 97 | 21.1 |
| Sep '10 | 28 | 7:54 | 24 | 86 | 8:00 | 20 | 96 | 262 | 99 | 21.0 |
| Sep '10 | 28 | 13:59 | 35 | 84 | 14:00 | 33 | 94 | 337 | 98 | 22.0 |
| Sep '10 | 28 | 15:00 | 40[a] | 84[a] | 15:00 | 40 | 88 | 354 | 100 | 21.9 |
| Sep '10 | 29 | 12:48 | 24 | 83 | 13:00 | 25 | 95 | 196 | 99 | 20.8 |

### *5.2.2 Fixed-Point Pumped Samples*

Physical samples of SSC were collected using the ISCO fixed-point pumping sampler on the east stream bank using methods described in the experimental approach. Over the 5 events, 251 samples were collected and analyzed. (An additional 15 samples were collected and analyzed, but omitted from this data set because they preceded event rises and had concentrations less than 10 mg/L.) The samples were collected at a one (typically) or two hour interval depending on storm duration. Analytical results from these samples were calibrated to EWI SSC measurements to provide a time series representing average cross-section conditions. These data then form the principal basis of comparison for the surrogate data. The sediment load is simply the product of the streamflow discharge and SSC summed for each time step over each storm event. Time series of the concentrations of these samples are shown in figure 5.21, together with discharge and turbidity time series data that will be discussed in later sections. Note that the SSC and turbidity are plotted on separate scales in the time series plots (left hand panel) of figure 5.21. The data are listed in Table 5.4.

Table 5.4 - Concurrent suspended sediment, turbidity, discharge, stage, velocity and temperature for 5 storms on Yellow River at Gees Mill Road near metropolitan Atlanta, Georgia (Velocity measured at station 143.6 feet by horizontal ADCP.)

| Event | Datetime | Stage ft | Dis-charge cfs | Temp-era-ture °C | Refer-ence Velo-city cm/s | Turb-idity FNU | SSC fixed-point mg/L | % Fines fixed-point | $SSC_{xs}$ mg/L |
|---|---|---|---|---|---|---|---|---|---|
| Aug '09 | 8/28/2009 1:00 | 2.86 | 75 | 25.0 | 10.2 | 7 | 9 | 89 | 10 |
| Aug '09 | 8/28/2009 3:00 | 2.89 | 81 | 24.7 | 4.2 | 7 | 7 | 74 | 7 |
| Aug '09 | 8/28/2009 5:00 | 2.87 | 76 | 24.7 | 5.5 | 6 | 7 | 58 | 7 |
| Aug '09 | 8/28/2009 7:00 | 2.92 | 86 | 24.1 | 10.7 | 16 | 24 | 91 | 27 |
| Aug '09 | 8/28/2009 9:00 | 2.98 | 97 | 24.0 | 9.3 | 10 | 10 | 92 | 11 |
| Aug '09 | 8/28/2009 11:00 | 3.30 | 167 | 23.3 | 25.7 | 41 | 55 | 84 | 64 |
| Aug '09 | 8/28/2009 13:00 | 4.10 | 366 | 23.0 | 25.4 | 156 | 297 | 66 | 370 |
| Aug '09 | 8/28/2009 15:00 | 5.16 | 639 | 23.5 | 39.8 | 156 | 258 | 54 | 320 |
| Aug '09 | 8/28/2009 17:00 | 6.70 | 1070 | 23.3 | 31.5 | 254 | 508 | 65 | 648 |
| Aug '09 | 8/28/2009 19:00 | 7.44 | 1330 | 23.4 | 33.3 | 286 | 461 | 71 | 586 |
| Aug '09 | 8/28/2009 21:00 | 7.86 | 1495 | 23.5 | 31.4 | 265 | 386 | 52 | 487 |
| Aug '09 | 8/28/2009 23:00 | 8.11 | 1598 | 23.5 | 29.8 | 222 | 326 | 59 | 408 |
| Aug '09 | 8/29/2009 1:00 | 8.23 | 1650 | 23.2 | 31.9 | 208 | 274 | 55 | 340 |
| Aug '09 | 8/29/2009 3:00 | 8.26 | 1663 | 23.0 | 25.0 | 192 | 275 | 59 | 342 |
| Aug '09 | 8/29/2009 5:00 | 8.27 | 1663 | 22.8 | 32.1 | 195 | 251 | 52 | 311 |
| Aug '09 | 8/29/2009 7:00 | 8.31 | 1685 | 22.5 | 24.7 | 193 | 256 | 67 | 317 |
| Aug '09 | 8/29/2009 13:00 | 8.53 | 1780 | 22.8 | 23.9 | 141 | 204 | 84 | 250 |
| Aug '09 | 8/29/2009 15:00 | 8.52 | 1778 | 23.1 | 23.1 | 124 | 175 | 85 | 213 |
| Aug '09 | 8/29/2009 17:00 | 8.40 | 1723 | 23.3 | 20.5 | 111 | 142 | 85 | 172 |
| Aug '09 | 8/29/2009 19:00 | 8.01 | 1555 | 23.5 | 30.3 | 101 | 134 | 85 | 161 |
| Aug '09 | 8/29/2009 21:00 | 7.40 | 1313 | 23.5 | 33.0 | 95 | 120 | 88 | 144 |
| Aug '09 | 8/29/2009 23:00 | 6.60 | 1043 | 23.4 | 36.8 | 91 | 111 | 91 | 133 |
| Aug '09 | 8/30/2009 1:00 | 5.93 | 849 | 23.4 | 32.6 | 84 | 106 | 94 | 126 |
| Aug '09 | 8/30/2009 3:00 | 5.40 | 702 | 23.3 | 27.3 | 79 | 100 | 93 | 119 |
| Aug '09 | 8/30/2009 5:00 | 5.04 | 609 | 23.3 | 18.3 | 73 | 90 | 94 | 107 |
| Aug '09 | 8/30/2009 7:00 | 4.86 | 561 | 23.3 | 24.4 | 67 | 82 | 92 | 97 |
| Aug '09 | 8/30/2009 9:00 | 4.65 | 508 | 23.3 | 17.0 | 62 | 73 | 96 | 86 |
| Aug '09 | 8/30/2009 11:00 | 4.56 | 483 | 23.5 | 12.3 | 59 | 70 | 93 | 82 |
| Aug '09 | 8/30/2009 13:00 | 4.55 | 480 | 23.6 | 9.5 | 54 | 64 | 94 | 75 |
| Aug '09 | 8/30/2009 15:00 | 4.57 | 485 | 23.4 | 10.0 | 84 | 126 | 90 | 151 |
| Aug '09 | 8/30/2009 17:00 | 4.54 | 479 | 23.3 | 7.5 | 82 | 102 | 92 | 121 |
| Aug '09 | 8/30/2009 19:00 | 4.41 | 446 | 23.3 | 3.0 | 62 | 73 | 95 | 86 |
| Aug '09 | 8/30/2009 21:00 | 4.32 | 421 | 23.4 | 5.3 | 51 | 65 | 95 | 76 |
| Aug '09 | 8/30/2009 23:00 | 4.24 | 401 | 23.3 | 6.9 | 47 | 60 | 94 | 70 |
| Aug '09 | 8/31/2009 1:00 | 4.20 | 391 | 23.3 | 3.2 | 43 | 55 | 95 | 64 |
| Aug '09 | 8/31/2009 3:00 | 4.33 | 425 | 23.3 | 6.0 | 42 | 63 | 9 | 73 |
| Aug '09 | 8/31/2009 5:00 | 5.14 | 635 | 23.3 | 9.7 | 59 | 97 | 87 | 115 |
| Aug '09 | 8/31/2009 7:00 | 5.78 | 806 | 23.2 | 18.2 | 77 | 120 | 90 | 144 |
| Aug '09 | 8/31/2009 9:00 | 6.07 | 888 | 22.8 | 30.5 | 91 | 154 | 87 | 187 |

Table 5.4 (continued) - Concurrent suspended sediment, turbidity, discharge, stage, velocity and temperature for 5 storms on Yellow River at Gees Mill Road near metropolitan Atlanta, Georgia (Velocity measured at station 143.6 feet by horizontal ADCP.)

| Event | Datetime | Stage ft | Dis-charge cfs | Temp-era-ture °C | Refer-ence Velo-city cm/s | Turb-idity FNU | SSC fixed-point mg/L | % Fines fixed-point | $SSC_{xs}$ mg/L |
|---|---|---|---|---|---|---|---|---|---|
| Aug '09 | 8/31/2009 11:00 | 6.20 | 925 | 22.7 | 15.1 | 139 | 196 | 93 | 240 |
| Aug '09 | 8/31/2009 14:00 | 6.16 | 914 | 22.3 | 24.8 | 163 | 182 | 92 | 222 |
| Aug '09 | 8/31/2009 16:00 | 6.05 | 883 | 22.5 | 17.9 | 130 | 132 | 92 | 159 |
| Aug '09 | 8/31/2009 18:00 | 5.90 | 842 | 22.6 | 18.4 | 109 | 130 | 90 | 156 |
| Aug '09 | 8/31/2009 20:00 | 5.71 | 787 | 22.6 | 12.0 | 98 | 110 | 90 | 131 |
| Aug '09 | 8/31/2009 22:00 | 5.47 | 721 | 22.5 | 14.9 | 91 | 102 | 94 | 121 |
| Aug '09 | 9/1/2009 0:00 | 5.24 | 660 | 22.4 | 15.3 | 86 | 94 | 95 | 112 |
| Aug '09 | 9/1/2009 2:00 | 4.98 | 593 | 22.4 | 13.3 | 82 | 82 | 93 | 97 |
| Aug '09 | 9/1/2009 4:00 | 4.77 | 538 | 22.3 | 8.1 | 78 | 76 | 94 | 89 |
| Aug '09 | 9/1/2009 6:00 | 4.60 | 495 | 22.2 | 9.6 | 74 | 76 | 94 | 89 |
| Aug '09 | 9/1/2009 8:00 | 4.46 | 461 | 22.2 | 4.4 | 70 | 70 | 92 | 82 |
| Aug '09 | 9/1/2009 10:00 | 4.34 | 428 | 22.1 | 6.1 | 66 | 68 | 96 | 80 |
| Aug '09 | 9/1/2009 12:00 | 4.25 | 405 | 22.1 | 5.4 | 62 | 58 | 95 | 67 |
| Aug '09 | 9/1/2009 14:00 | 4.16 | 380 | 22.1 | 6.8 | 58 | 59 | 95 | 69 |
| Aug '09 | 9/1/2009 16:00 | 4.07 | 359 | 22.2 | 3.3 | 52 | 54 | 96 | 63 |
| Aug '09 | 9/1/2009 18:00 | 4.00 | 339 | 22.2 | 3.8 | 49 | 51 | 95 | 59 |
| Aug '09 | 9/1/2009 20:00 | 3.93 | 325 | 22.1 | 1.5 | 45 | 44 | 97 | 51 |
| Aug '09 | 9/1/2009 22:00 | 3.87 | 308 | 22.1 | 4.3 | 42 | 44 | 97 | 51 |
| Aug '09 | 9/2/2009 0:00 | 3.82 | 295 | 22.0 | 6.5 | 39 | 41 | 97 | 47 |
| Aug '09 | 9/2/2009 2:00 | 3.77 | 281 | 22.0 | 11.3 | 35 | 39 | 97 | 45 |
| Aug '09 | 9/2/2009 4:00 | 3.74 | 276 | 21.9 | 7.1 | 34 | 34 | 98 | 39 |
| Aug '09 | 9/2/2009 6:00 | 3.73 | 272 | 21.8 | 1.9 | 32 | 37 | 97 | 42 |
| Aug '09 | 9/2/2009 8:00 | 3.71 | 267 | 21.7 | 13.6 | 30 | 35 | 97 | 40 |
| Aug '09 | 9/2/2009 10:00 | 3.48 | 211 | 21.9 | 9.3 | 28 | 29 | 99 | 33 |
| Aug '09 | 9/2/2009 12:00 | 3.48 | 212 | 22.4 | 10.0 | 25 | 28 | 97 | 32 |
| Mar '10 | 3/10/10 13:00 | 3.94 | 345 | 11.0 | 76.0 | 6 | 26 | 84 | 29 |
| Mar '10 | 3/10/10 15:00 | 4.23 | 444 | 10.9 | 90.3 | 20 | 41 | 90 | 47 |
| Mar '10 | 3/10/10 17:00 | 4.54 | 545 | 10.8 | 98.8 | 44 | 71 | 92 | 83 |
| Mar '10 | 3/10/10 19:00 | 4.67 | 589 | 10.8 | 108.1 | 34 | 50 | 89 | 58 |
| Mar '10 | 3/10/10 21:00 | 5.21 | 778 | 10.7 | 120.2 | 34 | 55 | 88 | 64 |
| Mar '10 | 3/10/10 23:00 | 6.04 | 1105 | 10.9 | 123.4 | 49 | 81 | 87 | 95 |
| Mar '10 | 3/11/10 1:00 | 6.83 | 1434 | 10.9 | 123.7 | 101 | 141 | 90 | 170 |
| Mar '10 | 3/11/10 3:00 | 7.39 | 1668 | 10.9 | 114.7 | 101 | 151 | 88 | 183 |
| Mar '10 | 3/11/10 5:00 | 7.76 | 1827 | 10.8 | 128.7 | 108 | 152 | 87 | 184 |
| Mar '10 | 3/11/10 7:00 | 8.05 | 1956 | 10.8 | 119.4 | 109 | 151 | 87 | 183 |
| Mar '10 | 3/11/10 9:00 | 8.28 | 2056 | 10.7 | 115.7 | 121 | 159 | 90 | 193 |
| Mar '10 | 3/11/10 11:00 | 8.54 | 2185 | 10.7 | 112.8 | 129 | 163 | 87 | 198 |
| Mar '10 | 3/11/10 13:00 | 8.82 | 2337 | 10.8 | 133.9 | 113 | 147 | 85 | 178 |
| Mar '10 | 3/11/10 15:00 | 9.00 | 2439 | 10.8 | 126.8 | 103 | 130 | 86 | 156 |

Table 5.4 (continued) - Concurrent suspended sediment, turbidity, discharge, stage, velocity and temperature for 5 storms on Yellow River at Gees Mill Road near metropolitan Atlanta, Georgia (Velocity measured at station 143.6 feet by horizontal ADCP.)

| Event | Datetime | Stage ft | Dis-charge cfs | Temp-era-ture °C | Refer-ence Velo-city cm/s | Turb-idity FNU | SSC fixed-point mg/L | % Fines fixed-point | $SSC_{xs}$ mg/L |
|---|---|---|---|---|---|---|---|---|---|
| Mar '10 | 3/11/10 17:00 | 9.17 | 2531 | 10.9 | 125.2 | 94 | 120 | 82 | 144 |
| Mar '10 | 3/11/10 19:00 | 9.28 | 2594 | 11.0 | 134.4 | 84 | 102 | 84 | 121 |
| Mar '10 | 3/11/10 21:00 | 9.30 | 2610 | 11.0 | 131.7 | 78 | 98 | 81 | 116 |
| Mar '10 | 3/11/10 23:00 | 9.31 | 2613 | 11.0 | 127.8 | 70 | 96 | 77 | 114 |
| Mar '10 | 3/12/10 1:00 | 9.25 | 2577 | 11.0 | 113.1 | 67 | 72 | 84 | 84 |
| Mar '10 | 3/12/10 3:00 | 9.05 | 2463 | 11.0 | 126.5 | 63 | 71 | 86 | 83 |
| Mar '10 | 3/12/10 5:00 | 8.80 | 2326 | 11.1 | 137.9 | 61 | 73 | 80 | 86 |
| Mar '10 | 3/12/10 7:00 | 8.50 | 2164 | 11.1 | 127.5 | 58 | 68 | 81 | 80 |
| Mar '10 | 3/12/10 9:00 | 8.12 | 1987 | 11.2 | 124.8 | 55 | 63 | 86 | 73 |
| Mar '10 | 3/12/10 11:00 | 7.69 | 1796 | 11.3 | 120.2 | 53 | 62 | 88 | 72 |
| Mar '10 | 3/12/10 15:00 | 6.91 | 1470 | 11.6 | 116.8 | 49 | 61 | 81 | 71 |
| Mar '10 | 3/12/10 17:00 | 6.74 | 1399 | 11.7 | 117.3 | 47 | 56 | 86 | 65 |
| Mar '10 | 3/12/10 19:00 | 6.60 | 1343 | 11.8 | 122.6 | 50 | 55 | 88 | 64 |
| Mar '10 | 3/12/10 21:00 | 6.53 | 1316 | 11.8 | 116.2 | 48 | 57 | 84 | 66 |
| Mar '10 | 3/12/10 23:00 | 6.49 | 1298 | 11.8 | 99.4 | 45 | 56 | 84 | 65 |
| Mar '10 | 3/13/10 1:00 | 6.41 | 1264 | 11.7 | 86.9 | 52 | 60 | 89 | 70 |
| Mar '10 | 3/13/10 3:00 | 6.37 | 1244 | 11.5 | 95.4 | 44 | 51 | 87 | 59 |
| Mar '10 | 3/13/10 5:00 | 6.41 | 1263 | 11.3 | 79.1 | 42 | 49 | 89 | 57 |
| Mar '10 | 3/13/10 7:00 | 6.48 | 1294 | 11.2 | 98.6 | 40 | 48 | 89 | 55 |
| Mar '10 | 3/13/10 9:00 | 6.52 | 1312 | 11.1 | 89.2 | 40 | 49 | 82 | 57 |
| Mar '10 | 3/13/10 11:00 | 6.48 | 1295 | 11.2 | 102.1 | 41 | 47 | 87 | 54 |
| Mar '10 | 3/13/10 13:00 | 6.41 | 1264 | 11.4 | 98.9 | 40 | 47 | 89 | 54 |
| Mar '10 | 3/13/10 15:00 | 6.27 | 1202 | 11.7 | 117.2 | 39 | 46 | 89 | 53 |
| Mar '10 | 3/13/10 17:00 | 6.15 | 1153 | 11.8 | 127.1 | 38 | 49 | 84 | 57 |
| Mar '10 | 3/13/10 19:00 | 6.03 | 1100 | 11.8 | 124.8 | 37 | 55 | 93 | 64 |
| Mar '10 | 3/13/10 21:00 | 5.90 | 1048 | 11.7 | 125.3 | 36 | 42 | 91 | 48 |
| Mar '10 | 3/13/10 23:00 | 5.80 | 1008 | 11.6 | 114.2 | 35 | 37 | 93 | 42 |
| Mar '10 | 3/14/10 1:00 | 5.70 | 965 | 11.4 | 122.0 | 35 | 39 | 90 | 45 |
| Mar '10 | 3/14/10 3:00 | 5.60 | 926 | 11.2 | 126.3 | 34 | 38 | 90 | 43 |
| Mar '10 | 3/14/10 5:00 | 5.49 | 883 | 11.0 | 119.7 | 32 | 37 | 93 | 42 |
| Mar '10 | 3/14/10 7:00 | 5.38 | 844 | 10.9 | 118.6 | 30 | 34 | 92 | 39 |
| Mar '10 | 3/14/10 9:00 | 5.27 | 802 | 10.7 | 123.0 | 30 | 35 | 92 | 40 |
| Mar '10 | 3/14/10 11:00 | 5.18 | 767 | 10.7 | 113.5 | 28 | 32 | 92 | 36 |
| Mar '10 | 3/14/10 13:00 | 5.12 | 746 | 11.0 | 119.4 | 27 | 31 | 87 | 35 |
| Mar '10 | 3/15/10 9:00 | 4.68 | 593 | 10.5 | 104.1 | 18 | 21 | 94 | 23 |
| Apr '10 | 4/24/10 14:00 | 3.53 | 205 | 18.9 |  | 8 | 46 | 87 | 53 |
| Apr '10 | 4/24/10 16:00 | 3.76 | 279 | 18.9 | 63.4 | 19 | 64 | 88 | 75 |
| Apr '10 | 4/24/10 18:00 | 4.05 | 385 | 18.7 | 73.9 | 49 | 106 | 80 | 126 |
| Apr '10 | 4/24/10 20:00 | 4.22 | 441 | 18.6 | 82.6 | 43 | 87 | 83 | 103 |

Table 5.4 (continued) - Concurrent suspended sediment, turbidity, discharge, stage, velocity and temperature for 5 storms on Yellow River at Gees Mill Road near metropolitan Atlanta, Georgia (Velocity measured at station 143.6 feet by horizontal ADCP.)

| Event | Datetime | Stage ft | Dis-charge cfs | Temp-era-ture °C | Refer-ence Velo-city cm/s | Turb-idity FNU | SSC fixed-point mg/L | % Fines fixed-point | $SSC_{xs}$ mg/L |
|---|---|---|---|---|---|---|---|---|---|
| Apr '10 | 4/24/10 22:00 | 4.64 | 581 | 18.4 | 100.8 | 40 | 85 | 86 | 100 |
| Apr '10 | 4/25/10 0:00 | 5.06 | 724 | 18.2 | 107.3 | 47 | 95 | 83 | 113 |
| Apr '10 | 4/25/10 2:00 | 5.46 | 874 | 18.5 | 115.2 | 81 | 136 | 89 | 164 |
| Apr '10 | 4/25/10 4:00 | 5.84 | 1021 | 18.6 | 121.3 | 68 | 125 | 89 | 150 |
| Apr '10 | 4/25/10 6:00 | 6.17 | 1163 | 18.5 | 115.8 | 77 | 153 | 89 | 185 |
| Apr '10 | 4/25/10 8:00 | 6.36 | 1240 | 18.4 | 119.9 | 80 | 145 | 88 | 175 |
| Apr '10 | 4/25/10 10:00 | 6.40 | 1258 | 18.4 | 114.9 | 84 | 146 | 90 | 177 |
| Apr '10 | 4/25/10 12:00 | 6.33 | 1228 | 18.6 | 119.8 | 89 | 148 | 89 | 179 |
| Apr '10 | 4/25/10 14:00 | 6.20 | 1175 | 19.0 | 125.4 | 93 | 157 | 90 | 190 |
| Apr '10 | 4/25/10 16:00 | 6.02 | 1095 | 19.4 | 118.1 | 90 | 138 | 92 | 166 |
| Apr '10 | 4/25/10 18:00 | 5.83 | 1020 | 19.6 | 123.2 | 74 | 116 | 90 | 139 |
| Apr '10 | 4/25/10 20:00 | 5.59 | 922 | 19.5 | 111.1 | 60 | 102 | 92 | 121 |
| Apr '10 | 4/25/10 22:00 | 5.34 | 826 | 19.5 | 113.3 | 51 | 83 | 88 | 98 |
| Apr '10 | 4/26/10 0:00 | 5.12 | 745 | 19.5 | 106.4 | 46 | 81 | 90 | 95 |
| Apr '10 | 4/26/10 2:00 | 4.94 | 682 | 19.3 | 105.6 | 41 | 79 | 91 | 93 |
| Apr '10 | 4/26/10 4:00 | 4.78 | 626 | 19.1 | 106.5 | 37 | 68 | 91 | 80 |
| Apr '10 | 4/26/10 6:00 | 4.66 | 585 | 18.9 | 99.0 | 33 | 58 | 91 | 67 |
| Apr '10 | 4/26/10 8:00 | 4.55 | 550 | 18.7 | 95.4 | 30 | 59 | 84 | 69 |
| Apr '10 | 4/26/10 10:00 | 4.46 | 520 | 18.8 | 94.0 | 26 | 52 | 94 | 60 |
| Apr '10 | 4/26/10 12:00 | 4.38 | 495 | 19.0 | 90.9 | 23 | 43 | 91 | 49 |
| Apr '10 | 4/26/10 14:00 | 4.28 | 462 | 19.1 | 87.6 | 20 | 48 | 93 | 55 |
| Apr '10 | 4/26/10 16:00 | 4.23 | 443 | 19.0 | 82.7 | 18 | 44 | 92 | 51 |
| Apr '10 | 4/26/10 18:00 | 4.15 | 418 | 18.9 | 80.9 | 16 | 40 | 94 | 46 |
| Apr '10 | 4/26/10 20:00 | 4.11 | 402 | 18.8 | 80.3 | 15 | 37 | 83 | 42 |
| Apr '10 | 4/26/10 22:00 | 4.05 | 383 | 18.6 | 77.3 | 14 | 32 | 71 | 36 |
| Apr '10 | 4/27/10 0:00 | 4.01 | 372 | 18.5 | 78.3 | 13 | 29 | 95 | 33 |
| Apr '10 | 4/27/10 2:00 | 3.98 | 359 | 18.4 | 74.7 | 12 | 35 | 94 | 40 |
| Apr '10 | 4/27/10 4:00 | 3.96 | 352 | 18.3 | 75.9 | 12 | 26 | 91 | 29 |
| May '10 | 5/3/2010 4:00 | 3.44 | 179 | 21.2 | 52.6 | 4 | 17 | 94 | 19 |
| May '10 | 5/3/2010 6:00 | 3.47 | 187 | 21.2 | 55.5 | 8 | 13 | 93 | 14 |
| May '10 | 5/3/2010 8:00 | 3.62 | 234 | 21.3 | 65.8 | 16 | 32 | 95 | 36 |
| May '10 | 5/3/2010 10:00 | 4.15 | 417 | 21.3 | 81.8 | 64 | 111 | 94 | 133 |
| May '10 | 5/3/2010 12:00 | 4.97 | 695 | 21.4 | 119.7 | 104 | 168 | 92 | 204 |
| May '10 | 5/3/2010 14:00 | 7.23 | 1603 | 21.2 | 124.1 | 145 | 270 | 87 | 335 |
| May '10 | 5/3/2010 16:00 | 8.59 | 2208 | 21.3 | 133.2 | 274 | 393 | 93 | 496 |
| May '10 | 5/3/2010 18:00 | 9.32 | 2615 | 21.3 | 140.8 | 212 | 314 | 91 | 392 |
| May '10 | 5/3/2010 20:00 | 9.86 | 2938 | 21.3 | 124.7 | 194 | 260 | 90 | 322 |
| May '10 | 5/3/2010 22:00 | 10.28 | 3198 | 21.2 | 115.6 | 182 | 228 | 90 | 281 |
| May '10 | 5/4/2010 0:00 | 10.72 | 3473 | 21.1 | 105.8 | 155 | 186 | 91 | 227 |

Table 5.4 (continued) - Concurrent suspended sediment, turbidity, discharge, stage, velocity and temperature for 5 storms on Yellow River at Gees Mill Road near metropolitan Atlanta, Georgia (Velocity measured at station 143.6 feet by horizontal ADCP.)

| Event | Datetime | Stage ft | Dis-charge cfs | Temp-era-ture °C | Refer-ence Velo-city cm/s | Turb-idity FNU | SSC fixed-point mg/L | % Fines fixed-point | $SSC_{xs}$ mg/L |
|---|---|---|---|---|---|---|---|---|---|
| May '10 | 5/4/2010 2:00 | 11.04 | 3678 | 21.1 | 132.5 | 138 | 168 | 86 | 204 |
| May '10 | 5/4/2010 4:00 | 11.35 | 3895 | 21.1 | 133.9 | 135 | 146 | 89 | 177 |
| May '10 | 5/4/2010 6:00 | 11.63 | 4105 | 21.0 | 156.3 | 132 | 145 | 89 | 175 |
| May '10 | 5/4/2010 8:00 | 11.84 | 4260 | 21.0 | 149.5 | 131 | 134 | 91 | 161 |
| May '10 | 5/4/2010 10:00 | 12.03 | 4410 | 21.0 | 149.7 | 126 | 130 | 91 | 156 |
| May '10 | 5/4/2010 12:00 | 12.27 | 4598 | 21.2 | 147.4 | 119 | 128 | 89 | 154 |
| May '10 | 5/4/2010 14:00 | 12.43 | 4728 | 21.4 | 158.4 | 113 | 113 | 90 | 135 |
| May '10 | 5/4/2010 16:00 | 12.58 | 4853 | 21.5 | 142.7 | 108 | 116 | 87 | 139 |
| May '10 | 5/4/2010 18:00 | 12.69 | 4938 | 21.6 | 150.8 | 100 | 101 | 88 | 120 |
| May '10 | 5/4/2010 20:00 | 12.80 | 5033 | 21.5 | 137.6 | 94 | 92 | 88 | 109 |
| May '10 | 5/4/2010 22:00 | 12.78 | 5018 | 21.4 | 153.2 | 86 | 91 | 80 | 108 |
| May '10 | 5/5/2010 0:00 | 12.62 | 4888 | 21.3 | 145.6 | 78 | 76 | 85 | 89 |
| May '10 | 5/5/2010 2:00 | 12.29 | 4613 | 21.1 | 154.3 | 71 | 70 | 91 | 82 |
| May '10 | 5/5/2010 4:00 | 11.78 | 4213 | 20.9 | 154.5 | 65 | 70 | 88 | 82 |
| May '10 | 5/5/2010 6:00 | 10.98 | 3643 | 20.7 | 146.7 | 64 | 65 | 90 | 76 |
| May '10 | 5/5/2010 8:00 | 9.91 | 2970 | 20.5 | 120.3 | 65 | 71 | 91 | 83 |
| May '10 | 5/5/2010 10:00 | 8.51 | 2173 | 20.4 | 107.8 | 68 | 123 | 75 | 148 |
| May '10 | 5/5/2010 12:00 | 7.35 | 1650 | 20.8 | 111.1 | 68 | 138 | 72 | 166 |
| May '10 | 5/5/2010 16:00 | 6.06 | 1113 | 21.6 | 111.3 | 60 | 134 | 74 | 161 |
| May '10 | 5/5/2010 18:00 | 5.78 | 999 | 21.7 | 107.4 | 58 | 97 | 86 | 115 |
| May '10 | 5/5/2010 20:00 | 5.57 | 916 | 21.7 | 104.0 | 53 | 73 | 93 | 86 |
| May '10 | 5/5/2010 22:00 | 5.45 | 869 | 21.7 | 91.3 | 51 | 73 | 92 | 86 |
| May '10 | 5/6/2010 0:00 | 5.33 | 824 | 21.7 | 91.8 | 47 | 65 | 94 | 76 |
| Sep '10 | 9/27/2010 14:00 | 3.14 | 170 | 23.6 | 60.4 | 12 | 29 | 93 | 33 |
| Sep '10 | 9/27/2010 15:00 | 3.38 | 225 | 24.2 | 73.8 | 25 | 45 | 91 | 52 |
| Sep '10 | 9/27/2010 16:00 | 3.50 | 254 | 24.1 | 77.8 | 29 | 52 | 90 | 60 |
| Sep '10 | 9/27/2010 17:00 | 3.53 | 263 | 23.8 | 78.3 | 26 | 41 | 93 | 47 |
| Sep '10 | 9/27/2010 18:00 | 3.52 | 262 | 23.5 | 77.3 | 22 | 36 | 91 | 41 |
| Sep '10 | 9/27/2010 19:00 | 3.51 | 258 | 23.2 | 78.6 | 19 | 33 | 91 | 37 |
| Sep '10 | 9/27/2010 20:00 | 3.49 | 253 | 22.8 | 76.5 | 17 | 29 | 90 | 33 |
| Sep '10 | 9/27/2010 21:00 | 3.49 | 252 | 22.5 | 75.9 | 18 | 28 | 89 | 32 |
| Sep '10 | 9/27/2010 22:00 | 3.49 | 252 | 22.2 | 77.0 | 18 | 29 | 88 | 33 |
| Sep '10 | 9/27/2010 23:00 | 3.48 | 249 | 22.0 | 73.3 | 17 | 25 | 93 | 28 |
| Sep '10 | 9/28/2010 0:00 | 3.45 | 242 | 21.9 | 70.3 | 15 | 23 | 97 | 26 |
| Sep '10 | 9/28/2010 1:00 | 3.43 | 236 | 21.8 | 68.3 | 16 | 25 | 95 | 28 |
| Sep '10 | 9/28/2010 2:00 | 3.41 | 233 | 21.7 | 67.1 | 16 | 23 | 93 | 26 |
| Sep '10 | 9/28/2010 3:00 | 3.41 | 233 | 21.6 | 67.9 | 15 | 22 | 94 | 25 |
| Sep '10 | 9/28/2010 4:00 | 3.44 | 239 | 21.5 | 69.7 | 15 | 21 | 95 | 23 |
| Sep '10 | 9/28/2010 5:00 | 3.47 | 246 | 21.4 | 71.6 | 15 | 23 | 94 | 26 |

Table 5.4 (continued) - Concurrent suspended sediment, turbidity, discharge, stage, velocity and temperature for 5 storms on Yellow River at Gees Mill Road near metropolitan Atlanta, Georgia (Velocity measured at station 143.6 feet by horizontal ADCP.)

| Event | Datetime | Stage ft | Dis-charge cfs | Temp-era-ture °C | Refer-ence Velo-city cm/s | Turb-idity FNU | SSC fixed-point mg/L | % Fines fixed-point | $SSC_{xs}$ mg/L |
|---|---|---|---|---|---|---|---|---|---|
| Sep '10 | 9/28/2010 6:00 | 3.49 | 252 | 21.3 | 72.0 | 15 | 24 | 92 | 27 |
| Sep '10 | 9/28/2010 7:00 | 3.50 | 255 | 21.2 | 73.2 | 16 | 21 | 97 | 23 |
| Sep '10 | 9/28/2010 8:00 | 3.53 | 263 | 21.1 | 76.3 | 16 | 20 | 96 | 22 |
| Sep '10 | 9/28/2010 9:00 | 3.54 | 267 | 21.1 | 73.9 | 16 | 22 | 96 | 25 |
| Sep '10 | 9/28/2010 10:00 | 3.54 | 267 | 21.2 | 77.5 | 15 | 20 | 96 | 22 |
| Sep '10 | 9/28/2010 11:00 | 3.56 | 272 | 21.4 | 79.3 | 17 | 24 | 96 | 27 |
| Sep '10 | 9/28/2010 12:00 | 3.62 | 289 | 21.7 | 85.0 | 17 | 22 | 97 | 25 |
| Sep '10 | 9/28/2010 13:00 | 3.72 | 316 | 22.0 | 89.5 | 19 | 26 | 94 | 29 |
| Sep '10 | 9/28/2010 14:00 | 3.79 | 337 | 22.1 | 91.4 | 21 | 33 | 94 | 37 |
| Sep '10 | 9/28/2010 15:00 | 3.85 | 354 | 22.1 | 92.6 | 23 | 40 | 88 | 46 |
| Sep '10 | 9/28/2010 16:00 | 3.88 | 364 | 21.9 | 95.0 | 24 | 42 | 90 | 48 |
| Sep '10 | 9/28/2010 17:00 | 3.89 | 367 | 21.8 | 98.1 | 24 | 38 | 90 | 43 |
| Sep '10 | 9/28/2010 18:00 | 3.88 | 364 | 21.6 | 97.1 | 24 | 36 | 89 | 41 |
| Sep '10 | 9/28/2010 19:00 | 3.85 | 355 | 21.5 | 95.4 | 24 | 36 | 88 | 41 |
| Sep '10 | 9/28/2010 20:00 | 3.82 | 345 | 21.3 | 95.4 | 23 | 42 | 86 | 48 |
| Sep '10 | 9/28/2010 21:00 | 3.78 | 333 | 21.2 | 92.4 | 22 | 36 | 89 | 41 |
| Sep '10 | 9/28/2010 22:00 | 3.75 | 326 | 21.1 | 89.8 | 23 | 33 | 92 | 37 |
| Sep '10 | 9/28/2010 23:00 | 3.71 | 313 | 21.0 | 88.9 | 22 | 33 | 88 | 37 |
| Sep '10 | 9/29/2010 0:00 | 3.69 | 307 | 20.9 | 88.0 | 22 | 35 | 78 | 40 |
| Sep '10 | 9/29/2010 1:00 | 3.65 | 296 | 20.8 | 86.5 | 21 | 30 | 88 | 34 |
| Sep '10 | 9/29/2010 2:00 | 3.62 | 287 | 20.7 | 84.8 | 20 | 31 | 90 | 35 |
| Sep '10 | 9/29/2010 3:00 | 3.58 | 277 | 20.6 | 81.7 | 20 | 29 | 90 | 33 |
| Sep '10 | 9/29/2010 4:00 | 3.55 | 269 | 20.6 | 80.2 | 21 | 29 | 90 | 33 |
| Sep '10 | 9/29/2010 5:00 | 3.51 | 259 | 20.5 | 76.8 | 21 | 27 | 92 | 30 |
| Sep '10 | 9/29/2010 6:00 | 3.48 | 249 | 20.4 | 74.7 | 21 | 29 | 94 | 33 |
| Sep '10 | 9/29/2010 7:00 | 3.44 | 240 | 20.3 | 74.7 | 22 | 28 | 94 | 32 |
| Sep '10 | 9/29/2010 8:00 | 3.41 | 231 | 20.2 | 73.5 | 22 | 29 | 94 | 33 |
| Sep '10 | 9/29/2010 9:00 | 3.38 | 225 | 20.1 | 71.2 | 23 | 29 | 95 | 33 |
| Sep '10 | 9/29/2010 10:00 | 3.35 | 217 | 20.3 | 68.8 | 23 | 27 | 95 | 30 |
| Sep '10 | 9/29/2010 11:00 | 3.32 | 210 | 20.5 | 67.2 | 22 | 26 | 94 | 29 |
| Sep '10 | 9/29/2010 12:00 | 3.30 | 203 | 20.8 | 65.5 | 23 | 26 | 93 | 29 |
| Sep '10 | 9/29/2010 13:00 | 3.27 | 197 | 20.9 | 63.9 | 21 | 25 | 95 | 28 |
| Sep '10 | 9/29/2010 14:00 | 3.24 | 190 | 21.2 | 62.3 | 20 | 25 | 97 | 28 |
| Sep '10 | 9/29/2010 16:00 | 3.18 | 177 | 21.3 | 57.6 | 17 | 22 | 98 | 24 |
| Sep '10 | 9/29/2010 18:00 | 3.15 | 170 | 21.0 | 55.1 | 17 | 22 | 97 | 25 |
| Sep '10 | 9/29/2010 20:00 | 3.09 | 158 | 20.7 | 53.1 | 16 | 21 | 97 | 24 |
| Sep '10 | 9/29/2010 22:00 | 3.07 | 155 | 20.4 | 52.9 | 16 | 19 | 99 | 21 |
| Sep '10 | 9/30/2010 0:00 | 3.06 | 153 | 20.2 | 53.0 | 16 | 22 | 99 | 25 |
| Sep '10 | 9/30/2010 2:00 | 3.05 | 151 | 20.2 | 52.3 | 15 | 20 | 96 | 22 |

Table 5.4 (continued) - Concurrent suspended sediment, turbidity, discharge, stage, velocity and temperature for 5 storms on Yellow River at Gees Mill Road near metropolitan Atlanta, Georgia (Velocity measured at station 143.6 feet by horizontal ADCP.)

| Event | Datetime | Stage ft | Dis-charge cfs | Temp-era-ture °C | Refer-ence Velo-city cm/s | Turb-idity FNU | SSC fixed-point mg/L | % Fines fixed-point | $SSC_{xs}$ mg/L |
|---|---|---|---|---|---|---|---|---|---|
| Sep '10 | 9/30/2010 4:00 | 3.07 | 155 | 20.2 | 53.3 | 15 | 22 | 94 | 25 |
| Sep '10 | 9/30/2010 6:00 | 3.09 | 158 | 20.1 | 54.4 | 16 | 20 | 95 | 23 |
| Sep '10 | 9/30/2010 8:00 | 3.08 | 156 | 20.1 | 53.7 | 15 | 19 | 97 | 21 |
| Sep '10 | 9/30/2010 10:00 | 3.08 | 156 | 20.3 | 54.3 | 14 | 22 | 81 | 25 |
| Sep '10 | 9/30/2010 12:00 | 3.11 | 162 | 20.7 | 55.8 | 13 | 17 | 88 | 19 |
| Sep '10 | 9/30/2010 14:00 | 3.17 | 174 | 21.2 | 59.6 | 14 | 19 | 97 | 21 |
| Sep '10 | 9/30/2010 16:00 | 3.24 | 190 | 21.4 | 63.5 | 15 | 20 | 98 | 23 |
| Sep '10 | 9/30/2010 18:00 | 3.30 | 204 | 21.1 | 65.5 | 17 | 22 | 93 | 25 |
| Sep '10 | 9/30/2010 20:00 | 3.37 | 222 | 20.8 | 69.7 | 22 | 31 | 94 | 35 |
| Sep '10 | 9/30/2010 22:00 | 3.63 | 291 | 20.3 | 85.1 | 74 | 79 | 97 | 93 |
| Sep '10 | 10/1/2010 0:00 | 3.80 | 339 | 20.2 | 93.0 | 62 | 64 | 100 | 74 |
| Sep '10 | 10/1/2010 2:00 | 3.76 | 329 | 20.3 | 91.9 | 31 | 43 | 95 | 49 |
| Sep '10 | 10/1/2010 4:00 | 3.67 | 301 | 20.3 | 85.1 | 25 | 36 | 93 | 41 |
| Sep '10 | 10/1/2010 6:00 | 3.58 | 276 | 20.2 | 80.2 | 21 | 29 | 95 | 33 |
| Sep '10 | 10/1/2010 8:00 | 3.50 | 256 | 20.0 | 77.5 | 18 | 24 | 95 | 27 |
| Sep '10 | 10/1/2010 10:00 | 3.46 | 246 | 20.1 | 77.3 | 16 | 23 | 98 | 25 |
| Sep '10 | 10/1/2010 12:00 | 3.41 | 232 | 20.6 | 74.5 | 16 | 21 | 96 | 23 |

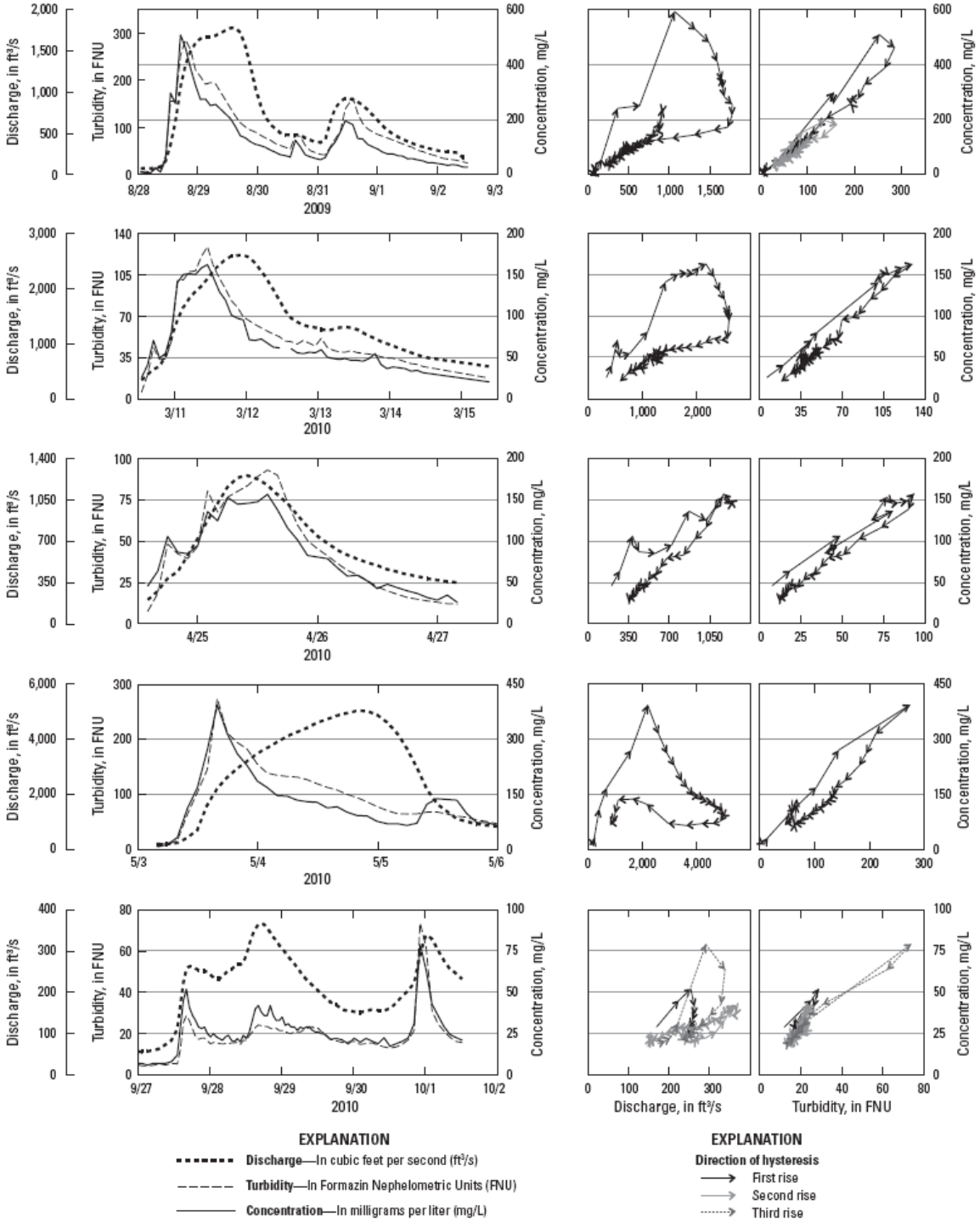


Figure 5.21 – Time series of streamflow discharge, turbidity, and mass suspended sediment concentration (fixed-point samples), and bivariate scatter plots of concentration and discharge, and concentration and turbidity, for 5 storm events in 2009 and 2010 on Yellow River at Gees Mill Road in metropolitan Atlanta, Georgia. (Note turbidity and concentration are plotted on separate axes in time series plots.)

### *5.2.3 Calibration of Fixed-Point to EWI Sample SSC*

The 33 concurrent measurements of SSC by EWI and adjusted single-vertical methods from the bridge section and by fixed-point pumping sampler were used to develop a regression model of cross section SSC ($SSC_{XS}$) as a function of fixed-point SSC ($SSC_{POINT}$). Log transformation of the data improved the linearity, correlation, model standard error, and the fit of residuals to normal quantiles, in comparison to untransformed data. The stream velocity at the time of the samples was statistically significant as an additional explanatory variable; but the improvement in model standard error was negligible (less than 0.009 in log-10 units), and thus velocity was not used in the final equation.

Retransformation into linear space from log space typically results in an estimate which is biased low (an underestimate). This retransformation bias was corrected using Duan's smoothing estimate (Duan, 1983; and Helsel and Hirsch, 1995) in which the mean of the retransformed residuals was 1.024. Results show that the retransformation bias was only -1 percent on average; but the correction was still applied to the final regression equation. The equation has an R-squared of 0.96, a model standard error of 0.095 (+/- 24%), and a p-value less than 0.0001, and is expressed as:

$$SSC_{XS} = 0.976\ (SSC_{POINT}\ )^{1.043} \qquad (12)$$

Figure 5.22 shows a scatter plot of the observed EWI SSC and the observed $SSC_{POINT}$, the fitted curve from equation 12, and the upper and lower 95 percent confidence interval for this curve. The variance in this relation is higher for higher concentrations. This is physically caused by the greater natural spatial variance in sand concentration associated with higher concentrations of sands. There is not, however, a bias in the least

squares regression fit, and the curve is well defined with low model error. Table 5.4 lists $SSC_{XS}$, $SSC_{POINT}$, discharge, stage, temperature, turbidity, and reference velocity for each time step for all 5 measured events.

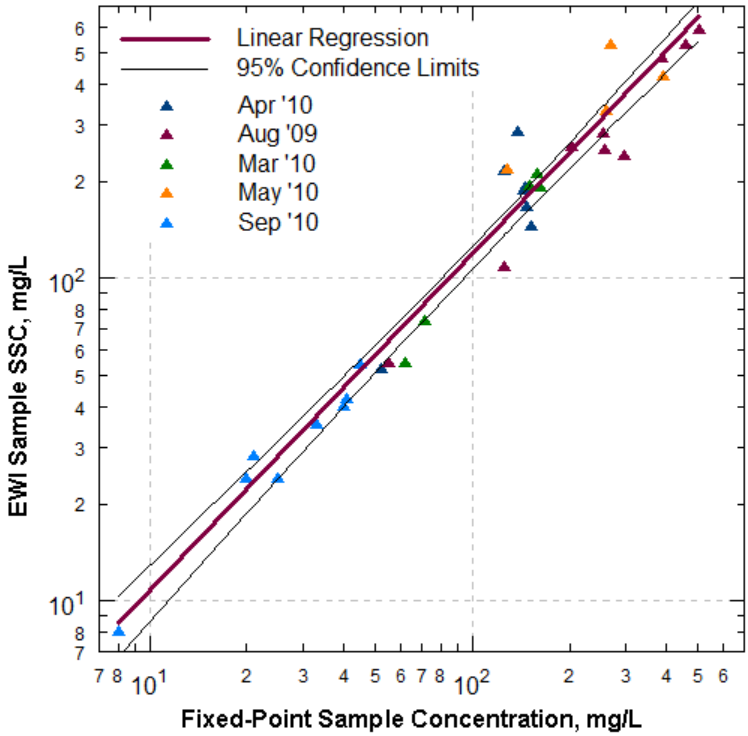


Figure 5.22 – Scatter plot of observed EWI suspended sediment concentration (SSC) and fixed-point SSC, and regression and upper and lower 95 percent confidence limits of model for Yellow River at Gees Mill Road

## 5.3 Turbidity Data Summary

The principals of operation, capabilities, and limitations of turbidity surrogates of sediment properties were discussed in the literature review. The turbidity time series data were collected at 15 minute intervals as described in the experimental methods section. The data quality and operation of the turbidity meter are very good, as indicated by the quality assurance, calibration checks, and data completeness. The data were averaged over one hour periods corresponding to the concurrent data time step for the SSC data. The average and maximum turbidity for each flow event are summarized in table 5.2. The concurrent hourly average turbidity data are given in table 5.4, and shown in figure 5.21 for all 5 measured storm events. The turbidity and concentration are plotted on separate scales in the time series plots of figure 5.21 (left panel) to facilitate graphical comparison of the shape of the time series data.

## 5.4 Laser-Diffraction Data Summary

Continuous time series of volumetric particle concentration (*VPC*) and particle size distribution (PSD) were measured using a LISST-Streamside laser-diffraction analyzer as discussed in the experimental approach. High resolution, environmental PSD are uniquely valuable in addressing many engineering, ecological, and water-quality issues related to sediment transport and source areas. The characteristics and limitations of this instrument and technology are discussed in the literature review. The average and maximum *VPC*, and the average volumetric *D10*, *D16*, *D50*, and *D84* for each flow event are listed in table 5.2.

An important finding of this research, discussed in the results, is that that *VPC* as measured by the LISST device and as reported here does not in fact equal true volumetric particle concentration, even within the instrument measurement size limits. If the mass concentration is converted to volumetric concentration using the mass density of sediment, the actual volumetric particle concentration would be smaller, by a factor of 2 to 5, than the *VPC* metric reported by the LISST.

### *5.4.1 Volumetric Particle Concentration*

Figure 5.23 show the time series of cross section mass $SSC_{XS}$ and fixed-point *VPC* for each of the 5 events. These data are used to develop the $SSC_{XS}$ to *VPC* relation as discussed in chapter 7. As discussed in the results section, the ratio of *VPC* to $SSC_{XS}$ changes with the portion of SSC that is unmeasured by *VPC*. Table 5.5 lists the *VPC* and volumetric particle size distribution data for the concurrent $SSC_{XS}$ measurements.

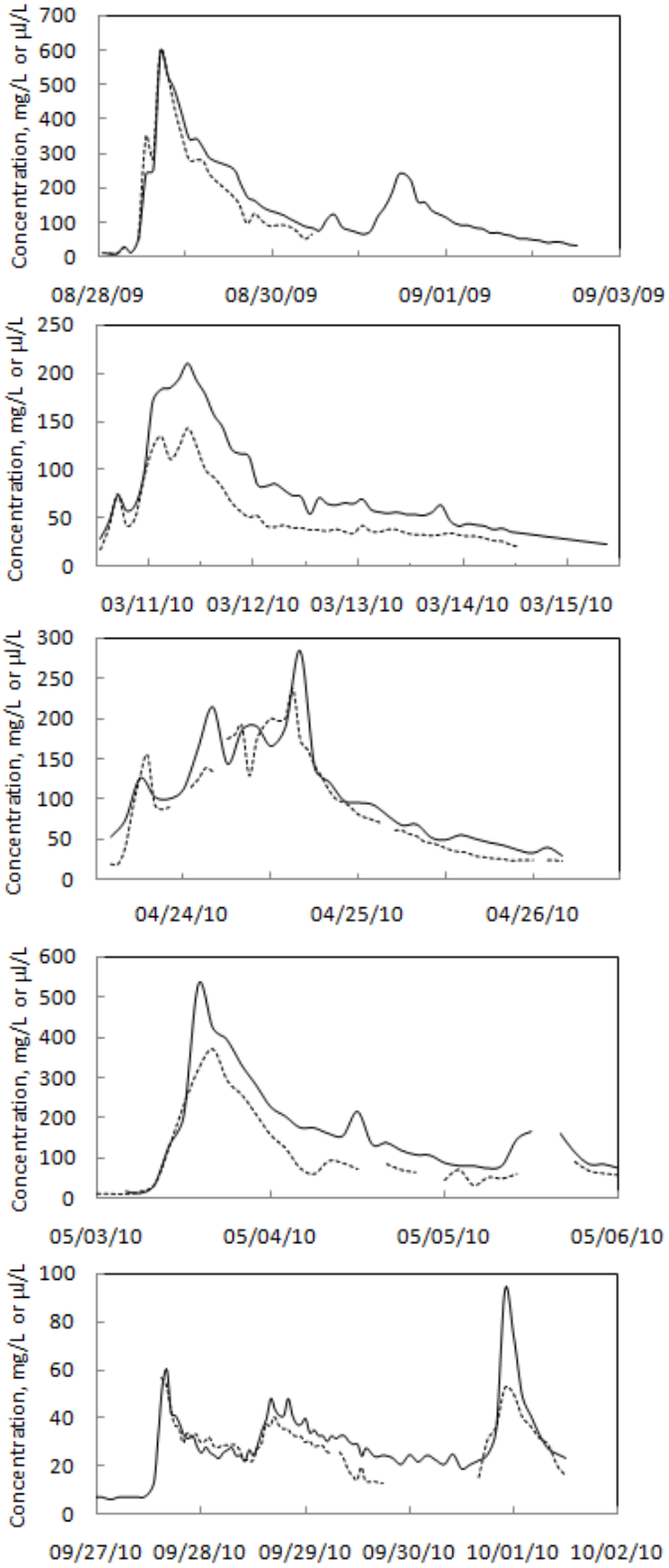


Figure 5.23 Time series of cross section mass $SSC_{XS}$ in mg/L (solid line) and fixed-point volumetric particle concentration in µl/L (dashed line)

Table 5.5 Laser-diffraction measured volumetric concentration and PSD

| Date and Time | Volu-metric Particle Concen-tration ul/L | *D10* microns | *D16* microns | *D50* microns | *D60* microns | *D84* microns |
|---|---|---|---|---|---|---|
| 8/28/2009 3:00 | 8.8 | 5 | 6 | 17 | 22 | 60 |
| 8/28/2009 5:00 | 8.3 | 5 | 7 | 18 | 24 | 114 |
| 8/28/2009 7:00 | 27.6 | 4 | 6 | 16 | 21 | 58 |
| 8/28/2009 11:00 | 49.0 | 5 | 6 | 19 | 25 | 66 |
| 8/28/2009 13:00 | 347.3 | 6 | 8 | 25 | 32 | 78 |
| 8/28/2009 15:00 | 287.8 | 6 | 9 | 26 | 35 | 85 |
| 8/28/2009 17:00 | 595.8 | 6 | 8 | 22 | 29 | 66 |
| 8/28/2009 19:00 | 528.6 | 6 | 8 | 23 | 30 | 72 |
| 8/28/2009 21:00 | 427.8 | 6 | 8 | 24 | 31 | 77 |
| 8/28/2009 23:00 | 349.4 | 6 | 8 | 24 | 32 | 81 |
| 8/29/2009 1:00 | 279.7 | 5 | 7 | 23 | 31 | 82 |
| 8/29/2009 3:00 | 281.7 | 6 | 8 | 24 | 32 | 85 |
| 8/29/2009 5:00 | 275.4 | 6 | 8 | 24 | 31 | 76 |
| 8/29/2009 7:00 | 234.4 | 5 | 7 | 23 | 31 | 80 |
| 8/29/2009 13:00 | 177.0 | 6 | 8 | 28 | 39 | 122 |
| 8/29/2009 15:00 | 147.8 | 6 | 8 | 28 | 40 | 137 |
| 8/29/2009 17:00 | 95.5 | 5 | 7 | 19 | 24 | 41 |
| 8/29/2009 19:00 | 124.7 | 6 | 9 | 29 | 42 | 144 |
| 8/29/2009 21:00 | 105.0 | 6 | 8 | 25 | 34 | 86 |
| 8/29/2009 23:00 | 89.3 | 6 | 7 | 22 | 28 | 58 |
| 8/30/2009 1:00 | 90.6 | 6 | 8 | 23 | 31 | 75 |
| 8/30/2009 3:00 | 91.6 | 6 | 8 | 25 | 34 | 95 |
| 8/30/2009 5:00 | 85.9 | 6 | 8 | 26 | 35 | 110 |
| 8/30/2009 7:00 | 71.5 | 6 | 8 | 23 | 30 | 71 |
| 8/30/2009 9:00 | 51.0 | 5 | 6 | 17 | 21 | 32 |
| 8/30/2009 11:00 | 65.4 | 6 | 8 | 23 | 32 | 97 |
| 3/10/10 13:00 | 17.1 | 5 | 7 | 20 | 26 | 63 |
| 3/10/10 15:00 | 40.5 | 5 | 7 | 19 | 25 | 52 |
| 3/10/10 17:00 | 75.1 | 5 | 7 | 19 | 25 | 55 |
| 3/10/10 19:00 | 42.2 | 5 | 6 | 18 | 23 | 52 |
| 3/10/10 21:00 | 50.1 | 5 | 6 | 19 | 25 | 61 |
| 3/10/10 23:00 | 92.0 | 5 | 6 | 18 | 23 | 60 |
| 3/11/10 1:00 | 122.9 | 5 | 6 | 17 | 23 | 59 |
| 3/11/10 3:00 | 134.6 | 5 | 6 | 19 | 25 | 67 |
| 3/11/10 5:00 | 111.3 | 4 | 6 | 17 | 23 | 61 |
| 3/11/10 7:00 | 123.2 | 5 | 6 | 17 | 22 | 56 |
| 3/11/10 9:00 | 143.3 | 5 | 6 | 17 | 22 | 61 |
| 3/11/10 11:00 | 125.6 | 4 | 6 | 16 | 21 | 56 |

Table 5.5 (continued) Laser-diffraction measured volumetric concentration and PSD

| Date and Time | Volu-metric Particle Concen-tration ul/L | *D10* microns | *D16* microns | *D50* microns | *D60* microns | *D84* microns |
|---|---|---|---|---|---|---|
| 3/11/10 11:00 | 125.6 | 4 | 6 | 16 | 21 | 56 |
| 3/11/10 13:00 | 100.8 | 4 | 5 | 16 | 21 | 53 |
| 3/11/10 15:00 | 92.4 | 4 | 5 | 16 | 22 | 60 |
| 3/11/10 17:00 | 81.4 | 4 | 6 | 17 | 23 | 63 |
| 3/11/10 19:00 | 66.6 | 4 | 5 | 16 | 22 | 59 |
| 3/11/10 21:00 | 57.7 | 4 | 5 | 16 | 23 | 63 |
| 3/11/10 23:00 | 51.0 | 4 | 5 | 16 | 23 | 63 |
| 3/12/10 1:00 | 52.4 | 4 | 6 | 19 | 27 | 80 |
| 3/12/10 3:00 | 42.0 | 4 | 5 | 15 | 21 | 57 |
| 3/12/10 5:00 | 40.8 | 4 | 5 | 16 | 22 | 63 |
| 3/12/10 7:00 | 42.7 | 4 | 5 | 17 | 24 | 67 |
| 3/12/10 9:00 | 39.9 | 4 | 5 | 16 | 22 | 57 |
| 3/12/10 11:00 | 40.1 | 4 | 6 | 17 | 23 | 62 |
| 3/12/10 15:00 | 37.7 | 4 | 5 | 17 | 23 | 56 |
| 3/12/10 17:00 | 36.6 | 4 | 5 | 16 | 22 | 58 |
| 3/12/10 19:00 | 38.7 | 4 | 5 | 15 | 21 | 52 |
| 3/12/10 21:00 | 35.9 | 4 | 5 | 16 | 21 | 58 |
| 3/12/10 23:00 | 34.1 | 4 | 5 | 16 | 21 | 55 |
| 3/13/10 1:00 | 42.4 | 4 | 5 | | | |
| 3/13/10 3:00 | 36.1 | 4 | 6 | 17 | 24 | 77 |
| 3/13/10 5:00 | 35.6 | 4 | 6 | 17 | 24 | 80 |
| 3/13/10 7:00 | 38.5 | 5 | 6 | 21 | 30 | 123 |
| 3/13/10 9:00 | 38.1 | 5 | 6 | 19 | 28 | 108 |
| 3/13/10 11:00 | 34.5 | 4 | 6 | 16 | 22 | 59 |
| 3/13/10 13:00 | 33.0 | 4 | 6 | 16 | 22 | 55 |
| 3/13/10 15:00 | 32.7 | 4 | 6 | 16 | 22 | 57 |
| 3/13/10 17:00 | 31.8 | 4 | 6 | 16 | 22 | 57 |
| 3/13/10 19:00 | 32.8 | 4 | 6 | 18 | 24 | 75 |
| 3/13/10 21:00 | 34.6 | 5 | 6 | | | |
| 3/13/10 23:00 | 32.8 | 5 | 6 | 19 | 27 | 102 |
| 3/14/10 1:00 | 31.2 | 4 | 6 | 18 | 26 | 94 |
| 3/14/10 3:00 | 31.2 | 5 | 6 | 20 | 28 | 109 |
| 3/14/10 5:00 | 29.4 | 5 | 6 | 19 | 28 | 111 |
| 3/14/10 7:00 | 26.6 | 5 | 6 | 18 | 26 | 94 |
| 3/14/10 9:00 | 26.1 | 5 | 6 | 19 | 26 | 103 |
| 3/14/10 11:00 | 22.5 | 4 | 6 | 16 | 22 | 66 |
| 3/14/10 13:00 | 19.9 | 4 | 5 | 15 | 21 | 54 |

Table 5.5 (continued) Laser-diffraction measured volumetric concentration and PSD

| Date and Time | Volu-metric Particle Concen-tration ul/L | *D10* microns | *D16* microns | *D50* microns | *D60* microns | *D84* microns |
|---|---|---|---|---|---|---|
| 4/24/10 14:00 | 19.2 | 5 | 7 | 21 | 27 | |
| 4/24/10 16:00 | 41.4 | 6 | 8 | 21 | 27 | 58 |
| 4/24/10 18:00 | 128.4 | 7 | 9 | 24 | 31 | 67 |
| 4/24/10 20:00 | 93.5 | 6 | 8 | 22 | 29 | 65 |
| 4/24/10 22:00 | 90.3 | 6 | 8 | 22 | 29 | 70 |
| 4/25/10 0:00 | | | | | | |
| 4/25/10 2:00 | 125.1 | 5 | 6 | 19 | 26 | 68 |
| 4/25/10 4:00 | 134.1 | 5 | 7 | 22 | 28 | 68 |
| 4/25/10 6:00 | 175.4 | 6 | 8 | 22 | 28 | 63 |
| 4/25/10 8:00 | 191.8 | 6 | 8 | 26 | 35 | 85 |
| 4/25/10 10:00 | 173.5 | 6 | 7 | 24 | 33 | 72 |
| 4/25/10 12:00 | 200.6 | 6 | 8 | 21 | 27 | 60 |
| 4/25/10 14:00 | 201.5 | 6 | 7 | 20 | 25 | 53 |
| 4/25/10 16:00 | 173.9 | 5 | 7 | 20 | 25 | 54 |
| 4/25/10 18:00 | 141.9 | 5 | 7 | 21 | 28 | 65 |
| 4/25/10 20:00 | 110.6 | 5 | 7 | 20 | 25 | 55 |
| 4/25/10 22:00 | 96.4 | 5 | 7 | 20 | 25 | 60 |
| 4/26/10 0:00 | 80.8 | 5 | 7 | 19 | 25 | 58 |
| 4/26/10 2:00 | 74.1 | 5 | 7 | 20 | 27 | 70 |
| 4/26/10 6:00 | 61.0 | 6 | 7 | 21 | 27 | 71 |
| 4/26/10 8:00 | 54.1 | 6 | 7 | 20 | 26 | 64 |
| 4/26/10 10:00 | 45.8 | 5 | 7 | 19 | 24 | 51 |
| 4/26/10 12:00 | 39.0 | 5 | 7 | 19 | 24 | 53 |
| 4/26/10 14:00 | 34.7 | 5 | 7 | 19 | 25 | 52 |
| 4/26/10 16:00 | 29.4 | 5 | 7 | 18 | 23 | 47 |
| 4/26/10 18:00 | 27.1 | 5 | 7 | 18 | 23 | 47 |
| 4/26/10 20:00 | 25.3 | 5 | 7 | 18 | 23 | 47 |
| 4/26/10 22:00 | 24.1 | 5 | 7 | 18 | 24 | 50 |
| 4/27/10 0:00 | 24.1 | 5 | 7 | 19 | 24 | 55 |
| 4/27/10 2:00 | 24.0 | 5 | 7 | 21 | 27 | 66 |
| 4/27/10 4:00 | 23.1 | 5 | 7 | 20 | 26 | 64 |
| 5/3/2010 4:00 | 9.2 | 5 | 6 | 15 | 19 | 37 |
| 5/3/2010 6:00 | 15.6 | 5 | 6 | 16 | 20 | 38 |
| 5/3/2010 8:00 | 33.9 | 5 | 6 | 16 | 21 | 43 |
| 5/3/2010 10:00 | 128.5 | 5 | 7 | 20 | 25 | 54 |
| 5/3/2010 12:00 | 231.3 | 6 | 7 | 23 | 30 | 78 |
| 5/3/2010 14:00 | 319.7 | 5 | 7 | 21 | 28 | 66 |

Table 5.5 (continued) Laser-diffraction measured volumetric concentration and PSD

| Date and Time | Volu-metric Particle Concen-tration ul/L | *D10* microns | *D16* microns | *D50* microns | *D60* microns | *D84* microns |
|---|---|---|---|---|---|---|
| 5/3/2010 16:00 | 368.6 | 4 | 5 | 18 | 26 | 80 |
| 5/3/2010 18:00 | 289.9 | 4 | 5 | 19 | 29 | 85 |
| 5/3/2010 20:00 | 255.1 | 4 | 5 | 18 | 26 | 91 |
| 5/3/2010 22:00 | 205.7 | 4 | 5 | 16 | 23 | 66 |
| 5/4/2010 0:00 | 154.9 | 3 | 5 | | | |
| 5/4/2010 2:00 | 123.2 | 4 | 5 | 14 | 19 | 51 |
| 5/4/2010 4:00 | 74.4 | 3 | 4 | 10 | 14 | 65 |
| 5/4/2010 6:00 | 59.1 | 2 | 3 | 8 | 10 | 30 |
| 5/4/2010 8:00 | 91.6 | 3 | 4 | 14 | 20 | 70 |
| 5/4/2010 10:00 | 85.7 | 3 | 4 | 13 | 18 | 50 |
| 5/4/2010 12:00 | 71.0 | 3 | 4 | 12 | 17 | 98 |
| 5/4/2010 16:00 | 83.7 | 3 | 5 | 19 | 30 | 141 |
| 5/4/2010 18:00 | 69.3 | 3 | 5 | 16 | 25 | 123 |
| 5/4/2010 20:00 | 63.2 | 3 | 5 | 16 | 24 | 132 |
| 5/5/2010 0:00 | 43.8 | 3 | 4 | | | |
| 5/5/2010 2:00 | 69.4 | 4 | 7 | | | |
| 5/5/2010 4:00 | 30.8 | 3 | 4 | 11 | 16 | 82 |
| 5/5/2010 6:00 | 50.6 | 4 | 5 | 19 | 29 | 138 |
| 5/5/2010 8:00 | 47.7 | 4 | 5 | 15 | 21 | 74 |
| 5/5/2010 10:00 | 59.7 | 4 | 5 | | | |
| 5/5/2010 20:00 | 66.4 | 5 | 6 | 19 | 25 | 90 |
| 5/5/2010 22:00 | 60.4 | 5 | 6 | 17 | 23 | 59 |
| 5/6/2010 0:00 | 56.2 | 5 | 6 | 17 | 22 | 52 |
| 9/27/2010 15:00 | 56.5 | 6 | 7 | 20 | 26 | 59 |
| 9/27/2010 16:00 | 54.5 | 5 | 6 | 17 | 22 | 50 |
| 9/27/2010 17:00 | 45.7 | 5 | 6 | 16 | 21 | 47 |
| 9/27/2010 18:00 | 37.3 | 5 | 6 | 15 | 19 | 41 |
| 9/27/2010 19:00 | 35.9 | 5 | 6 | 16 | 21 | 49 |
| 9/27/2010 20:00 | 29.7 | 5 | 6 | 15 | 19 | 42 |
| 9/27/2010 21:00 | 33.9 | 5 | 6 | 16 | 22 | 56 |
| 9/27/2010 22:00 | 31.9 | 5 | 6 | 17 | 22 | 63 |
| 9/27/2010 23:00 | 33.3 | 5 | 6 | 16 | 22 | 59 |
| 9/28/2010 0:00 | 30.1 | 5 | 6 | 17 | 22 | 70 |
| 9/28/2010 1:00 | 30.3 | 5 | 6 | 16 | 21 | 59 |
| 9/28/2010 2:00 | 32.0 | 5 | 6 | 17 | 23 | 73 |
| 9/28/2010 3:00 | 28.4 | 5 | 6 | 17 | 23 | 80 |
| 9/28/2010 4:00 | 27.7 | 5 | 6 | 18 | 24 | 124 |

Table 5.5 (continued) Laser-diffraction measured volumetric concentration and PSD

| Date and Time | Volu-metric Particle Concen-tration ul/L | *D10* microns | *D16* microns | *D50* microns | *D60* microns | *D84* microns |
|---|---|---|---|---|---|---|
| 9/28/2010 5:00 | 28.6 | 5 | 6 | 18 | 24 | 107 |
| 9/28/2010 6:00 | 28.6 | 5 | 6 | 17 | 23 | 82 |
| 9/28/2010 7:00 | 28.8 | 5 | 6 | 17 | 24 | 105 |
| 9/28/2010 8:00 | 28.9 | 5 | 6 | 19 | 26 | 154 |
| 9/28/2010 9:00 | 26.8 | 5 | 6 | 17 | 23 | 84 |
| 9/28/2010 10:00 | 22.7 | 5 | 6 | 14 | 18 | 41 |
| 9/28/2010 11:00 | 22.7 | 4 | 5 | 13 | 16 | 34 |
| 9/28/2010 12:00 | 22.2 | 4 | 5 | 13 | 17 | 36 |
| 9/28/2010 13:00 | 27.1 | 5 | 5 | 14 | 18 | 37 |
| 9/28/2010 14:00 | 29.1 | 5 | 6 | 15 | 19 | 42 |
| 9/28/2010 15:00 | 37.3 | 5 | 6 | 16 | 21 | 54 |
| 9/28/2010 16:00 | 36.5 | 5 | 6 | 16 | 21 | 52 |
| 9/28/2010 17:00 | 40.3 | 5 | 6 | 16 | 21 | 53 |
| 9/28/2010 18:00 | 37.1 | 5 | 6 | 15 | 19 | 42 |
| 9/28/2010 19:00 | 35.4 | 5 | 6 | 15 | 20 | 49 |
| 9/28/2010 20:00 | 35.5 | 5 | 6 | 15 | 19 | 42 |
| 9/28/2010 21:00 | 33.2 | 5 | 6 | 15 | 20 | 46 |
| 9/28/2010 22:00 | 32.4 | 5 | 6 | 15 | 20 | 51 |
| 9/28/2010 23:00 | 32.5 | 5 | 6 | 15 | 20 | 50 |
| 9/29/2010 0:00 | 29.9 | 5 | 6 | 15 | 19 | 48 |
| 9/29/2010 1:00 | 30.6 | 5 | 6 | 16 | 21 | 60 |
| 9/29/2010 2:00 | 28.3 | 5 | 6 | 16 | 21 | 70 |
| 9/29/2010 3:00 | 28.4 | 5 | 6 | 16 | 22 | 79 |
| 9/29/2010 4:00 | 28.7 | 5 | 6 | 16 | 22 | 92 |
| 9/29/2010 5:00 | 26.1 | 5 | 6 | 16 | 21 | 79 |
| 9/29/2010 6:00 | 25.5 | 4 | 5 | 15 | 21 | 85 |
| 9/29/2010 8:00 | 25.9 | 4 | 6 | | | |
| 9/29/2010 9:00 | 23.0 | 4 | 5 | 15 | 21 | |
| 9/29/2010 10:00 | 18.3 | 4 | 5 | 11 | 15 | 32 |
| 9/29/2010 11:00 | 16.2 | 3 | 4 | 11 | 14 | 26 |
| 9/29/2010 12:00 | 14.3 | 3 | 4 | 10 | 13 | 26 |
| 9/29/2010 13:00 | 19.6 | 4 | 5 | 11 | 14 | 26 |
| 9/29/2010 14:00 | 13.9 | 4 | 5 | 11 | 14 | 26 |
| 9/29/2010 16:00 | 13.7 | 4 | 5 | 11 | 14 | 28 |
| 9/29/2010 18:00 | 12.9 | 4 | 5 | 11 | 13 | 25 |
| 9/30/2010 16:00 | 15.4 | 4 | 5 | 11 | 15 | 29 |
| 9/30/2010 18:00 | 30.9 | 4 | 5 | 13 | 17 | 34 |
| 9/30/2010 20:00 | 36.3 | 4 | 5 | 14 | 18 | 40 |

Table 5.5 (continued) Laser-diffraction measured volumetric concentration and PSD

| Date and Time | Volu-metric Particle Concen-tration ul/L | *D10* microns | *D16* microns | *D50* microns | *D60* microns | *D84* microns |
|---|---|---|---|---|---|---|
| 9/30/2010 22:00 | 52.3 | 3 | 3 | 9 | 11 | 27 |
| 10/1/2010 0:00 | 49.9 | 3 | 4 | 11 | 15 | 39 |
| 10/1/2010 2:00 | 40.4 | 4 | 5 | 14 | 19 | 63 |
| 10/1/2010 4:00 | 36.5 | 5 | 6 | 15 | 20 | 68 |
| 10/1/2010 6:00 | 31.6 | 5 | 6 | 15 | 20 | 75 |
| 10/1/2010 8:00 | 28.9 | 5 | 6 | 16 | 23 | 158 |
| 10/1/2010 10:00 | 20.4 | 4 | 5 | 12 | 16 | 34 |
| 10/1/2010 12:00 | 16.1 | 4 | 5 | 11 | 15 | 28 |

### *5.4.2 Volumetric Particle Size Distribution*

The time series of volumetric PSD are shown for each sampled event in figures 5.24 to 5.28. Some of the volumetric PSD measurements have been filtered out because of errors typically associated with the presence of bubbles in the sample flow. The particle sizes for which 10, 16, 50, 60, and 84 percent of the total volume is finer by volume (*D10*, *D16*, *D50*, *D60*, and *D84*), for the measured range between 2 and 381 microns, are shown for the concurrent measurement periods in table 5.5. In figures 5.24 to 5.28 some variation in PSD is evident within and between events. As discussed in the results, relatively small changes in the PSD are significant to the relation of $SSC_{XS}$ to *VPC*, and of $SSC_{XS}$ to turbidity.

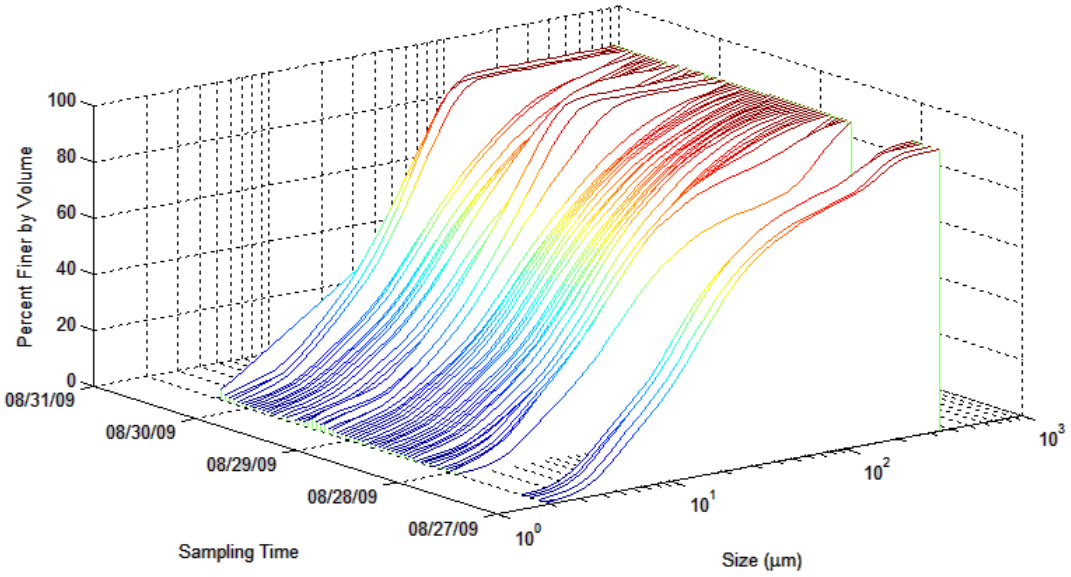


Figure 5.24– Time series of volumetric PSD from LISST-SS laser-diffraction analyzer for August 2009 event

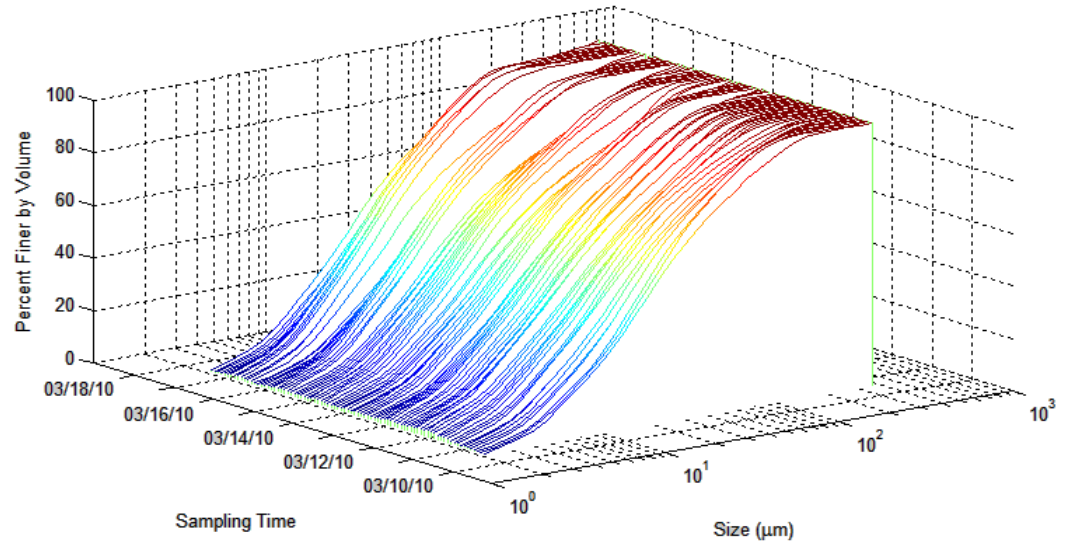


Figure 5.25– Time series of volumetric PSD from LISST-SS laser-diffraction analyzer for March, 2010 event

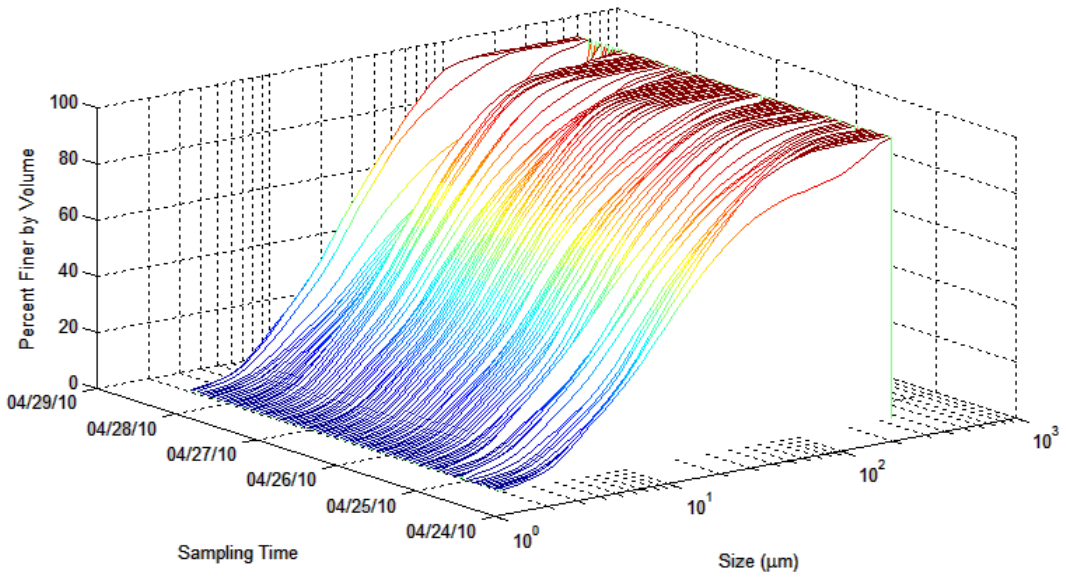


Figure 5.26 – Time series of volumetric PSD from LISST-SS laser-diffraction analyzer for April, 2010 event

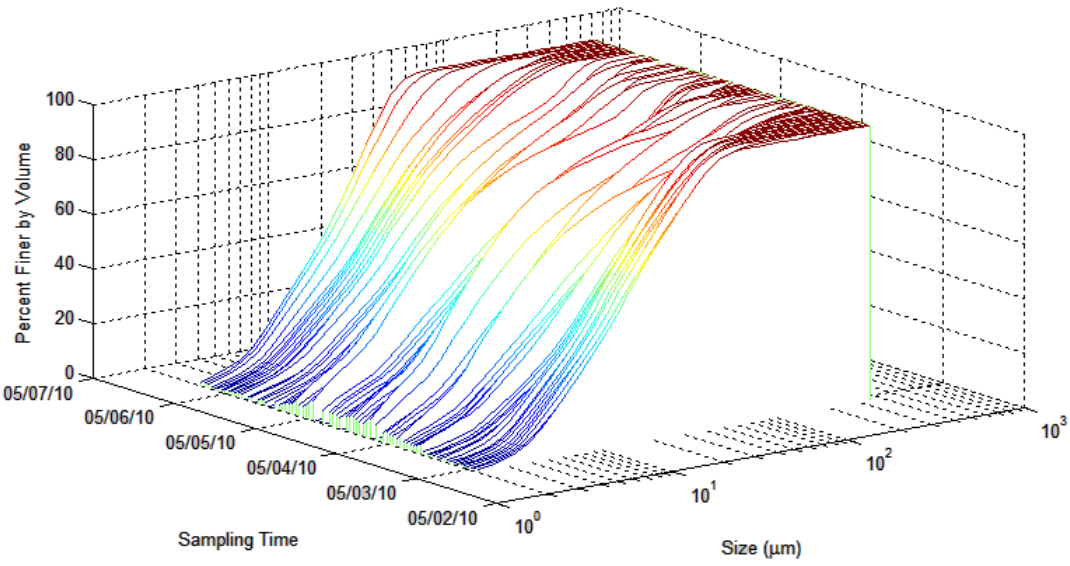


Figure 5.27 – Time series of volumetric PSD from LISST-SS laser-diffraction analyzer for May, 2010 event

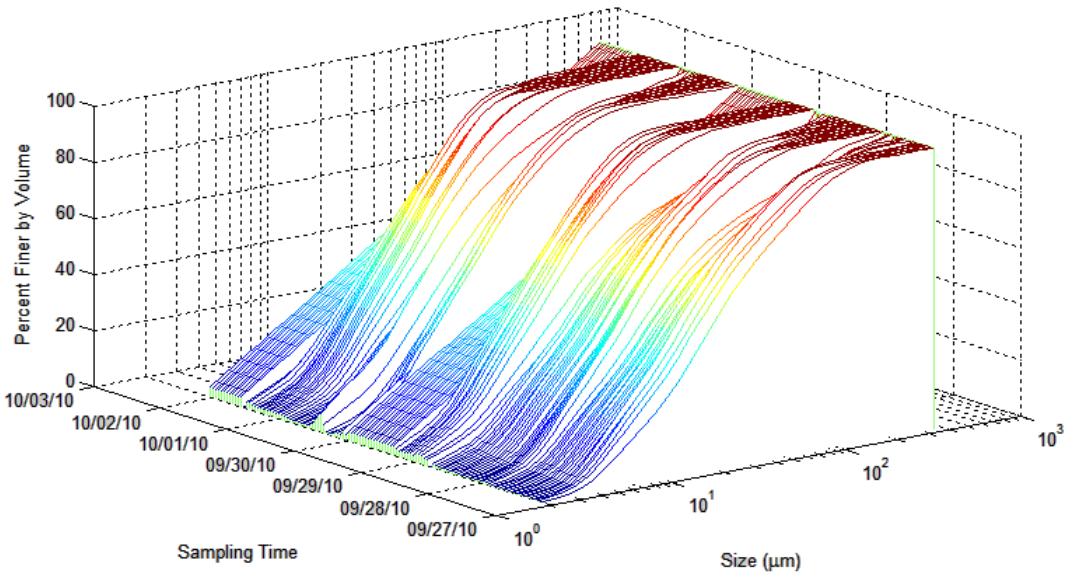


Figure 5.28 – Time series of volumetric PSD from LISST-SS laser-diffraction analyzer for September, 2010 event

### *5.4.3 Comparison of Volumetric and Mass PSD*

The PSD reported for a sediment sample always depends on the method of PSD analysis, so it is a “methods based result”. However, this does not mean that results from different methods cannot or should not be quantitatively comparable. This is particularly important as more volumetric PSD data are collected with increasing use of LISST devices, and as constituent loads are increasingly estimated using turbidity which is strongly affected by PSD. Understanding how and why PSD results are different for different methods is essential for comparability of data, for traceability when methods change, and for helping understand why surrogate methods with size-concentration ambiguity behave as they do for a specific stream.

In-situ PSD will typically be different than laboratory, or even streamside-analyzed PSD. In the case of laboratory PSD by settling velocities, typically dispersants are used that can affect colloidal size materials and create significant changes relative to in-situ PSD. The LISST-Streamside PSD results also may differ from in-situ PSD because of the effects of non-isokinetic-pumping plus mechanical disturbance of the sample.

Differences may also occur because of different analytical PSD size limits. Mass PSD ($PSD_{mass}$) is analyzed by USGS laboratories using wet sieve methods for particle sizes larger than 62.5 microns, and fall-velocity methods for particles smaller than 62.5 microns (diameter of a spherical particle having the same fall velocity as that measured in a pipette in the lab). The minimum fall diameter reported is 2 microns, and the mass (or percent of total mass) finer than this size is reported. Thus, the total mass is included in the PSD even though the smallest size class is less than 2 microns. The LISST technology measures the angles of light scattering by individual particles to obtain volumetric PSD ($PSD_{vol}$)over a fixed range from 2 to 381 microns, as described previously (section 2.3.2). If all of the environmental suspended sediment sample were between 2 and 381 microns, and there were no changes in density for the particle sizes within the sample, then $PSD_{mass}$ and $PSD_{vol}$ should be equal.

The median percent finer than 2 microns for this site is 35%, and the interquartile range is from 31% to 41%, based on 13 full $PSD_{mass}$ analyses. (Note, most of these were flagged as having insufficient mass; but they all agree reasonably well). This causes large differences in laser-diffraction-based $PSD_{vol}$ versus $PSD_{mass}$ from depth-integrated samples, as indicated in figures 5.29 to 5.31. Another cause of differences in these PSDs are the pumped versus EWI location and methods (discussed in section 5.2.3).

In this study, a simple method was developed to adjust $PSD_{vol}$ to equivalent $PSD_{mass}$ for comparative purposes only. The method adjusts the $PSD_{vol}$ for the unmeasured size fractions, based on the results of the $PSD_{mass}$ results. For example, for the April 2010 event, an average of 34 percent of the $PSD_{mass}$ was finer than 2 microns; while an average of 15 percent was larger than about 381 microns. The portion of the sample unmeasured by $PSD_{vol}$ was then about 49 percent by mass. In this method, the $PSD_{vol}$ data were multiplied by 0.51 (the 'measured' fraction) and then the 2 micron fraction of 34 percent (from $PSD_{mass}$) was added to all values. The resulting adjusted $\mathbf{PSD_{vol}}$ shown in figure 5.31 are roughly comparable with the $PSD_{mass}$ results. The difference between the laser-diffraction measured $\mathbf{PSD_{vol}}$ and concurrent $PSD_{mass}$ results is due to the size limitations. It does not apparently provide an explanation for the discrepancy between the LISST-Streamside measured *VPC* (as used here) and actual volumetric particle concentration. This is described further in chapter 7. For the purposes of further analysis in this study, the unadjusted $PSD_{vol}$ data are used, as they clearly provide a quantitative, relative measure of changes in sediment PSD over the events.

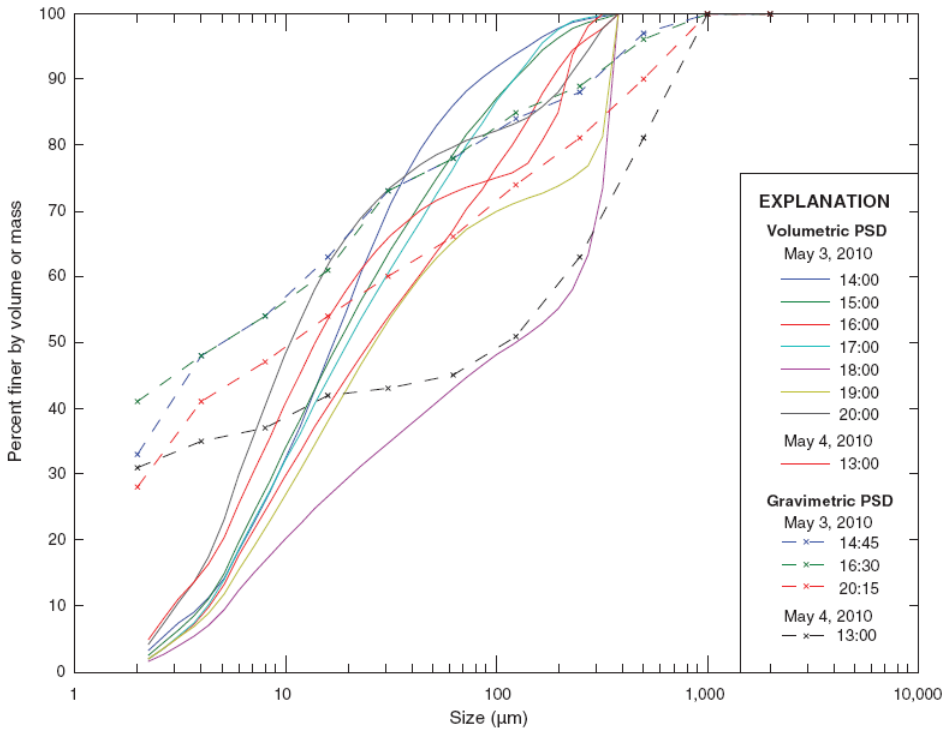


Figure 5.29 – Laser-diffraction volumetric and physical sample gravimetric particle size distributions, Yellow River at Gees Mill Road, May 3-4, 2010.

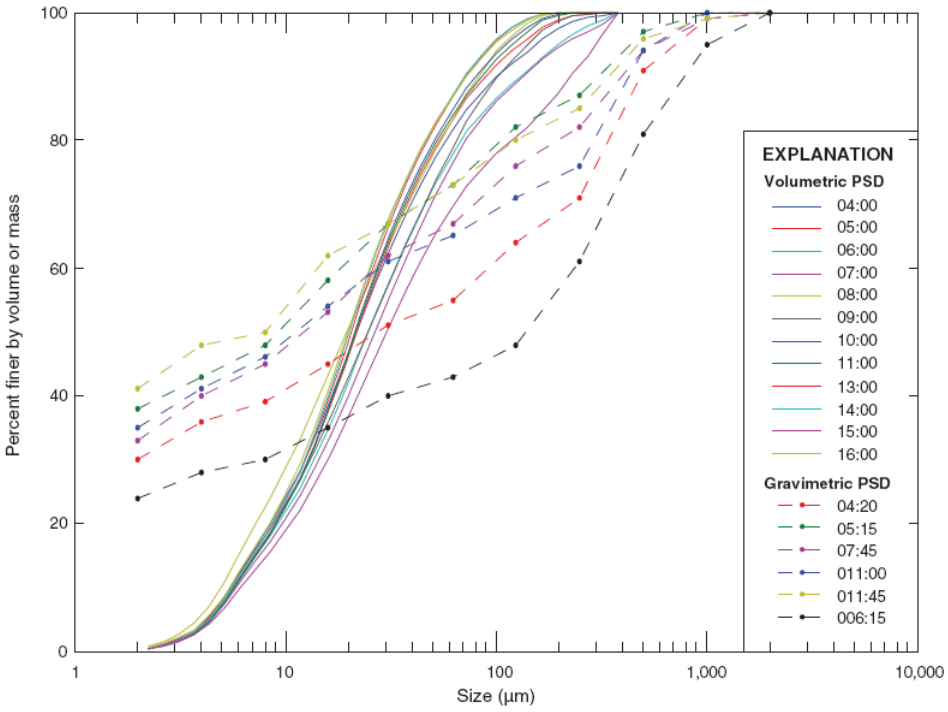


Figure 5.30 - Laser-diffraction volumetric and physical sample gravimetric particle size distributions, Yellow River at Gees Mill Road, April 25, 2010

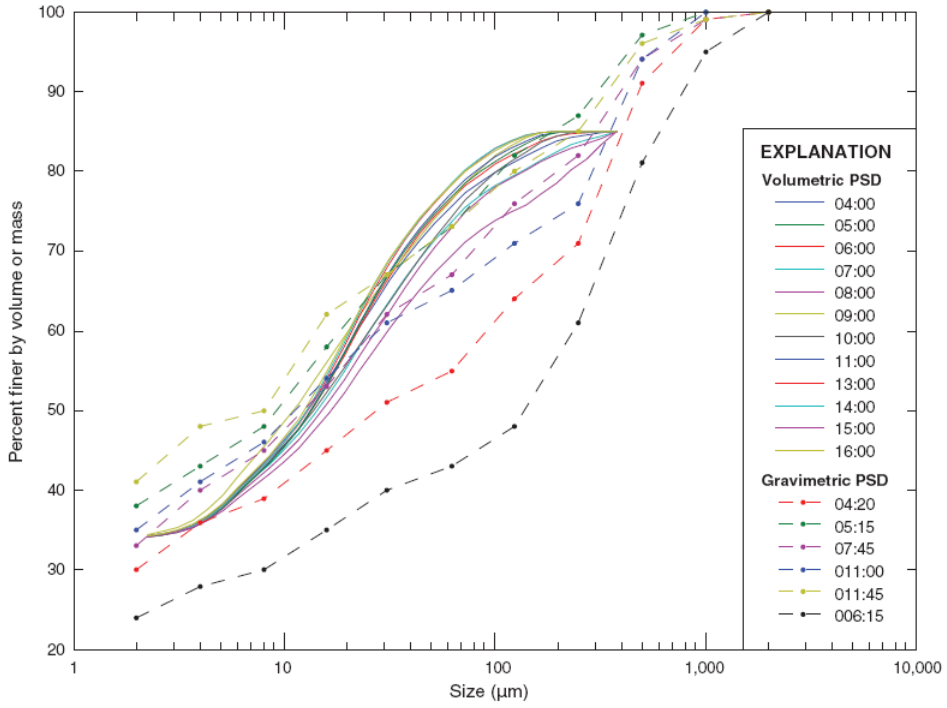


Figure 5.31 – Adjusted laser-diffraction volumetric and physical sample gravimetric particle size distributions, Yellow River at Gees Mill Road April 25, 2010

## 5.5 Acoustic Backscatter Data Summary

Acoustic backscatter is measured by acoustic velocity meters as a data quality indicator, because accurate velocity measurement is possible only when the measured backscatter signal is significantly greater than the ambient acoustic noise. Acoustic backscatter is affected by characteristics of the instrument, suspended sediment, fluid, and two-way distance from the transducer to the ensonified volume, as discussed in the literature review. Variation in acoustic backscatter over an event for a given frequency instrument is due primarily to changes in sediment concentration and size characteristics. The measured acoustic backscatter intensity is referred to here as reverberation level (RL), after Urick (1975), as discussed previously.

As with velocity data, *RL* data were stored at 15 minute intervals for each cell of the horizontal profile for each beam of each ADCP. The *RL* values from the two beams at each point in the profile were not significantly different, and thus were averaged for each instrument to create a single profile of *RL* values for each time step for each ADCP.

As noted in the velocity data summary, the August 2009 event data were corrupted by debris caught on the bridge pier in the acoustic path of the ADCPs. After extensive efforts to correct these data, they were determined to be unusable for the August 2009 event. During the May 2010 flow event, the 1.2MHz RDI ADCP was not recording because the memory card was full. After this event, the memory was cleared and the unit performed as before.

The raw *RL* data in decibels are shown for selected cells in the horizontal profile for the 1.2, 1.5, and 3.0 MHz side-looking ADCPs in figures 5.32 to 5.42. The *RL* is lower for the more distant cells because *RL* decreases with distance from the transceiver due to

simple signal spreading. The complexity of the relation of *RL* to $SSC_{XS}$ is apparent by comparing the *RL* and $SSC_{XS}$ time series. Raw *RL* does not necessarily correlate with SSC because of the offsetting effects of increased acoustic scatter and increased acoustic attenuation with increased $SSC_{XS}$; and possibly because of the effects of changing PSD on these metrics. In chapter 8, the raw *RL* data are used to compute the acoustic attenuation and relative backscatter, adjusted for signal spreading and attenuation due to fluid and sediment properties.

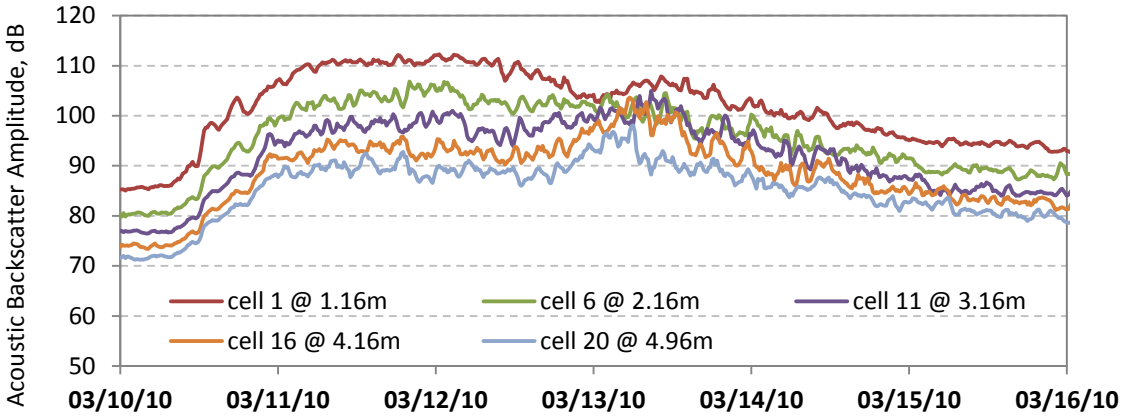


Figure 5.32 - Acoustic backscatter amplitude, average of beams one and two, 1.2MHz instrument, for cells 1, 6, 11, 16, and 20, March 10-15, 2010.

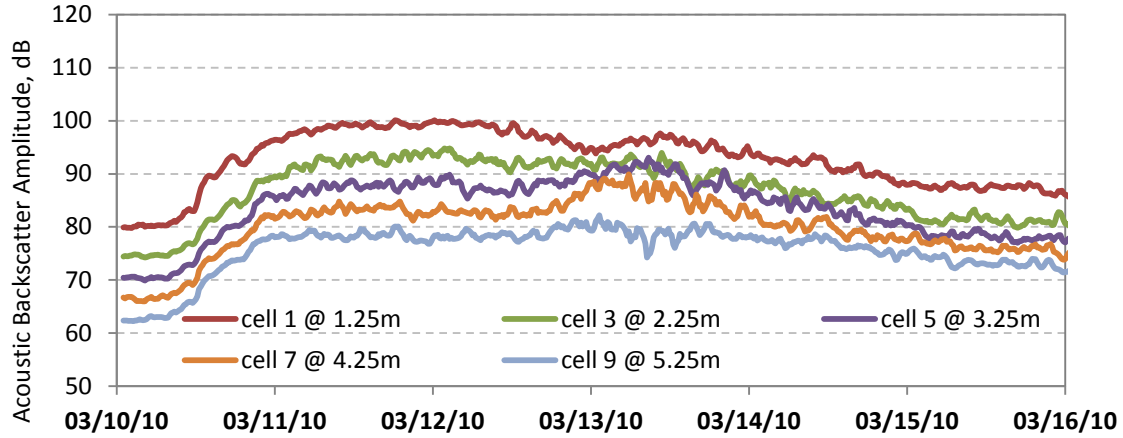


Figure 5.33 - Acoustic backscatter amplitude, average of beams one and two, 1.5MHz instrument, for cells 1, 3, 5, 7, and 9, March 10-15, 2010.

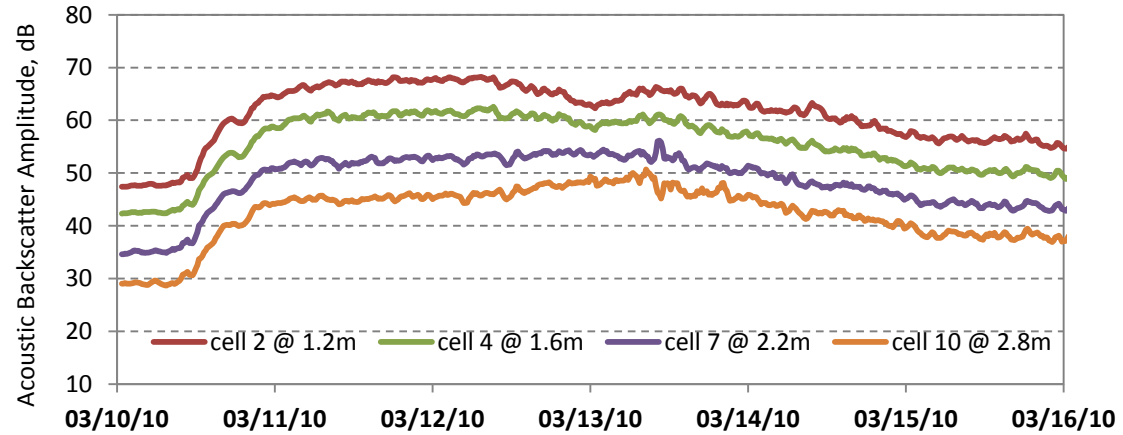


Figure 5.34 - Acoustic backscatter amplitude, average of beams one and two, 3.0MHz instrument, for cells 2, 4, 7, and 10, March 10-15, 2010.

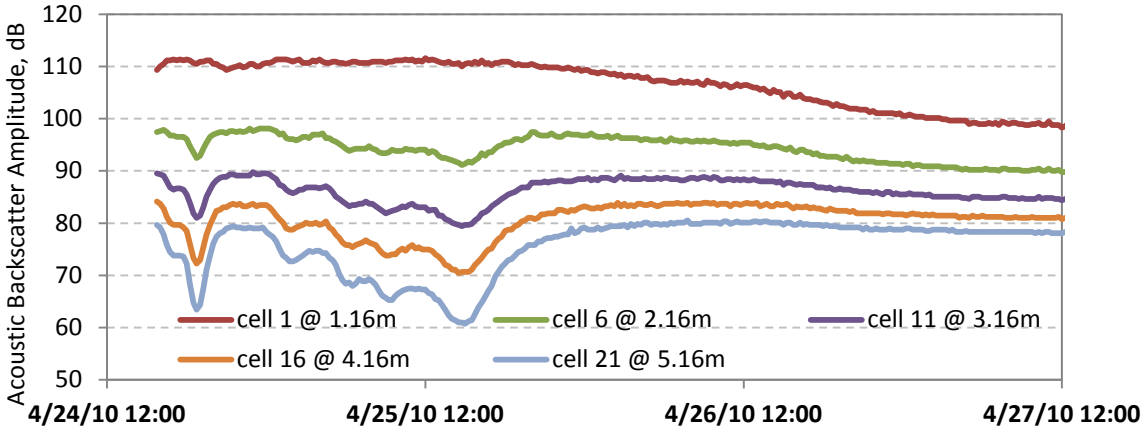


Figure 5.35 - Acoustic backscatter amplitude, average of beams one and two, for 1.2MHz instrument, for cells 1, 6, 11, 16, and 21, April 24-27, 2010.

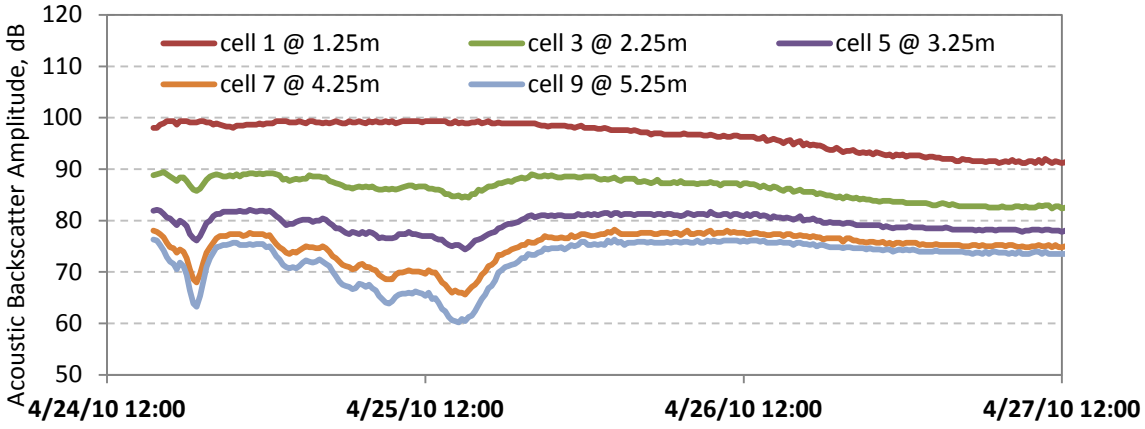


Figure 5.36 - Acoustic backscatter amplitude, average of beams one and two, for 1.5MHz instrument, for cells 1, 3, 5, 7, and 9, April 24-27, 2010.

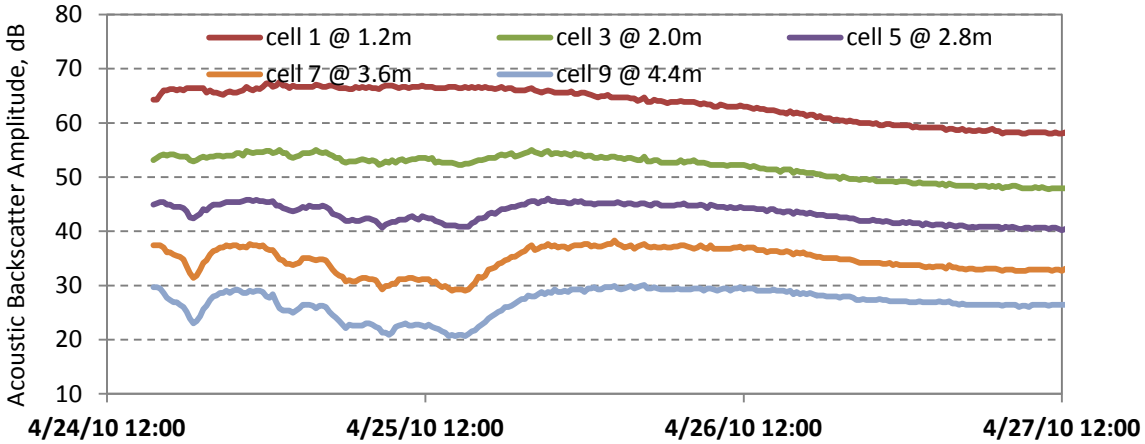


Figure 5.37 - Acoustic backscatter amplitude, average of beams one and two, for 3.0MHz instrument, for cells 1, 3, 5, 7, and 9, April 24-27, 2010.

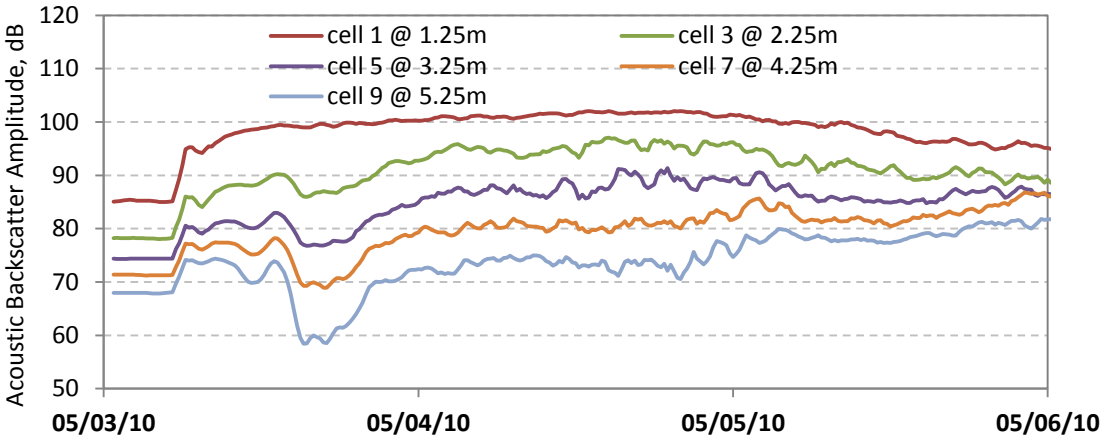


Figure 5.38- Acoustic backscatter amplitude, average of beams one and two, for 1.5MHz instrument, for cells 1, 3, 5, 7, and 9, May 3–5, 2010.

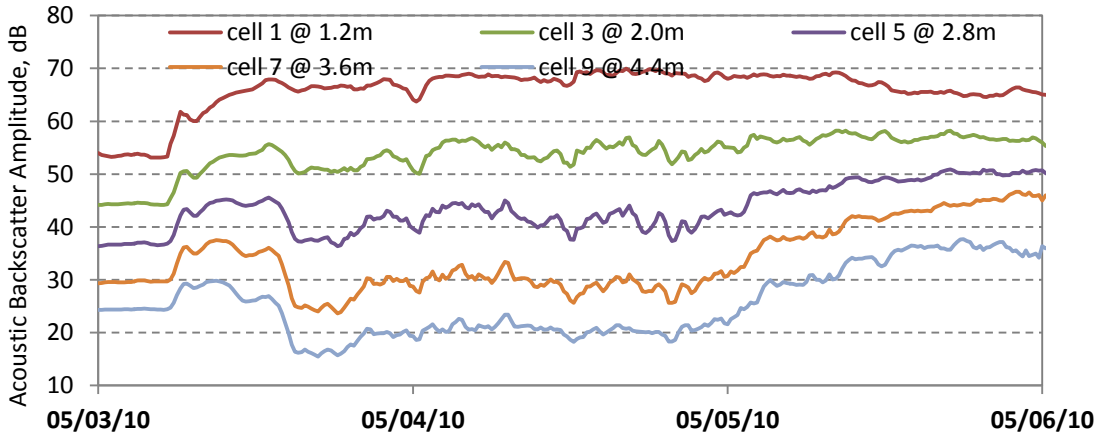


Figure 5.39 - Acoustic backscatter amplitude, average of beams one and two, for 3.0MHz instrument, for cells 1, 3, 5, 7, and 9, May3–5, 2010.

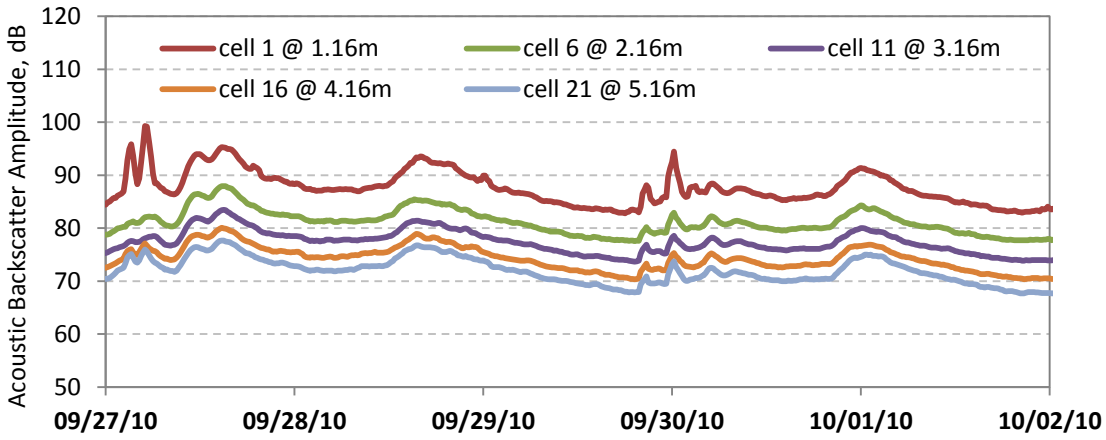


Figure 5.40 - Acoustic backscatter amplitude, average of beams one and two, 1.2MHz instrument, for cells 1, 6, 11, 16, and 21, Sep 27-Oct 1, 2010.

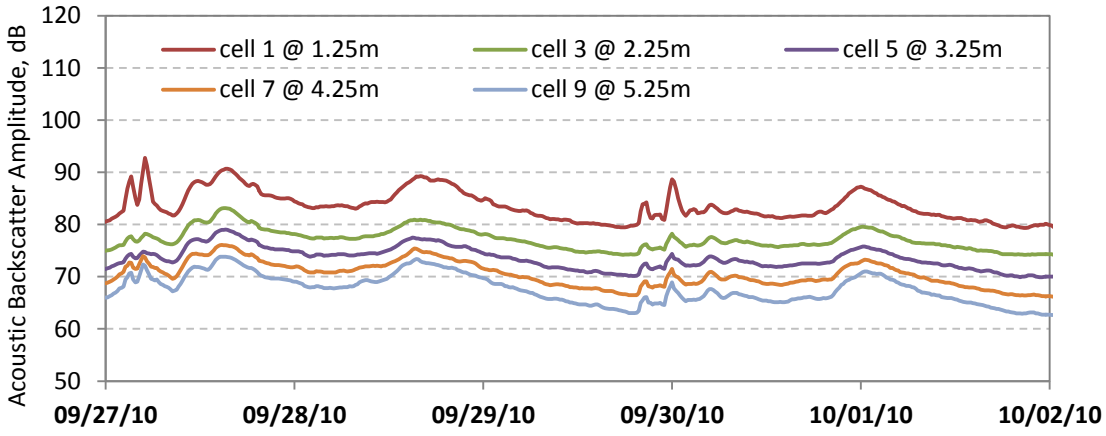


Figure 5.41 - Acoustic backscatter amplitude, average of beams one and two, 1.5MHz instrument, for cells 1, 3, 5, 7, and 9, for Sep 27-Oct 1, 2010.

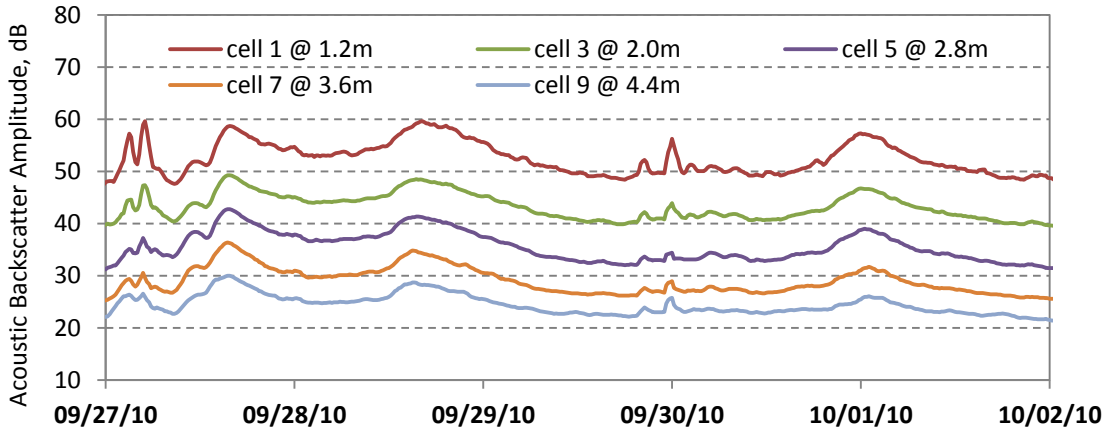


Figure 5.42 - Acoustic backscatter amplitude, average of beams one and two, 3.0MHz instrument, for cells 1, 3, 5, 7, and 9, Sep 27-Oct 1, 2010.

# 6 Suspended Sediment Characteristics from Turbidity as a Surrogate

Turbidity is widely used as a sediment surrogate to estimate suspended sediment concentration and load with typically greater accuracy, much higher temporal resolution, and potentially lower cost than traditional SSC~Q rating curve methods. Turbidity (*T*) is known to be affected by several parameters, particularly sediment size, in addition to SSC; but those parameters are typically assumed to be stable during runoff events and for a site specific SSC~T rating (Lewis 1996; Rasmussen et al. 2009; Loperfido, et al., 2010). One of the major findings of this study as described in this chapter is that hysteresis in SSC~T ratings is quantifiable and significant; it is shown to be related to changing sediment PSD, and indicative of sediment transport processes in the watershed. This section describes the measured occurrence, causes, and effects on computed sediment load of SSC~T hysteresis for the five storm events measured in 2009-2010.

## 6.1 SSC – Turbidity Hysteresis Background

Hysteresis in the relation of suspended sediment concentration (SSC) to fluvial discharge (Q) for single storm events is a well documented source of the uncertainty in SSC~Q rating curves (Walling, 1977; Wood, 1977; Williams, 1989), which is a primary reason for the increasing use of sediment surrogates such as turbidity. Hysteresis in SSC to turbidity relations (SSC~T) for single storm events is caused by factors distinct from SSC~Q hysteresis and has received almost no discussion, although it has been observed by a few authors (Gilvear and Petts, 1985; Lewis, 1996; Lenzi and Marchi, 2000; Minella et.al, 2008). Hysteresis produces uncertainty in the SSC~T rating curve,

but also may contain valuable information on hydrograph rise-to-recession changes in physical and(or) optical sediment characteristics. Evaluation of SSC~T hysteresis and isolation, to the extent possible, of its causes may explain uncertainty and provide qualitative or quantitative information on changing sediment characteristics over a runoff event, yielding another benefit of sediment surrogate metrics.

Hysteresis is evidenced graphically as a difference in the timing and(or) shape of the time series response of two variables, such as SSC and discharge. In a bivariate plot, hysteresis is indicated by a loop in the chronologically ordered data, as in the conceptual bivariate plots of figure 6.1. If two variables have a similar shaped, but non-synchronous time series, then it will produce ‘leading’, clockwise, or ‘trailing’, counterclockwise hysteresis. For example, in figure 6.1, the concentration peak leads the discharge peak and this produces clockwise SSC~Q hysteresis. Williams (1989) identified five classes of hysteresis in SSC~Q relations. In addition to leading and trailing hysteresis, Williams (1989) described how clockwise or counterclockwise hysteresis can occur where two variables have synchronous peaks, but different slopes with respect to time during the hydrograph rise or recession. Turbidity and SSC generally have near-synchronous peaks, but they will exhibit hysteresis if there is a consistent difference in the turbidity to SSC ratio between the SSC rise and the SSC recession. For example, in figure 6.1, the turbidity to SSC ratio is consistently higher on the recession than on the rise, producing clockwise hysteresis. In order to facilitate comparison of the shape of the time series data, the turbidity and concentration are plotted on separate scales in figure 5.21 and 6.1. The terminology in this paper for hysteresis of SSC~T will be consistent with traditional usage in reference to SSC~Q hysteresis. Thus, if the turbidity per unit concentration is consistently greater on the recession than on the rise, we refer to this as clockwise hysteresis.

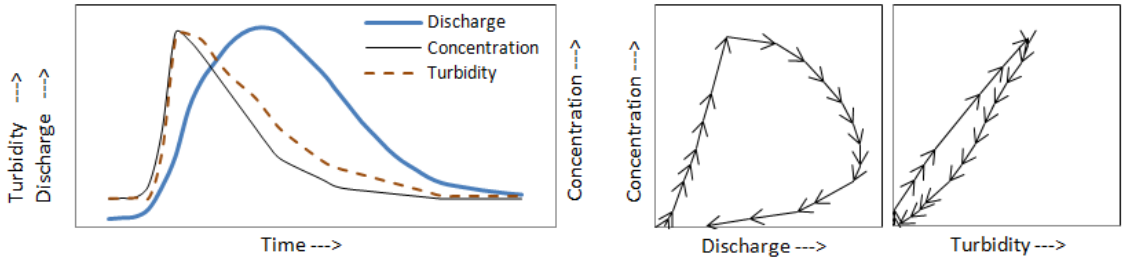


Figure 6.1 – Conceptual hysteresis due to differences in timing or shape of time series data (Note turbidity and concentration are conceptually shown on separate axes.)

Analysis of SSC~Q hysteresis has been used to evaluate uncertainty in sediment rating curves, and to evaluate watershed sediment transport characteristics (Walling, 1977; Wood, 1977; Lawler et al., 2006). The SSC~Q relation is determined by the sediment supply and the transport capacity of discharge; thus SSC~Q hysteresis provides information on these processes. Causes of SSC~Q hysteresis have been identified as early suspension of material deposited in the stream channel in prior event recessions; hillslope erosion and transport; changing ground water and throughflow hydrograph contributions; and the effects of main-stem backwater on tributary sediment flux (Wood, 1977; Williams, 1989; Howoritz, 2008). The SSC~Q relation typically exhibits clockwise hysteresis (center panel, figures 5.21 and 6.1) which is often ascribed to resuspension on the event rise of sediment stored in the stream channel, and to relatively limited sediment supply on the event recession. Lagging SSC~Q hysteresis, in which the SSC peak occurs after the Q peak, may indicate an influx of sediment during the discharge recession from an upstream tributary or mass wasting of stream banks on event recessions (Lawler et.al, 2006). Characteristics of SSC~Q hysteresis may change seasonally due to changing antecedent and erosion characteristics and long-term due to changing land use and climate (Wood, 1977).

The SSC~T relation for a given turbidity meter is determined by the effect on light scattering of suspended sediment particle concentration, sediment physical properties, and suspension optical properties (Downing et al., 1981; Lewis, 1996; ISO, 1999; Davies-Colley and Smith, 2001, Boss et al., 2009). Thus, hysteresis in SSC~T may contain information on changing sediment characteristics which could not be interpreted from SSC or T independently, nor from SSC~Q hysteresis. Lewis (1996) observed SSC~T hysteresis in over half of sampled storm events in a small (949 acre) forested watershed in coastal northern California, USA. The hysteresis was clockwise and turbidity and SSC peaked synchronously for events measured in the study; but potential causes of the hysteresis were not discussed. At a monitoring station below a reservoir and unregulated tributary confluence in Wales, U.K., Gilvear and Petts (1985) found counterclockwise SSC~T hysteresis during an event dominated by tributary runoff and clockwise SSC~T hysteresis for an event dominated by reservoir release flow. The authors stated that both events implied changes in the sediment particle sizes or density over the flow events. These and other authors (Walling, 1977) recommend sampling over the rise and recession of runoff events to reduce uncertainty and bias in load estimation if SSC~T hysteresis is observed.

## 6.2 Occurrence of Measured Hysteresis in SSC-to-Discharge and SSC-to-Turbidity Ratings

Hysteresis in the SSC~Q and SSC~T relations are indicated graphically in the time series and bivariate plots of figure 5.21. If hysteresis in SSC~Q and SSC~T for single storm events is evident graphically, then it can be evaluated quantitatively in the range and coefficient of variation of the ratio of *Q/SSC* and *T/SSC*, respectively. Selected statistical characteristics of *Q/SSC* and *T/SSC* are listed in table 6.1.

Table 6.1 – Statistical characteristics of ratio of turbidity to SSC (*T/SSC* in FNU/mg/L) and discharge to SSC (*Q/SSC* in cfs/mg/L)

| Event Begin Date | 8/28/ 2009 | 3/10/ 2010 | 4/24/ 2010 | 5/3/ 2010 | 9/27/ 2010 |
|---|---|---|---|---|---|
| Average *T/SSC* | 0.82 | 0.80 | 0.51 | 0.80 | 0.70 |
| Maximum *T/SSC* | 1.06 | 0.95 | 0.65 | 1.02 | 0.97 |
| Minimum *T/SSC* | 0.50 | 0.49 | 0.29 | 0.45 | 0.42 |
| Coefficient of Variation *T/SSC* | 0.167 | 0.116 | 0.169 | 0.231 | 0.134 |
| Average *Q/SSC* | 6.62 | 22.47 | 8.90 | 27.30 | 8.94 |
| Maximum *Q/SSC* | 12.13 | 35.79 | 13.53 | 65.89 | 13.35 |
| Minimum *Q/SSC* | 1.23 | 7.68 | 3.63 | 3.75 | 3.69 |
| Coefficient of Variation *Q/SSC* | 0.309 | 0.306 | 0.250 | 0.735 | 0.212 |

The SSC~Q hysteresis is always clockwise for the 5 events sampled in this study, but its shape and magnitude vary significantly with changing antecedent conditions and storm characteristics (center panel of figure 5.21). Clockwise SSC~Q hysteresis due to stored sediment in the channel is indicated in figure 5.21 by lower magnitude SSC~Q hysteresis for secondary within-event rises in August 2009 and September 2010. The hydrograph shape for the May 2010 event indicates that greater rainfall amounts in the upper watershed contribute to the SSC~Q hysteresis of this event. The minimum and maximum *Q/SSC* for the 5 events are 14 and 241 percent of the mean, respectively, and the standard deviation ranges from 21 to 74 percent of the mean *Q/SSC* ratio (table 6.1). The magnitude of SSC~Q hysteresis observed for these storms is not surprising and, as discussed previously, is strong motivation for using surrogate metrics other than discharge to estimate sediment concentration and load.

The SSC~T hysteresis for these five events is much less pronounced than SSC~Q hysteresis, but is consistent in its occurrence and clockwise direction as shown previously in the center panel bivariate plots of figure 5.21. The only exception for the

clockwise SSC~T hysteresis in these data is the third rise within the September 2010 event, which has a linear SSC~T relation. The SSC and turbidity time series peaks are nearly synchronous for all events, and the SSC~T hysteresis is evident graphically as a consistently higher *T/SSC* ratio on the receding SSC limb versus the rising SSC limb (right hand panel of figure 5.21). The SSC and turbidity have separate scales in figure 5.21 to highlight this graphical explanation of SSC~T hysteresis. The minimum and maximum *T/SSC* are 56 and 139 percent of the mean, respectively, and the standard deviation ranges from 13 to 23 percent of the mean *Q/SSC* ratio (table 6.1). The magnitude of the hysteresis observed in these data is significant and indicates that SSC~T hysteresis should be evaluated as a matter of course when estimating sediment loads using turbidity.

The occurrence of SSC~T hysteresis also was evaluated in this study for the first time in 4 other urban watersheds in the metropolitan Atlanta area where discrete SSC samples were collected over storm events occurring between 2003 and 2007 (fluxes evaluated in Horowitz et al., 2008). The watersheds are located in the same physiographic province as Yellow River at Gees Mill, but are smaller with sizes from 22.5 to 86.8 square miles, and are generally more urbanized. Hysteresis was evaluated for all runoff events with at least 5 total SSC samples and with at least 2 samples each collected during the rising and falling SSC time series. These criteria were met for 24 sampled storm events in 2003-2007 in the 4 watersheds; and of these 23 events had clockwise SSC~T hysteresis, while the 24$^{th}$ had no SSC~T hysteresis. The samples were not analyzed for sediment size.

## 6.3 Potential Causes of SSC-to-Turbidity Hysteresis

Hysteresis in the SSC~T relation for a single event can be caused by a rise to recession change in sediment physical properties (size, shape, density), optical properties (index of refraction), flocculation characteristics, instrument performance (such as fouling), or SSC sample bias (Downing et al., 1981; Lewis, 1996; ISO, 1999; Davies-Colley and Smith, 2001, Boss et al., 2009). SSC is the first order determinant of turbidity (Downing, 2006) and SSC typically has much higher variance than other factors for a given turbidity sensor and stream site. Potential causes of SSC~T hysteresis are evaluated here in the variation of SSC-normalized turbidity computed as T/SSC. This section will discuss potential causes of SSC~T hysteresis that were determined to be of insignificant or minor impact, followed by sections on changing PSD characteristics and how these impact SSC~T hysteresis.

Flow velocity is a direct measure of the erosion and transport capacity of the main channel flow, and is highly correlated with SSC. If the SSC to velocity relation were significantly different for rising versus falling SSC, then this could be a source of observed hysteresis in other relations. For these data, there was no hysteresis between SSC and velocity. Velocity also was insignificant in relation to the ratio of *T/SSC* and in relation to residuals of a SSC~T regression model. Sediment particle index of refraction strongly affects light scattering, as discussed by Sutherland et al (2000); and color from dissolved constituents affects light absorption. Quantitative analyses of sediment and water color were not conducted in this study ; however there was no visually notable change in sediment color during events nor seasonally, and the water appears colorless, so it is unlikely that sediment color contributed to any hysteresis effects..

SSC~T hysteresis would be produced by a significant difference in sediment density between rising and falling SSC. This could occur, for example, if tributary sediment arriving after the peak had significantly different density characteristics. Changing sediment density would have an equal linear affect on, and thus be evidenced in a positive correlation between, *T/SSC* and *VPC/ $SSC_{xs}$*. The correlation between *T/SSC* and *VPC/ $SSC_{xs}$* for these data is actually weakly negative (r= – 0.45 at p-value < 0.001) indicating that any changing sediment density over the measured events is more than overwhelmed by other factors. Laboratory analysis of sediment density was not performed in this study; but is recommended in future studies using optical surrogates.

Limitations and sampling errors associated with fixed-point pumping samplers are discussed by Edwards and Glysson (1999), and could potentially produce a bias in SSC on the rise versus recession under some conditions. However, there is no rise to recession bias in the differences between SSC from the fixed-point pumping sampler and SSC from 33 concurrent cross section samples obtained 100 feet downstream. The turbidity meter functioned well throughout the study as verified in regular calibration checks and the same turbidometer was used throughout the study. Thus, changes in sediment PSD and(or) possibly sediment shape are likely to be the primary determinants of SSC~T hysteresis.

## 6.4 Particle Size Distribution Trends in Runoff Events

The high-resolution time series of volumetric PSD measured by the laser-diffraction analyzer provide valuable data that are used here to evaluate sediment transport characteristics and the effects of particle size on SSC~T hysteresis. Trends in PSD in single runoff events were evaluated in the time series of sediment diameters for the $10^{th}$, $16^{th}$, median, and $84^{th}$ percentile of the volumetric PSD (*D10*, *D16*, *D50*, and *D84*). For

all 5 storm events the sizes of the *D10* and *D16* have decreasing trends over the rising streamflow hydrograph; with flat or increasing trends on the hydrograph recession, as shown in figure 6.2 for the storm event of May 3-6, 2010. The time series for the *D50* and *D84* sizes have much higher variance than the finer fractions of the PSD and do not consistently indicate an increasing or decreasing trend after an initial jump in size at the beginning of the event. The trends in size of the fine fractions of the PSD cover a very narrow size range, from 2 to 9 microns; however they are well defined and correlate well with the independently measured ratio of turbidity to $SSC_{xs}$ as discussed further below.

The trend of decreasing size in the *D10* and *D16* of the PSD time series over the event rise indicates that the source of sediment is changing during runoff events at this site. If the PSD of the sediment source(s) were unchanging over the flow event, and if suspended sediment were limited only by the entrainment and transport capacity of the flow (capacity-limited transport) then the entire suspended sediment PSD would be coarsening with rising discharge and velocity. A coarsening in suspended particle sizes over the event would also be expected if the supply of very fine silt and smaller particles were limited, due to winnowing of these sediments. A constant source sediment PSD is generally assumed in sediment transport studies. However, these results prove that assumption to be invalid in this stream.

The increase in the relative concentration of particles less than the *D16* size is likely due to a limited supply of these fine to very fine silt size sediments (less than about 9 microns for these data) available for entrainment in the channel bed and banks; and to their availability and transport from hill slope sources affected by rainfall impact, rill, and gully erosion. These smaller particles may not be stored in the stream bed between flow events because low velocities are adequate to transport them. For example, base flow velocity prior to each of the measured flow events at the velocity reference location was

greater than the computed critical velocity at this location for incipient motion of 8 micron sediment at the channel bed (0.479 feet per second (0.146 m/s)). The limited availability of small size in the channel is further indicated by the difference between the percent of the material smaller than 63 microns in the sampled bed-material sediment (less than 1 percent) versus that of the $SSC_{xs}$ samples (89 percent for the fixed-point samples and 79 percent for the EWI samples).

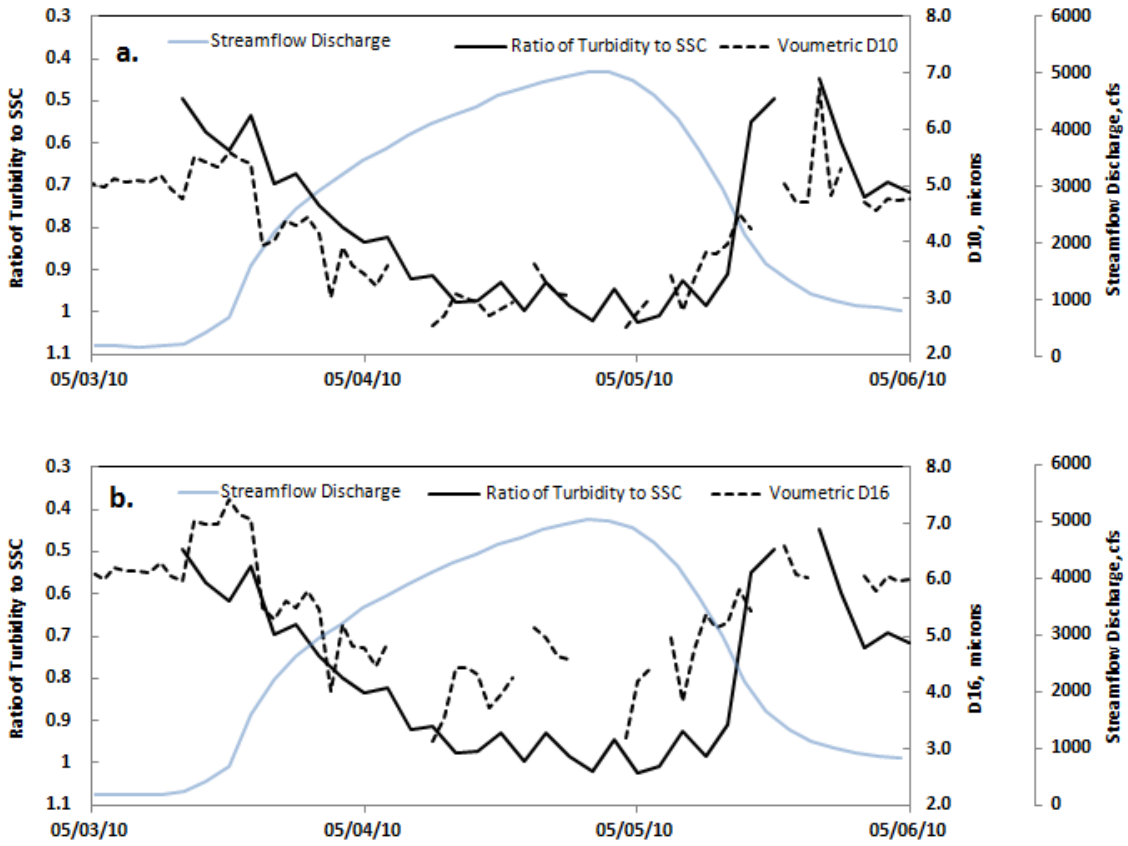


Figure 6.2 - Time series of discharge, ratio of turbidity to mass suspended sediment concentration ($SSC_{xs}$), and sediment diameter for (a.) 10$^{th}$ and (b.) 16$^{th}$percentiles of volumetric particle size distribution for event of May 2-5, 2010 on Yellow River at Gees Mill Road.

Prior studies have observed an increase in the percent of very fine material with discharge for some watersheds and have cited similar causes (Slattery and Burt, 1997; Lawler et al., 2006). For a small (1.9 mi$^2$) alpine watershed in northeastern Italy, Lenzi

and Marchi (2000) found that the SSC~T relation is affected by changing particle size distributions due both to changing entrainment velocities and changing influx of silty material eroded from failed channel banks and from hillslopes. They developed separate SSC~T rating curves for changing particle sizes, but did not assess SSC~T hysteresis. Observed SSC~T hysteresis would not in itself confirm the underlying causes and sediment transport dynamics. However, SSC~T hysteresis in storm events is a useful indicator of potential event changes in PSD, and of driving watershed transport processes.

## 6.5 Changing Sediment Size Effects on SSC-to-Turbidity Hysteresis

The effect of sediment size on turbidity creates a size-concentration ambiguity that has been widely noted (for example Lewis, 1996; Gray and Gartner, 2009). In Mie scattering theory, if the effects of sediment concentration, density, irradiance, and shape are unchanging or normalized for, then the amount of light scattered by homogenous spheres is a function of the scattering surface area (van de Hulst, 1981; Sutherland et al., 2000; Claveno et al., 2007; Boss et al., 2009). Summarizing data for sands between about 30 and 1000 microns from previous studies, Downing (2006) found an inverse relation between sediment size and concentration-normalized optical backscatter, after adjusting for other factors affecting light scattering. Although the effect of sediment size on turbidity is a known limitation of turbidity surrogates, the stability of PSD over runoff events is generally assumed and corrections for SSC~T hysteresis have not been attempted in prior studies.

The correlation of concentration-normalized turbidity (*T/SSC*) and the *D10* and *D16* sediment sizes is evident in the time series data shown for the May 3-6, 2010 event in figure 6.2. This relation is summarized for the 251 samples from all 5 storm events in

figure 6.3 in which the data are from 3 independently measured metrics: mass SSC, turbidity, and laser-diffraction-based volumetric *D10* and *D16*. Variance in the bivariate plots is large, but the least squares fit has a slope in logarithmic space close to $D^{-1}$, in agreement with the results of Downing (2006) and Sutherland et al. (2000). The $D^{-1}$ curve is shown in figure 6.3 with a logarithmic intercept equal to the mean product of *T/SSC* and *D10* or *D16*. The variance in the observed relation between *T/SSC* and *D10* or *D16* may be due to effects of particle shape, other sediment size fractions, measurement errors, and(or) variance in sediment density and index of refraction.

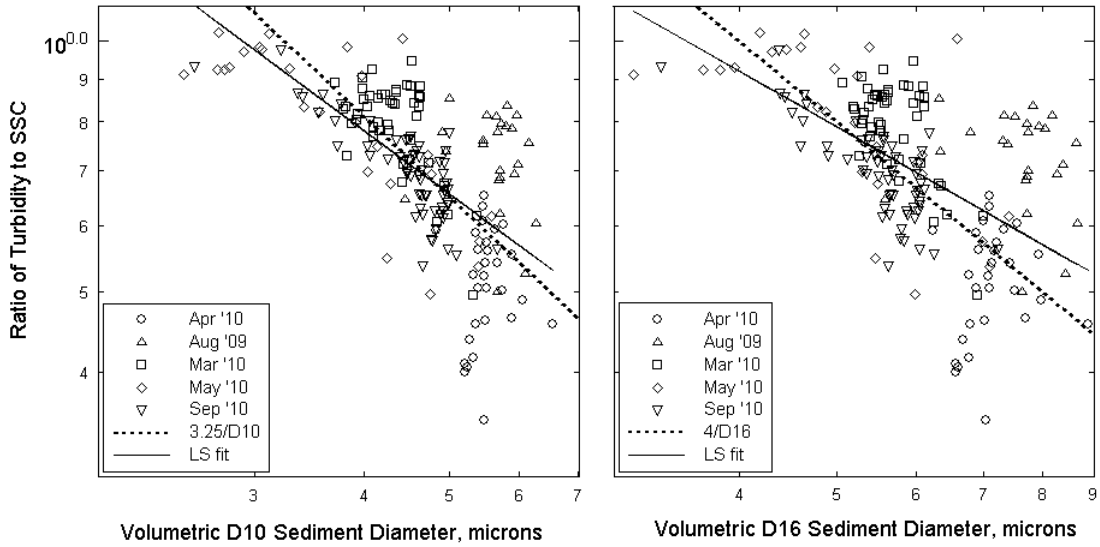


Figure 6.3 – Sediment diameter for tenth (*D10*) and sixteenth (*D16*) percentile of volumetric size distribution and ratio of turbidity to mass suspended sediment concentration (SSC) with least squares regression (LS fit) and theoretical $D^{-1}$ curves

Table 6.2 – Results of regression of log-transformed, SSC-normalized turbidity (*T/SSC*) on sediment diameter (D) for 10th, 16th, 50th, 60th, and 84th percentiles of volumetric particle size distribution PSD for Yellow River at Gees Mill Road

| | Diameter for N$^{th}$ Percentile of Volumetric PSD | | | | |
|---|---|---|---|---|---|
| | *D10* | *D16* | *D50* | *D60* | *D84* |
| Slope | -0.76 | -0.66 | -0.35 | -0.24 | 0.07 |
| R-squared | 0.44 | 0.32 | 0.14 | 0.07 | 0.02 |
| p-value < | 0.0001 | 0.0001 | 0.0001 | 0.0004 | 0.08 |

The results of log-transformed least squares regressions of (*T/SSC*) and sediment diameter for the 10th, 16th, 50th, 60th, and 84th PSD percentiles are given in Table 6.2 and shown in figure 6.4 (in which the sediment size data were centered for graphical comparison). The magnitudes of the regression slope values and the $R^2$ values increase with decreasing PSD percentile, and thus sediment size. These results show that the influence of particle size on turbidity is not constant over the PSD, but increases for the finer fractions of the PSD for these data. These results are in agreement with the theoretical results of Claveno et al. (2007) who found that for modeled PSDs of non-spherical shapes with particle sizes ranging from 0.2 to 200 microns, at least 50% of the contribution to light scattering, attenuation, and absorption comes from particles smaller than 10 microns. For these data, changes of only a few microns in the fractions of the PSD between 2 and 9 microns significantly affect turbidity and create observed SSC~T hysteresis. The relation of normalized turbidity to *D84* is not statistically significant for these data in which *D84* is between 25 and 158 microns.

These results indicate that although turbidity is a bulk indicator of optical properties of the sediment-water mixture, it does not respond to all properties equally. In studies of systems where most of the suspended sediment is sand sized, the SSC~T relation may be dependent on a relatively small fraction of the fine silt and clay sized particles in the

PSD, and minor changes in the PSD over single events and(or) over time could have a large influence on the SSC~T relation. Similarly, studies focused on fine silt and clay size particles and(or) adsorbed constituents may benefit from greater responsiveness of turbidity to these size sediments. In any case, turbidity is only a bulk optical indicator and real information on changes in the PSD and how these may affect the SSC~T relation and the fluvial system will require independent measurements.

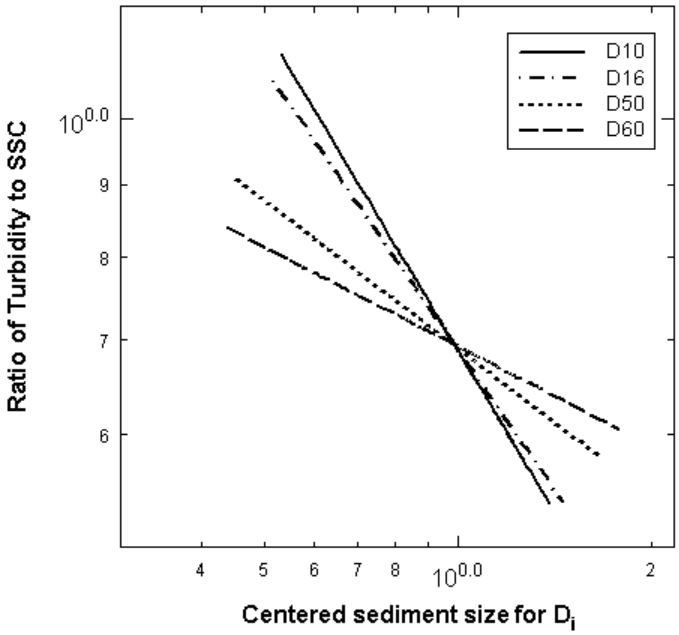


Figure 6.4—Regression model curves for ratio of turbidity to $SSC_{point}$ and centered volumetric sediment size for 5 percentiles of PSD

## 6.6 SSC and Load from Turbidity Surrogates

Turbidity was used as a surrogate to estimate $SSC_{xs}$ using least square regression on the log-transformed variables. Retransformation into linear space from log space typically results in an estimate which is biased low (an underestimate). This retransformation bias was corrected using Duan's smoothing estimate (Duan, 1983; and Helsel and Hirsch, 1995). Ordinary least squares regression was used in the initial analysis of variance to determine the principal explanatory variables for $SSC_{xs}$. The regression models and statistics are shown in table 6.3.

Models of $SSC_{xs}$ ~*T* and $SSC_{xs}$ as a function of both turbidity and *D10* were developed using the 194 data points for which *D10* is available. The $SSC_{xs}$ ~*T* model developed from the 194 points has a $R^2$ of 0.91 and the standard error is 0.113 (in logarithmic units of $SSC_{xs}$) or 30%, the same (within significant digits) as for the $SSC_{xs}$ ~*T* model developed from the entire 251 point data set. The model of $SSC_{xs}$ as a function of turbidity and *D10* is slightly improved, with a $R^2$ of 0.94 and standard error of 0.092 or 24%.

Table 6.3—Results of multiple linear regression of $SSC_{xs}$ on surrogate metrics of discharge, turbidity, and volumetric *D10*

| Explan-atory Variables | $R^2$ | DF | Res Std Err | Res Std Err % | $R^2_{pred}$ | Linear Regression Model |
|---|---|---|---|---|---|---|
| Discharge | 0.57 | 249 | 0.238 | 73 | 0.56 | $SSC_{XS} = 1.245 \ \ Discharge^{0.648}$ |
| Turbidity | 0.90 | 249 | 0.113 | 30 | 0.90 | $SSC_{XS} = 2.111 \ Turbidity^{0.941}$ |
| Turbidity | 0.91 | 192 | 0.113 | 30 | 0.90 | $SSC_{XS} = 2.184 \ Turbidity^{0.932}$ |
| Turbidity *D10* | 0.94 | 191 | 0.092 | 24 | 0.93 | $SSC_{XS} = 0.598 \ Turbidity^{0.949} \ D10^{0.820}$ |

Because the data come from concurrent time series, the residual errors may be autocorrelated (a relationship between values separated from each other by a given time lag), which violates the assumptions of least squares regression. The traditional test for the presence of first-order autocorrelation is the Durbin–Watson statistic which tests for the null hypothesis that the errors are serially independent (not autocorrelated) against the alternative that they follow a first order autoregressive process. For the regression of $SSC_{xs}$ on turbidity, the DW statistic is 0.59, which indicates the presence of positive first order autoregression (AR-1) at a 1-percent significance level.

The AR-1 does not affect the computed intercept or explanatory variable coefficients; but can affect the computed model standard error and p-values. If the time series data contained no gaps, then an Auto Regressive Integrated Moving Average (ARIMA) method could be used to estimate the model residual statistics. Another alternative, appropriate for this data set, is to use maximum likelihood estimation (MLE) which allows for autocorrelated residuals. In this study, MLE was used in a generalized least squares model for each regression model between $SSC_{xs}$ and explanatory variables. The p-values remained less than 0.001 for all explanatory variables and the model standard error was not greater than that computed using ordinary least squares, within reported significant digits. Thus, although the residuals of the $SSC_{xs}$ and turbidity model are autocorrelated, the ordinary least squares statistics are not significantly affected for these data.

Errors of prediction for the $SSC_{xs}$ models were evaluated using the prediction residual sum of squares (PRESS) statistic (Helsel and Hirsch, 1995). The PRESS residual for a specific observation is obtained by computing the regression model from a data set excluding that specific observation. This is done (n-1) times to obtain the PRESS statistic for a model. The observations were not themselves used to estimate the models

for the PRESS statistic. The prediction $R^2$, or $R^2_{pred}$ is computed as one minus the ratio of the PRESS statistic to the total sum of squared errors for the observed data. Thus, values of PRESS and $R^2_{pred}$ are indicators of how well the regression model predicts new observations. For all of the models, values of the $R^2_{pred}$ were equal to or slightly less than the model $R^2$, as shown in table 6.3.

The effect of $SSC_{xs}$ ~$Q$ hysteresis on the $SSC_{xs}$ ~$Q$ rating is evident in figure 6.5, particularly in the pattern of points for specific events. The least-squares regression for the $SSC_{xs}$ ~$Q$ rating curve has an $R^2$ of 0.57, and a model standard error of 0.238. These models were developed using all 251 concurrent sample data points.

Compared to the $SSC_{xs}$ ~$Q$ rating, the effect of $SSC_{xs}$ ~$T$ hysteresis is much smaller and the $SSC_{xs}$ ~$T$ rating has a much better fit as shown in figure 6.6. The least-squares regression for the $SSC_{xs}$ ~$T$ rating curve has an $R^2$ of 0.90, and a model standard error of 0.113; less than half that of the $SSC_{xs}$ ~$Q$ rating curve.

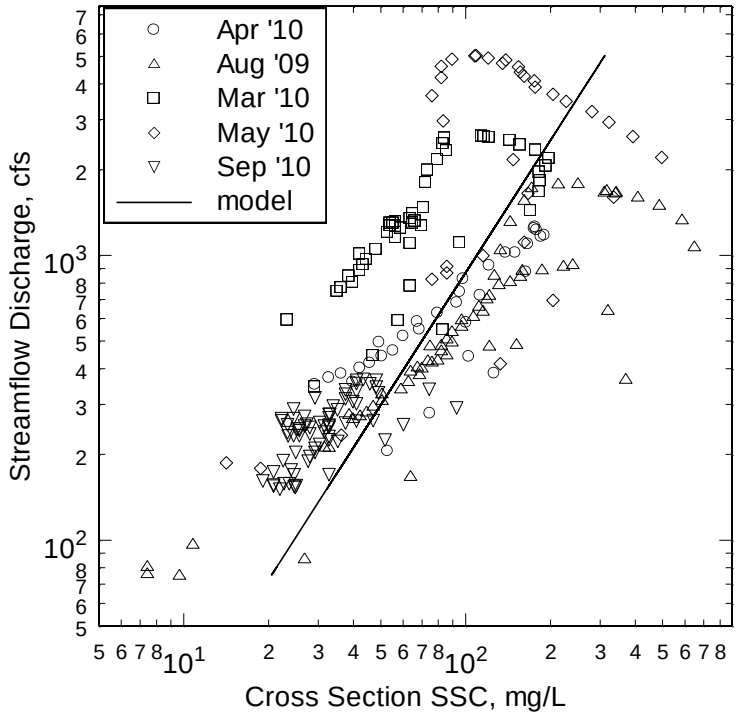


Figure 6.5 – Observed cross section SSC, streamflow discharge, and regression model curve

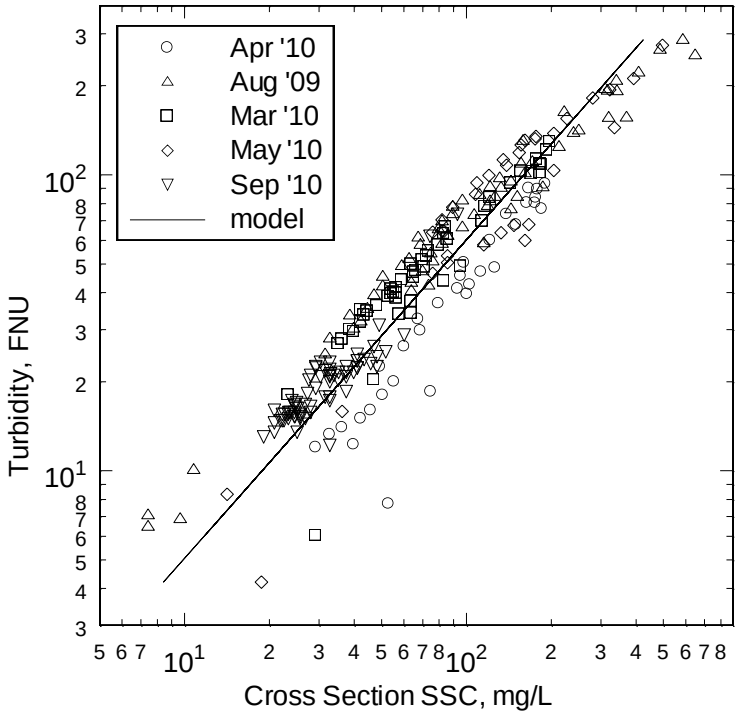


Figure 6.6 – Observed cross section SSC, turbidity, and regression model curve

The simple logarithmic $SSC_{xs}$ ~$T$ rating (second equation in table 6.3) was selected for the turbidity-based sediment surrogate in this study. The observed and predicted $SSC_{xs}$ results and 95% confidence limits for individual predicted values are shown in figure 6.7

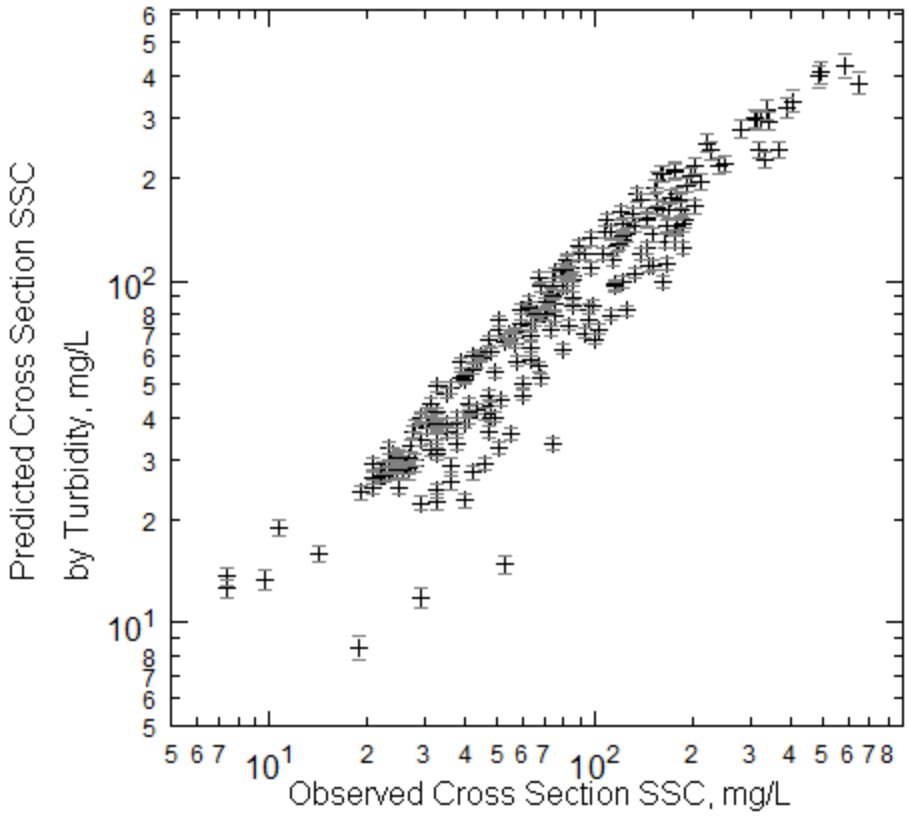


Figure 6.7 - Observed and predicted cross section SSC and 95% confidence interval, with predicted values from turbidity

Suspended sediment load is a highly effective indicator of many cumulative watershed processes. Computation of suspended sediment load often is the primary purpose of SSC sampling and monitoring of sediment surrogates such as turbidity, in addition to discharge. Measurements of streamflow (as discussed in section 5.1.1) and of $SSC_{xs}$ are used to compute sediment flux (discharge) for a specific stream location. Sediment fluxes are often integrated over a runoff event or a specific time period such as a year to obtain sediment loads. Sediment flux is obtained as the product of the streamflow discharge ($Q_s$) and $SSC_{xs}$ for a selected time step using the equation $Q_s = Q_w\, SSC_{XS}\, k$ where $Q_s$ is suspended-sediment flux, in mass per unit time; $Q_w$ is water discharge, in volume per unit time; and $k$ is a coefficient based on the unit of measurement of $Q_s$ and $SSC_{xs}$.

The sediment fluxes were computed and integrated over each sampled flow event to compute event load, with results shown in table 6.4. Errors of estimate for the SSC load are determined from the difference between the observed and the computed SSC load. This method does not split the data set into a model-development and verification data sets; and thus is not a true error of prediction. However, it is a strong indicator of the relative error between the methods.

The $SSC_{xs}$ ~$Q$ error of load estimate ranges from -48 to 58 percent for individual events and is 21 percent overall as shown in table 6.4. The $SSC_{xs}$ ~$T$ error of load estimate ranges from -23 to 12 percent for individual events and is only 1.6 percent overall (table 6.4). This clearly demonstrates the advantages of turbidity over discharge as a surrogate measure of $SSC_{xs}$ and for computation of sediment load.

Table 6.4 – Measured and estimated sediment load and errors of load estimate for Yellow River at Gees Mill Road (a—the total measured load concurrent with this sample subset is 7225 tons)

| | | Discharge Surrogate | | Turbidity Surrogate | | Turbidity and *D10* Surrogate | |
|---|---|---|---|---|---|---|---|
| EVENT | Measured Load Tons | Esti-mated Load Tons | Error of Pred-iction Percent | Esti-mated Load Tons | Error of Pred-diction Percent | Est-imated Load Tons | Error of Pred-diction Percent |
| Aug '09 | 2367 | 1235 | -47.8 | 2169 | -8.4 | 2025 | 7.7 |
| Mar '10 | 1594 | 2504 | 57.1 | 1731 | 8.6 | 1659 | 4.1 |
| Apr '10 | 591 | 467 | -21.0 | 452 | -23.4 | 525 | -8.2 |
| May '10 | 3532 | 5584 | 58.1 | 3850 | 9.0 | 2795 | -9.8 |
| Sep '10 | 89 | 115 | 29.5 | 100 | 12.2 | 83 | 4.9 |
| Samples | 251 | 251 | | 251 | | 194 | |
| Totals | 8172 | 9905 | 21 | 8302 | 1.6 | 7087[a] | -1.9 |

The error of load estimate for SSC load for individual storms is lowest where $SSC_{xs}$ is estimated as a function of both turbidity and *D10*, for 4 of the 5 measured storm events. The observed SSC~T hysteresis would affect computed sediment load if the collection of samples were significantly biased to the rising or falling limb of the SSC time series. The effect of SSC~T hysteresis becomes negligible, however, as more samples are included on rising and falling limbs, where a best fit modeling approach is used. Thus, inclusion of *D10* in the turbidity model to estimate $SSC_{xs}$ results in significant improvements in individual storm estimates, with the maximum event reduced from -23.4% to -9.8%. Also, the individual event loads themselves are significantly different when *D10* is included, with an 18.8% and 16.1% differences in computed load for the May 2010 and August 2009 events, respectively. However, the magnitude of the overall error is not significantly different for load computed using $SSC_{xs}$ models with turbidity only versus turbidity and *D10*; with an error of 1.6 versus -1.9 %. This tends to confirm that a best-fit modeling approach will resolve the effects of minor SSC~T hysteresis where samples are well represented on rising and falling limbs of the SSC time series. . The SSC~T and

SSC~Q predictive results are compared with results using acoustic and laser-diffraction surrogates in chapter 10.

# 7 Suspended Sediment Characteristics from Laser-Diffraction Surrogates

The principals of operation, capabilities, and limitations of laser-diffraction based *VPC* and volumetric PSD data were discussed in the literature review. The time series of *VPC* and $SSC_{XS}$ are shown in figure 5.23 and listed in table 5.5. These data were used to develop models of $SSC_{XS}$ from the laser-diffraction metrics to compute sediment load for each measured event.

Ordinary least squares regression of logarithmic-transformed data was used in the initial analysis of variance to determine the principal explanatory variables for $SSC_{XS}$ using laser-diffraction surrogates. The Durbin-Watson test for autocorrelation of the time series data (described in section 6.6) indicates the presence of positive first order autoregression (AR-1) at a 1-percent significance level for the residuals of $SSC_{XS}$ in the tested models using laser-diffraction surrogates. Reanalyzing the models using MLE in a generalized least square model indicated that the p-values remained less than 0.001 for all explanatory variables and the model standard error was not significantly greater than that computed using ordinary least squares. Thus, although the residuals of the $SSC_{XS}$ and laser-diffraction models are autocorrelated, the ordinary least squares statistics are not significantly affected for these data. All models were also corrected for minor retransformation bias using Duan's smoothing estimate (Duan, 1983).

Errors of prediction for the $SSC_{XS}$ models were evaluated using the prediction residual sum of squares (PRESS) statistic (Helsel and Hirsch, 1995) to compute the prediction $R^2$, or $R^2_{pred}$ as described in section 6.6. The $R^2_{pred}$ is an indicator of how well the

regression model predicts new observations. For all of the models, values of the $R^2_{pred}$ were equal to or slightly less than the model $R^2$ as shown in table 7.1.

Table 7.1—Results of multiple linear regression of $SSC_{xs}$ on acoustic surrogate metrics

| Explan-atory Variables | $R^2$ | DF | Res Std Err | Res Std Err % | $R^2_{pred}$ | Linear Regression Model |
|---|---|---|---|---|---|---|
| *VPC* | 0.90 | 192 | 0.115 | 30 | 0.90 | $SSC_{XS} = 1.640\ VPC^{0.957}$ |
| *VPC D10* | 0.94 | 190 | 0.093 | 24 | 0.94 | $SSC_{XS} = 5.221\ VPC^{1.010}\ D10^{-0.902}$ |

The relation of $SSC_{xs}$ to *VPC* is strong in logarithmic space as shown in figure 7.1. Least-squares regression in log space for $SSC_{XS}$ as a function of *VPC* has an $R^2$ of 0.90, standard error of 0.115 (in logarithmic units of $SSC_{xs}$) or 30%, and p-value less than 0.0001 as summarized in table 7.1. The laser-diffraction measurements are not affected by size-concentration ambiguity as are turbidity and acoustic metrics; however there is still significant variance in the relation of $SSC_{XS}$ to *VPC*, as seen in figure 7.1. This scatter is due primarily to the variable fraction of $SSC_{XS}$ that is unmeasured by *VPC*.

The $SSC_{XS}$ ~*VPC* relation is affected by changes in the percent of $SSC_{XS}$ that is unmeasured in *VPC* because of instrument measurement size limits, as discussed in the laser-diffraction data summary. This affect will be more significant for particles below the minimum size limit (2 microns), which comprises a larger portion of the unmeasured $SSC_{XS}$ than particles larger than the maximum size limit (381 microns) for the suspended sediments in this study. The median percent finer than 2 microns for this site is 35%, based on 13 full $PSD_{mass}$ analyses. Changes in *D10* can indicate changes in the fraction

of $SSC_{XS}$ that is unmeasured by *VPC*, because as *D10* decreases the relative concentration of fine silt and clay size particles, including particles less than 2 microns, increases. This is evident in the figure 7.2 scatter plot of *D10* and the residuals of $SSC_{XS}$ as a function of *VPC*. In figure 7.2, $SSC_{XS}$ is over estimated for larger *D10*, and underestimated for smaller *D10* because the fraction of $SSC_{XS}$ less than 2 microns that is unmeasured by *VPC* will increase with decreasing *D10*. This variable unmeasured fraction of $SSC_{XS}$ by *VPC* is also evidenced in a weak but consistent counter-clockwise hysteresis for single events at this site, because the ratio of *VPC* to $SSC_{XS}$ is smaller on the SSC recession than the SSC rise.

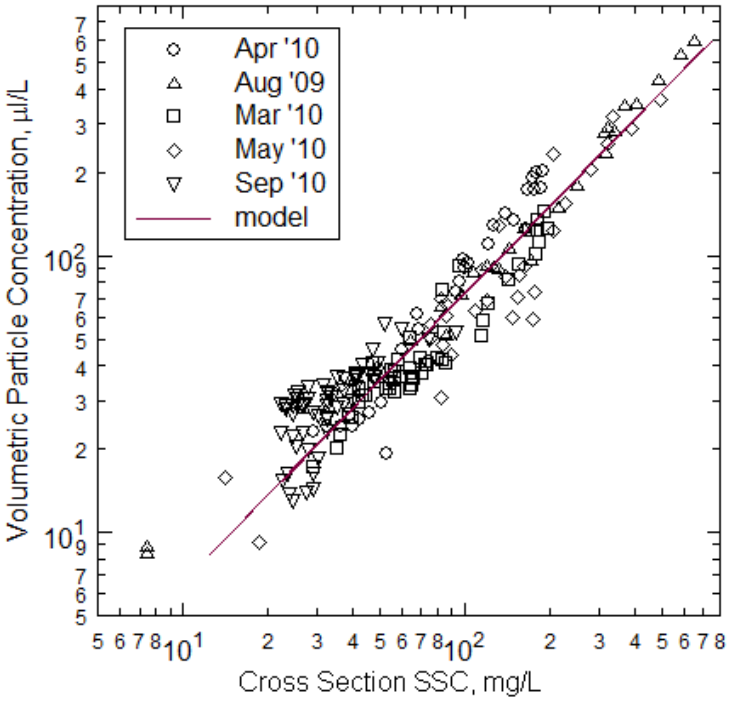


Figure 7.1 Observed cross section SSC, volumetric particle concentration, and regression model curve

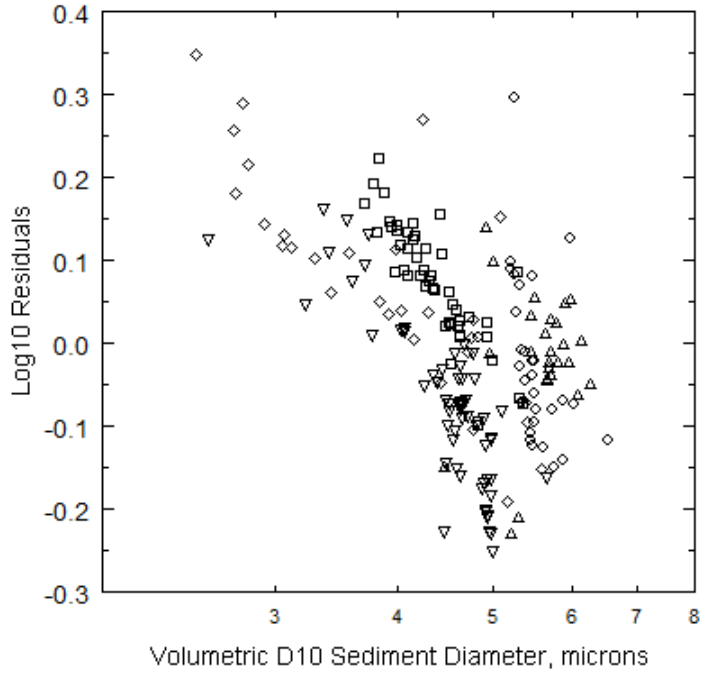


Figure 7.2 - Sediment diameter for tenth percentile of volumetric size distribution and residuals of regression of log($SSC_{xs}$) on VPC

The *VPC* and volumetric size data can be used together to improve the estimate of $SSC_{xs.}$ Multiple least-squares regression in log space for $SSC_{XS}$ as a function of *VPC* and *D10* has an $R^2$ of 0.94, standard error of 0.093, and p-value less than 0.0001 as shown in table 7.1. The effects of density difference and other factors are included in the coefficients and/or the uncertainty of this equation. The scatter plot of observed and predicted $SSC_{XS}$ is shown in figure 7.3.

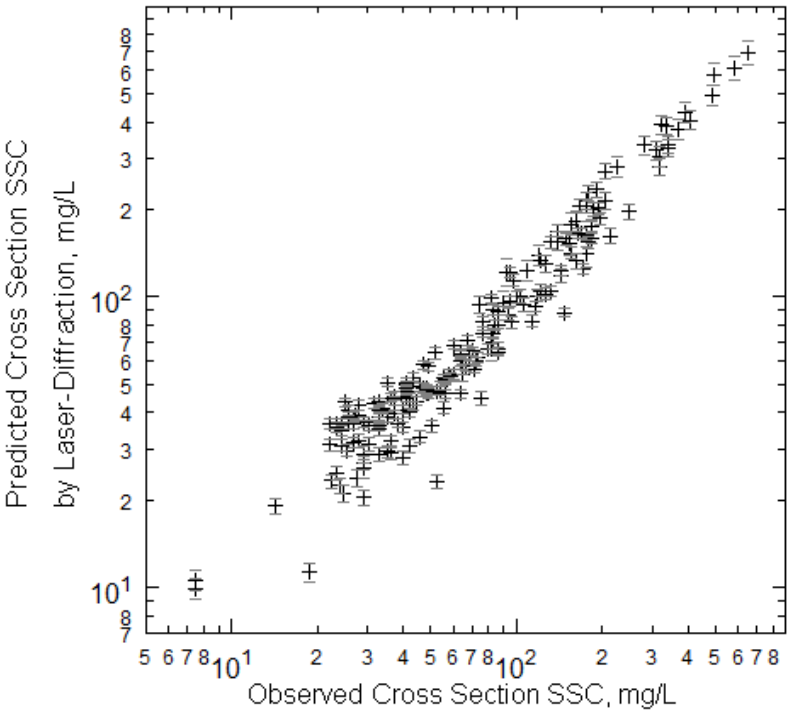


Figure 7.3 - Observed and predicted cross section SSC and 95% confidence interval, with predicted values from laser-diffraction-based volumetric particle concentration and D10 sediment size

This is the first study to suggest using fine fractions (*D10*) of volumetric size together with *VPC* to estimate $SSC_{XS.}$, and to show that this method provides an improved surrogate model. Multiple least-squares regression in log space for $SSC_{XS}$ as a function of *VPC* and *D10*, as compared with a model using *VPC* alone, improves the $R^2$ from 0.90 to 0.94, and decreases the model residual standard error from 30 to 24 percent (table 7.1). This model has the lowest model error and error of prediction of any of the surrogate metrics used in this study. Further research is needed into the use and application of laser-diffraction for continuous PSD and *VPC* monitoring in fluvial systems, and into methods to adjust the measured metrics for the unmeasured fractions of $SSC_{XS}$.

This study also found, for the first time, that the *VPC*, as reported by the LISST-Streamside, is not a true volumetric particle concentration. This is evident in the ratios of measured SSC to *VPC*. The ratio of mass SSC to true volumetric particle concentration, after adjusting for units, should equal the sediment specific gravity, which is close to 2.6 for predominantly silica sediment of this stream. The effect of the fraction of SSC that is unmeasured by *VPC* would increase the SSC (in mg/L) to *VPC* (in µl/L) ratio to a number larger than sediment density. Instead, the indicated specific gravity from the SSC-to-*VPC* ratio for the concurrent measurements of this study has a median value of 1.12 and an interquartile range from 0.94 to 1.41 (dimensionless relative density). Given the unmeasured fraction of roughly 45% of the sample for this site, the *VPC* differs from actual volumetric concentration by a factor of 2.5 to 4 within the interquartile range of SSC to *VPC* ratios. This problem is not unique to the specific LISST-Streamside purchased for this research. The problem was first communicated by this researcher to the manufacturer of the LISST-Streamside, Sequoia Scientific, in 2009, with a request for detailed review of their system software. In October 2011, a similar issue was discovered by this investigator and colleagues in the USGS for another LISST device

designed for fluvial systems, the LISST-SL. Further research is now being conducted by Sequoia Scientific, and the issue is likely to be resolved soon in the algorithms used to compute the volumetric particle concentration.

The observed SSC load and the prediction from the *VPC* and *D10* metrics for the time steps with concurrent laser-diffraction data, and the errors are summarized in chapter 10.

# 8 Suspended Sediment Size Characteristics from Acoustic Attenuation Surrogates

The methods used here to estimate sediment characteristics from acoustic metrics are built on the methods described in the literature review with innovations unique to this research plan. In the following section the acoustic attenuation and relative backscatter results are described and shown graphically. Section 8.2 describes a new method for estimating sediment size characteristics from measured and theoretical acoustic attenuation, exactly as described in the research proposal. Section 8.3 presents the experimental results of applying this method for single-frequency data in this study, and section 8.4 presents the results using multi-frequency instruments. Section 8.5 describes a purely empirical fitting of the multi-frequency attenuation to sediment size relation. These methods are used to estimate $SSC_{xs}$ and load in chapter 9.

## 8.1 Acoustic Attenuation and Relative Backscatter

The acoustic metrics that relate to sediment concentration and size are (a) the acoustic attenuation due to sediment properties; and (b) the acoustic backscatter, adjusted for signal spreading and attenuation due to fluid and sediment properties. The acoustic backscatter is typically the stronger indicator of SSC and acoustic attenuation is often assumed to be negligible; though the validity of this is assumption has rarely been tested. The raw acoustic backscatter data (RL) for selected locations in the ensonified acoustic profile for the 1.2, 1.5, and 3.0 MHz ADCPs were presented in section 5.5. Raw *RL* does not necessarily correlate with SSC because of the offsetting effects of increased acoustic scatter and increased acoustic attenuation with increased SSC. Data were analyzed for acoustic surrogates for the four events in 2010, but not the event

beginning in August 2009, which had acoustic interference from debris caught on the bridge..

The relative backscatter (RB) is equivalent to the total scattering by suspended particles. *RB* is in units of decibels, which is in logarithmic space by definition so that it is related to logarithmic $SSC_{xs}$. The *RB* is computed following Urick's (1975) method as *RB = RL+2TL,* with all units in logarithms, using equations 6 and 7 as described in section 2.1.4 of this thesis. Recalling equations 6 and 7, the relative backscatter, RB, may be written as:

$$RB = RL + 20\log_{10}(\psi r) + 2r(\alpha_w + \alpha_s) \qquad (13)$$

Attenuation in pure water at depths less than 100 meters is a function of temperature and acoustic frequency only and may be computed as (Fisher and Simmons, 1977):

$$\alpha_w = 8.686\, f^2\, (55.9 - 2.37\mathrm{T} + 0.0477\mathrm{T}^2 - 0.000348\mathrm{T}^3)\, 10^{-15} \qquad (14)$$

where *f* is in Hz, T is in centigrade, and $\alpha_w$ is in dB/m. Temperature is measured and stored by each acoustic meter at each measurement interval, so continuous time series of $\alpha_w$ can be computed.

The sediment-associated acoustic attenuation, $\alpha_s$, is the acoustic energy attenuation per unit distance due to viscous and scattering losses. The coefficient of acoustic attenuation by sediment is defined as:

$$\alpha_s = -\frac{1}{2}\frac{d}{dr}(RL + 20\log_{10}(\psi r) + 2r\alpha_w) \qquad (15)$$

Methods to determine $\alpha_s$ prior to Topping et al. (2004) required iterative numerical estimates and/or extensive assumptions as describe in section 2.1. Following Topping et al. (2004), $\alpha_s$ may be measured using *RL* profiles from ADCPs, because all of the terms on the right hand side of equation 15 are known. Topping et al. do not adjust for near field effects in their method; but this is a potentially important correction when using multiple frequencies with different near-field distances.

Because ADCPs measure acoustic backscatter (*RL*) at multiple locations (cells) along the profile, equation 15 can be solved practically as negative ½ times the slope along the range of the acoustic beam of the term in brackets. This is the same basic method described by Topping et al (2007) for obtaining $\alpha_s$. Profiles of ($RL + 20log_{10}(\psi r) + 2r(\alpha_w)$) were plotted at hourly time steps over each flow event for each instrument. An example of these plots for the 3.0 MHz ADCP is shown in figure 8.1. The steeper profiles with the larger value intercepts near the transducer are associated with higher concentrations during this event of April 2010. Based on evaluation of these plots, the entire acoustic profile range was used for computation of $\alpha_s$ and of *RB* for each instrument for each event. The acoustic profile ranges and cell locations are defined in section 4.2.4 of this thesis. Sediment acoustic attenuation was computed for each of the 3 frequencies to obtain $\alpha_{s1.2}$, $\alpha_{s1.5}$, and $\alpha_{s3.0}$. The acoustic attenuation was computed at hourly time steps from the 15-minute adjusted *RL* profiles.

The acoustic attenuation values were used in equation 13 to compute hourly relative backscatter profiles for each event for each ADCP. An example of the *RB* profiles for the 3.0 MHz unit for the April 2010 event is shown in figure 8.2. This example illustrates the expected results of SSC surrogate values for a well-mixed system in which the SSC may be increasing closer to the channel thalweg, at the greatest distance from the transducer. For some time steps during periods of low sediment concentrations the

computed acoustic attenuation was negative, which is theoretically impossible. These negative attenuation values are included in the data set shown in table 8.1, but were filtered out of the analysis in computing RB and in evaluations of sediment size.

Figure 8.3 shows the time series of profile average *RB* for the 1.5 MHz ADCP for the 4 events in 2010. The $SSC_{xs}$ and index velocity time series are repeated in figure 8.3 for reference. Figure 8.4 shows the profile average $\alpha_s$, used in the computation of RB, for the 1.5 MHz ADCP for the 4 events in 2010. The $SSC_{xs}$ and streamflow discharge are repeated in figure 8.4 for reference. The inclusion of velocity in figure 8.3 and discharge in 8.4 is for reference only and is not based on a perceived causal relation between the plotted parameters. The horizontal gridlines shown in figures 8.3 and 8.4 are for the concentration, referenced to the far right axis on the plots. The results for the 1.2 and 3.0 MHz ADCPs are similar to those for the 1.5MHz unit shown here. The data are also listed in table 8.1.

The time series and scatter plots in figures 8.3 and 8.4 illustrate the within event and event-to-event variation in the $SSC_{xs}$ ~*RB* and $SSC_{xs}$ ~Attenuation relations. The ratio of *RB* to SSC and of Attenuation to SSC is greater on the SSC recession than on the SSC rise for all except the April 2010 event, creating clockwise hysteresis.

Table 8.1 - Acoustic relative backscatter (RB) and attenuation (full profile and sub profile) for 1.5, 3.0, and 1.2 MHz ADCPs.

| Date and Time | 1.5 MHz RB | 1.5 MHz $\alpha_s$ full | 1.5 MHz $\alpha_s$ sub | 3.0 MHz RB | 3.0 MHz $\alpha_s$ full | 3.0 MHz $\alpha_s$ sub | 1.2 MHz RB | 1.2 MHz $\alpha_s$ full | 1.2 MHz $\alpha_s$ sub |
|---|---|---|---|---|---|---|---|---|---|
| 3/10/10 13:00 | 91.9 | 0.06 | 0.31 | 65.2 | 1.06 | 0.80 | 103.1 | 0.80 | 0.99 |
| 3/10/10 15:00 | 93.0 | 0.00 | 0.36 | 68.3 | 1.09 | 0.66 | 104.0 | 0.75 | 1.00 |
| 3/10/10 17:00 | 96.7 | 0.20 | 0.79 | 71.4 | 1.29 | 0.78 | 109.8 | 1.09 | 1.50 |
| 3/10/10 19:00 | 95.7 | -0.01 | -0.02 | 70.3 | 1.03 | 0.59 | 106.6 | 0.69 | 1.14 |
| 3/10/10 21:00 | 99.5 | 0.04 | -0.15 | 73.9 | 1.10 | 0.76 | 111.5 | 0.78 | 0.78 |
| 3/10/10 23:00 | 100.8 | 0.08 | 0.04 | 76.1 | 1.43 | 1.25 | 112.3 | 0.59 | 0.87 |
| 3/11/10 1:00 | 101.1 | 0.08 | 0.07 | 76.3 | 1.36 | 1.20 | 113.1 | 0.72 | 1.19 |
| 3/11/10 3:00 | 103.8 | 0.37 | 0.42 | 77.7 | 1.46 | 1.52 | 117.0 | 1.09 | 1.08 |
| 3/11/10 5:00 | 103.4 | 0.24 | -0.15 | 77.1 | 1.35 | 1.17 | 118.6 | 1.27 | 1.68 |
| 3/11/10 7:00 | 105.6 | 0.50 | 0.04 | 78.7 | 1.51 | 1.64 | 118.1 | 0.94 | 0.80 |
| 3/11/10 9:00 | 104.9 | 0.44 | 0.12 | 79.1 | 1.83 | 1.57 | 116.3 | 0.79 | 0.75 |
| 3/11/10 11:00 | 105.7 | 0.54 | 0.30 | 80.4 | 2.13 | 1.72 | 117.9 | 1.02 | 0.63 |
| 3/11/10 13:00 | 104.6 | 0.36 | 0.28 | 79.3 | 1.80 | 1.55 | 118.2 | 0.99 | 1.63 |
| 3/11/10 15:00 | 106.3 | 0.59 | 0.31 | 79.7 | 1.73 | 1.77 | 118.8 | 1.14 | 0.64 |
| 3/11/10 17:00 | 104.9 | 0.41 | -0.33 | 79.8 | 1.78 | 1.44 | 120.0 | 1.17 | 0.87 |
| 3/11/10 19:00 | 106.0 | 0.52 | 0.55 | 80.3 | 1.94 | 1.56 | 120.0 | 1.28 | 2.02 |
| 3/11/10 21:00 | 107.0 | 0.75 | 0.07 | 80.6 | 1.92 | 1.92 | 121.9 | 1.55 | 0.42 |
| 3/11/10 23:00 | 108.2 | 0.88 | 0.10 | 80.8 | 1.91 | 1.91 | 122.9 | 1.65 | 1.04 |
| 3/12/10 1:00 | 107.8 | 0.71 | 0.15 | 80.1 | 1.86 | 1.69 | 123.0 | 1.62 | 0.92 |
| 3/12/10 3:00 | 107.3 | 0.73 | 0.31 | 80.8 | 1.97 | 1.64 | 121.4 | 1.50 | 0.29 |
| 3/12/10 5:00 | 103.9 | 0.35 | 1.34 | 81.4 | 2.31 | 2.19 | 117.7 | 1.18 | 2.00 |
| 3/12/10 7:00 | 106.9 | 0.73 | 0.50 | 81.5 | 2.07 | 2.13 | 119.4 | 1.34 | 1.42 |
| 3/12/10 9:00 | 105.0 | 0.51 | 0.96 | 81.3 | 1.94 | 2.24 | 119.4 | 1.54 | 2.80 |
| 3/12/10 11:00 | 102.8 | 0.28 | 0.38 | 79.4 | 1.95 | 1.64 | 114.3 | 0.78 | 1.86 |
| 3/12/10 15:00 | 103.8 | 0.30 | 0.41 | 77.3 | 1.11 | 1.29 | 117.0 | 0.94 | 1.27 |
| 3/12/10 17:00 | 104.7 | 0.45 | -0.58 | 75.0 | 0.51 | 0.57 | 119.2 | 1.29 | 0.20 |
| 3/12/10 19:00 | 102.9 | 0.10 | 0.15 | 75.8 | 0.72 | 1.05 | 116.4 | 0.96 | 0.31 |
| 3/12/10 21:00 | 102.3 | -0.18 | -0.63 | 72.1 | -0.04 | 0.08 | 112.4 | 0.12 | -0.78 |
| 3/12/10 23:00 | 102.8 | -0.21 | -1.95 | 71.8 | -0.32 | -0.24 | 112.4 | -0.23 | -0.60 |
| 3/13/10 1:00 | 102.9 | -0.27 | -0.88 | 71.9 | -0.20 | 0.07 | 112.9 | -0.17 | 0.36 |
| 3/13/10 3:00 | 103.2 | -0.01 | -1.72 | 72.3 | -0.25 | 0.08 | 113.6 | -0.63 | -1.54 |
| 3/13/10 5:00 | 104.4 | 0.17 | -1.59 | 73.3 | 0.22 | -0.43 | 113.9 | -1.10 | -0.61 |
| 3/13/10 7:00 | 103.5 | 0.08 | -2.10 | 73.9 | 0.11 | -0.28 | 113.2 | -0.69 | -1.37 |
| 3/13/10 9:00 | 103.9 | 0.34 | -1.97 | 73.1 | 0.14 | -0.68 | 112.4 | -0.61 | -2.24 |
| 3/13/10 11:00 | 104.4 | 0.25 | -1.05 | 75.1 | 0.64 | 0.28 | 111.8 | -0.04 | -0.66 |
| 3/13/10 13:00 | 103.2 | 0.16 | -1.50 | 73.9 | 0.29 | -0.26 | 112.2 | 0.05 | -1.27 |
| 3/13/10 15:00 | 100.3 | -0.31 | 0.04 | 75.2 | 1.16 | 0.90 | 108.5 | -0.03 | -0.55 |
| 3/13/10 17:00 | 100.7 | -0.31 | -1.14 | 73.6 | 0.75 | 0.22 | 111.2 | 0.32 | -0.56 |
| 3/13/10 19:00 | 100.9 | -0.03 | -1.20 | 72.1 | 0.44 | 0.03 | 109.9 | -0.02 | -2.00 |

Table 8.1 - (continued) Acoustic relative backscatter (RB) and attenuation (full profile and sub profile) for 1.5, 3.0, and 1.2 MHz ADCPs.

| Date and Time | 1.5 MHz RB | 1.5 MHz $\alpha_s$ full | 1.5 MHz $\alpha_s$ sub | 3.0 MHz RB | 3.0 MHz $\alpha_s$ full | 3.0 MHz $\alpha_s$ sub | 1.2 MHz RB | 1.2 MHz $\alpha_s$ full | 1.2 MHz $\alpha_s$ sub |
|---|---|---|---|---|---|---|---|---|---|
| 3/13/10 21:00 | 99.8 | -0.16 | -1.63 | 73.2 | 0.94 | 0.30 | 108.3 | 0.27 | -1.14 |
| 3/13/10 23:00 | 99.7 | -0.17 | -0.34 | 74.0 | 1.01 | 0.44 | 109.5 | 0.11 | -0.57 |
| 3/14/10 1:00 | 99.4 | -0.09 | -1.10 | 72.6 | 0.60 | 0.18 | 109.0 | 0.39 | -0.06 |
| 3/14/10 3:00 | 98.4 | -0.22 | -1.24 | 71.3 | 0.59 | 0.43 | 107.4 | 0.37 | 0.04 |
| 3/14/10 5:00 | 98.5 | -0.18 | -1.11 | 71.1 | 0.58 | 0.28 | 105.8 | 0.08 | -1.29 |
| 3/14/10 7:00 | 98.6 | -0.28 | -1.89 | 72.7 | 1.05 | 0.31 | 105.4 | 0.00 | -0.55 |
| 3/14/10 9:00 | 98.1 | -0.32 | -1.31 | 73.6 | 1.40 | 0.83 | 105.8 | 0.01 | -0.71 |
| 3/14/10 11:00 | 98.0 | -0.50 | -0.56 | 72.8 | 1.31 | 0.26 | 105.3 | -0.43 | -1.11 |
| 3/14/10 13:00 | 96.9 | -0.45 | -0.68 | 69.9 | 0.63 | 0.18 | 104.0 | 0.07 | -0.98 |
| 3/15/10 9:00 | 93.5 | -0.46 | -0.66 | 66.2 | 0.68 | 0.18 | 100.9 | 0.23 | 0.54 |
| 4/24/10 16:00 | 104.1 | 1.10 | 2.27 | 75.0 | 1.68 | 1.73 | 116.7 | 2.02 | 3.09 |
| 4/24/10 18:00 | 107.8 | 2.15 | 3.29 | 78.2 | 2.48 | 2.66 | 117.8 | 2.98 | 4.08 |
| 4/24/10 20:00 | 105.8 | 1.58 | 2.91 | 76.6 | 2.05 | 2.24 | 116.7 | 2.62 | 3.78 |
| 4/24/10 22:00 | 103.7 | 1.06 | 2.29 | 76.3 | 1.82 | 1.97 | 114.9 | 1.95 | 2.96 |
| 4/25/10 0:00 | 104.7 | 1.20 | 2.36 | 77.8 | 2.04 | 2.31 | 116.2 | 2.12 | 3.20 |
| 4/25/10 2:00 | 107.2 | 1.98 | 3.18 | 78.8 | 2.55 | 2.81 | 117.5 | 2.86 | 3.99 |
| 4/25/10 4:00 | 106.5 | 1.75 | 2.94 | 79.0 | 2.49 | 2.74 | 117.3 | 2.66 | 3.91 |
| 4/25/10 6:00 | 108.5 | 2.48 | 3.55 | 79.2 | 2.90 | 3.21 | 117.7 | 3.26 | 4.27 |
| 4/25/10 8:00 | 108.5 | 2.52 | 3.71 | 79.3 | 2.92 | 3.25 | 117.6 | 3.28 | 4.36 |
| 4/25/10 10:00 | 109.6 | 2.83 | 3.90 | 79.7 | 3.04 | 3.38 | 118.8 | 3.63 | 4.56 |
| 4/25/10 12:00 | 109.5 | 2.76 | 3.85 | 79.9 | 3.02 | 3.36 | 118.3 | 3.52 | 4.52 |
| 4/25/10 14:00 | 110.8 | 3.33 | 4.31 | 80.1 | 3.29 | 3.74 | 118.8 | 4.04 | 4.91 |
| 4/25/10 16:00 | 110.2 | 3.10 | 4.13 | 79.7 | 3.11 | 3.42 | 118.6 | 3.93 | 4.77 |
| 4/25/10 18:00 | 106.9 | 2.01 | 3.33 | 78.5 | 2.56 | 2.81 | 116.8 | 2.93 | 4.11 |
| 4/25/10 20:00 | 105.8 | 1.57 | 2.74 | 77.6 | 2.17 | 2.31 | 116.4 | 2.47 | 3.61 |
| 4/25/10 22:00 | 104.2 | 1.24 | 2.47 | 76.3 | 1.91 | 2.06 | 115.0 | 2.14 | 3.25 |
| 4/26/10 0:00 | 103.3 | 1.05 | 2.41 | 75.7 | 1.80 | 2.01 | 114.1 | 1.94 | 3.07 |
| 4/26/10 2:00 | 102.6 | 0.95 | 2.25 | 74.6 | 1.62 | 1.79 | 113.2 | 1.79 | 2.87 |
| 4/26/10 4:00 | 101.9 | 0.86 | 2.17 | 74.0 | 1.54 | 1.65 | 112.3 | 1.66 | 2.73 |
| 4/26/10 6:00 | 101.3 | 0.78 | 1.79 | 73.5 | 1.51 | 1.47 | 111.6 | 1.56 | 2.46 |
| 4/26/10 8:00 | 101.0 | 0.74 | 1.86 | 73.5 | 1.49 | 1.43 | 111.3 | 1.51 | 2.43 |
| 4/26/10 10:00 | 100.7 | 0.69 | 1.73 | 72.6 | 1.39 | 1.30 | 110.9 | 1.46 | 2.29 |
| 4/26/10 12:00 | 100.4 | 0.67 | 1.71 | 72.2 | 1.35 | 1.30 | 110.4 | 1.41 | 2.27 |
| 4/26/10 14:00 | 99.6 | 0.61 | 1.63 | 71.5 | 1.32 | 1.20 | 109.3 | 1.30 | 2.15 |
| 4/26/10 16:00 | 98.9 | 0.56 | 1.57 | 70.9 | 1.29 | 1.19 | 108.4 | 1.23 | 2.00 |
| 4/26/10 18:00 | 97.9 | 0.50 | 1.49 | 70.0 | 1.24 | 1.07 | 107.0 | 1.12 | 1.87 |
| 4/26/10 20:00 | 96.9 | 0.42 | 1.25 | 69.1 | 1.16 | 0.94 | 106.0 | 1.04 | 1.76 |
| 4/26/10 22:00 | 96.4 | 0.41 | 1.11 | 68.7 | 1.16 | 0.93 | 105.1 | 0.98 | 1.67 |
| 4/27/10 0:00 | 95.8 | 0.36 | 1.11 | 68.4 | 1.15 | 0.98 | 104.5 | 0.93 | 1.60 |

Table 8.1 - (continued) Acoustic relative backscatter (RB) and attenuation (full profile and sub profile) for 1.5, 3.0, and 1.2 MHz ADCPs.

| Date and Time | 1.5 MHz RB | 1.5 MHz $\alpha_s$ full | 1.5 MHz $\alpha_s$ sub | 3.0 MHz RB | 3.0 MHz $\alpha_s$ full | 3.0 MHz $\alpha_s$ sub | 1.2 MHz RB | 1.2 MHz $\alpha_s$ full | 1.2 MHz $\alpha_s$ sub |
|---|---|---|---|---|---|---|---|---|---|
| 4/27/10 2:00 | 95.4 | 0.34 | 1.02 | 67.8 | 1.10 | 0.94 | 104.0 | 0.89 | 1.57 |
| 4/27/10 4:00 | 95.0 | 0.31 | 1.05 | 67.5 | 1.08 | 0.90 | 103.5 | 0.85 | 1.49 |
| 5/3/10 8:00 | 98.4 | 0.53 | 1.30 | 70.6 | 1.31 | 1.20 | | | |
| 5/3/10 10:00 | 102.9 | 1.12 | 2.02 | 75.7 | 2.02 | 2.05 | | | |
| 5/3/10 12:00 | 104.8 | 1.40 | 2.29 | 78.5 | 2.56 | 2.68 | | | |
| 5/3/10 14:00 | 107.2 | 1.94 | 2.64 | 80.7 | 3.35 | 3.67 | | | |
| 5/3/10 16:00 | 109.8 | 2.92 | 3.93 | 81.2 | 4.13 | 5.01 | | | |
| 5/3/10 18:00 | 109.7 | 2.77 | 3.83 | 80.3 | 4.10 | 5.24 | | | |
| 5/3/10 20:00 | 107.3 | 1.83 | 2.48 | 79.5 | 3.48 | 3.81 | | | |
| 5/3/10 22:00 | 109.9 | 1.92 | 2.08 | 83.0 | 3.78 | 3.65 | | | |
| 5/4/10 0:00 | 109.2 | 1.63 | 1.32 | 77.1 | 3.29 | 3.30 | | | |
| 5/4/10 2:00 | 111.6 | 1.91 | 1.11 | 84.5 | 3.87 | 3.72 | | | |
| 5/4/10 4:00 | 110.6 | 1.67 | 1.48 | 85.3 | 4.01 | 4.22 | | | |
| 5/4/10 6:00 | 110.2 | 1.56 | 1.16 | 83.3 | 3.75 | 4.25 | | | |
| 5/4/10 8:00 | 108.8 | 1.39 | 1.54 | 81.3 | 3.50 | 4.03 | | | |
| 5/4/10 10:00 | 111.1 | 1.73 | 1.67 | 81.1 | 3.56 | 4.06 | | | |
| 5/4/10 12:00 | 110.1 | 1.69 | 2.35 | 80.6 | 3.88 | 5.30 | | | |
| 5/4/10 14:00 | 112.3 | 1.80 | 1.22 | 85.1 | 4.12 | 5.13 | | | |
| 5/4/10 16:00 | 112.6 | 1.78 | 0.63 | 85.8 | 4.11 | 4.62 | | | |
| 5/4/10 18:00 | 113.0 | 1.84 | 1.01 | 83.9 | 4.07 | 5.43 | | | |
| 5/4/10 20:00 | 113.2 | 1.96 | 1.17 | 82.2 | 3.89 | 5.39 | | | |
| 5/4/10 22:00 | 110.9 | 1.48 | 0.58 | 81.5 | 3.53 | 3.91 | | | |
| 5/5/10 0:00 | 110.7 | 1.45 | 0.36 | 82.0 | 3.45 | 3.93 | | | |
| 5/5/10 2:00 | 108.0 | 0.93 | 0.01 | 82.4 | 3.06 | 2.94 | | | |
| 5/5/10 4:00 | 104.3 | 0.49 | 0.24 | 80.3 | 2.42 | 2.58 | | | |
| 5/5/10 6:00 | 103.7 | 0.60 | 1.24 | 77.7 | 1.95 | 2.40 | | | |
| 5/5/10 8:00 | 104.8 | 0.76 | 1.61 | 81.4 | 2.43 | 2.92 | | | |
| 5/5/10 10:00 | 102.8 | 0.54 | 1.07 | 77.0 | 1.48 | 1.60 | | | |
| 5/5/10 12:00 | 103.3 | 0.64 | 1.00 | 77.3 | 1.55 | 1.47 | | | |
| 5/5/10 16:00 | 100.2 | 0.14 | 0.12 | 75.4 | 1.12 | 0.77 | | | |
| 5/5/10 18:00 | 99.8 | -0.04 | -0.47 | 73.5 | 0.78 | 0.66 | | | |
| 5/5/10 20:00 | 99.7 | -0.21 | -1.09 | 74.4 | 0.95 | 0.21 | | | |
| 5/5/10 22:00 | 100.4 | -0.18 | -0.66 | 75.9 | 1.23 | 0.74 | | | |
| 5/6/10 0:00 | 99.8 | -0.41 | -0.68 | 73.8 | 0.92 | 0.10 | | | |
| 9/27/10 14:00 | 92.1 | -0.04 | 0.15 | 63.3 | 0.65 | 0.41 | 99.5 | 0.53 | 0.89 |
| 9/27/10 15:00 | 92.8 | 0.05 | 0.32 | 66.1 | 0.91 | 0.68 | 100.0 | 0.56 | 0.98 |
| 9/27/10 16:00 | 92.1 | 0.02 | 0.35 | 66.0 | 0.95 | 0.71 | 99.0 | 0.53 | 0.99 |
| 9/27/10 17:00 | 91.0 | -0.03 | 0.02 | 64.9 | 0.92 | 0.72 | 97.4 | 0.47 | 0.77 |
| 9/27/10 18:00 | 90.2 | -0.09 | -0.12 | 63.8 | 0.87 | 0.71 | 95.9 | 0.39 | 0.63 |

Table 8.1 - (continued) Acoustic relative backscatter (RB) and attenuation (full profile and sub profile) for 1.5, 3.0, and 1.2 MHz ADCPs.

| Date and Time | 1.5 MHz RB | 1.5 MHz $\alpha_s$ full | 1.5 MHz $\alpha_s$ sub | 3.0 MHz RB | 3.0 MHz $\alpha_s$ full | 3.0 MHz $\alpha_s$ sub | 1.2 MHz RB | 1.2 MHz $\alpha_s$ full | 1.2 MHz $\alpha_s$ sub |
|---|---|---|---|---|---|---|---|---|---|
| 9/27/10 19:00 | 89.8 | -0.03 | -0.12 | 63.1 | 0.85 | 0.62 | 95.7 | 0.43 | 0.61 |
| 9/27/10 20:00 | 88.7 | -0.08 | -0.18 | 62.8 | 0.88 | 0.82 | 94.2 | 0.33 | 0.56 |
| 9/27/10 21:00 | 88.5 | -0.09 | -0.16 | 62.3 | 0.86 | 0.85 | 94.1 | 0.36 | 0.62 |
| 9/27/10 22:00 | 88.3 | -0.13 | -0.19 | 61.5 | 0.83 | 0.79 | 93.8 | 0.32 | 0.58 |
| 9/27/10 23:00 | 88.2 | -0.09 | -0.17 | 62.0 | 0.86 | 0.86 | 93.5 | 0.32 | 0.48 |
| 9/28/10 0:00 | 88.0 | -0.14 | -0.41 | 61.4 | 0.77 | 0.72 | 93.4 | 0.31 | 0.49 |
| 9/28/10 1:00 | 87.3 | -0.12 | -0.31 | 60.5 | 0.75 | 0.77 | 92.8 | 0.32 | 0.45 |
| 9/28/10 2:00 | 87.0 | -0.12 | -0.39 | 60.3 | 0.74 | 0.79 | 92.3 | 0.30 | 0.46 |
| 9/28/10 3:00 | 87.2 | -0.09 | -0.31 | 60.4 | 0.77 | 0.87 | 92.3 | 0.29 | 0.47 |
| 9/28/10 4:00 | 87.0 | -0.08 | -0.28 | 60.4 | 0.74 | 0.88 | 92.5 | 0.32 | 0.39 |
| 9/28/10 5:00 | 87.1 | -0.07 | -0.34 | 60.9 | 0.79 | 0.95 | 92.4 | 0.32 | 0.39 |
| 9/28/10 6:00 | 87.2 | -0.07 | -0.31 | 61.4 | 0.83 | 0.93 | 92.5 | 0.30 | 0.41 |
| 9/28/10 7:00 | 87.1 | -0.14 | -0.37 | 60.4 | 0.69 | 0.73 | 92.2 | 0.26 | 0.37 |
| 9/28/10 8:00 | 87.6 | -0.23 | -0.37 | 60.9 | 0.72 | 0.81 | 92.0 | 0.22 | 0.39 |
| 9/28/10 9:00 | 87.9 | -0.20 | -0.23 | 61.6 | 0.78 | 0.88 | 92.5 | 0.24 | 0.43 |
| 9/28/10 10:00 | 87.9 | -0.15 | -0.21 | 61.6 | 0.81 | 0.99 | 92.6 | 0.24 | 0.44 |
| 9/28/10 11:00 | 88.1 | -0.17 | -0.20 | 62.3 | 0.85 | 0.87 | 92.8 | 0.26 | 0.44 |
| 9/28/10 12:00 | 88.6 | -0.21 | -0.23 | 62.9 | 0.86 | 0.87 | 93.2 | 0.24 | 0.54 |
| 9/28/10 13:00 | 89.8 | -0.20 | -0.03 | 64.5 | 0.91 | 0.82 | 94.6 | 0.27 | 0.60 |
| 9/28/10 14:00 | 90.7 | -0.17 | 0.08 | 65.6 | 0.94 | 0.86 | 95.6 | 0.26 | 0.59 |
| 9/28/10 15:00 | 91.4 | -0.20 | 0.26 | 66.4 | 1.00 | 1.11 | 96.6 | 0.29 | 0.80 |
| 9/28/10 16:00 | 91.2 | -0.12 | 0.31 | 66.8 | 1.10 | 1.16 | 96.7 | 0.32 | 0.74 |
| 9/28/10 17:00 | 91.0 | -0.15 | 0.18 | 66.1 | 1.03 | 1.07 | 96.2 | 0.29 | 0.73 |
| 9/28/10 18:00 | 90.7 | -0.12 | 0.01 | 65.6 | 1.00 | 1.01 | 95.9 | 0.28 | 0.56 |
| 9/28/10 19:00 | 90.4 | -0.10 | 0.28 | 66.1 | 1.12 | 1.21 | 95.9 | 0.33 | 0.74 |
| 9/28/10 20:00 | 89.9 | -0.12 | 0.25 | 65.2 | 1.05 | 1.14 | 95.6 | 0.32 | 0.87 |
| 9/28/10 21:00 | 89.4 | -0.18 | -0.07 | 63.7 | 0.86 | 0.94 | 94.6 | 0.29 | 0.53 |
| 9/28/10 22:00 | 89.1 | -0.21 | -0.34 | 63.7 | 0.96 | 0.97 | 94.1 | 0.24 | 0.33 |
| 9/28/10 23:00 | 88.5 | -0.24 | -0.29 | 62.9 | 0.93 | 1.11 | 93.0 | 0.16 | 0.37 |
| 9/29/10 0:00 | 88.1 | -0.17 | 0.00 | 62.8 | 0.94 | 1.19 | 93.4 | 0.26 | 0.60 |
| 9/29/10 1:00 | 87.6 | -0.17 | -0.35 | 61.3 | 0.79 | 0.95 | 92.6 | 0.25 | 0.47 |
| 9/29/10 2:00 | 87.2 | -0.17 | -0.38 | 60.6 | 0.77 | 0.98 | 92.0 | 0.21 | 0.46 |
| 9/29/10 3:00 | 86.9 | -0.11 | -0.35 | 60.5 | 0.78 | 0.96 | 92.1 | 0.27 | 0.40 |
| 9/29/10 4:00 | 86.6 | -0.15 | -0.33 | 59.7 | 0.73 | 0.97 | 91.8 | 0.25 | 0.48 |
| 9/29/10 5:00 | 86.3 | -0.09 | -0.25 | 59.6 | 0.73 | 1.17 | 91.6 | 0.26 | 0.45 |
| 9/29/10 6:00 | 86.0 | -0.12 | -0.41 | 58.1 | 0.60 | 1.11 | 91.3 | 0.25 | 0.31 |
| 9/29/10 7:00 | 85.5 | -0.07 | -0.36 | 57.9 | 0.62 | 1.21 | 90.7 | 0.26 | 0.35 |
| 9/29/10 8:00 | 85.0 | -0.08 | -0.36 | 57.4 | 0.58 | 1.11 | 90.4 | 0.26 | 0.36 |
| 9/29/10 9:00 | 85.1 | -0.07 | -0.25 | 57.4 | 0.59 | 1.21 | 90.4 | 0.28 | 0.38 |

Table 8.1 - (continued) Acoustic relative backscatter (RB) and attenuation (full profile and sub profile) for 1.5, 3.0, and 1.2 MHz ADCPs.

| Date and Time | 1.5 MHz RB | 1.5 MHz $\alpha_s$ full | 1.5 MHz $\alpha_s$ sub | 3.0 MHz RB | 3.0 MHz $\alpha_s$ full | 3.0 MHz $\alpha_s$ sub | 1.2 MHz RB | 1.2 MHz $\alpha_s$ full | 1.2 MHz $\alpha_s$ sub |
|---|---|---|---|---|---|---|---|---|---|
| 9/29/10 10:00 | 84.8 | -0.06 | -0.38 | 56.7 | 0.51 | 1.10 | 89.8 | 0.23 | 0.39 |
| 9/29/10 11:00 | 84.4 | -0.06 | -0.38 | 56.2 | 0.48 | 1.08 | 89.3 | 0.23 | 0.35 |
| 9/29/10 12:00 | 84.1 | -0.04 | -0.29 | 56.2 | 0.53 | 1.24 | 89.2 | 0.24 | 0.30 |
| 9/29/10 13:00 | 84.0 | -0.02 | -0.29 | 55.5 | 0.46 | 1.14 | 89.0 | 0.25 | 0.31 |
| 9/29/10 14:00 | 84.0 | -0.03 | -0.24 | 55.5 | 0.44 | 1.12 | 88.9 | 0.22 | 0.30 |
| 9/29/10 16:00 | 83.7 | 0.02 | -0.23 | 55.0 | 0.42 | 1.08 | 88.9 | 0.30 | 0.42 |
| 9/29/10 18:00 | 83.7 | 0.08 | -0.16 | 55.1 | 0.44 | 1.14 | 88.8 | 0.34 | 0.43 |
| 9/29/10 20:00 | 86.6 | 0.17 | -0.03 | 58.9 | 0.70 | 1.65 | 91.3 | 0.40 | 0.43 |
| 9/29/10 22:00 | 85.4 | 0.09 | -0.22 | 56.3 | 0.45 | 1.13 | 90.5 | 0.33 | 0.32 |
| 9/30/10 0:00 | 89.7 | 0.31 | 0.74 | 60.0 | 0.83 | 2.17 | 96.5 | 0.62 | 1.05 |
| 9/30/10 2:00 | 86.1 | 0.11 | -0.09 | 57.9 | 0.62 | 1.61 | 92.2 | 0.46 | 0.72 |
| 9/30/10 4:00 | 86.3 | -0.03 | -0.36 | 57.3 | 0.48 | 0.97 | 92.1 | 0.32 | 0.42 |
| 9/30/10 6:00 | 86.1 | 0.03 | -0.25 | 56.8 | 0.48 | 0.98 | 92.4 | 0.38 | 0.52 |
| 9/30/10 8:00 | 86.5 | -0.01 | -0.25 | 57.3 | 0.51 | 1.03 | 92.9 | 0.37 | 0.50 |
| 9/30/10 10:00 | 85.8 | 0.01 | -0.33 | 55.6 | 0.39 | 1.01 | 92.1 | 0.37 | 0.48 |
| 9/30/10 12:00 | 85.3 | 0.05 | -0.24 | 56.4 | 0.50 | 1.17 | 91.4 | 0.38 | 0.52 |
| 9/30/10 14:00 | 85.3 | 0.05 | -0.26 | 55.9 | 0.44 | 0.95 | 91.0 | 0.36 | 0.40 |
| 9/30/10 16:00 | 85.4 | 0.00 | -0.31 | 57.3 | 0.54 | 0.95 | 91.3 | 0.37 | 0.45 |
| 9/30/10 18:00 | 85.7 | 0.03 | -0.26 | 59.0 | 0.74 | 1.26 | 91.4 | 0.37 | 0.53 |
| 9/30/10 20:00 | 86.2 | 0.04 | -0.16 | 60.3 | 0.82 | 1.18 | 91.9 | 0.39 | 0.51 |
| 9/30/10 22:00 | 88.4 | -0.07 |  | 63.7 | 1.06 | 1.30 | 94.2 | 0.35 | 0.63 |
| 10/1/10 0:00 | 89.7 | -0.10 | 0.13 | 65.0 | 1.05 | 1.25 | 95.7 | 0.37 | 0.82 |
| 10/1/10 2:00 | 89.0 | -0.22 | -0.03 | 63.8 | 0.97 | 1.21 | 94.4 | 0.27 | 0.70 |
| 10/1/10 4:00 | 87.9 | -0.19 | -0.11 | 61.9 | 0.86 | 1.16 | 92.8 | 0.22 | 0.50 |
| 10/1/10 6:00 | 86.9 | -0.19 | -0.17 | 60.0 | 0.73 | 1.14 | 91.5 | 0.18 | 0.40 |
| 10/1/10 8:00 | 86.1 | -0.13 | -0.28 | 59.1 | 0.68 | 1.12 | 91.1 | 0.23 | 0.40 |
| 10/1/10 10:00 | 85.5 | -0.06 | -0.28 | 58.5 | 0.66 | 1.17 | 91.1 | 0.30 | 0.54 |
| 10/1/10 12:00 | 85.0 | -0.04 | -0.32 | 57.3 | 0.58 | 1.07 | 90.2 | 0.28 | 0.29 |

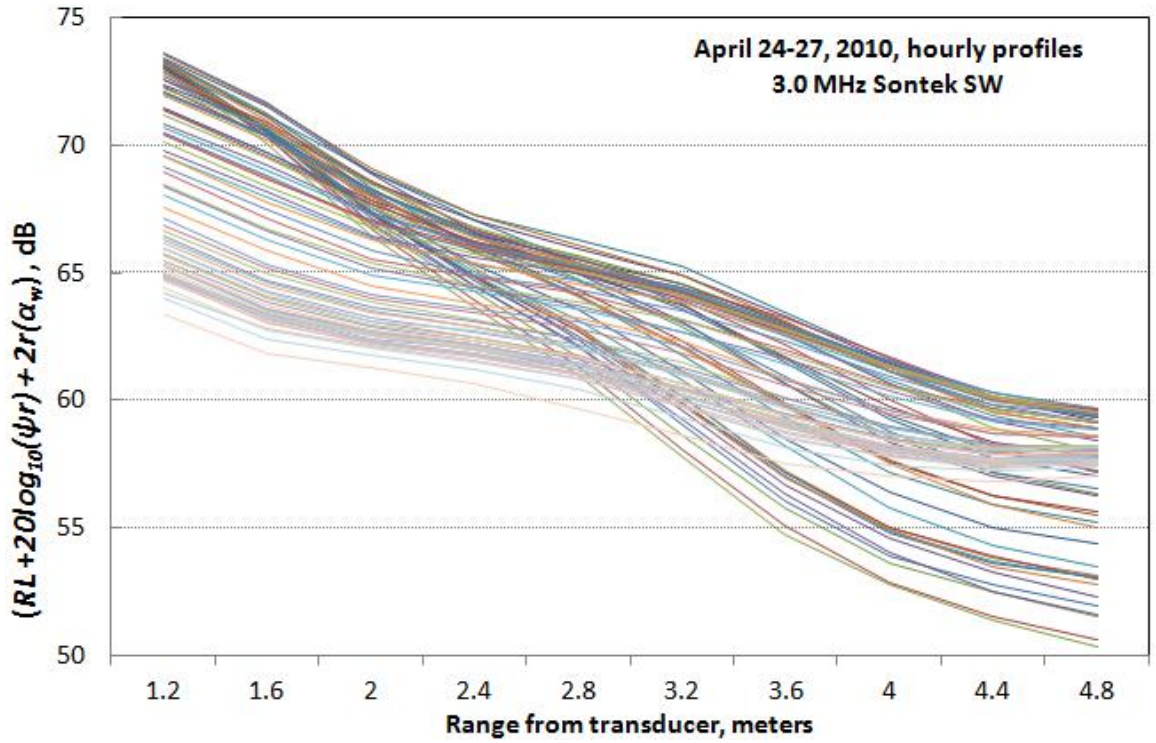


Figure 8.1 – Hourly profiles of acoustic backscatter adjusted for signal spreading and water attenuation for 3.0 MHz ADCP for event of April 24-27, 2010 for Yellow River at Gees Mill Road

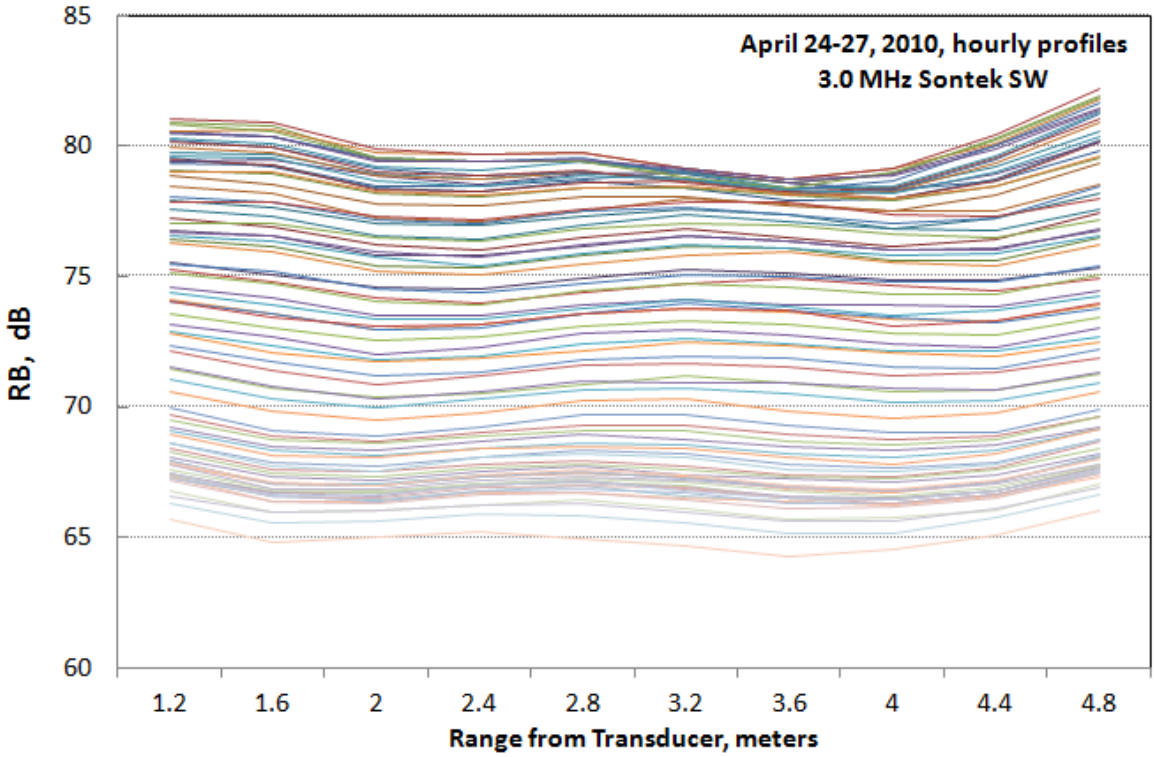


Figure 8.2 – Hourly profiles of relative backscatter for 3.0 MHz ADCP for event of April 24-27, 2010 for Yellow River at Gees Mill Road

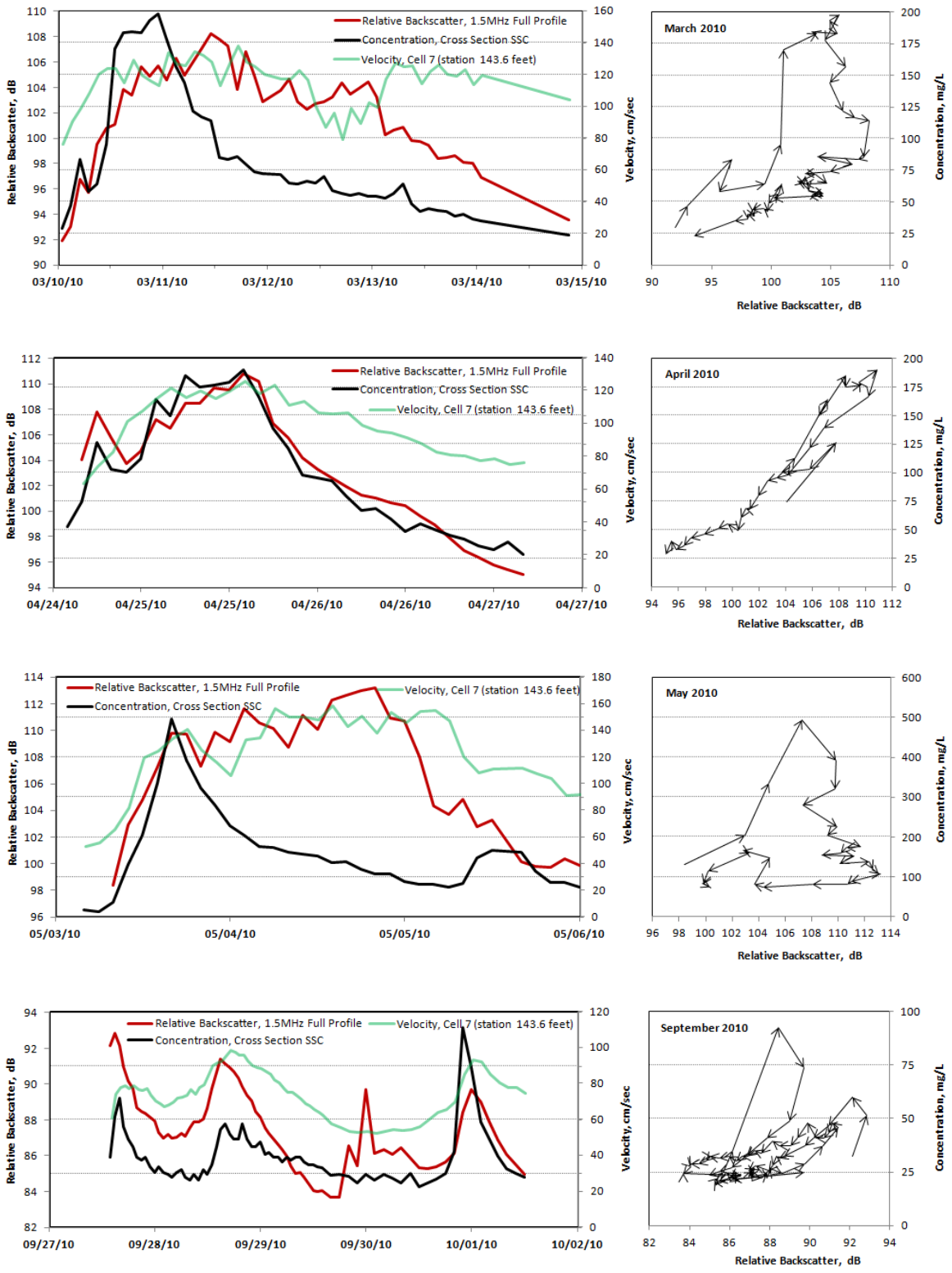


Figure 8.3 – Time series of relative backscatter, SSC, and reference velocity; and scatter plots of relative backscatter and concentration for storm events in March, April, May, and September 2010 at Yellow River at Gees Mill Road.

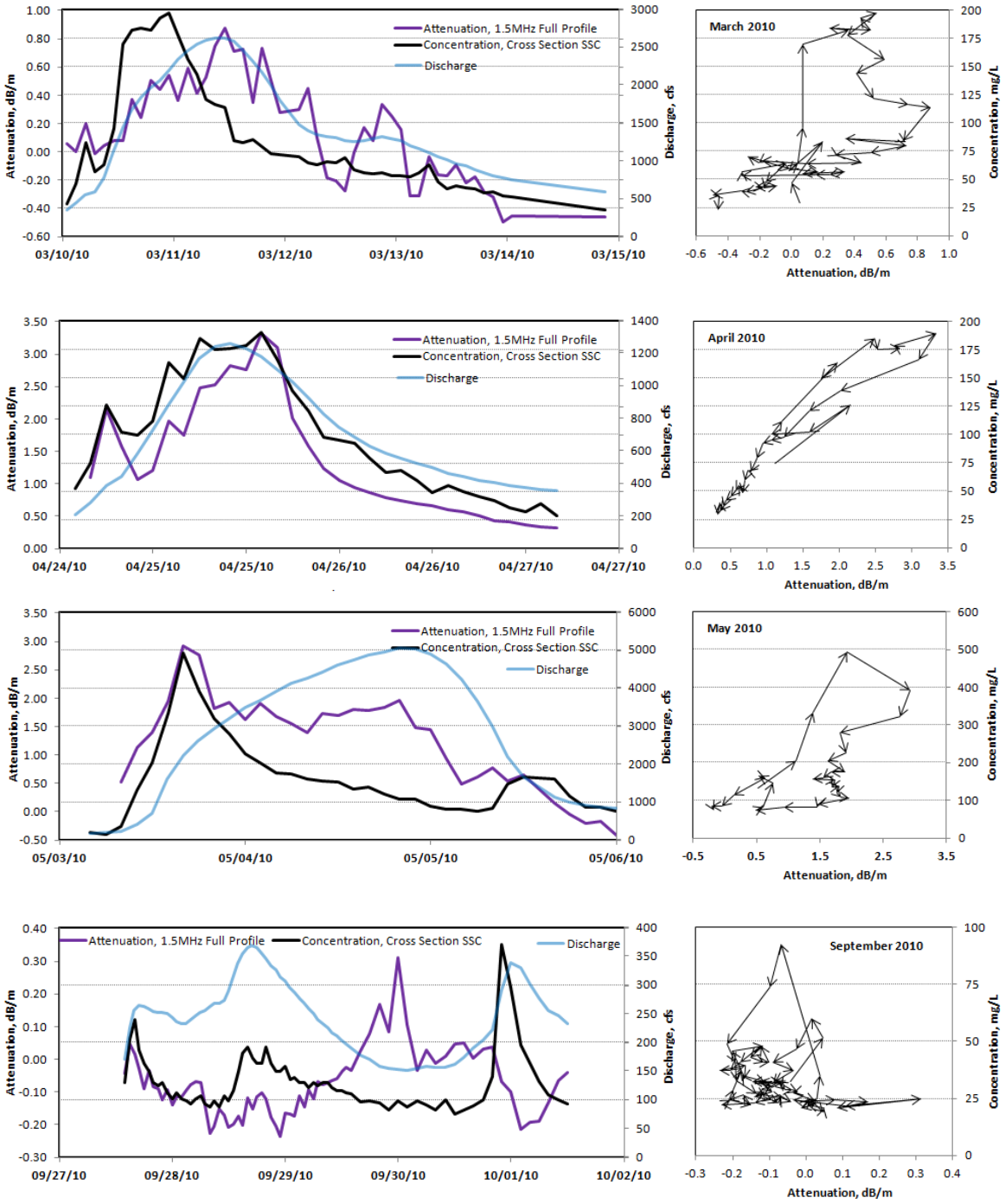


Figure 8.4 – Time series of acoustic attenuation, SSC, and discharge; and scatter plots of acoustic attenuation and concentration for storm events in March, April, May, and September 2010 at Yellow River at Gees Mill Road.

## 8.2 Proposed method for sediment size from acoustic attenuation

Sediment size data are needed to understand sediment transport and its impacts, and to adjust ratings between SSC and acoustic metrics for the effects of changing PSD. Several authors have proposed methods to estimate sediment size characteristics from acoustic metrics, as reviewed in section 2.1. The following section describes a new method to derive sediment size from acoustic metrics, as presented in the proposal for this research.

As described in section 2.1, the theoretical development and experimental evaluation of equation 1 and equation 2 generally assumed single-size particles in suspension. This single size has been represented as a mean representative sediment size affecting attenuation. The prior discussion noted that the minimum attenuation occurs in the transition from viscous to scattering losses. Solving for the transition sediment size occurring at this minimum attenuation yields particle diameters of 90, 74, and 42 microns for frequencies of 1.2, 1.5, and 3.0 MHz, respectively. These diameters roughly bracket the defined 63 micron size break between sediments classified as sands or coarser and those classified as silts or clays (fines). During high flow conditions fluvial suspended sediment typically has size distributions that include particles coarser and finer than 63 microns.

In this research it is observed that natural suspended sediment mixtures containing sizes both larger and smaller than the transition particle size for a given frequency will cause acoustic attenuation due to both viscous losses from the finer sizes and scattering losses from particles coarser than the transition particle size. Based on this observation, it is proposed for the first time in this research that equation 3 be reformulated as:

$$\alpha_S = SSC_V \left[ k(\gamma - 1)^2 \left\{ \frac{s_v}{s_v^{\,2} + (\gamma + \tau_v)^2} \right\} + \left\{ \frac{k^4 a_{nv}^{\,3}}{5(1 + 1.3k^2 a_{nv}^{\,2} + 0.24k^4 a_{nv}^{\,4})} \right\} \right] \quad 4.34\ (16)$$

where $a_{nv}$ is the average particle radius causing scattering (*nv=non-viscous*) attenuation, $s_v$ is equal to $[9/(4\beta a_v)][1+1/(\beta a_v)]$, $\tau_v$ is equal to $[0.5+9/(4\beta a_v)]$, in which $a_v$ is the average particle radius causing viscous attenuation. Values for $a_{nv}$ are constrained to be coarser than the transition particle size while values for $a_v$ are constrained to be less than the transition particle size for the frequency for which $\alpha_s$ is measured. Other variables and units are as defined previously.

If SSC is measured or estimated, then equation 16 may be solved in an optimization procedure to obtain values of $a_{nv}$ and $a_v$ using a single frequency $\alpha_s$ such that the difference between the measured and computed $\alpha_s$ is minimized. Equation 16 contains the typical *viscous* particle size, $a_v$ to the powers of -1 through -4, and the typical *scattering* particle size, $a_{nv}$ to the power of 3. Solutions to equation 16 were obtained using a Generalize Reduced Gradient optimization method (Lasdon, 1978). This method works for smooth functions and computes the gradient values at trial solutions, then moves the solution in the direction of the negative gradient (when minimizing). The method also uses second derivative analysis to follow the curvature as well as the direction of the functions. The optimum solution minimizes the difference between the measured and computed $\alpha_s$ by adjusting the values of $a_{nv}$ and $a_v$ where these values are constrained as:

$0.5um \leq [a_v] \leq a_T$

$a_T \leq [a_{nv}] \leq 2000\mu m$

where $a_T$ is the frequency-specific transition sediment size.

A second method proposed for the first time herein is to evaluate sediment size using ratios of measured acoustic attenuation for separate frequencies. Equation 16, the theoretical acoustic attenuation due to sediment, is written for each frequency as described previously. The ratio of theoretical acoustic attenuation at different frequencies is equated to the concurrently measured attenuation at separate frequencies, *i* and *j,* [$\alpha_{si}$ / $\alpha_{sj}$] obtained from equation 15. The solution no longer requires known SSC because it cancels out so that values of $a_{nv}$ and $a_v$ may be solved using equation 16 in an optimization procedure such that the difference between measured and estimated [$\alpha_{si}$ / $\alpha_{sj}$] is minimized. This procedure could be computed for any time step or [$\alpha_{si}$ / $\alpha_{sj}$] could be averaged over durations in which the particle size distribution could be assumed to be unchanging. The ratio of frequencies may provide a more robust result than a single frequency solution; although the result would still be frequency dependent because the particle sizes by this method are related to acoustic wavelength. Three frequencies should provide three ratios of [$\alpha_{si}$ / $\alpha_{sj}$] and three sets of estimated $a_{nv}$ and $a_v$.

This proposed method is conceptually similar to the method of Hay and Sheng (1992) in which sediment size is obtained from the ratio of sediment form function ($\langle f_i \rangle / \langle f_j \rangle$ ) at different frequencies (equation 9), as described in section 2.1.6. That approach requires information on the transducer specific characteristics ($K_t$) and/or an iterative solution and is applicable for a limited range of $k\langle a_s \rangle$ (the product of the wave number and sediment size). If $k\langle a_s \rangle$ is larger than about 2 or less than about 0.2, then there is no size information in $\langle f_i \rangle / \langle f_j \rangle$ (Thorne and Hanes, 2002).

## 8.3 Experimental results for proposed method for sediment size from single-frequency acoustic attenuation

The method proposed in this thesis for determining sediment size characteristics from acoustic attenuation due to sediment requires that acoustic attenuation follows the Urick-Sheng-Hay relation (equation 3, reformulated as equation 16), which is based on theory and has been verified in laboratory studies using single size sediments, as described previously.

Figures 8.5 to 8.7 show the measured data points and the theoretical acoustic attenuation from the hybrid Urick-Sheng-Hay relation (equation 16) for the 1.2, 1.5, and 3.0 MHz frequencies. The results in figures 8.5 to 8.7 are for unit concentration. The $SSC_V$ in equation 16 was set to one, and the measured acoustic attenuation values were divided by the product of concurrently measured mass SSC and 2.65 (assumed density) to obtain volumetric concentration. The theoretical curves are shown for pure water at a temperature of 20$^o$C. The sensitivity of these curves to changes in temperature and viscosity is negligible over the 11$^o$C to 23$^o$C range of temperatures for this data set. The measured attenuation values for each frequency were obtained from the slope of the full ensonified profile. Negative attenuation values were omitted from the analysis. Three independent technologies are represented in the measured data: gravimetric analysis of physical SSC samples, laser-diffraction analyzed PSD, and acoustic attenuation from the ADCP data. Figure 8.5 shows the curves for particles from 1 to 1000 microns, and figures 8.6 and 8.7 zoom into the range of observed particle sizes for the *D50* and *D10*, respectively.

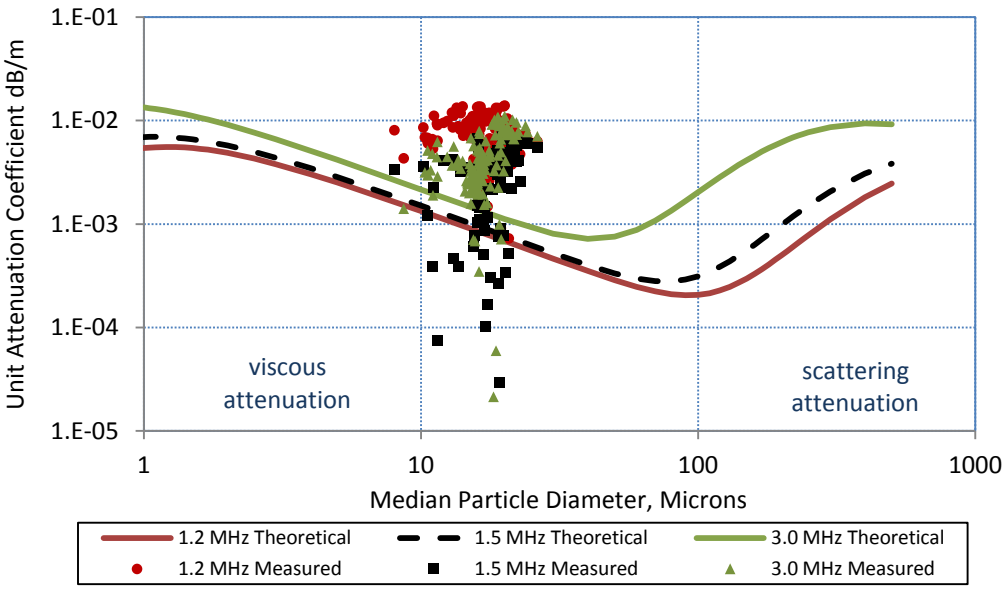


Figure 8.5- Particle size and acoustic attenuation due to suspended sediment (theoretical curves and measured values), for 1.2, 1.5, and 3.0 MHz frequencies at unit volumetric concentration and volumetric D50

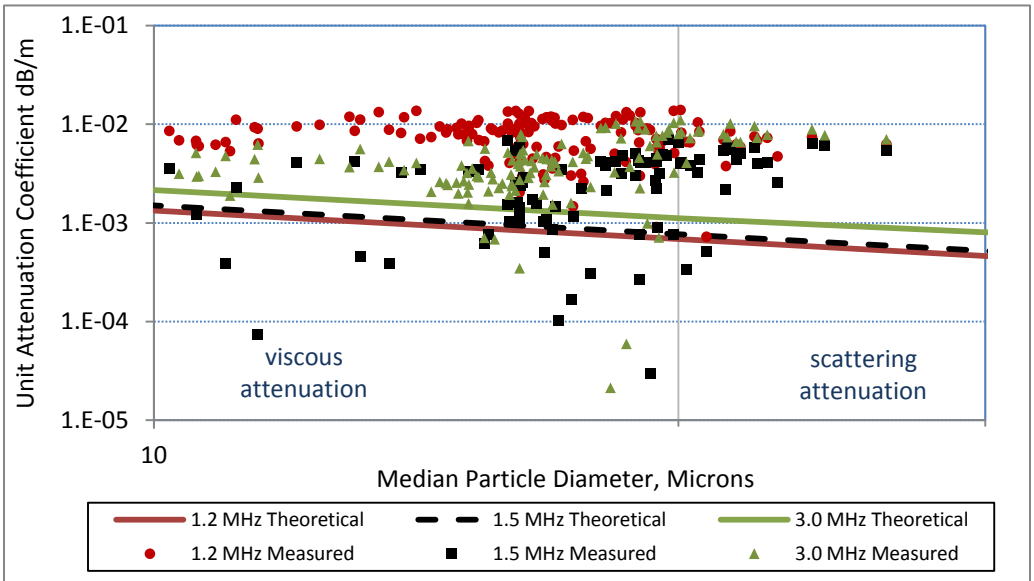


Figure 8.6 - Particle size and acoustic attenuation due to suspended sediment (theoretical curves and measured values), for 1.2, 1.5, and 3.0 MHz at unit volumetric concentration and volumetric D50 from 10 to 30 microns

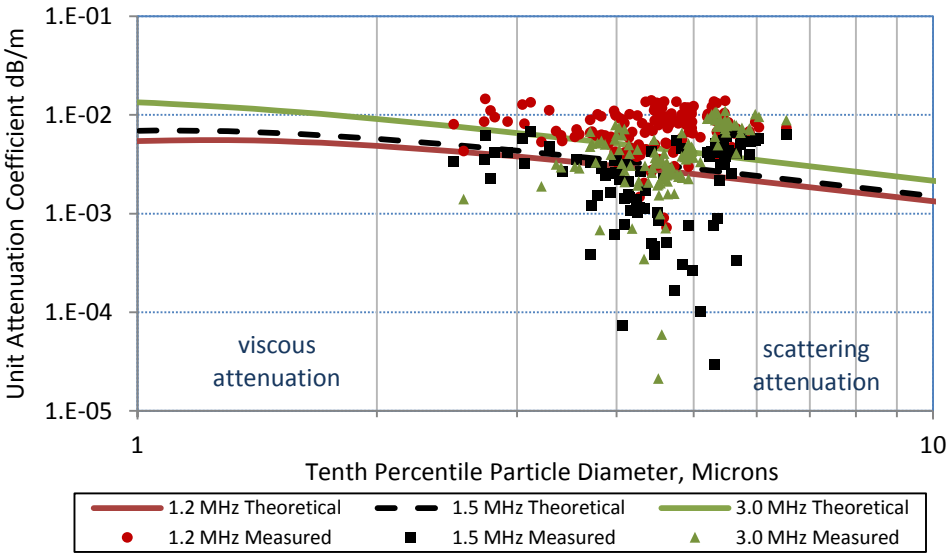


Figure 8.7 - Particle size and acoustic attenuation due to suspended sediment (theoretical curves and measured values), for 1.2, 1.5, and 3.0 MHz, unit volumetric concentration, and D10 from 1 to 10 microns

These figures illustrate that the observed data do not fit the Urick-Sheng-Hay relation and that the variance of the observed unit attenuation is much greater than the change in theoretical attenuation over the observed sediment size range. The theoretical curve is nearly flat over the measured sediment size range, indicating that theoretical attenuation is a weak function of sediment size. Even if we allow the observed unit attenuation and/or the sediment size to shift by a constant, they do not fit the theoretical curve. Furthermore, linear regressions of unit attenuation and logarithmic sediment size for the (volumetric) *D10*, *D50*, and *D84* for all three frequencies produce either an insignificant slope, or a slope that increases with increasing sediment size. This is contrary to the theoretical relation in which attenuation decreases with increasing size for sediment in this size range (viscous attenuation range). Analysis of variance indicates

that the minimum residual error is for the purely empirical relation between sediment size and unit attenuation at the frequency of 1.5MHz, with a positive slope and an $R^2$ of only 0.37. Alternate measures of sediment PSD that were evaluated in relation to acoustic attenuation include the concentration less than specific sediment sizes and the percent finer than specific sediment sizes. These alternative measures of PSD did not improve the relation with acoustic attenuation.

The observed unit acoustic attenuation values are within an order of magnitude of the theoretical curves. Also, the volumetric size data indicate that the attenuation losses are all in the viscous attenuation range. The volumetric *D50* sediment sizes are less than the acoustic transition sediment size for all 3 frequencies for all events; and the *D84* sizes are less than the transition size for all but one event for the 1.2 and 1.5 MHz frequencies. Thus, equation 16 can be constrained to solve for only the viscous sediment size solution.

The theoretical sediment size was determined for the median of the measured attenuation values for each event by solving equation 16, assuming only viscous attenuation. Table 8.2 shows the theoretical sediment size obtained by solving equation 16 for the median unit acoustic attenuation. For comparison, Table 8.2 also shows the volumetric PSD data for each event. Although the data do not fit the theoretical relation, the computed values are within an order of magnitude of the volumetric *D50* for all events. However, the results in table 8.2 are shown simply as an exercise and should not be considered as producing useful results based on the lack of fit with the theoretical relation.

Table 8.2 – Median measured acoustic sediment attenuation per unit SSC and associated theoretical sediment size, for 1.2, 1.5, and 3.0 MHz ADCPs, with laser-diffraction measured PSD data

| Event Begin Date | 3/10/2010 | 4/24/2010 | 5/3/2010 | 9/27/2010 |
|---|---|---|---|---|
| Median Unit Attenuation ($\alpha_s$) 3.0 MHz, dB/m | 5.84E-03 | 7.37E-03 | 7.61E-03 | 8.93E-03 |
| Median Unit Attenuation ($\alpha_s$) 1.5 MHz, dB/m | 1.12E-03 | 4.39E-03 | 3.30E-03 | 4.61E-04 |
| Median Unit Attenuation($\alpha_s$) 1.2 MHz, dB/m | 3.25E-03 | 8.33E-03 | -- | 3.70E-03 |
| Number of Measurements of $\alpha_s$ | 49 | 32 | 34 | 72 |
| Theoretical sediment size for ($\alpha_s$) 3.0 MHz, µm | 3.4 | 2.6 | 2.5 | 2.1 |
| Theoretical sediment size for ($\alpha_s$) 1.5 MHz, µm | 14 | 3.0 | 4.2 | 34 |
| Theoretical sediment size for ($\alpha_s$) 1.2 MHz, µm | 3.7 | no solution | -- | 3.1 |
| Laser-Diffraction Measured Average *D10*, µm | 4 | 6 | 4 | 5 |
| Laser-Diffraction Measured Average *D16*, µm | 6 | 7 | 5 | 6 |
| Laser-Diffraction Measured Average *D50*, µm | 17 | 21 | 16 | 15 |
| Laser-Diffraction Measured Average *D84*, µm | 69 | 61 | 76 | 57 |

There may be a significant limitation in the application of the theoretical relations of Urick (1948) and Sheng and Hay (1988) to natural fluvial environments with well graded suspended sediment. Urick (1948) proved the viscous acoustic attenuation using sediment from 0.9 to 2.2 microns with frequencies from 1 to 25 MHz. Flammer (1962) and Sheng and Hay (1988, using primarily Flammer's data) proved the scattering acoustic attenuation for particle sizes from about 40 to 500 microns. The literature search did not find any prior laboratory or field investigations that compare measured and theoretical attenuation for well graded natural fluvial streams. This is an important finding of this research and further comparisons are recommended for future research.

In conclusion it appears that either deterministic factors other than sediment size are dominating the variance in observed acoustic attenuation; or that acoustic attenuation

from a natural, non-uniform PSD cannot be uniquely related to a characteristic sediment size fraction, or that measurement errors cause a range of variance that overwhelms the resolution of the theoretical relation. This finding of no significant size information in the single frequency attenuation results is in general agreement with prior theoretical evaluations; but has been verified using this method through these experimental results shown here for the first time.

## 8.4 Experimental result for proposed method for sediment size from multi-frequency acoustic attenuation

The method proposed in this thesis for determining sediment size characteristics from multi-frequency acoustic attenuation, as for single frequency, is based on the theoretical Urick-Sheng-Hay relation. As shown in the previous section, the data do not fit this relation. However, using the ratio of the attenuation from two ADCP frequencies may mitigate or normalize for some of the causes and/or measurement errors that render the single-frequency method ineffective.

Figures 8.8 to 8.10 show the measured and theoretical attenuation ratios for a range of particle sizes for the frequency ratios: 3.0 to 1.2 MHz; 3.0 to 1.5 MHz; and 1.5 to 1.2 MHz. Negative measured attenuation values were omitted from the analysis. The theoretical ratios are for the Urick-Sheng-Hay relation. The theoretical curves are shown for pure water at a temperature of 20$^{o}$C. The sensitivity of these curves to changes in temperature and viscosity is negligible over the 11$^{o}$C to 23$^{o}$C range of temperatures for this data set. The attenuation ratios were evaluated over the full ensonified profile and over sub-sections of the profile. The full acoustic profiles for the three frequency units do not overlap entirely, as discussed in chapter 4 (see figure 4.9). Figures 8.8 to 8.10 show the spatially concurrent attenuation ratios for the profile sub range located from about 1.5 to 3.0 meters from the transducer faces.

Figures 8.8 to 8.10 illustrate that the range of the observed attenuation ratios far exceeds the theoretical range over the observed particle sizes. Thus there is no sediment size information in the individual measurements and the proposed theoretical method will not yield usable size information from individual measurements.

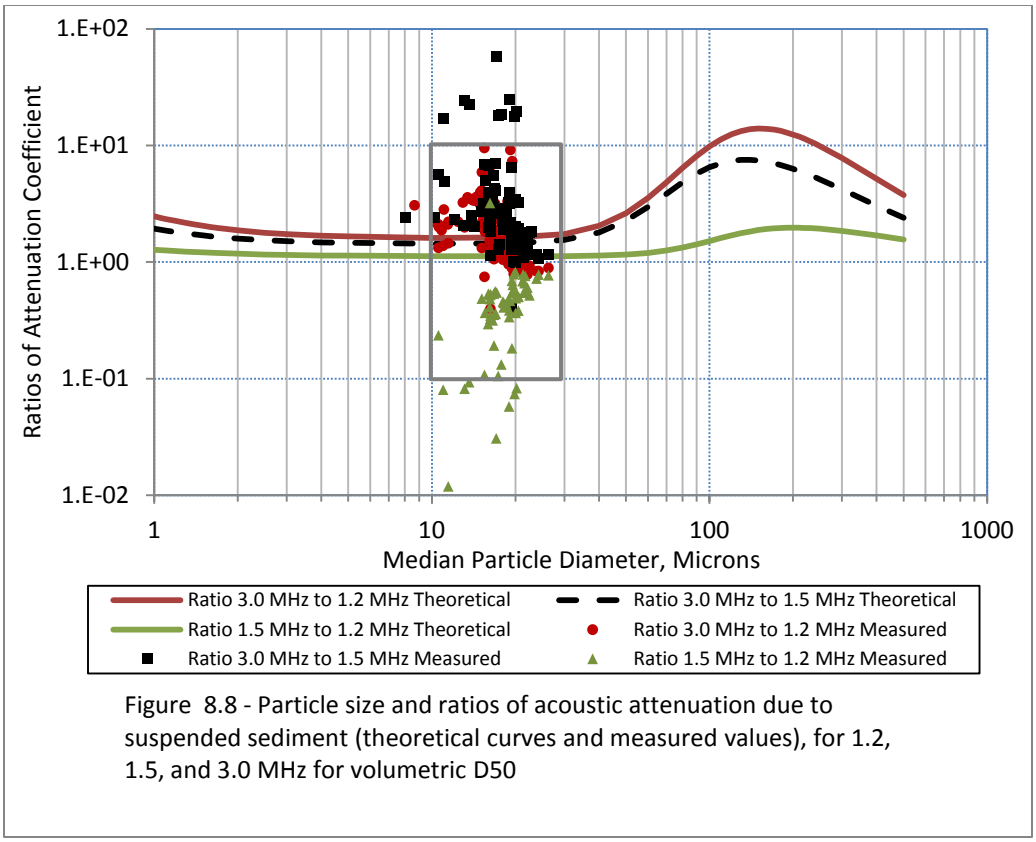


Figure 8.8 - Particle size and ratios of acoustic attenuation due to suspended sediment (theoretical curves and measured values), for 1.2, 1.5, and 3.0 MHz for volumetric D50

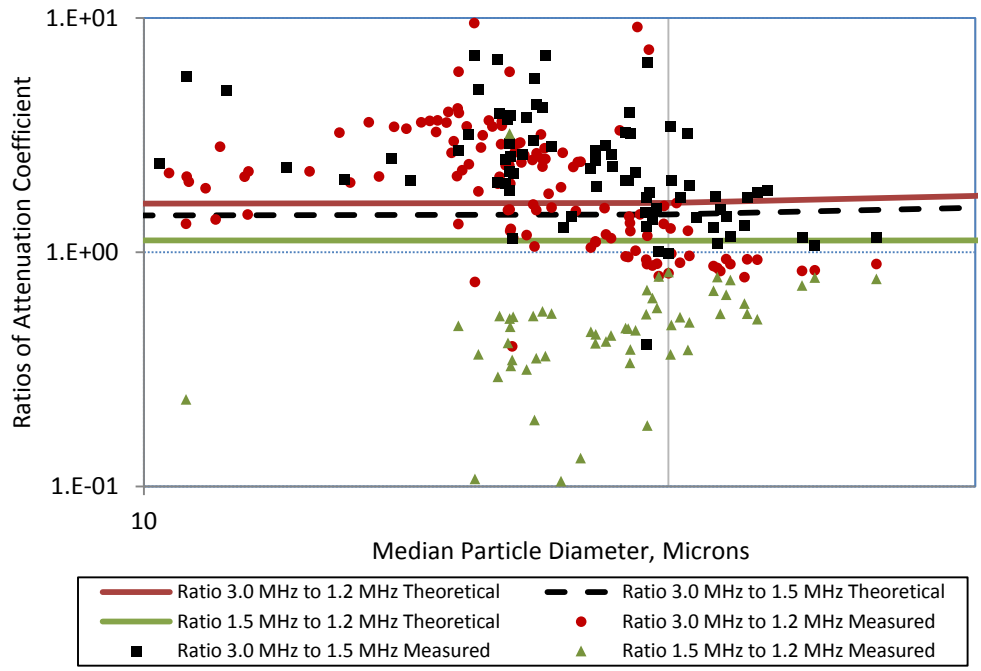


Figure 8.9 - Particle size and ratios of acoustic attenuation due to suspended sediment (theoretical curves and measured values), for 1.2, 1.5, and 3.0 MHz, for volumetric D50 from 10 to 30 microns and ratios from 0.1 to 10

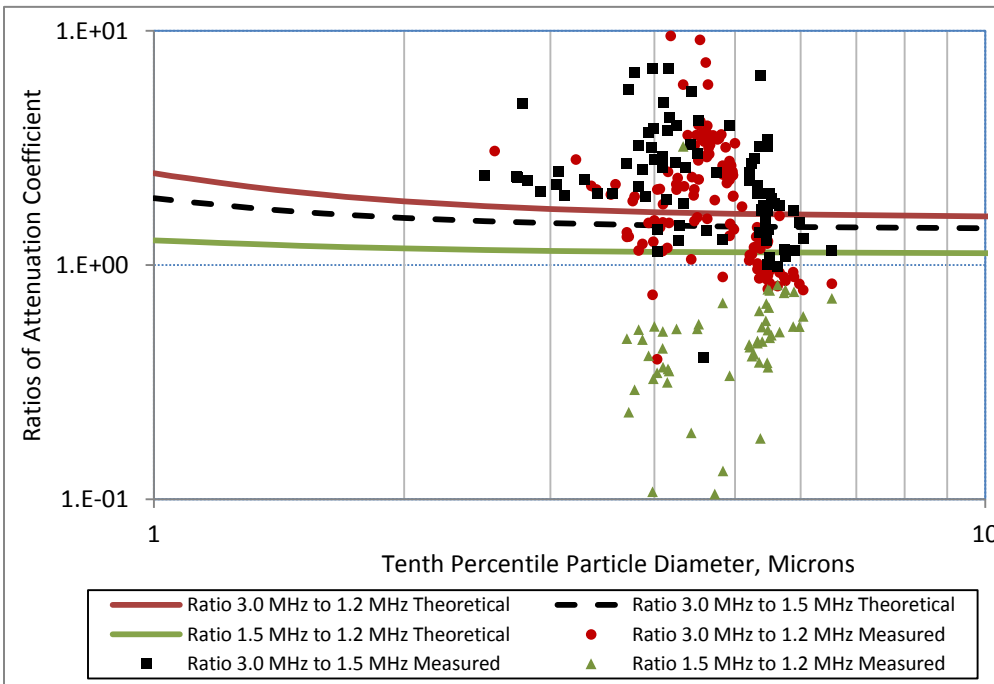


Figure 8.10 - Particle size and ratios of acoustic attenuation due to suspended sediment (theoretical curves and measured values), for 1.2, 1.5, and 3.0 MHz, for volumetric D10 from 1 to 10 microns and ratios from 0.1 to 10

Also, the measured attenuation ratios are often less than one, which is theoretically incorrect. The sediment attenuation is theoretically higher for higher frequencies (smaller wavelengths) for a given sediment size. Thus the computed ratio is expected to be always greater than one for the frequency ratios used here: 3.0 to 1.2 MHz; 3.0 to 1.5 MHz; and 1.5 to 1.2 MHz. However, as shown in the figures and in table 8.3 the observed attenuation ratios are often less than one. The reasons for this may be related to non-uniform sediment sizes and/or to differences in acoustic signal characteristics. The 1.2MHz unit, manufactured by RDI, uses a broadband width signal in default mode; while the 1.5 and 3.0 MHz units, manufactured by Sontek/YSI Inc., use a narrowband width. The 1.2MHz unit was programmed to operate in narrowband mode so that results would be comparable; however the actual signal processing to achieve this conversion within the RDI software may lead to signal results that are affected by factors other than frequency. This is particularly evident in the ratios of the 1.5MHz to 1.2MHz results, which are nearly always less than 1.0.

The lack of agreement between observed and theoretical sediment attenuation ratios may be related to the sensitivity and response of the frequencies used in this study to the observed sediment sizes. The scattering attenuation will depend on the ratio of the particle size and the acoustic wavelength, which is usually expressed as $k\langle a_s \rangle$ (the product of the wave number and sediment size). In the form function ratio method of Hay and Sheng (1992) for estimating sediment size, the optimal $k\langle a_s \rangle$ is equal to 1, which would occur for sediment diameters of 394, 315, and 157 μm for frequencies of 1.2, 1.5, and 3.0 MHz, respectively (optimal $\langle a_s \rangle$ varies linearly with wavelength). The method of Hay and Sheng (1992) is applicable only for a limited range of $k\langle a_s \rangle$ where $k$ is the wave number and $\langle a_s \rangle$ is the average sediment radius. If $k\langle a_s \rangle$ (dimensionless) is larger than about 2 or less than about 0.2, then there is no size information in $\langle f_i \rangle / \langle f_j \rangle$. Taking the

radius of the volumetric *D50* to represent $<a_s>$, the average *kD50* values for the 1.2, 1.5, and 3.0MHz units for this data set are 0.045, 0.056, and 0.112, respectively. Thus, the form function method would also not be expected to indicate meaningful sediment size. The method proposed in this thesis is derived independently of the form function method, from a different theoretical equation. However, both rely on quantifiable changes with sediment size in ratios of frequency-specific acoustic metrics.

Table 8.3—Median ratio of measured acoustic sediment attenuation and associated theoretical sediment size for 1.2, 1.5, and 3.0 MHz ADCPs.

| Event Begin Date | 3/10/2010 | 4/24/2010 | 5/3/2010 | 9/27/2010 |
|---|---|---|---|---|
| Median $\alpha_s$ Ratio 3.0 to 1.2 MHz | 1.251 | 0.619 | -- | 2.089 |
| Median $\alpha_s$ Ratio 3.0 to 1.5 MHz | 5.229 | 0.834 | 2.431 | 4.202 |
| Median $\alpha_s$ Ratio 1.5 to 1.2 MHz | 0.296 | 0.770 | -- | 0.325 |
| Sediment size for $\alpha_s$ Ratio 3.0 to 1.2 MHz | no solution | no solution | -- | 1.4 |
| Sediment size for $\alpha_s$ Ratio 3.0 to 1.5 MHz | 84 | no solution | 52 | 74 |
| Sediment size for $\alpha_s$ Ratio 1.5 to 1.2 MHz | no solution | no solution | -- | no solution |

Neither the individual sediment ratio measurements, nor the median ratios provide meaningful sediment size data. As an exercise, Table 8.3 shows the theoretical sediment size for the median of the measured ratios of acoustic attenuation for each event. The theoretical ratios only contained solutions for four of the observed median ratios; and the particle sizes for these theoretical solutions do not appear to relate to the observed volumetric PSD.

Potential causes for the lack of agreement between observed and theoretical sediment attenuation ratios include unaccounted for deterministic factors, an inability for the theoretical relation to represent characteristic sediment size for a typical well graded,

fluvial PSD, and/or measurement errors that overwhelm the resolution of the theoretical relation. Even is one had relatively uniform sediment sizes, the theoretical attenuation ratio is only weakly related to sediment size for the range of size measured here, as indicated by the relatively flat curves in figures 8.9 and 8.10. This finding does not provide the acoustically based, theoretically grounded sediment size evaluation tool that was hoped for in the research proposal. This finding is significant because multi-frequency approaches have been described as having significant promise (Gray and Gartner, 2009) for accounting for sediment size effects and is the basis for other ongoing research studies.

## 8.5 Empirical evaluation of sediment size from multi-frequency acoustic attenuation

In the previous section the measured attenuation was found to have a variance larger than the resolution of theoretical relations. In the current section, a purely empirical approach is taken to relate the ratio of measured acoustic attenuation to sediment PSD. As noted in section 8.3, there is no significant relation between single frequency sediment attenuation and sediment PSD. However, analysis of variance indicates that the ratios of measured acoustic attenuation are related to sediment PSD. Also, as shown in table 8.4, sediment attenuation tends to increase with decreasing sediment size, as indicated in the negative slope of linear regression of logarithmic PSD size fractions on attenuation ratios. This agrees with the theory for attenuation ratios of higher frequency to lower frequency.

The results show that the relation between acoustic attenuation ratios and PSD sizes is strongest at the *D16* size class and becomes weaker for the *D50* and *D60*, and is not statistically significant for the *D84* size class. The reason for the strongest relation

occurring at the *D16* size fraction is not apparently related to optimum sediment size for the acoustic wavelength; as these would theoretically be maximizing at much larger particle sizes as discussed previously. Particle shape may be causative for the observed results, as shape is likely changing significantly for the smaller size fractions (*D16* and *D10*) versus larger size fractions. The smaller size fractions are primarily fine to very fine silt which characteristically have flatter shapes and greater surface area, which leads to increased viscous attenuation.

Table 8.4—Results of analysis of variance for volumetric particle size classes and ratios of acoustic attenuation at frequencies of 1.2, 1.5, and 3.0 MHz

| Dependent ~ Independent Variable (logarithmic space) | $R^2$ | Resi-dual Std Err | Std Err % | Slope | p<0.001 |
|---|---|---|---|---|---|
| *D10* ~ Ratio $\alpha_{s3.0} / \alpha_{s1.2}$ | 0.54 | .0389 | 9 | -0.15 | Y |
| *D16* ~ Ratio $\alpha_{s3.0} / \alpha_{s1.2}$ | 0.64 | .0352 | 8 | -0.17 | Y |
| *D50* ~ Ratio $\alpha_{s3.0} / \alpha_{s1.2}$ | 0.53 | .0549 | 13 | -0.21 | Y |
| *D60* ~ Ratio $\alpha_{s3.0} / \alpha_{s1.2}$ | 0.33 | .0734 | 18 | -0.20 | Y |
| *D84* ~ Ratio $\alpha_{s3.0} / \alpha_{s1.2}$ | 0.02 | .1466 | | | N |
| *D10* ~ Ratio $\alpha_{s3.0} / \alpha_{s1.5}$ | 0.38 | .0782 | 28 | -0.14 | Y |
| *D16* ~ Ratio $\alpha_{s3.0} / \alpha_{s1.5}$ | 0.39 | .0679 | 17 | -0.12 | Y |
| *D50* ~ Ratio $\alpha_{s3.0} / \alpha_{s1.5}$ | 0.32 | .0710 | 18 | -0.11 | Y |
| *D60* ~ Ratio $\alpha_{s3.0} / \alpha_{s1.5}$ | 0.23 | .0736 | 18 | -0.09 | Y |
| *D84* ~ Ratio $\alpha_{s3.0} / \alpha_{s1.5}$ | 0.0 | .115 | | | N |
| *D10* ~ Ratio $\alpha_{s1.5} / \alpha_{s1.2}$ | 0.35 | .0464 | 11 | 0.09 | Y |
| *D16* ~ Ratio $\alpha_{s1.5} / \alpha_{s1.2}$ | 0.40 | .0438 | 11 | 0.10 | Y |
| *D50* ~ Ratio $\alpha_{s1.5} / \alpha_{s1.2}$ | 0.39 | .0457 | 11 | 0.10 | Y |
| *D60* ~ Ratio $\alpha_{s1.5} / \alpha_{s1.2}$ | 0.32 | .0470 | 11 | 0.09 | Y |
| *D84* ~ Ratio $\alpha_{s1.5} / \alpha_{s1.2}$ | 0.04 | .0638 | | | N |

The results in table 8.4 also show that the relation between acoustic attenuation ratios and PSD sizes is stronger for the ratio of 3.0 to 1.2 MHz (figure 8.11) compared to the other frequency ratios, although the reasons for this are unknown. Alternate measures of sediment PSD that were evaluated in relation to acoustic attenuation include the concentration less than specific sediment sizes and the percent finer than specific sediment sizes. These alternative measures of PSD did not have an improved relation with acoustic attenuation. These empirical results will be used in the analysis of the relation of SSC to relative backscatter.

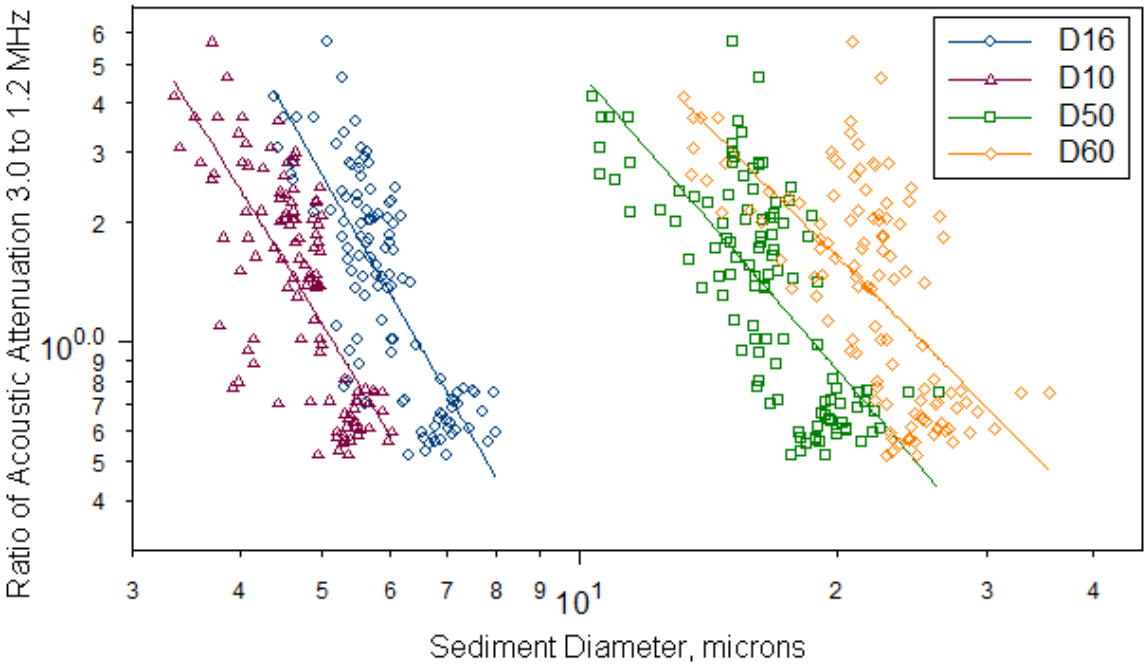


Figure 8.11—Sediment diameter for size fractions of volumetric PSD and $\alpha_{s3.0}$ / $\alpha_{s1.2}$ (ratio of acoustic attenuation for 3.0 to 1.2 MHz ADCPs)

# 9 Suspended Sediment Concentration from Acoustic Surrogates

The primary acoustic surrogate metric for $SSC_{xs}$ is relative backscatter, *RB* as described in prior chapters. The relation of logarithmic $SSC_{xs}$ to *RB* (which is logarithmic by definition) is shown in figures 9.1 to 9.3 for the 1.2, 1.5, and 3.0MHz units. Table 9.1 shows results of analysis of variance (ANOVA) and simple linear regression (SLR) for selected acoustic metrics and logarithmic $SSC_{xs}$. For reference, table 9.1 also shows results for logarithmic $SSC_{xs}$ and logarithmic index velocity (at station 143.6 feet; 4.25 meters from the transducer face, near the channel thalweg and about 2.3 feet above the bed). The relative backscatter, as described previously, is determined using $\alpha_s$ from the full ensonified profile. The subprofile attenuation is taken from the ensonified subprofile located about 1.5 to 3.0 meters from the transducer face.

The *RB* explains from 75 to 77 % of the observed variance in the log-transformed $SSC_{xs.}$ The attenuation was used to adjust the acoustic return level in the computation of *RB*. However, attenuation is a measure of sediment-acoustic interaction that is separate from scattering, particularly where viscous acoustic losses are dominant, as for this site. Thus, it is theoretically reasonable to include both *RB* and $\alpha_s$ in a multiple linear regression (MLR) model of $SSC_{xs}$.

Inclusion of both *RB* and $\alpha_s$ in a multiple linear regression (MLR) model explains from 80 to 83 percent of the observed variance in log-transformed $SSC_{xs.}$ Inclusion of both *RB* and $\alpha_s$ does not cause multicollinearity in the model, as indicated by the variance inflation factor (VIF, Helsel and Hirsch, 2002). Multicollinearity is considered to be

significant at VIF values greater than about 10. The VIF values for *RB* and full-profile $\alpha_s$ for the 1.2, 1.5, and 3.0 MHz results are 1.6, 1.8, and 1.9, respectively. The VIF values for *RB* and sub-profile $\alpha_s$ for the 1.2, 1.5, and 3.0 MHz results are 1.2, 1.3, and 1.2, respectively. The single parameter correlation with $SSC_{xs}$ is greater for full-profile $\alpha_s$ than for sub-profile $\alpha_s$, as seen in table 9.1. However, when included with *RB* in MLR, the sub-profile $\alpha_s$ provides more explanatory information, as indicated by the $R^2$ and model standard error.

As an additional test in the regression model development, the logarithmic $SSC_{xs}$ was related to $\alpha_s$ and ($RL + 20log_{10}(\psi r) + 2r(\alpha_w)$) (RL values, adjusted for signal spreading and water attenuation, but not sediment attenuation), to see if an improved model results when $\alpha_s$ is not used to adjust backscatter following theory. This test stochastically determines how $\alpha_s$ and ($RL + 20log_{10}(\psi r) + 2r(\alpha_w)$) relate to logarithmic $SSC_{xs}$. The resulting models had slightly higher standard error and lower $R^2$ than the models using *RB* and $\alpha_s$.

Table 9.1 SLR and ANOVA results for log($SSC_{xs}$) and surrogate acoustic metrics

| Dependent ~ Independent Parameters | $R^2$ | Residual Standard Error | Slope | p< 0.001 | Degrees of Freedom |
|---|---|---|---|---|---|
| $log(SSC_{xs}) \sim RB_{1.5MHz}$ | 0.76 | 0.159 | 0.032 | Y | 182 |
| $log(SSC_{xs}) \sim full\ \alpha_{s\ 1.5MHz}$ | 0.57 | 0.211 | 0.298 | Y | 182 |
| $log(SSC_{xs}) \sim sub\ \alpha_{s\ 1.5MHz}$ | 0.38 | 0.256 | 0.151 | Y | 181 |
| $log(SSC_{xs}) \sim RB_{3.0.5MHz}$ | 0.77 | 0.157 | 0.032 | Y | 183 |
| $log(SSC_{xs}) \sim full\ \alpha_{s\ 3.0MHz}$ | 0.61 | 0.204 | 0.244 | Y | 183 |
| $log(SSC_{xs}) \sim sub\ \alpha_{s\ 3.0MHz}$ | 0.43 | 0.244 | 0.175 | Y | 183 |
| $log(SSC_{xs}) \sim RB_{1.2MHz}$ | 0.75 | 0.140 | 0.022 | Y | 150 |
| $log(SSC_{xs}) \sim full\ \alpha_{s\ 1.2MHz}$ | 0.47 | 0.204 | 0.210 | Y | 150 |
| $log(SSC_{xs}) \sim sub\ \alpha_{s\ 1.2MHz}$ | 0.31 | 0.232 | 0.115 | Y | 150 |
| $log(SSC_{xs}) \sim log(velocity)$ | 0.60 | 0.207 | 2.036 | Y | 184 |

It is interesting that for all frequencies, *RB* explains more of the observed variance in log($SSC_{xs}$) than log(*velocity*) alone. This implies that surrogate metrics can be more effective than deterministic ones in explaining changing suspended sediment characteristics, in part because of the more complex, overlapping, multi-determinant relations between SSC and deterministic parameters like velocity and discharge. Velocity could be used in a MLR of log($SSC_{xs}$) on *RB*, $\alpha_s$ and log(*velocity*), since all are acoustically determined in this case. Inclusion of velocity in the MLR improved the results slightly, by about 2 percent, for the 1.5 and 1.2 MHz acoustics; but not for the 3.0MHz acoustics. The decision was made to use only the actual surrogate metrics of $\alpha_s$ and *RB* in the acoustic surrogate models for $SSC_{xs}$ for this study.

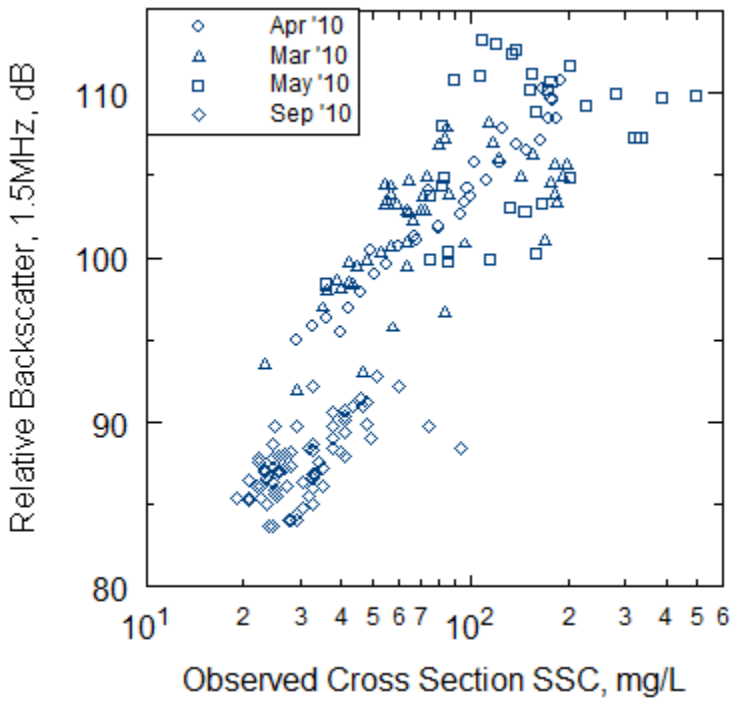


Figure 9.1--Relative backscatter for 1.5MHz ADCP and cross section average SSC

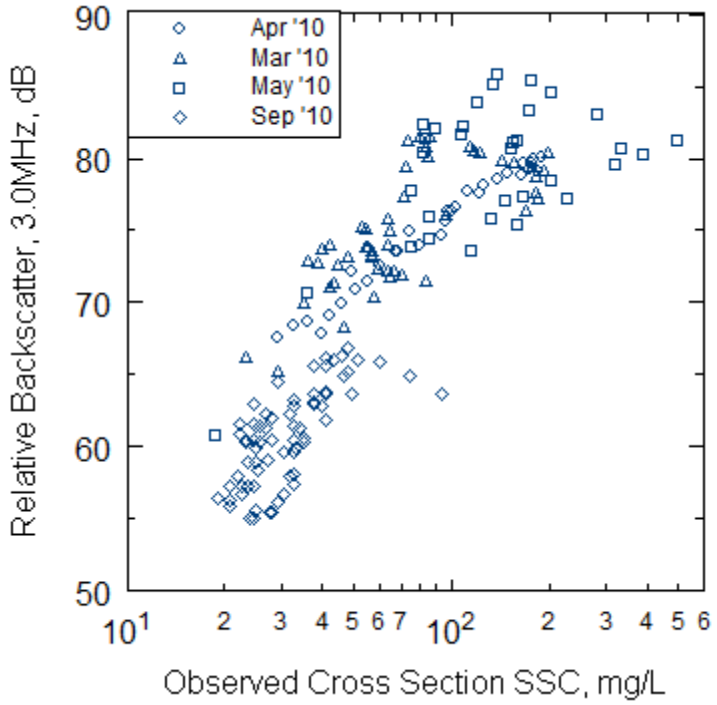


Figure 9.2--Relative backscatter for 3.0MHz ADCP and cross section average SSC

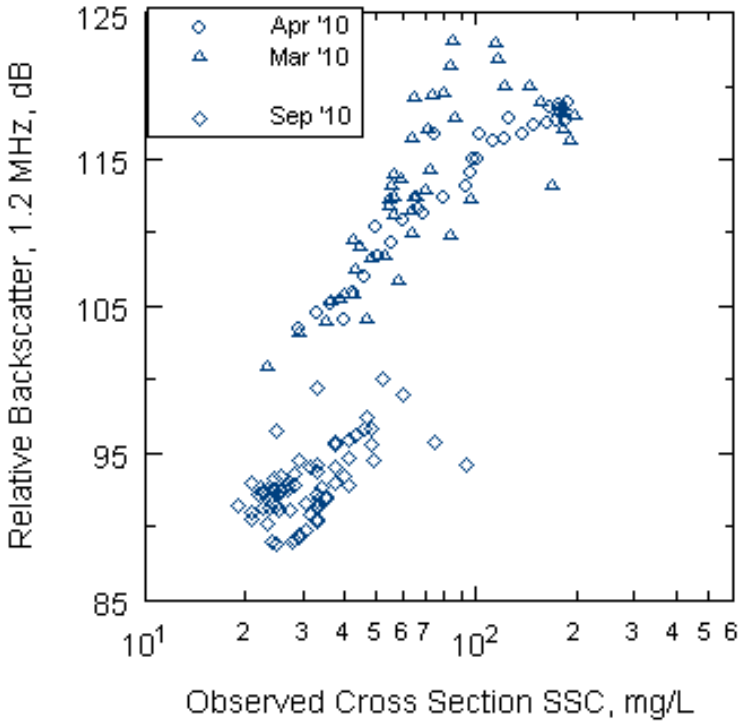


Figure 9.3-Relative backscatter for 1.2 MHz ADCP and cross section average SSC

One goal of the Chapter 8 analysis to obtain sediment size information from acoustic metrics was to reduce the variance in observed $SSC_{xs}$~$RB$ relations, which is assumed to be affected by changing sediment size characteristics. A surprising result of this analysis is that the sediment PSD was not related to residuals of the SLR of log($SSC_{xs}$) and $RB$, nor to residuals of the MLR of log($SSC_{xs}$) and $RB$+ $\alpha_{s.}$ Sediment PSD parameters were not statistically significant (at a p-value of 0.01) to the residual variance and did not improve MLR of log($SSC_{xs}$) on acoustic metrics for the 1.5 and 3.0 MHz results; and were only marginally, and perhaps spuriously related for the 1.2 MHz results (best $R^2$=0.07 at p=0.0012). Graphical analysis of the 1.2MHz results did not confirm the statistical significance). These tests were conducted using several measures of the

sediment PSD from the laser-diffraction results including sediment size for *D10*, *D16*, D15, *D50*, *D60*, and *D84*, concentration less than specific sizes, and percent concentration less than specific sizes. Also, the ratio of acoustic attenuation coefficients, $\alpha_{s3.0}$ / $\alpha_{s1.2}$ was not related to the residuals. This is shown in figure 9.4 for the volumetric *D50* and for $\alpha_{s3.0}$ / $\alpha_{s1.2}$.

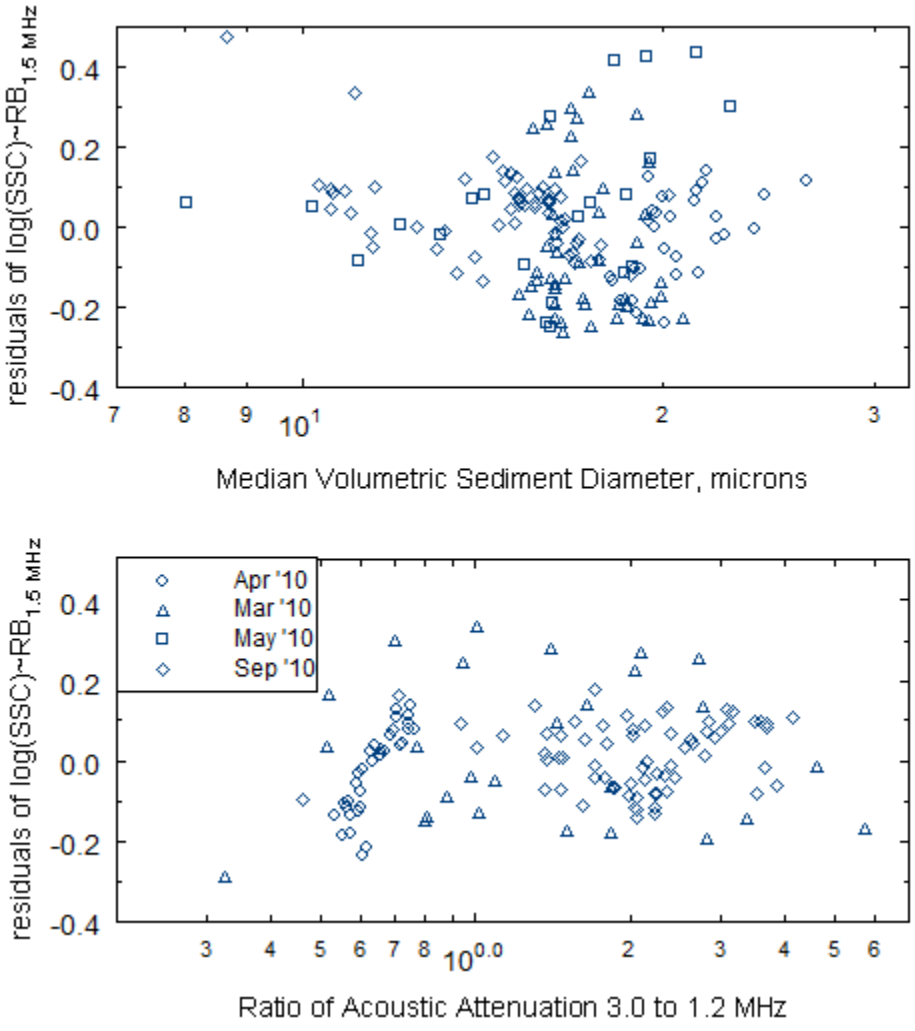


Figure 9.4—Residuals of simple linear regression of SSCxs on *RB* for 1.5MHz ADCP with median volumetric sediment size (A) and with the ratio of $\alpha_{s3.0}$ / $\alpha_{s1.2}$.

The single frequency $\alpha_s$ results are not related to sediment size, as described in section 8.3; thus their significance in explaining variance in $SSC_{xs}$ is apparently not related to sediment size effects. Residuals of SLR of $SSC_{xs}$ and ($RL + 20log_{10}(\psi r) + 2r(\alpha_w)$), also do not vary significantly with sediment size parameters. Thus, while it is known theoretically that hydroacoustics are affected by sediment PSD characteristics, these effects are not apparent in this extensive data set for a natural fluvial system. As discussed in Chapter 8, this may be due to unaccounted for deterministic factors, an inability for the theoretical relation to represent characteristic sediment size for a typical well graded, fluvial PSD, and/or measurement errors that overwhelm the resolution of the theoretical relation.

The final selected MLR models of $SSC_{xs}$ as a function of acoustic metrics for the 1.2, 1.5, and 3.0MHz frequencies are shown in table 9.2. The *RB* is from the full ensonified profile and the $\alpha_s$ is taken from the subprofile located from about 1.5 to 3.0 meters from the transducers. The DF (degrees of freedom) for the 1.2MHz system is smaller than the other frequencies because this unit was not recording during the May 2010 event.

Table 9.2—Results of multiple linear regression of SSCxs on acoustic surrogate metrics

| Explan-atory Variables | $R^2$ | DF | Res Std Err | Res Std Err % | $R^2_{pred}$ | Linear Regression Model |
|---|---|---|---|---|---|---|
| $RB_{1.5MHz}$ $\alpha_{s\ 1.5MHz}$ | 0.80 | 180 | 0.1437 | 39 | 0.80 | $SSC_{XS} = 0.120\ 10^{[0.0277\ RB_{1.5MHz} + 0.0543\ \alpha s_{1.5MHz}}$ |
| $RB_{3.0MHz}$ $\alpha_{s\ 3.0MHz}$ | 0.80 | 182 | 0.1447 | 40 | 0.79 | $SSC_{XS} = 0.591\ 10^{[0.0276\ RB_{3.0MHz} + 0.0611\ \alpha s_{3.0MHz}}$ |
| $RB_{1.2MHz}$ $\alpha_{s\ 1.2MHz}$ | 0.79 | 149 | 0.1273 | 34 | 0.79 | $SSC_{XS} = 0.446\ 10^{[0.0196\ RB_{1.2MHz} + 0.0476\ \alpha s_{1.2MHz}}$ |

Ordinary least squares regression of logarithmic parameters was used in the initial analysis of variance to determine the principal explanatory variables for $SSC_{XS}$ for acoustic surrogate parameters. The Durbin-Watson test for autocorrelation of the time series data (described in section 6.6) indicates the presence of positive first order autoregression (AR-1) at a 1-percent significance level for the residuals of $SSC_{XS}$ for the models in table 9.2. Reanalyzing the models in table 9.2 using MLE in a generalized least square model indicated that the p-values remained less than 0.001 for all explanatory variables and the model standard error was not significantly greater than that computed using ordinary least squares. Thus, although the residuals of the $SSC_{XS}$ and acoustic surrogate models are autocorrelated, the ordinary least squares statistics are not significantly affected for these data.

Errors of prediction for the SSC models were evaluated using the prediction residual sum of squares (PRESS) statistic (Helsel and Hirsch, 1995) to compute the prediction $R^2$, or $R^2_{pred}$ as described in section 6.6. The $R^2_{pred}$ is an indicator of how well the regression model predicts new observations. For all of the models in table 9.2, values of the $R^2_{pred}$ were equal to or slightly less than the model $R^2$.

The model residual standard error from the three units ranges from 34 to 40 percent. The coefficients for *RB* and $\alpha_s$ are similar for all three frequencies. The rounded coefficients for *RB* range from 0.02 to 0.03, and for $\alpha_s$ from 0.05 to 0.06. This consistency in coefficients for three independent instruments indicates a consistent physical process driving the sediment-hydroacoustic interaction. The observed and predicted values are plotted in figures 9.5 to 9.7, with the 95% confident intervals for each estimate. The SSC loads for each event using these models are summarized and compared in Chapter 10.

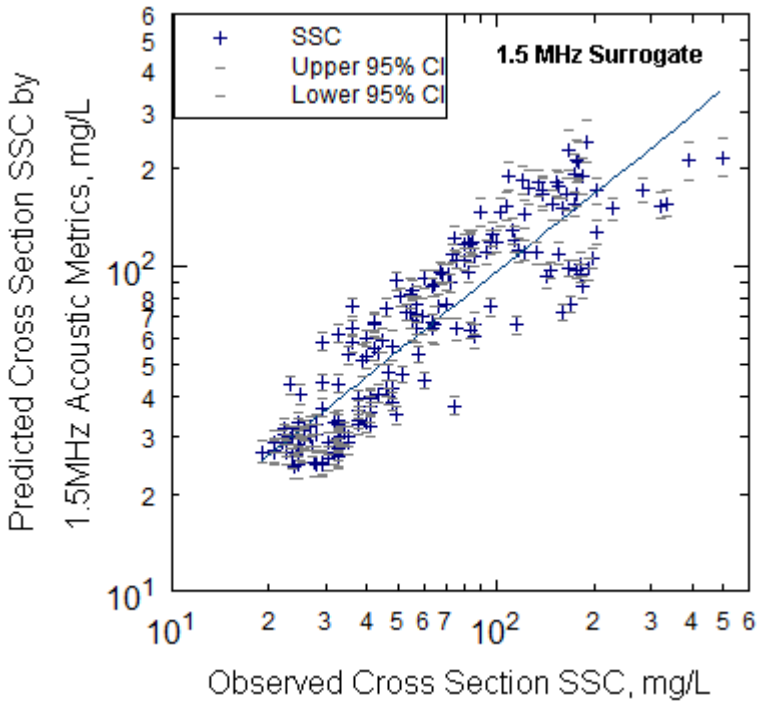


Figure 9.5 - Cross section SSC, observed and predicted as a function of 1.5MHz relative backscatter and attenuation, with 95 % confidence intervals

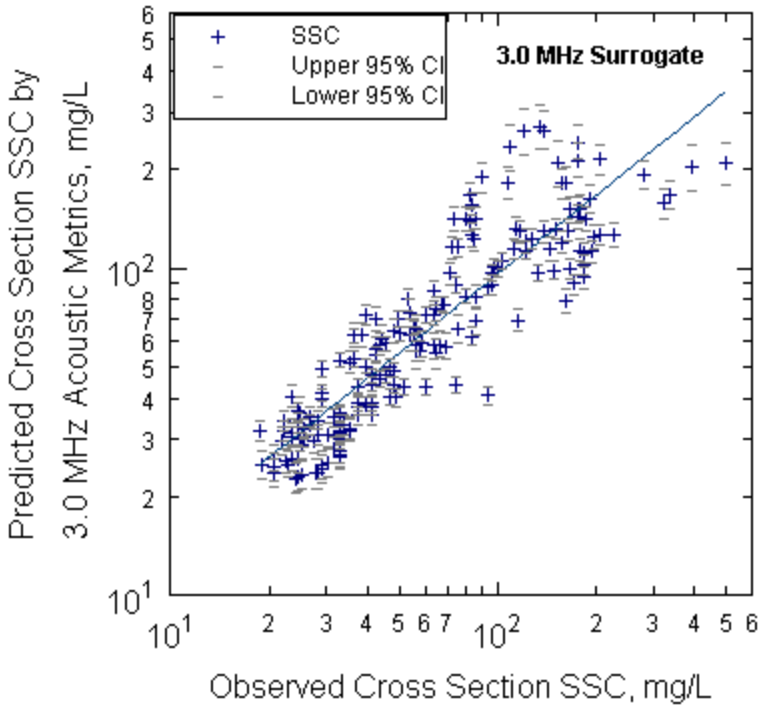


Figure 9.6 - Cross section SSC, observed and predicted as a function of 3.0 MHz relative backscatter and attenuation, with 95 % confidence intervals

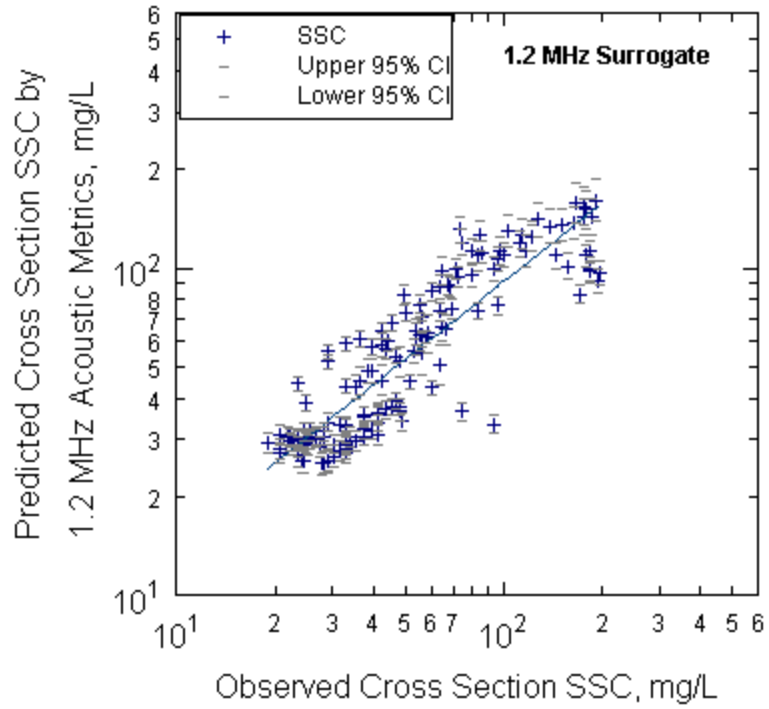


Figure 9.7 - Cross section SSC, observed and predicted as a function of 1.2 MHz relative backscatter and attenuation, with 95 % confidence intervals

# 10 Comparison of Fluvial Suspended Sediment Characteristics by High-Resolution, Surrogate Metrics of Turbidity, Laser-Diffraction, Acoustic Backscatter, and Acoustic Attenuation

This chapter addresses the fundamental hypothesis of this research, that fluvial suspended sediment characteristics may be determined by high-resolution, surrogate metrics of multi-frequency acoustic, optical turbidity, and laser-diffraction characteristics with greater accuracy and resolution than traditional methods that are based on streamflow alone; and that some metrics will be more accurate and informative sediment surrogates than others. Several of the specific questions posed in Chapter 3 also are addressed here.

## 10.1 Comparison of Operational Characteristics of SSC Surrogate Instruments

One of the specific questions for this research is: What are the operational and maintenance aspects of using these surrogate technologies? The sediment surrogate parameters investigated here each have differing operational advantages and limitations in terms of the volume sampled, the SSC size limits, the instrument robustness, the extent to which methods are well proven for a broad range of conditions, ease of deployment, operation, and maintenance, and cost. These features are summarized in table 10.1

The ‘best’ surrogate will depend on the given set of conditions (hydrologic, hydraulic, sedimentologic, cost, sampling logistics, experience of personnel) and on the type and accuracy of sediment information needed to address the purpose of the study. Study design factors include the specific engineering, ecological, and/or agricultural questions the monitoring is designed to address; the accuracy needed for suspended sediment

size, concentration, and/or load; the importance of understanding the watershed sediment source areas; budget; and manpower considerations. A study to address sediment loads affecting benthic macroinvertebrates, for example, may require higher accuracy focused on smaller sediment sizes than a study to address sedimentation rates of a navigation channel. Environmental factors include the streamflow depth, velocity, and range of stage; the quality of mixing at the monitoring location; the sediment PSD and concentration characteristics and variability; and seasonal and temperature variations (snow and ice flows). Logistical factors include ability to safely and accurately make cross section SSC measurements for calibration, secure and representative locations for installation of surrogate instruments; potential damage or loss from debris, floods, or vandalism; accessibility during high flow conditions; and existing power and communications infrastructure. These factors must all be carefully evaluated in selecting the surrogate instrument(s) for a study.

The cost of obtaining more accurate sediment characteristic data using surrogate parameters compared to using less accurate traditional discharge-based methods will likely be higher during the period of calibrating the SSC-to-surrogate model, because of the additional capital and maintenance cost of the surrogate instrumentation. However, after the SSC-to-surrogate model is calibrated, costs using sediment surrogate methods will likely be lower than traditional methods because fewer samples will be needed for ongoing verification the more accurate and stable surrogate model. Physical sample analytical cost (about $100 per sample at the time of this study) and manpower costs are significant. Thus, cost savings from fewer physical samples can be much greater than the additional capital and maintenance costs of surrogate instruments. Also, the surrogate instrument data may have added value or be required for other water-quality

(as for turbidity water-quality standards) or hydraulic (as for acoustic velocity data) purposes.

Operationally, the ADCPs are the most robust, followed by turbidity, and then laser-diffraction instruments. The turbidometer and ADCPs are both in-situ meters, but the ADCPs have a much larger measurement volume. Proper installation of turbidity meters and ADCPs requires careful site evaluation and experience. In shallow streams, adequate flow depth can be a significant limitation for ADCPs. The laser-diffraction meter is a pumped sampler, which can introduce bias, particularly for sand fractions. However, correct placement of the pump intake and detailed sampling for calibration can overcome this limitation. The laser-diffraction instrument is the only one to measure high-temporal resolution volumetric PSD data, which can provide the essential data needed to address key sediment related scientific questions.

Table 10.1. – Summary of selected operational attributes of tested sediment-surrogate technologies [Modified from Gray and Gartner, 2009]

| Technology | Turbidity | Laser | Hydroacoustics | |
|---|---|---|---|---|
| **Instrument or Type** | In Situ Turbidity meter | Fixed-Point Pump Sampling LISST-Streamside | In Situ Single-Frequency ADCP | In Situ Multiple-Frequency ADCP |
| **Price Relative to In Situ Turbidimeter** | $5,000—$8,000 Summer 2011 | About 3X-4X | About 2X-3X | About 3X-6X |
| **Approximate Concentration Measurement Range** | Standard 0-2 g/L<br><br>Available at larger ranges | Depending on versions: 0-2 g/L (particle size dependent) | 0.02-5g/L Variable as function of PSD and frequency | 0.02-5g/L Variable as function of PSD and frequency |
| **Measurement of PSD** | Does not measure PSD | Volumetric PSD from 1.9 to 381 microns | Does not measure PSD | May measure or qualify PSD |
| **Measurement Metric** | Flormazin Nephelometric or Nephelometric Turbidity Units or Optical Backscatter | Volumetric Particle Concentration and PSD within instrument sediment size limits | Relative Acoustic Backscatter and Attenuation | Relative Acoustic Backscatter and Attenuation for multiple frequencies |
| **Ancillary Measurements** | None | None for this model | Index velocity Depth, Temperature | Index velocity. Depth, Temperature |
| **Reliability, Robustness, and Frequency of Servicing** | Reliable technology. For wiped sensor models, cleaning every 2 to 6 weeks depending on stream and temperature. | Technology is new to applications in fluvial systems. Initial robustness and reliability is low. Cleaning every 1 to 3 weeks. | Very reliable and robust. More or less unaffected by fouling. | Very reliable and robust. More or less unaffected by fouling. |
| **Region of Measurement** | Fixed point | Fixed Point | Conic volume of beams | Conic volume of beams |

## 10.2 Summary and Comparison of Models of SSC from Surrogate Metrics

Analysis and development of the models of $SSC_{xs}$ based on each surrogate metric were described in the previous chapters of this thesis and are summarized in table 10.2. The data sets are not entirely overlapping, as indicated by the DF, because of instrument malfunctions during some of the measurements. However, the data set is large enough to allow the performance of the surrogates to be compared based on these model results.

Ordinary least squares regression was used in the initial analysis of variance to determine the principal explanatory variables for $SSC_{xs}$ for each surrogate. However, because the data come from concurrent time series, the residual errors may be autocorrelated, which violates the assumptions of least squares regression. For each

Table 10.2—Summary of regression models for cross section $SSC_{xs}$ and surrogate metrics

| Explanatory Variables | $R^2$ | DF | Res Std Err | Res Std Err % | $R^2_{pred}$ | Linear Regression Model |
|---|---|---|---|---|---|---|
| Discharge | 0.57 | 249 | 0.238 | 73 | 0.56 | $SSC_{XS} = 1.245\ Discharge^{0.648}$ |
| Turbidity | 0.90 | 249 | 0.113 | 30 | 0.90 | $SSC_{XS} = 2.111\ Turbidity^{0.941}$ |
| *VPC D10* | 0.94 | 190 | 0.093 | 24 | 0.94 | $SSC_{XS} = 5.221\ VPC^{1.010}\ D10^{-0.902}$ |
| $RB_{1.5MHz}$ $\alpha_{s\ 1.5MHz}$ | 0.80 | 180 | 0.144 | 39 | 0.80 | $SSC_{XS} = 0.120\ 10^{[0.0277\ RB_{1.5MHz} + 0.0543\ \alpha s_{1.5MHz}}$ |
| $RB_{3.0MHz}$ $\alpha_{s\ 3.0MHz}$ | 0.80 | 182 | 0.145 | 40 | 0.79 | $SSC_{XS} = 0.591\ 10^{[0.0276\ RB_{3.0MHz} + 0.0611\ \alpha s_{3.0MHz}}$ |
| $RB_{1.2MHz}$ $\alpha_{s\ 1.2MHz}$ | 0.79 | 149 | 0.127 | 34 | 0.79 | $SSC_{XS} = 0.446\ 10^{[0.0196\ RB_{1.2MHz} + 0.0476\ \alpha s_{1.2MHz}}$ |

one of the regression models shown in table 10.2, the Durbin–Watson statistic (traditional test for the presence of first-order autocorrelation) indicates the presence of positive first order autoregression (AR-1) at a 1-percent significance level. The AR-1 does not affect the computed intercept or explanatory variable coefficients; but can affect the computed model standard error and p-values. In this study, maximum likelihood estimation (MLE) which allows for autocorrelated residuals was used in a generalized least squares model for each regression model shown in table 10.2. The p-values remained less than 0.001 for all explanatory variables and the model standard error was not significantly greater than that computed using ordinary least squares. Thus, although the residuals are autocorrelated, the ordinary least squares statistics are not significantly affected for these models.

Regression models of $SSC_{xs}$ were developed using logarithmic-transformed units for parameters of discharge, turbidity, and laser diffraction. The acoustic parameters were already in logarithmic units of decibels. Retransformation into linear space from log space typically results in an estimate which is biased low (an underestimate). This retransformation bias was corrected using Duan's smoothing estimate (Duan, 1983; and Helsel and Hirsch, 1995).

Errors of prediction for the $SSC_{xs}$ models were evaluated using the prediction residual sum of squares (PRESS) statistic (Helsel and Hirsch, 1995). The PRESS residual for a specific observation is obtained by computing the regression model from a data set excluding that specific observation. This is done (n-1) times to obtain the PRESS statistic for a model. The observations were not themselves used to estimate the models for the PRESS statistic. Thus, values of PRESS and the prediction $R^2$, or $R^2_{pred}$ are indicators of how well the regression model predicts new observations. The $R^2_{pred}$ is computed as one minus the ratio of the PRESS statistic to the total sum of squared

errors for the observed data. For all of the models, values of the $R^2_{pred}$ were equal to or slightly less than the model $R^2$.

All of the surrogate metrics provide major improvements over the traditional SSC~discharge model, with reductions in residual standard errors from 33 to 49 percent. This answers the fundamental hypothesis of this research, that fluvial suspended sediment characteristics can be determined by these high-resolution surrogates with greater accuracy and resolution than traditional methods using streamflow alone; and that some surrogates will be more accurate and informative than others. In this study which has the same temporal resolution for $SSC_{xs}$ and discharge and its surrogate metrics, the improved accuracy is due primarily to improved correlation with $SSC_{xs}$, rather than improved temporal resolution.

The laser-diffraction metrics of volumetric particle concentration (*VPC*) and *D10* sediment size provide the best regression model for $SSC_{xs}$, explaining 94% of the observed variance and having a residual standard error of 24 percent. Changes in *D10* can indicate changes in the fraction of $SSC_{xs}$ that is unmeasured by *VPC* (less than 2 microns), because as *D10* decreases the relative concentration of fine silt and clay size particles, including particles less than 2 microns, increases. The coefficient for *VPC* rounds to 1.0, as expected theoretically, and the coefficient for *D10* would vary with the percent of $SSC_{xs}$ finer than the minimum sediment size limit of the laser-diffraction instrument. This is the first study to suggest using fine fractions (*D10*) of volumetric size together with *VPC* to estimate $SSC_{xs}$., and to show that this method provides an improved surrogate model.

Turbidity provides the second-best model, explaining 90% of the observed variance and having a residual standard error of 30%. The coefficient for turbidity is also close to 1, as is typical (Rasmussen et al., 2009).

Acoustic metrics also perform well, explaining between 79% and 80% of the observed variance. The consistency in coefficients for the *RB* and $\alpha_s$ from three independent instruments indicates consistent physical process driving the sediment-hydroacoustic interaction. This is the first time that *RB* and $\alpha_s$ have been used as separate explanatory variables in a multiple regression to estimate SSC in a fluvial environment.

All of these sediment surrogate models are applicable for the Yellow River at Gees Mill Road in metropolitan Atlanta, Georgia. The specific models are not transferrable to other streams. There is general agreement in the literature and here that sediment surrogate models require calibration for each stream and cannot be fully generalized. However, the ranges of coefficients are expected to be indicative of general relations between SSC and the sediment surrogate parameter.

## 10.3 Summary and Comparison of Measured and Predicted Suspended Sediment Load

Suspended sediment load is a highly effective indicator of many cumulative watershed processes. Computation of suspended sediment load often is the primary purpose of SSC sampling and monitoring of sediment surrogates such as turbidity, in addition to discharge. Measurements of streamflow (as discussed in section 5.1.1) and of $SSC_{xs}$ are used to compute sediment flux (discharge) for a specific stream location. Sediment fluxes are often integrated over a runoff event or a specific time period such as a year to

obtain sediment loads. Sediment flux is obtained as the product of the streamflow discharge ($Q_s$) and SSC for a selected time step using the equation $Q_s = Q \quad SSC_{XS}\, k$ where $Q_s$ is suspended-sediment flux, in mass per unit time; $Q$ is water discharge, in volume per unit time; and $k$ is a coefficient based on the unit of measurement of $Q_s$ and $SSC_{xs}$.

The sediment fluxes were computed for each surrogate using the equation noted in table 10.2 and integrated over each sampled flow event to obtain measured event load. The measured load, predictions, and errors of predicted load for each surrogate are summarized in table 10.3 and figure 10.1.

Table 10.3—SSC load in tons, measured and predicted by surrogate parameters for sampled storm events

| | SSC Load Measured, Tons | | SSC Load Predicted by Surrogates, Tons | | | | | |
|---|---|---|---|---|---|---|---|---|
| EVENT | Measured Load Tons | Subset of Measured Load Concurrent with Laser | Discharge Surrogate | Turbidity Surrogate | Laser-Diffrac-tion Surrogate | Acoustic 1.5MHz Surrogate | Acoustic 3.0 MHz Surrogate | Acoustic 1.2 MHz Surrogate |
| Aug '09 | 2367 | 1881 | 1235 | 2169 | 1742 | | | |
| Mar '10 | 1594 | 1594 | 2504 | 1731 | 1431 | 1451 | 1567 | 1458 |
| Apr '10 | 591 | 591 | 467 | 452 | 656 | 723 | 545 | 581 |
| May '10 | 3532 | 3532 | 5584 | 3850 | 3765 | 3290 | 4046 | -- |
| Sep '10 | 89 | 88 | 115 | 100 | 107 | 78 | 86 | 81 |
| n | 251 | 194 | 251 | 251 | 194 | 187 | 187 | 153 |
| Total | 8172 | 7686 | 9905 | 8302 | 7700 | -- | -- | -- |

The differing magnitude of the loads for the 5 storms demonstrates the typically exponential increase of SSC load with storm magnitude. The SSC flux for the May 2010 event, which had a 0.50 annual exceedence probability for streamflow, was more than 39 times larger that of the smallest sampled event in September 2010. The acoustic measurements had irresolvable interference from debris lodged on the pier for the August 2009 event; and the 1.2 MHz unit was not functioning for the May 2010 event. The measured load for the 194 samples during which the laser-diffraction meter was operational are shown for comparisons with those surrogate estimates.

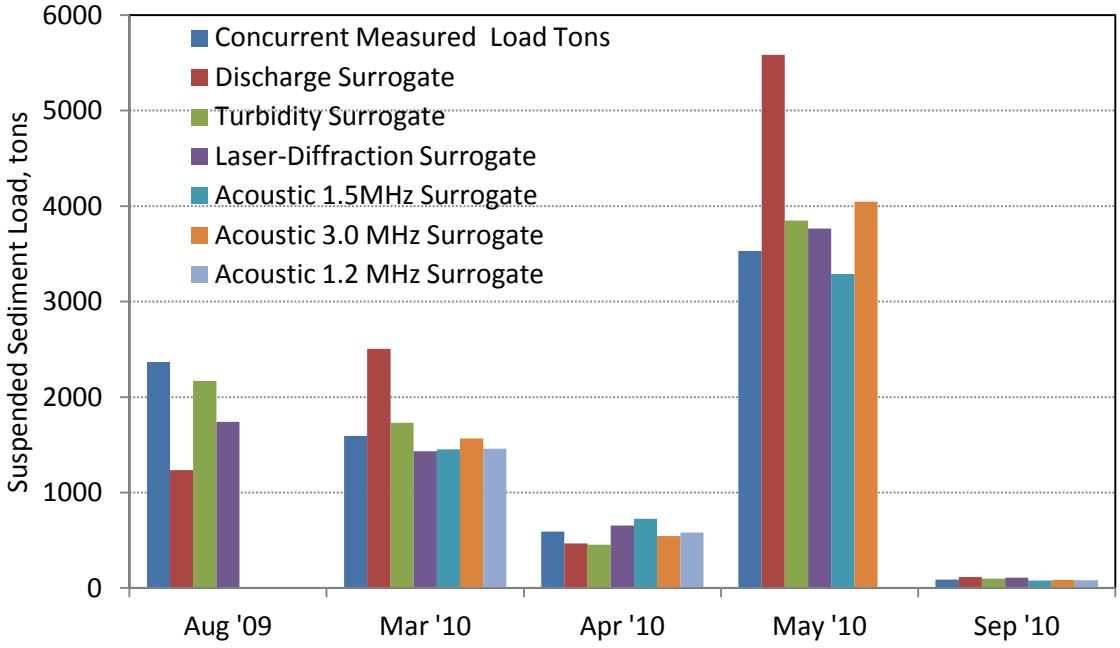


Figure 10.1—Measured and estimated event suspended sediment load for surrogate metrics of discharge, turbidity, laser-diffraction, and acoustics. (Acoustics are not available for August ’09 event. Laser-diffraction was inoperable during portion of August ’09 event.)

### *10.3.1 Error of measured suspended sediment load*

The ‘best’ estimate of SSC and suspended sediment load is from analysis of physical samples collected using correct methods and instruments with adequate temporal resolution over the sediment-hydrologic conditions and with adequate spatial resolution for the overall stream cross section. The error associated with measured load results from errors in the stream discharge data, sampling and analytical errors in the sediment samples, and errors in the calibration of fixed-location samples to cross section samples. Discharge errors at the 95% confidence limit are likely to be less than ±5-8 % at this site and using these techniques (Kennedy, 1983; Sauer and Meyer, 1992). Laboratory analytical errors from gravimetric analysis of SSC are higher for very low concentrations, and decrease rapidly with increasing concentration. Sampling errors for SSC measurements vary with grain-size distribution, concentration, sampler equipment, training and experience of the field crew, and sampling conditions. However, analytical results from replicate field samples at concentrations above 20 mg/l typically have differences of ±10% (Edwards and Glysson, 1999; Horowitz et al., 2001a, Horowitz, 2008). For the DH-95 sediment sampler used under the conditions of this study, the sampler is expected to have been within +/- 5 percent of isokinetic conditions and accuracy is likely to be better than 5 percent for silt-clay sizes and better than 10 percent for fine sand sizes. The temporal variability in SSC due to turbulence from the bridge piers is likely to be the primary source of variation in sample results. Based on these references and the measurement conditions for this research, the measured load is expected to have an accuracy of +/- 15%.

### *10.3.2 Errors of suspended sediment load estimated from surrogate parameters*

The observed and predicted sediment load of the individual and combined runoff events, for each sediment surrogate is shown in table 10.3; and the errors are shown in table 10.4. Errors for the SSC load are determined from the difference between the observed and the computed SSC load. This method does not split the data set into a model-development and verification data sets; and thus is not a true, independent measure of error of prediction for SSC load.

The error of predicted load estimated from streamflow discharge ranges from -48 to 58 percent for individual events and is 21 percent the combined event load as shown in table 10.4. The error of predicted load estimated from turbidity ranges from -23 to 12 percent for individual events and is only 1.6 percent for the combined event load. The error of predicted load estimated from laser-diffraction surrogates ranges from -10 to 21 percent for individual events and is only 0.2 percent for the combined event load. The error of predicted load estimated from acoustic surrogates ranges from -12 to 22 percent for individual events and ranges from -7 to 8 percent for the combined event load. The improved accuracy obtained for the combined load versus individual event estimates is due to the effect of averaging random errors across individual events.

Table 10.4—Summary of event and combined errors of predicted load

| EVENT | Discharge Surrogate | Turbidity Surrogate | Laser-Diffrac-tion Surrogate | Acoustic 1.5MHz Surrogate | Acoustic 3.0 MHz Surrogate | Acoustic 1.2 MHz Surrogate |
|---|---|---|---|---|---|---|
| Aug '09 | -47.8 | -8.4 | -7.4 | | | |
| Mar '10 | 57.1 | 8.6 | -10.2 | -8.9 | -1.6 | -8.5 |
| Apr '10 | -21.0 | -23.4 | 11.0 | 22.4 | -7.7 | -1.8 |
| May '10 | 58.1 | 9.0 | 6.6 | -6.8 | 14.6 | |
| Sep '10 | 29.5 | 12.2 | 21.4 | -12.0 | -3.1 | -9.3 |
| Combined | 21.2 | 1.6 | 0.2 | -4.5 | 7.6 | -6.8 |
| n | 251 | 251 | 194 | 187 | 187 | 153 |

The error in predicted load for each event is shown in figure 10.4. The relative magnitude of the error for the traditional discharge to sediment rating is evident. It is also apparent from table 10.4 and figure 10.2 that there is not a bias in any of the methods to consistently over or underestimate the load. Also, the magnitude and direction of predicted errors do not have a trend with sediment size characteristics (as indicated in the SSC model residual analysis), nor with overall magnitude of event load (as shown in figure 10.2). Thus, in response to one of the specific questions of Chapter 3, for the range of conditions measured in this study, there is not a clear difference in accuracy for changing sediment conditions. However, for each individual event most of the predicted loads tend to consistently over or underestimate the measured load. Investigations of causes of errors and potential biases or limitations for specific surrogates are needed for a wider range of sediment sizes and concentrations.

Turbidity, laser-diffraction, and acoustic surrogate metrics all provide load estimates with overall errors (ranging from 0.2% to 7.6%) that are less than the likely overall uncertainty

of the measured sediment load (about +/- 15%), and much less than the error of estimate obtained using a traditional SSC~discharge rating curve (21%). The minimum error of predicted load is obtained for the laser-diffraction surrogate, followed by turbidity and then the acoustic surrogate metrics. This is the same accuracy order as for the model standard error.

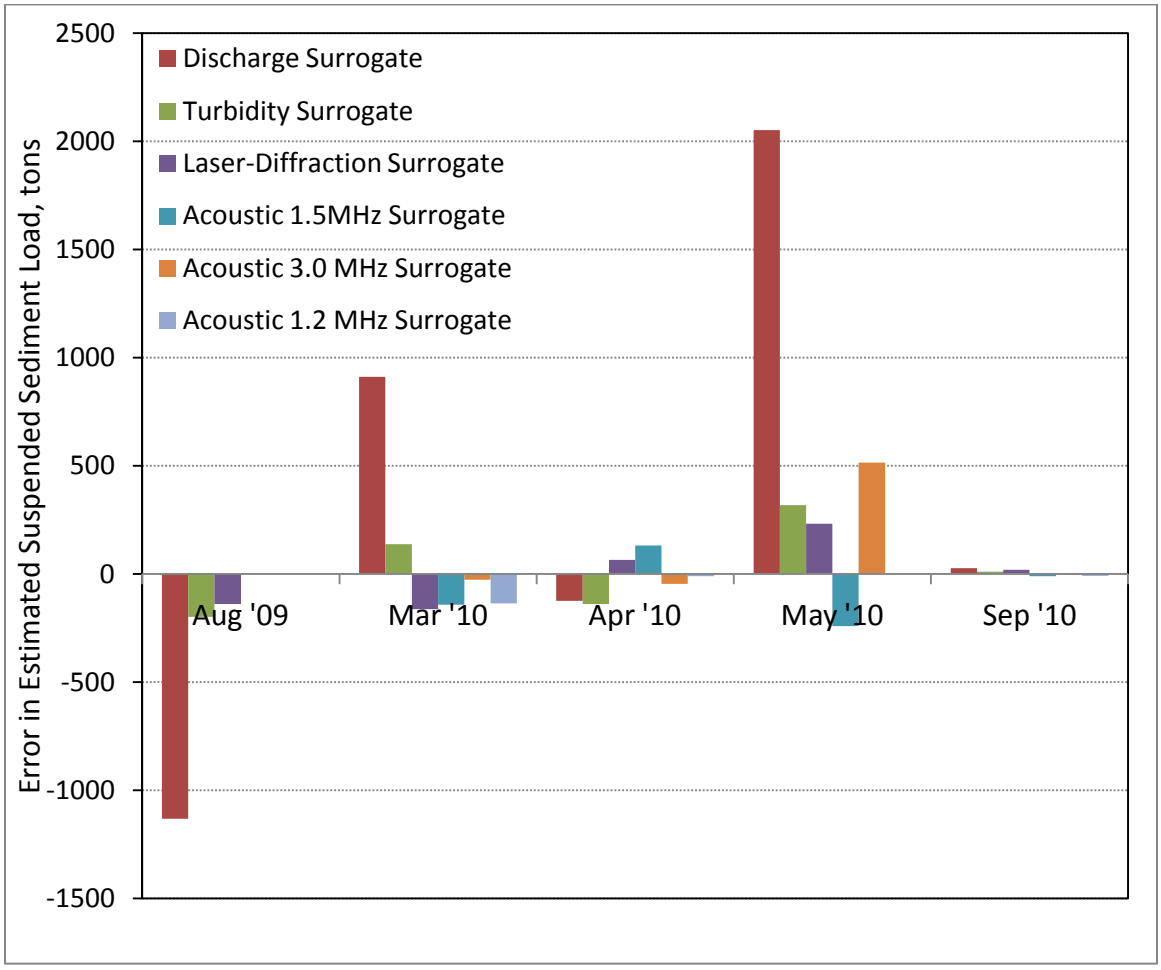


Figure 10.2—Error in estimated event suspended sediment load for surrogate metrics of discharge, turbidity, laser-diffraction, and acoustics. (Acoustics are not available for August ’09 event. Laser-diffraction was inoperable during portion of August ’09 event.)

# 11 Conclusions, Contributions, and Recommendations for Further Research

In this study, a field investigation was conducted to compare measurements of sediment characteristics including size, size distribution, concentration, and sediment load using sediment surrogates. More than 250 comprehensive, concurrent hydrologic, sediment, and multi-parameter surrogate measurements were obtained from the Yellow River at Gees Mill Road near Atlanta, Georgia for five storm events that occurred in August 2009, and March, April, May, and September 2010. Maximum measured cross section suspended sediment concentration $SSC_{xs}$ for the 5 events ranged from 93 to 648 mg/L.

The surrogate instruments and parameters evaluated in this research include concurrent measurements of nephelometric turbidity, laser-diffraction-based particle size distribution (PSD) and volumetric particle concentration (*VPC*), and acoustic backscatter and acoustic attenuation from acoustic doppler current profilers (ADCPs) with frequencies of 1.2, 1.5, and 3.0 MHz. These data were collected for this thesis and are the basis for the evaluations and comparisons of fluvial suspended sediment characteristics by high-resolution, surrogate metrics at both storm and seasonal time scales at a level of detail not previously achieved. Significant new contributions to the science of sediment surrogates are made in the research conducted within this graduate program and reported herein as described below. Suggestions for future research are also given.

## 11.1 Conclusions

1. **Fluvial suspended sediment characteristics can be determined by high-resolution surrogate parameters of turbidity, laser-diffraction and acoustics with greater accuracy and resolution than traditional methods using streamflow alone**. The fundamental hypothesis of this research has clearly been proven true by these results, as shown in Chapter 10. The turbidity, laser-diffraction, and acoustic surrogate metrics all provide errors of predicted sediment load (ranging from 0.2% to 7.6% for the combined events) that are less than the overall, inherent uncertainty of the measured sediment load (about +/- 15%) which comprise the calibration data. The errors in predicted load for the individual event and combined event load using surrogate methods is much less than the error of predicted load obtained using a traditional $SSC_{xs}$ to streamflow discharge rating curve (21% for the combined events).The surrogate-based models and load estimates were more accurate than models based on measured stream index velocity and/or discharge and velocity combined. Thus, surrogate parameters can be more effective than physical deterministic parameters in explaining changing suspended sediment characteristics during storm events and on a seasonal basis.
2. **The model error and predicted load error is lowest for laser-diffraction-based *VPC* and volumetric *D10*, followed by turbidity, and acoustic surrogate metrics.** Laser-diffraction-based *VPC* and *D10* explained 94% of the observed variance in $SSC_{xs}$, with model residual standard error of 24% and error of $SSC_{xs}$ load of 0.2%.Turbidity surrogates explained 90% of the observed variance in $SSC_{xs}$, with model residual standard error of 30% and error of $SSC_{xs}$ load of 1.6%. Acoustic backscatter and attenuation for 1.2, 1.5, and 3.0MHz ADCPs explained 79 to 80% of the observed variance in $SSC_{xs}$, with model residual standard error of 34 to 40% and

error of $SSC_{xs}$ load of 4.5 to 7.6%. The prediction $R^2$ for all of the models is equal to or slightly less than the model $R^2$**.**

The 'best' sediment surrogate parameter will depend on the study purpose, the accuracy required to address the study questions, and field conditions as discussed regarding operational considerations in section 10.1.The best monitoring solution may involve multiple surrogate parameters, because the combined data can have synergistic rather than redundant value for the characterization of fluvial suspended sediment.

3. **Hysteresis in sediment-turbidity relations for single storm events was observed and quantitatively related to PSD changes of less than 10 microns in the fine silt to clay size range.** Concentration-normalized turbidity is related to concurrent *D10* and *D16* sediment sizes with an $R^2$ of –0.76 and –0.66, respectively at p-values less than 0.0001, and the least squares fit has a slope in logarithmic space close to $D^{-1}$, in agreement with the laboratory results of Downing (2006) and Sutherland et al. (2000). The influence of sediment size on concentration normalized turbidity was found to increase with decreasing sediment size. These results are in agreement with the theoretical results of Claveno et al. (2007) who found that for modeled PSDs of non-spherical shapes with particle sizes ranging from 0.2 to 200 microns, at least 50% of the contribution to light scattering, attenuation, and absorption comes from particles smaller than 10 microns. For these data, changes of only a few microns in the *D10* for sizes between 2 and 9 microns significantly affect turbidity and create observed hysteresis. This is the first time this has been shown quantitatively for $SSC_{xs}$ to turbidity ($SSC_{xs} \sim T$) ratings using field data.
4. **Because sediment to turbidity ratings are affected by small changes in suspended sediment PSD, these ratings cannot be generalized from stream to**

**stream but must always be fully calibrated for each monitoring site.** In studies of streams where most of the suspended sediment is sand sized, the $SSC_{xs} \sim T$ relation may be dependent on a relatively small fraction of the fine silt and clay sized particles in the PSD, and minor changes in the PSD over single events and(or) over time could have a large influence on the $SSC_{xs} \sim T$ relation. Studies focused on fine silt and clay size particles and(or) adsorbed constituents may benefit from greater responsiveness of turbidity to those sediments. Hysteresis in single event $SSC_{xs} \sim T$ ratings can indicate changes in sediment PSD over flow events, yielding insight into dynamic sediment sources, storage, and transport. In this study, the increased relative concentration of fine silt and clay size particles during event recessions is likely due to a limited supply of these size sediments available for entrainment in the channel bed; and to their availability and transport from hill slope sources affected by rainfall impact, rill, and gully erosion.

5. **High temporal resolution volumetric PSD data from laser diffraction instruments may provide uniquely valuable information on dynamic sediment source and transport conditions; and may suggest improved methods using other surrogates which, unlike laser diffraction, have a size-concentration ambiguity.** Although PSD is highly significant to the engineering, water-quality, and ecological roles of sediment in the environment, it is rarely measured in field studies; and very rarely with the spatial and(or) temporal resolution needed to characterize the dynamics of PSD. The high resolution PSD data were uniquely valuable in this study to evaluate causes of uncertainty in turbidity and acoustic surrogates, and to evaluate dynamic sediment sources over single flow events.
6. **The particle size detection limits of laser-diffraction instruments are a significant limitation for measurement of *VPC* and PSD in most fluvial environments.** The LISST-Streamside instrument can only detect particles between

2 and 381 microns. Gravimetric PSD analyses for this site indicate that typically about 35% (median result) of the sediment is finer than 2 microns. This study shows that the unmeasured SSC fraction is an important limitation in both *VPC* and PSD measurements from laser-diffraction analyzers for fluvial environments where large fractions of the suspended sediment are clay sized and/or larger than medium sand sized. Although laser-diffraction measurements are not affected by size-concentration ambiguity, there is still significant variance in the relation of $SSC_{xs}$ to *VPC* due primarily to the variable fraction of $SSC_{xs}$ that is unmeasured by *VPC*.

7. **Changes in volumetric *D10* can indicate changes in the fraction of SSC that is unmeasured by *VPC***. This occurs because as *D10* decreases, the relative concentration of fine silt and clay size particles, including particles less than 2 microns, increases. This is the first study to suggest using the size of fine fractions of the PSD together with *VPC* to estimate $SSC_{XS.}$, and to show that this provides an improved surrogate model. Multiple least-squares regression in log space for $SSC_{XS}$ as a function of *VPC* and *D10*, as compared with a model using *VPC* alone, improves the $R^2$ from 0.90 to 0.94, and the model residual standard error from 30 to 24 percent. This model has the lowest model error and predicted load error of any of the surrogate metrics used in this study.
8. **The *VPC*, as reported by the LISST-Streamside, is not a true volumetric particle concentration.** This conclusion, which is reported in this study for the first time, is evident in the ratios of measured $SSC_{xs}$ to *VPC*. The ratio of mass $SSC_{xs}$ (in mg/L) to true volumetric particle concentration (in µl/L) should equal the sediment specific gravity, which is close to 2.65 for predominantly silica sediment of this stream. Furthermore, the effect of the fraction of $SSC_{xs}$ that is unmeasured by *VPC* would increase the $SSC_{xs}$ to *VPC* ratio to a number larger than sediment specific gravity. Instead, the indicated specific gravity from the $SSC_{xs}$ -to-*VPC* ratio for the concurrent

measurements of this study has a median value of 1.12 and an interquartile range from 0.94 to 1.41 (dimensionless relative density). Given the unmeasured fraction of roughly 45% of the sample for this site, the *VPC* differs from actual volumetric concentration by a factor of 2.5 to 4 within the interquartile range of $SSC_{xs}$ to *VPC* ratios. This problem was first reported to the manufacturer by this study, and is common to LISST devices designed for fluvial environments.

9. **The variance of the measured acoustic attenuation due to sediment in this study is greater than the change in theoretical attenuation over the observed sediment size range, so that representative particle sizes could not be determined from the theoretical acoustic for single acoustic frequencies nor for ratios of multiple acoustic frequencies.** This conclusion addresses a specific hypothesis of the overall investigation. The measured acoustic attenuation values due to sediment for this data set range over an order of magnitude and do not fit the Urick-Sheng-Hay relation (normalized for SSC). The theoretical acoustic attenuation curves (for single frequencies and multi-frequency ratios) are nearly flat over the measured sediment size range, indicating that theoretical attenuation is a weak function of sediment size for the PSD of this stream. The observed acoustic attenuation values are within an order of magnitude of the theoretical curves. Also, the volumetric sediment size data indicate that the attenuation losses are all in the viscous attenuation range.

   This result may indicate a significant limitation in the application of the theoretical relations of Urick (1948) and Sheng and Hay (1988), which were developed from relatively uniform sediment sizes, to natural fluvial environments with well graded suspended sediment. The literature search did not find any prior laboratory or field investigations that compare measured and theoretical attenuation for well graded natural fluvial streams. Deterministic factors other than sediment size may be

dominating the variance in observed acoustic attenuation; or acoustic attenuation from a fluvial, non-uniform PSD may not be uniquely related to theoretical characteristic sediment size, or measurement errors may cause a range of variance that overwhelms the weak sensitivity of the theoretical relation.

10. **Suspended sediment PSD is significantly correlated with ratios of measured acoustic attenuation at different frequencies.** The three ratios of acoustic attenuation for the 1.2, 1.5, 3.0 MHz frequencies explain from 32 to 64% of the variance in sediment sizes of the volumetric *D10*, *D16*, and *D50* for this site and are statistically significant (p-value<0.001). The results show that the relation between acoustic attenuation ratios and PSD sizes is strongest at the *D16* size class for all frequency ratios, becomes weaker for the *D10*, *D50* and *D60*, and is not statistically significant for the *D84* size class. The acoustic attenuation ratio that is most highly related to PSD is for the ratio of 3.0 to 1.2 MHz frequencies; and this ratio explains 64% of the variance in volumetric *D16* sediment size, and has a residual standard error of only 8% (see table 8.4).
11. **The methods proposed by Topping et al. (2007) to empirically measure acoustic attenuation from profiling ADCP measurements do apply for a stream in the southeastern USA.** In contrast to the methods of previous authors, Topping et al. (2007) propose a direct measurement of acoustic attenuation from profiling ADCP measurements. This method has practical and potential accuracy advantages over the approach used by other authors; however it has had almost no published testing outside the Colorado River and none in streams of the eastern United States. The method worked well for the Yellow River at Gees Mill Road near Atlanta, Georgia.
12. **Using both relative acoustic backscatter (*RB*) and acoustic attenuation as explanatory variables results in a significantly improved model of $SSC_{xs}$,**

**compared with traditional sonar equations using only *RB*.** The acoustic metrics that relate to sediment concentration and size are the acoustic attenuation due to sediment properties ($\alpha_s$) and the relative acoustic backscatter, adjusted for signal spreading and attenuation due to fluid and sediment properties. These two acoustic metrics indicate distinct mechanisms of sediment-acoustic interaction, particularly where the sediment PSD is dominated by smaller particles that cause primarily viscous acoustic attenuation, as for this site. Thus, it is theoretically reasonable to include *RB* and $\alpha_s$ in a multiple linear regression (MLR) model of $SSC_{xs}$. Using the previously published sonar equation to estimate $SSC_{xs}$, *RB* explains from 75 to 77 % of the observed variance in the log-transformed $SSC_{xs}$. In this study, for the first time, both *RB* and $\alpha_s$ were used in a MLR model that explains from 80 to 83 percent of the observed variance in log-transformed $SSC_{xs}$, a significant improvement over the model using *RB* as the only explanatory variable.

13. **All surrogate technologies require calibration to the specific stream site for the range of sediment characteristics (concentration and PSD) and surrogate metric conditions to be modeled.** This study confirms that $SSC_{xs}$ to surrogate relations are affected by changing sediment and instrument characteristics, and thus require calibration with cross section $SSC_{xs}$ measurements for each site where they are used. Initial physical sampling requirements would not be reduced by surrogate technology, until calibration and rating curves are established. The methods developed in this study will be transferrable and applicable to other stream sites and conditions. However, the model calibrations will not be transferrable.
14. **Operation and maintenance of the surrogate instruments was easiest for the ADCPs, and most difficult for the laser-diffraction instruments.** The ADCPs are generally unaffected by fouling and maintenance is required primarily for

programming the units correctly and downloading stored data. The turbidity sensor performed well through the study with cleaning and calibration checks every 3 to 6 weeks. After resolving a number of instrument issues, the LISST-Streamside functioned well during the majority of the data collection period. The unit requires significant expertise for programming and set up, and regular (at least every other week) cleaning and maintenance. For all surrogate technologies, site selection and installation are critical to data quality and monitoring success. An established monitoring and quality assurance plan, data management including all relevant metadata, and data review are also essential to reliable SSC monitoring. The cost of obtaining more accurate sediment characteristic data using surrogate parameters compared to using less accurate traditional discharge-based methods will likely be higher during the period of calibrating the SSC-to-surrogate model, because of the additional capital and maintenance cost of the surrogate instrumentation. However, after the SSC-to-surrogate model is calibrated, costs using sediment surrogate methods will likely be lower than traditional methods because fewer samples will be needed for ongoing verification the more accurate and stable surrogate model.

## 11.2 Contributions

The following findings are made in this study for the first time:

- Sediment-to-turbidity hysteresis is quantitatively related to PSD changes of less than 10 microns in the fine silt to clay size range for field data.
- Laser-diffraction can be used for continuous monitor PSD in an urban river in the southeastern United States.
- The sediment size of fine fractions of volumetric PSD can be used to estimate the unmeasured SSC below instrument detection limits, to improve laser-diffraction-based surrogates of $SSC_{XS}$ using the method proposed herein.
- The *VPC*, as reported by the LISST-Streamside, is not a true volumetric particle concentration.
- A proposed method to determine characteristic suspended sediment sizes from theoretical and measured acoustic attenuation is not effective.
- Ratios of acoustic attenuation at different frequencies can be used to empirically estimate characteristic suspended sediment size.
- Acoustic attenuation can be determined from profiling ADCP measurements for a stream in the southeastern USA.
- Use of both relative backscatter and acoustic attenuation to model $SSC_{XS}$ result in significant improvement over the traditional sonar equation methods.

## 11.3 Recommendations for Further Research

This study has identified the following needs for further research:

- Document and define the causes of $SSC_{xs}$ to turbidity hysteresis for a wide range of sediment and stream conditions. The requisite data sets for this research will include concurrent, discrete measurements of $SSC_{xs}$, turbidity, discharge, and size distribution data over runoff events.
- Evaluate the effective use and interpretation of laser-diffraction measurements for continuous PSD and *VPC* monitoring in fluvial systems. Determine methods to quantitatively relate laser-diffraction-based, volumetric PSD to gravimetric PSD analytical results. Determine methods to adjust the measured metrics for the undetected fractions of $SSC_{xs}$.
- Resolve the problem in the LISST inversion algorithms so that true volumetric particle concentration (within instrument detection limits) is reported. This research is underway by Sequoia Scientific, Inc.
- Evaluate measured and theoretical acoustic attenuation for characterization of suspended sediment size. In particular, determine whether the theoretical attenuation, developed for single sediment sizes, is applicable to well graded sediment size distributions typical of fluvial systems. The data needed for this research includes concurrent measurements of SSC, full PSD, and multi-frequency profiles of acoustic backscatter and attenuation on different streams having diverse sediment characteristics.
- Test, validate, and develop generalized methods for use of acoustic backscatter and attenuation for estimation of suspended sediment concentration and load.

# References


Ainslie, M. A., and McColm, J. G. (1998), A simplified formula for viscous and chemical absorption in sea water. J. Acoustical Society of America, 103 (3), 1671-1672

Agrawal, Y. C., McCave, I. N., and Riley, J. B. (1991). Laser diffraction size analysis. *In:* J.M.P. Syvitski, Editor, Principles, Methods and Application of Particle Size Analysis, Cambridge University Press, New York, 119–128.

Agrawal, Y. C. and Pottsmith, H. C. (1994). Laser diffraction particle sizing in STRESS. Con. Shelf Res., 14, 1101-1121.

Agrawal, Y. C. and Pottsmith, H. C. (2000). Instruments for particle size and settling velocity observations in sediment transport. Marine Geology, 168, 89-114.

Agrawal, Y. C., and H. C. Pottsmith, (2006). The isokinetic streamlined suspended-sediment profiling LISST-SL – status and field results. Proceedings of the 8th Federal Inter-Agency Sedimentation Conference, Reno, NV, April 2–6, 2006, 288–295

Agrawal, Y. C., Whitemore, A., Mikkelsen, O. A., and Pottsmith, H. C. (2008). Light scattering by random shaped particles and consequences on measuring suspended sediments by laser diffraction. J. Geophys. Res., 113, CO4023

Agrawal, Y. C., and H. C. Pottsmith (2000), Instruments for particle size and settling velocity observations in sediment transport, Mar. Geol., 168(1–4), 89–114.

Anderson, C.A. (2005), Turbidity, in, U.S. Geological Survey National Field Manual for the collection of water-quality data. U.S.G.S. Techniques of Water-Resources Investigations, Book 9, Ch. 6.7

Andrews, S. W., D. M. Nover, J. E. Reuter, and S. G. Schladow (2011), Limitations of laser diffraction for measuring fine particles in oligotrophic systems: Pitfalls and potential solutions, Water Resour. Res., 47

Andrews S, Nover D, Schladow SG (2011): Using laser diffraction data to obtain accurate particle size distributions: the role of particle composition. Limnology & Oceanography:Methods 8: 507-526.

Aquatec Group, 2011 (http://www.aquatecgroup.com/aquascat.html)

ASTM International (2007), D4410, in terminology for fluvial sediment, annual book of standards, water and environmental technology: West Conshohocken, Pennsylvania, ASTM International, 7 p.

Atlanta Regional Commission, 2009, LandPro09, vector digital land-use data, available at: http://www.atlantaregional.com/info-center/gis-data-maps/gis-data

Baker, E. T., and J. W. Lavelle (1984), The Effect of Particle Size on the Light Attenuation Coefficient of Natural Suspensions. J. Geophys. Res., 89(C5), 8197–8203.

Bogen, J., T. Fergus, and D. E. Walling (2003), Erosion and sediment transport in rivers, technological and methodological advances. Internat. Assoc. of Hydrological Sciences, Publication 283, 238 pp.

Boss, E., et al. (2009), Comparison of inherent optical properties as a surrogate for particulate matter concentration in coastal waters, Limnol. Oceanogr. Methods, 7, 803–810

Braithwaite, H. (1974), Some measurements of acoustic conditions in rivers. Journal of Sound and Vibration, 37, 557-560

Braithwaite KM, Bowers DG, Nimmo Smith WAM, Graham GW, Agrawal YC, Mikkelsen OA (2010): Observations of particle density and scattering in the Tamar Estuary. Marine Geology 277(1-4): 1-10.

Brown, E. H., and Clifford, S. F. (1976), On the attenuation of sound by turbulence. J. Acoustical Society of America, 60, 788–794

Christensen, V. G., Xiaodong, J. (2000) Regression analysis and real-to estimate constituent concentrations, the Little Arkansas River. U.S. Geological Survey Water-Report 00–4126, 36 pp.

Clavano, W.R., E. Boss, and L. Karp-Boss, 2007. Inherent Optical Properties of Non-Spherical Marine-Like Particles - From Theory to Observations, in Oceanography and Marine Biology: An Annual Review, 2007, 45, 1-38, CRC Press

Cobb, E. D., and Landers, M. N. (1993) Broad-band Acoustic Doppler Current Profiler for Discharge Measurements in Streams. AWRA 29th Annual Conference, Tucson, AZ, proceedings, 288

Collins, A. L., Walling, D. E. and Leeks, G. J. L. (1997), Source type ascription for fluvial suspended sediment based on a quantitative composite fingerprinting technique. Catena 29, 1–27

Conner, C. S. and A. M. De Visser (1992), A laboratory investigation of particle size effects on optical backscatterance sensor. Mar. Geol., 108, 151-159

Crawford, A. M., Hay, A. E. (1993). Determining suspended sand size and concentration from multi-frequency acoustic backscatter. Journal of the Acoustical Society of America, 94, 3312-3324

Crosson, P. (1997), Will erosion threaten agricultural productivity?, Environment, 38

Clesceri, L. S., Greenberg, A. E., and Eaton, A. D., eds. (1998), Standard methods for the examination of water and wastewater (20th ed.): American Waterworks Association and Water Environment Federation, 1,200 p.

Conner, C. S. and De Visser, A. M. (1992), A laboratory investigation of particle size effects on optical backscatterance sensor. Mar. Geol., 108, 151–159

Davies-Colley, R. J., and Smith, D. G. ( 2001), Turbidity, suspended sediment, and water clarity–a review. Journal of American Water Resources Association, v. 37, 1085–1101.

Davis, B. E. (2005), A guide to the proper selection and use of Federally approved sediment and water-quality samplers. U. S.G.S. Open-File Report 2005–1087, 20 pp.

Diplas P., Kuhnle R., Gray J., Glysson D., and Edwards T., 2008, Sediment transport measurements, ASCE Manual 110, Chapter 5

Downing, J. P., Sternberg, R. W. and Lister, C. R. B. (1981), New instrumentation for the investigation of sediment suspension processes in the shallow marine environment. Mar. Geol., 42, 19–34.

Downing, A., Thorne, P. D. and Vincent, C. E. (1995), Backscattering from a suspension in the near field of a piston transducer. J. Acoust. Soc. Am. 97, 1614–1620.

Downing, J. P. (1996), Suspended sediment and turbidity measurements in streams: What they do and do not mean. Automatic Water Quality Monitoring Workshop, Richmond, B.C., 12–13 February.

Downing, J. (2006), Twenty-five years with OBS sensors—the good, the bad, and the ugly. Continental Shelf Research, 20 p.

Duan N. 1983. Smearing estimate: a nonparametric retransformation method. Journal of the American Statistical Society 78: 605–610.

Edwards, T. E., and Glysson, G. D. (1999), Field methods for collection of fluvial sediment. U.S.G.S. Techniques of Water-Resources Investigations Book 3, Chp C2, 89 p.

Fisher, F. H., and Simmons, V. P. (1977), Sound absorption in sea water. J. Acoustical Society of America, 62 (3), 558-564

Flagg, C. N. and Smith, S. L. (1989), On the use of the acoustic Doppler current profiler to measure zooplankton abundance. Deep-Sea Res., 36, 455–474

Flammer, G. H. (1962), Ultrasonic measurement of suspended sediment. U.S.G.S. Bul. 1141–A, 48 pp

Freemen, L. (2006), Estimation of particle sizes for a range of narrow size distributions of natural sands suspended in water using multi-frequency acoustic backscatter. Proceedings of the 8th Federal Inter-Agency Sedimentation Conference, Reno, NV, April 2–6, 2006, 555–559

Gartner, J. W., Cheng, R. T. (2001), Promises and Pitfalls of estimating TSS from Backscatter. Proceedings of the 7th Federal Interagency Sedimentation Conference, Vol. III, Reno, Nevada, 25-29

Gartner, J. W., Cheng, R. T., Wang, P. F. and Richter, K. (2001), Laboratory and field evaluations of LISST-100 instrument for suspended particle size determinations. Marine Geology, 175, 199–219.

Gartner, J. W., Mueller, D. S., Wall, G. R. and Gray, J. R. (2003), Breakout session 4: Other fluvial-sediment surrogates, in Proceedings of the Federal Interagency Workshop on Turbidity and Other Sediment Surrogates, Reno, Nevada, 21-27, 30 April-2 May, 2002.

Gartner, J. W. (2004), Estimating suspended solids concentrations from backscatter intensity measured by acoustic Doppler current profiler in San Francisco Bay, California. Marine Geology, 211, 169–187

Gilvear, D. J. and Petts, G. E. (1985), Turbidity and suspended solids variations downstream of a regulating reservoir. Earth Surface Processes and Landforms, 10: 363–373

Gippel, C. J. (1989), The use of turbidimeters in suspended sediment research. Hydrobiologia 176/177, 465-480

Glysson, G. D. (1987), Sediment-transport curves. U.S.G.S. Open-File Report 87-218, 47 pp.

Gray, J. R., Glysson, G. D. and Mueller, D. S. (2002) Comparability and accuracy of fluvial-sediment data – a view from the U.S. Geological Survey, in Proceedings of the ASCE Specialty Conference, Hydraulic Measurements & Experimental Methods, Estes Park, Colorado, 28 July-1 August, 6 pp.

Gray, J.R. (2005), ed., Proceedings of the Federal Interagency Sediment Monitoring Instrument and Analysis Research Workshop, Flagstaff, Arizona, 9-11 September, U.S.G.S. Circular 1276, 46 pp.

Gray, J. R., Glysson, G. D. and Edwards, T. K. (2008), Suspended-sediment samplers and sampling methods. Sedimentation Engineering, ASCE Manual 110, chapter 5.3, 318-337.

Gray, J. R., and Gartner, J. W. (2009) Technological advances in suspended-sediment surrogate monitoring. Water Resources Research., 45, W00D29

Gray, J. R., and J. W. Gartner, 2010, Surrogate technologies for monitoring suspended-sediment transport in rivers, in Sedimentology of Aqueous Systems, edited by Poleto, C. and Charlesworth, S. Blackwell Publishing

Guerrero, M., Szupiany, R.N., Amsler, M., 2011, Comparison of acoustic backscattering techniques for suspended sediments investigation, Flow Measurement and Instrumentation, Vol 22, 5, 392-401

Hach, C.C. (1972), Understanding Turbidity Measurement. Industrial Water Engineering, 9, 18-22

Hamilton, L. J., Shi, Z. and Zhang, S. Y. (1998). Acoustic backscatter measurements of estuarine suspended cohesive sediment concentration profiles. J. of Coastal Res., 14, 1213-1224.

Hay, A. E. (1983), On the Remote Acoustic Detection of Suspended Sediment at Long Wavelengths. J. Geophys. Res., 88(C12), 7525–7542

Hay, A. E. and Sheng, J. (1992), Vertical profiles of suspended sand concentration and size from multi-frequency acoustic backscatter. J. of Geo. Res., 97, 15661-15677.

Helsel, D.R., and Hirsch, R.M., 2002, Statistical methods in water resources—hydrologic analysis and interpretation: U.S. Geological Survey Techniques of Water-Resources Investigations, book 4, chap. A3, 510 p.

Hess, F. R., and Bedford K. W. (1985), Acoustic Backscatter System (ABSS): The instrument and some preliminary results. Marine Geology, 66, 357-379

Hill, P. S., E. Boss, J. P. Newgard, B. A. Law, and T. G. Milligan (2011), Observations of the sensitivity of beam attenuation to particle size in a coastal bottom boundary layer, J. Geophys. Res., 116

Holdaway, G. P., Thorne, P. D., Flatt, D., Jones, S. E. and Prandle, D. (1999), Comparison between ADCP and transmissometer measurements of suspended sediment concentration. Con. Shelf Res., 19, 421–441

Horowitz, A. J. (1991), A primer on sediment-trace element chemistry: Second ed., Chelsea, Mich., Lewis Publishers, 136 p.

Horowitz, A. J., Elrick, K. A., Smith, J. J. (2001), Annual suspended sediment and trace element fluxes in the Mississippi, Columbia, Colorado, and Rio Grande drainage basins. Hydrological Processes 15, 1169–1207

Horowitz, A. J., Elrick, K. A., Smith, J. J. (2008), Monitoring urban impacts on suspended sediment, trace element, and nutrient fluxes within the City of Atlanta, Georgia, USA: program design, methodological considerations, and initial results. Hydrological Processes, 22, 1473–1496

Horowitz, A. J. (2008), Determining annual suspended sediment and sediment-associated trace element and nutrient fluxes. Science of the Total Environment, 400, 315–343

International Organization for Standardization (1999), Water-quality determination of turbidity, method 7027: International Organization for Standardization, 10 p.

Jastram, J.D., Moyer, D.L. and Hyer, K.E. (2009), A Comparison of Turbidity-Based and Streamflow-Based Estimates of Suspended Sediment Concentrations In Three Chesapeake Bay Tributaries. U.S.G.S. Scientific Investigations Report 2009-5165

Jean P. G., Minella, G., Merten, H., Reichert, J. M., Clarke, R. T. (2008), Estimating suspended sediment concentrations from turbidity measurements and the calibration problem. Hydrological Processes, 22

Julien, P. Y. (1995). Erosion and sedimentation. Cambridge: Cambridge University Press.280 pgs; (pgs 225-232)

Kennedy, E. J. (1983) Computation of continuous records of streamflow. U.S.G.S. Techniques of Water Resources Investigations, U.S. Geological Survey, A13, Book 3, 58 pp.

Kineke, G. C. and R. W. Sternberg (1992), Measurements of high concentration suspended sediments using the optical backscatterance sensor, Mar. Geol., 108, 253-258.

Konrad, C., H. C. Pottsmith, Melis, T. S., and Rubin, D. M. (2006), Real-time analysis of concentrated fluvial suspended sediments. Proceedings of the 8th Federal Inter-Agency Sedimentation Conference, Reno, NV, April 2–6, 2006, 585–591

Lamb, H., 1916, Hydrodynamics, 4$^{th}$ edition, Cambridge University Press, 708pp

Land, J. M. and Jones, P. D. (2001), Acoustic measurement of sediment flux in rivers and near-shore waters. Proceedings of the 7th Federal Interagency Sedimentation Conference, Vol. III, Reno, Nevada, 25-29 March, 127-134.

Landers, M. N., and Mueller, D. S. (1996), Evaluation of selected pier-scour equations using field data. Transportation Research Record: Journal of the Transportation Research Board, 1523, 186-195

Landers, M. N.(2003), Summary of blind sediment reference sample measurement session. Proceedings of the Federal Interagency Workshop on Turbidity and Other Sediment Surrogates, Reno, Nevada, 30 April-2 May, U.S.G.S. Circular 1250, 29-30.

Landers, M.N., Ankcorn, P.D., and McFadden, K.W. (2007), Watershed effects on streamflow quantity and quality in six watersheds of Gwinnett County, Georgia, U.S.G.S. Scientific Investigations Report 2007-5132, 54 .

Landers, M.N., 2010, Review of methods to estimate fluvial sediment characteristics from acoustic surrogate metrics, in Proceedings of the 9th Federal Interagency Sedimentation Conference, Las Vegas, NV

Lasdon, L.S., Waren, A.D., Jain, A., and Ratner, M.(1978), Design and testing of a generalized reduced gradient code for nonlinear programming, ACM Transactions on Mathematical Software (TOMS), 4, 34-50

Lawler, D.M., Petts, G.E., Foster, I.D.L., Harper, S., 2006, Turbidity dynamics during spring storm events in an urban headwater river system: The Upper Tame, West Midlands, UK, Science of The Total Environment, V 360, pp 109-126,

Lawrence, S. J. (2006), BacteriALERT: A Cooperative Program for Water-quality Monitoring and Prediction of Escherichia coli Bacteria in the Chattahoochee River, Georgia: 5th National Monitoring Conference, Monitoring Networks: Connecting for Clean Water, May 7-11, 2006 San Jose, California, National Water Quality Monitoring Council

Lenzi, Mario A., and Marchi, Lorenzo, 2000, Suspended sediment load during floods in a small stream of the Dolomites (northeastern Italy), CATENA, Volume 39, Issue 4, Pages 267-282

Lewis, J. (1996), Turbiditycontrolled suspended sediment sampling for runoff event load estimation. Water Resources Research, 32, 2299–2310.

Lewis, J. (2002), Estimation of suspended sediment flux in streams using continuous turbidity and flow data coupled with laboratory concentrations. Proceedings of the Federal

Interagency Workshop on Turbidity and Other Sediment Surrogates, Reno , Nevada, 30 April-2 May, U.S.G.S. Circular 1250

Loperfido, J. V., Just, C. L., Papanicolaou, A. N., and Schnoor, J. L., 2010, In situ sensing to understand diel turbidity cycles, suspended solids, and nutrient transport in Clear Creek, Iowa , Water Resour. Res. , 46

Lynch, J.F., Irish, J.D., Sherwood, C.R., Agrowal, Y.C. (1994), Determining suspended sediment particle size information from acoustical and optical backscatter measurements. Continental Shelf Research 14 (10/11), 1139-1165.

Melis, T. S., Topping, D. J. and Rubin, D. M. (2003), Testing laser-based sensors for continuous in situ monitoring of suspended sediment in the Colorado River, Arizona, in Erosion and Sediment Transport Measurement in Rivers, Technological and Methodological Advances edited by J. Bogen et al., International Association of Hydrological Sciences Publication 283, 21-27.

Minella, J. P. G., Merten, G. H., Reichert, J. M. and Clarke, R. T. (2008), Estimating suspended sediment concentrations from turbidity measurements and the calibration problem. Hydrological Processes, 22: 1819–1830.

Multi-Resolution Land Characteristics (MRLC) Consortium (2001), National Land Cover Database 2001. <http://www.mrlc.gov/mrlc2k_nlcd.asp>

Muste,M., Vermeyen,T., Hotchkiss,R., and Oberg,K. (2007), Acoustic Velocimetry for Riverine Environments, J. Hydr. Engrg. V 133, 1297-1298

National Research Council, Committee on Assessment of Water Resources Research (2004), Confronting the Nation's Water Problems: The Role of Research, ISBN: 978-0-309-09258-6, 324 pages.

Noir, D. T., and George, A. R. (1978), Absorption of sound by homogeneous turbulence. Journal of Fluid Mechanics, 86 (3), 593-608

Nolan, K. M., Gray, J. R. and Glysson, G. D. (2005), Introduction to suspended-sediment sampling, U.S.G.S. Scientific Investigations Report 2005-5077

Pimentel, D., Harvey, C., Resosudarmao, P., Sinclair, K., Kurz, D., McNair, M., Crist, S., Shpritz, L., Fitton, L., Saffouri, R. and Blair, R. (1995), Environmental and economic costs of soil erosion and conservation benefits, Science, 267, 1117-1123

Porterfield, G. (1972), Computation of fluvial-sediment discharge, U.S. Geological Survey Techniques of Water-Resource Investigations Book 3, Chapter C3, 66 pp.

Preisendorfer, R. W. (1986), Secchi disk science: visual optics of natural waters, Limnology and Oceanography, 31, 909-926

Rasmussen, T. J., Ziegler, A. C., and Rasmussen P. P. (2005), Estimation of constituent concentrations, densities, loads, and yields on lower Kansas River, northeast Kansas, using regression models and continuous water-quality modeling, January 2000 through December 2003. U.S.G.S. Scientific Investigations Report 2005–5165, 117 p.

Rasmussen, P. P., Gray, J. R., Glysson, D. G., and Ziegler, A. C. (2009), Guidelines and Procedures for Computing Time-Series Suspended-Sediment Concentrations and Loads from In-Stream Turbidity-Sensor and Streamflow Data. U.S.G.S. Techniques and Methods Report Book 3, Chapter C4, 66p

Rayleigh, Lord (J. W. Strutt) (1896), Theory of Sound, Macmillan and Co. Ltd, New York, 2, 2nd ed., 504 pp

Rayleigh, Lord (1937), The Surface Layer of Polished Silica and Glass with Further Studies on Optical Contact. Proceedings of the Royal Society of London. Series A, Mathematical and Physical Sciences, 160, no. 903, 507-526

Reichel, G., and Nachtnebel, H. P. (1994), Suspended sediment monitoring in a fluvial environment: Advantages and limitations applying an acoustic Doppler current profiler. Water Resources, 28, 751-761

Reynolds, R. A., D. Stramski, V. M. Wright, and S. B. Woźniak (2010), Measurements and characterization of particle size distributions in coastal waters, J. Geophys. Res., 115

Ross, T. and Lueck, R. (2005), Estimating turbulent dissipation rates from acoustic backscatter. Deep Sea Research, 52, 2353-2365

Sauer, V. B., Meyer, R. W. (1992), Determination of error in individual discharge measurements, U.S.G.S. Open-File Report. 92-144, 21 pp.

Schoellhamer, D. H. and Wright, S. A. (2003), Continuous measurement of suspended-sediment discharge in rivers by use of optical backscatterance sensors, in Bogen, J., T. Fergus, and D. E. Walling (2003), Erosion and sediment transport in rivers, technological and methodological advances: Internat. Assoc. of Hydrological Sciences, Publication 283, 28-36.

Sequoia Scientific, Inc. (2008), Home page. http://www.sequoiasci.com/

Sewell, C. J. T. (1910), The extinction of sound in a viscous atmosphere by small obstacles of cylindrical and spherical form: Philosophical Transactions of the Royal Soc. of London, Series A, 210, 239-270

Sheng, J. and Hay, A. E. (1988), An examination of the spherical scatter approximation in aqueous suspensions of sand. J. Acoust. Soc. Am., 83(2), 598-610.

Simmons, S. M., Parsons, D. R., Best, J. L., Orfeo, O., Lane, S. N., Kostaschuk, R., Hardy, R. J., West, G., Malzone, C., Marcus, J., and Pocwiardowski, P. (2010), Monitoring Suspended Sediment Dynamics Using MBES, J. Hydr. Engrg. 136, 45-49

Simpson, M. R. (2001) Discharge measurements using a broad-band acoustic doppler current profiler, U.S.G.S. Open File Report 01-1, 123 pp

Slattery, M.C., Burt, T.P., 1997, Particle size characteristics of suspended sediment in hillslope runoff and stream flow, Earth Surface Processes Landforms 22 _8., 705–719

Smith, C. K., Wren, D., and Chambers, J. (2006), Estimation of particle sizes for a range of narrow size distributions of natural sands suspended in water using multi-frequency acoustic backscatter. Proceedings of the 8th Federal Inter-Agency Sedimentation Conference, Reno, NV, April 2–6, 2006, 531–538

Sturm, T.W. (2006), Scour around bankline and setback abutments in compound channels, Journal of Hydraulic Engineering, 132, 21-32

Sung, C. C., Huang, Y. J., Lai, J. S., and Hwang, G. W. (2008), Ultrasonic measurement of suspended sediment concentrations: an experimental validation of the approach using kaolin suspensions and reservoir sediments under variable thermal conditions. Hydrological Processes 22, 3149–3154

Sutherland, T. F., Lane, P. M., Amos, C. L. and Downing, J. (2000), The calibration of optical backscatter sensors for suspended sediment of varying darkness levels. Mar. Geol. 162, 587-597

Thevenot, M. M., and Kraus, N. C. (1993), Comparison of acoustical and optical measurements of suspended material in the Chesapeake Estuary. J. Mar. Env. Eng., 1, 65-79.

Thorne, P. D., Vincent, C. E., Harcastle, P. J., Rehman, S. and Pearson, N. (1991), Measuring suspended sediment concentrations using acoustic backscatter devices. Mar. Geol., 98, 7-16.

Thorne, P. D., Hardcastle, P. J. (1997), Acoustic measurements of suspended sediments in turbulent currents and comparison with in-situ samples. Journal of the Acoustical Society of America, 101, 2603-2614

Thorne, P.D., Hanes, D.M. (2002), A review of acoustic measurement of small-scale sediment processes, Continental Shelf Research, 22, 603-632

Thorne, Peter D., Hurther, David, Moate, Benjamin D., 2011, Acoustic inversions for measuring boundary layer suspended sediment processes, J. Acoustical. Soc. Am. Volume 130, Issue 3, pp. 1188-1200

Topping, D. J., Melis, T. S., Rubin, D. M. and Wright, S. A. (2004), High-resolution monitoring of suspended-sediment concentration and grain size in the Colorado River in Grand Canyon using a laser acoustic system, in Proceedings of the 9th International Symposium on River Sedimentation, Yichang, China, 18-21 October, Tsinghua University Press, 2507-2514.

Topping, D. J., Wright, S. A., Melis, T. S., and Rubin, D. M. (2006), High-resolution monitoring of suspended-sediment concentration and grain size in the Colorado River using laser-diffraction instruments and a three-frequency acoustic system. Proceedings of the 8th Federal Inter-Agency Sedimentation Conference, Reno, NV, April 2–6, 2006, 555–559

Topping, D. J., Wright, S. A., Melis, T. S. and Rubin, D. M. (2007), High-resolution measurement of suspended-sediment concentrations and grain size in the Colorado River in Grand Canyon using a multi-frequency acoustic system, in Proceedings of the 10th International Symposium on River Sedimentation, Moscow, Russia, 1-4 August, 330-339

Traykovski, P., Latter, R. J. and Irish, J. D. (1999), A laboratory evaluation of the LISST instrument using natural sediments. Mar. Geol., 159, 355–367

Uhrich, M. A., and Bragg, H. M. (2003), Monitoring instream turbidity to estimate continuous suspended-sediment loads and yields and clay-water volumes in the Upper North Santiam River Basin, Oregon, 1998–2000, U.S.G.S. Water-Resources Investigations Report 03-4098, 44 pp.

Urick, R.J. (1948), The absorption of sound in suspensions of irregular particles, Acoustical Society of America, 20, 283-289

Urick, R. J. (1975), Principles of underwater sound, 2nd ed., McGraw Hill, N. Y., 384 pp.

U.S. Army Corps of Engineers (2008), Annual Dredging Costs, Navigation Data Center, http://www.iwr.usace.army.mil/ndc/dredge/ddhisbth.htm

U.S. Environmental Protection Agency (1979), Methods for chemical analysis of water and wastes: Cincinnati, Ohio, U.S. Environmental Monitoring Laboratory, Office of Research and Development 600/4/79/020, 180.1–1 to 180.1–3

U.S. Environmental Protection Agency (1999), Guidance manual for compliance with the Interim Enhanced Surface Water Treatment rule – Turbidity provisions: Washington , D.C., USEPA, Office of Water, EPA 815-R-99-010

U. S. Environmental Protection Agency (2008), Handbook for Developing Watershed Plans to Restore and Protect Our Waters, Office of Water, Nonpoint Source Control Branch, EPA 841-B-08-002, 400 pgs

Vanoni, V.A. (editor), 2006, Sedimentation Engineering, American Society of Civil Engineers, Manuals and Reports on Engineering Practice; no. 54

van de Hulst, H.C. 1981. Light Scattering by Small Particles. New York: Dover.

Wall, G. R., Nystrom, E. A., and Litten, S. (2006), Use of an ADCP to Compute Suspended-Sediment Discharge in the Tidal Hudson River, New York, USGS SIR 2006-5055

Walling, D. E. (1977), Assessing the Accuracy of Suspended Sediment Rating Curves for a Small Basin, Water Resour. Res., 13(3), 531–538.

Warner, R. and Sturm, T. (2002), Turbidity as a Surrogate to Estimate the Effluent Suspended Sediment Concentration of Sediment Controls at a Construction Site in the Southeastern United States, Proc., U.S.G.S. Turbidity and Other Sediment Surrogates Workshop

Williams, Garnett P., 1989, Sediment Concentration versus water discharge during single hydrologic events in rivers, Journal of Hydrology, 111, pp89-106

Wood, P.A., 1977. Controls of variation in suspended sediment concentration in the River Rother, West Sussex, England. Sedimentology 24 _3., 437–445.

Wood P.J., Armitage, P.D. (1997) Biological effects of fine sediment in the lotic environment. Environmental Management 21: 203-217

Young, R. A., Merrill, J. T., Clarke, T. L. and Proni, J. R. (1982), Acoustic Profiling of Suspended Sediments in the Marine Bottom Boundary Layer, Geophys. Res. Lett., 9(3), 175–178

Ziegler, A. C. (2003)a, Breakout session 1 – Definition of optical methods for turbidity and data reporting, in Proceedings of the Federal Interagency Workshop on Turbidity and

Other Sediment Surrogates, 30 April-2 May, Reno, Nevada, U.S.G.S. Circular 1250, 9-13.

Ziegler, A. C., (2003)b, Issues related to use of turbidity measurements as a surrogate for suspended sediment, in Gray, J.R., and Glysson, G.D., eds., Proceedings of the Federal Interagency Workshop on Turbidity and Other Sediment Surrogates, April 30–May 2, 2002, Reno, Nevada: U.S.G.S. Circular 1250, p. 16–18